Synthesis and Morphological Characterization of Segmented and Branched Polydimethylsiloxane-Polyester Copolymers

By

Abduelmaged Basher Elmabrok Abduallah

Dissertation is presented in partial fulfillment of the requirements for the degree of PhD in Polymer Science at the University of Stellenbosch

Promoter: Prof. Peter Mallon

Department of Chemistry and Polymer Science

March 2010

Abstract

Polydimethylsiloxane–polyester (PDMS-PES) copolymers produce materials which have enhanced properties and take advantage of the unique properties of the two very dissimilar components. The dissimilar nature of the components results in these types of materials typically having complex morphologies in the solid state as a result of phase segregation. When the polyester component is crystallisable, an even richer variation in morphology can be expected. The chain structure of the copolymer in terms of the distribution of the various segments along the chain and the variation in the composition also has a dramatic impact on the solid state morphology. In this study, two different types of polyesters were used to synthesise five series of PDMS-PES segmented copolymers and one series of PDMS-PES branched copolymer. The two polyester segments selected were polybutyleneadipate (PBA) and polybuthylenecyclohexancarboxylate (PBCH). The copolymers were synthesised via polycondensation in the melt state. Insights on many variations in the PDMS-PES copolymer synthesis are given. The copolymer series synthesized gave systematic series where the influence of the polyester type, chain architecture, bulk composition, block length, crystallinity and processing condition on the bulk and surface morphology could be studied. The remarkable variations in the properties of the copolymer were attributed to the differences in the copolymers morphology in terms of the microphase segregation, crystallization and the free volume properties. These variations were also found to alter the nature of the surface compositions and the related surface properties. Multiphase morphology exhibited in all the PDMS-PES copolymers and the type of morphology observed was dependent on PDMS contents, PDMS segment length and the degree of branching. Three types of morphology were observed: spherical micro-domains of PDMS in a matrix of PES, bicontinuous double diamond type morphology, and spherical micro-domains of PES in a matrix of PDMS. Spherical domains of the PDMS were also observed for low PDMS content copolymers between the crystalline polyester lamellae. The complexity of the PDMS-PBCH copolymer morphology was further investigated, using an extensive set of experimental data that has been drawn together with using positron annihilation lifetime spectroscopy (PALS) and developing and applying a new type of hyphenated technique between fractionation (chromatography) and microscopy (atomic force microscopy) techniques. The outcome has provided a unique perspective regarding the complexity of the PDMS-PBCH copolymer morphology, which is believed to provide basis for a theoretical structure-properties relationship in this fascinating class of thermoplastic material.

Opsomming

Polidimetielsiloksaan–poliëster (PDMS–PES) kopolimere lewer verbindings met goeie eienskappe en trek voordeel uit die unieke eienskappe van die twee baie verskillende komponente. Aangesien die aard van hierdie twee verbindings baie verskil het hulle ‘n gekompliseerde morfologie in die vastetoestand as gevolg van faseskeiding. Wanneer die poliëster komponent kristalliseerbaar is kan ‘n nog ryker variasie in morfologie verwag word. Die kettingstruktuur van die kopolimere in terme van die verspreiding van die verskillende segmente al langs die ketting en die variasie in samestelling, het ook ‘n groot invloed op die vastetoestandmorfologie. In hierdie studie is twee verskillende tipes poliëster gebruik om vyf reekse PDMS–PES gesegmenteerde kopolimere en een reeks vertakte PDMS–PES kopolimere te berei. Die twee poliëstersegmente is polibutileenadipaat (PBA) en polibutileensikloheksaankarboksilaat (PBCH). Die kopolimere is berei deur middel van polikondensasie in die smeltfase. Inligting aangaande verskeie faktore in the bereiding van die PDMS–PES kopolimere is ingewin. Die reekse kopolimere wat berei is, het dit moontlik gemaak om die invloed van die tipe poliëster, kettingargitektuur, grootmaatsamestelling, bloklengte, kristalliniteit en reaksiekondisies op die oppervlakte en interne morfologie te bestudeer. Die opmerklike verskille in the eienskappe van die kopolimere word toegeskryf aan die verskille in die kopolimeermorfologie in terme van die mikrofaseskeiding, kristalliniteit en vryevolume eienskappe. Hierdie verskille het ook veranderings in die oppervlakte samestellings en verwante oppervlakte eienskappe teweeggebring. Multifase morfologie, in alle PDMS–PES kopolimere en die tipe morfologie wat waargeneem is, is afhanklik van die PDMS inhoud, die PDMS segmentlengte en die graad van vertakking. Drie tipes morfologie is waargeneem: sferiese mikro-gebiede van PDMS in ‘n PES matriks, ‘n bi-kontinueerlike dubbele-diamant tipe en sferiese mikro-gebiede van PES in ‘n PDMS matriks. Sferiese gebiede van die PDMS is ook waargeneem in kopolimere met ‘n lae PDMS inhoud tussen die kristallyne poliëster lae. Die kompleksiteit van die PDMS–PBCH kopolimeermorfologie is verder ondersoek deur gebruik te maak van ‘n wye reeks eksperimentele data afkomstig van positronvernietigingsleeftydspektroskopie (PALS), gevolg deur die ontwikkeling en toepassing van ‘n nuwe soort gekoppelde tegniek – tussen fraksionering (chromatografie) en mikroskopie (atoomkragmikroskopie) tegnieke. Die resultate het ‘n unieke perspektief gegee wat betref die kompleksiteit van die PDMS–PBCH kopolimeermorfologie en dien as ‘n basis vir die teoretiese struktuur–eienskapverwantskap van hierdie interessante klas termoplastiese materiale.

Declaration

I, the undersigned, hereby declare that the work contained in this thesis is my own original work and that I have not previously in its entirety or in part submitted it at any university for a degree.

Signature: …….

Abduelmaged

Date: ……..

Acknowledgements

All praise and thanks are due to God almighty for granting me the chance and ability to successfully complete this study.

My sincere thanks are due to the following people and organizations:

- My family and friends for their support and help
- Prof. P.E. Mallon (my promoter) for his guidance and support
- Dr M. J. Hurndall for her assistance in compiling this thesis
- Elsa Malherbe and Jean McKenzie for running the NMR samples
- Remy Bucher from iTemba LABS for the WAXD analysis
- Mohamed Jaffer from the University of Cape Town for the TEM analysis
- My colleagues in the 134 lab and the AFM lab
- All the staff in the Department of Chemistry and Polymer Science
- The Centre for Macromolecular Chemistry in Tripoli, Libya for financial support

during this work.

Dedication

To my parents

To my wife

To all the members of my family

To everyone, who believed in me and supported me.

TABLE OF CONTENT

CHAPTER ONE: INTRODUCTION AND OBJECTIVES.....1

1.1 INTRODUCTION.....2

1.2 OBJECTIVES.....4

1.3 LAYOUT OF THE THESIS.....5

1.4 REFERENCES.....6

CHAPTER TWO: LITERATURE REVIEW AND BACKGROUND.....8

2.1 INTRODUCTION.....10

2.2 POLYDIMETHYLSILOXANE PROPERTIES AND SYNTHESIS.....10

2.3 PDMS MULTIBLOCK COPOLYMERS SYNTHESIS.....13

2.3.1 Polymer–monomer condensation.....14

2.3.2 Polymer–polymer condensation.....15

2.3.3 PDMS-polyester copolymer synthesis.....16

2.4 PDMS COPOLYMER MORPHOLOGY.....19

2.4.1 Microphase separation in PDMS copolymers.....20

2.4.2 Crystallization of PDMS copolymers.....24

2.4.3 Free volume of PDMS copolymers.....26

2.4.4 Surface morphology of PDMS copolymers.....29

2.4.5 Morphology characterizations of PDMS copolymers.....30

2.5 FRACTIONATION PROCESS USING CHROMATOGRAPHIC SYSTEMS.....31

2.5.1 Size exclusion chromatography.....32

2.5.2 Gradient elution chromatography.....33

2.6 CONCLUSION.....34

2.7 REFERENCES.....34

CHAPTER THREE: SYNTHESIS OF MULTIBLOCK PDMS-PES COPOLYMERS VIA MELT POLYCONDENSATION AND THEIR CHARACTERIZATION.....42

3.1 INTRODUCTION.....44

3.2 EXPERIMENTAL.....46

3.2.1 Materials.....46

3.2.2 Synthesis of PDMS oligomers.....48

3.2.2.1 Preparation of tetramethylammonium hydroxide siloxanolate catalyst.....48

3.2.2.2 Synthesis of PDMS oligomers terminated with an aminopropyl group 49
3.2.2.3 PDMS amine end group deactivation reaction 50
3.2.2.4 End-capping of polydimethylsiloxane 51
3.2.3 Synthesis of PDMS-PES copolymers via the one-prepolymer method.....52
3.2.3.1 PDMS-s-PBA copolymers 52
3.2.3.2 PDMS-s-PBCH copolymers 53
3.2.3.3 PDMS-br-PBCH copolymers 55
3.2.4 Synthesis of PDMS-PBCH copolymers via the two-prepolymer method 56
3.2.4.1 PBCH homopolymers 57
3.2.4.2 PDMS-s-PBCH copolymers 57
3.2.5 Characterization techniques 58
3.2.5.1 Nuclear magnetic resonance spectroscopy (NMR) 58
3.2.5.2 Fourier-transform infrared spectroscopy (FTIR).....59
3.2.5.3 High performance liquid chromatography (HPLC).....59
3.2.5.4 Size exclusion chromatography (SEC) 60
3.2.5.5 Gradient elution chromatography (GEC).....60
3.2.5.6 Size exclusion chromatography-multi angle laser light scattering (SEC-MALLS).....61
3.3 RESULTS AND DISCUSSION 62
3.3.1 PDMS and PBCH oligomers characterization 62
3.3.1.1 Chemical characterization of PDMS and PBCH oligomers.....62
3.3.1.2 Determination of PDMS molar mass and the removal of cyclic components 68
3.3.2 PDMS-s-PES copolymer characterization 71
3.3.2.1 PDMS-s-PBA copolymer 71
3.3.2.2 PDMS-s-PBCH copolymer 78
3.3.2.3 PDMS-br-PBCH copolymer.....87
3.4 CONCLUSIONS 91
3.5 REFERENCES 92
CHAPTER FOUR: MORPHOLOGY OF SEMI-CRYSTALLINE POLYDIMETHYLSILOXANE-POLYESTER COPOLYMERS: 95
1 EFFECT OF THE PDMS CONTENT AND THE POLYESTER TYPE 95
4.1 INTRODUCTION 97

4.2 EXPERIMENTAL 99
4.2.1 Copolymers *99*
4.2.2 Characterization *100*
4.2.2.1 Dynamic mechanical analysis (DMA) 100
4.2.2.2 Differential scanning calorimetry (DSC) 101
4.2.2.3 Wide-angle X-ray diffraction (WAXD) 101
4.2.2.4 Atomic force microscopy (AFM) 101
4.2.2.5 Transmission electron microscopy (TEM) 103
4.3 RESULTS AND DISCUSSION 103
4.3.1 Copolymer characterization *103*
4.3.2 Microscopic surface morphology of the copolymers *106*
4.3.3 Microscopic bulk morphology of the copolymers *114*
4.3.4 Adhesive force and surface roughness measurements *119*
4.4 CONCLUSIONS 121
4.5 REFERENCES 122

CHAPTER FIVE: MORPHOLOGY OF SEMI-CRYSTALLINE POLYDIMETHYLSILOXANE-POLYESTER COPOLYMERS: 126

2 EFFECT OF THE PDMS MOLAR MASS AND THE BRANCHING DEGREE 126

5.1 INTRODUCTION 128
5.2 EXPERIMENTAL 129
5.2.1 Copolymers *129*
5.2.2 Characterization *130*
5.3 RESULTS AND DISCUSSION 130
5.3.1 Copolymer characterization *130*
5.3.2 Microscopic surface and bulk morphology of the copolymers *135*
5.3.3 Adhesive force and surface roughness *146*
5.4 CONCLUSIONS 149
5.5 REFERENCES 150

CHAPTER SIX: MEASUREMENT OF FREE VOLUME IN PDMS-PBCH COPOLYMERS USING POSITRON ANNIHILATION LIFETIME SPECTROSCOPY 153

6.1 INTRODUCTION 155

6.2 EXPERIMENTAL 157
6.2.1 PDMS-PBCH samples 157
6.2.2 Sample preparation 159
6.2.3 Data analysis 159
6.3 RESULTS AND DISCUSSION 161
6.3.1 PDMS and PBCH homopolymers 161
6.3.2 PDMS-PBCH copolymers 163
6.3.3 Glass transition temperature and free volume 172
6.4 CONCLUSIONS 174
6.5 REFERENCES 175

CHAPTER SEVEN: SURFACE MORPHOLOGY OF PDMS-S-PBCH COPOLYMERS AND HPLC-LC-TRANSFORM MICROSCOPIC HYPHENATED TECHNIQUES 177

7.1 INTRODUCTION 179
7.2 EXPERIMENTAL 181
7.2.1 PDMS-s-PBCH samples 181
7.2.2 Characterization techniques 181
7.2.2.1 Fractionation by size exclusion chromatography 181
7.2.2.2 Fractionations by gradient elution chromatography 182
7.2.2.3 SEC-LC-FTIR analysis 182
7.2.2.4 Surface morphology investigation of the PDMS-s-PBCH copolymers 182
7.3 RESULTS AND DISCUSSION 184
7.3.1 Surface morphology of alternating PDMS-s-PBCH copolymers 184
7.3.2 HLPC-LC-transform-AFM investigation of PDMS-PBCH copolymers 186
7.3.3 Adhesive force investigation of PDMS-PBCH copolymer fractions 195
7.4 CONCLUSIONS 200
7.5 REFERENCES 201

CHAPTER EIGHT: CONCLUSIONS AND RECOMMENDATIONS 203

8.1 CONCLUSIONS 204
8.1.1 Synthesis, characterization and properties of the PDMS-PES copolymers 204
8.1.2 Morphology of PDMS-PES copolymers 205
8.2 RECOMMENDATIONS FOR FUTURE WORK 208

8.3 POSTERS AND PUBLICATIONS 209

APPENDIXES 210

APPENDIX A: PDMS OLIGOMER 211

APPENDIX B: PDMS-PBCH COPOLYMERS 215

APPENDIX C: PDMS-POLYBUTYLENE 1,4-CYCLOHEXANE DICARBOXYLATE-CO-TEREPHTHALATE (PDMS-PBCH-PBT) COPOLYMERS 224

APPENDIX D: PRELIMINARY STUDY OF ELECTROSPINNING OF SEGMENTED AND BRANCHED POLYDIMETHYLSILOXANE-POLYESTER COPOLYMERS 232

List of Abbreviations

a	Mark Houwink constant
AA	Adipic acid
AFM	Atomic force microscopy
BD	1,4-butanediol
C	Empirical scaling constant
CCD	Chemical composition distribution
D_3	Hexamethylcyclotrisiloxane
D_4	Octamethylcyclotrisiloxane
D-chloroform	Deuterated chloroform
DIS.	Distilled
DMA	Dynamic mechanical analysis
DMCH	1,4-dimethylcyclohexanedicarboxylate
DSC	Differential scanning calorimetry
ELSD	Evaporating light scattering detector
F	Adhesive force
ffv	Average of the free volume fractions
FTIR	Fourier-transform infrared spectroscopy
fv	Free volume fraction
fv	Average of the free volume holes
FWHM	Full width at half maximum
g	Branching index
GEC	Gradient elution chromatography
I_c	Area under the crystalline peaks
I_{tot}	Total area under of the amorphous and the crystalline peaks
HPLC	High performance liquid chromatography
HPLC-DPFM-AFM	Hyphenated technique of HPLC and digital pulsed force mode of AFM
I_3	Average intensity of the ortho-positronium formation
k	Spring constant of the AFM cantilever
k	Mark Houwink constant
LC	Liquid chromatography
LC-CC	Liquid chromatography at critical conditions
LT	Positron lifetime (spectra)

M_m	Average molar mass
M_n	Number average molar mass
M_w	Weight average molar mass
N	Number of accumulated coincidences
N	Degree of polymerization
NMR	Nuclear magnetic resonance spectroscopy
NP	Normal phase
o-Ps	Ortho-positronium
PALS	Positronium annihilation lifetime spectroscopy
PBA	Polybutyleneadipate
PBCH	Polybutylenecyclohexanedicarboxylate
PBT	Polybutyleneterephthalate
PCL-PDMS-PCL	Polycaprolactone-PDMS-polycaprolactone
PDI	Polydispersity index
PDMS	Polydimethylsiloxane
PDMS-BPAC	PDMS-bisphenol polycarbonate
PDMS-br-PBCH	Polydimethylsiloxane-polybutylenecyclohexanedicarboxylate branched copolymer
PDMS-s-PBA	Polydimethylsiloxane-polybutyleneadipate segmented copolymer
PDMS-s-PBCH	Polydimethylsiloxane-polybutylenecyclohexanedicarboxylate segmented copolymer
PDMS-PES	Polydimethylsiloxane-polyester
PEO-PDMS-PEO	Poly(ethylene oxide)-PDMS-poly(ethylene oxide)
PES	Polyester
PPO-PDMS-PPO	Poly(propylene oxide)-PDMS-poly(propylene oxide) copolymer
Ps	Positronium
p-Ps	Para-positronium
R	Spherical domain radius
R	Average radius of the free volume holes
R^2	Mean square radius of gyration
Ra	Mean surface roughness
RI	Refractive index detector
R_o	Infinite spherical potential radius
RP	Reversed-phase
S	Sensitivity of the photodiode in the AFM

SEC	Size exclusion chromatography
SEC-MALLS	Size exclusion chromatography-multi angle laser light scattering
t	Flow time
TEM	Transmission electron microscopy
T_g	Glass transition temperature
T_gH	Higher T_g (T_g of the PES segments)
T_gL	Lower T_g (T_g of the PDMS segment)
THF	Tetrahydrofuran
TIP	Titanium tetraisopropoxide
T_m	Melting temperature
TMS	Tetramethylsiloxane
UND.	Undistilled
UV	Ultraviolet
V	Average voltage value
Vf	Mean hole volume
WAXD	Wide-angle X-ray diffraction
XPS	X-ray photoelectron spectroscopy

List of Figures

Figure 2.1: Various diblock copolymer architectures. 19

Figure 2.2: Schematic illustration of the four different types of copolymer morphology: spheres, cylinder, lamellae and gyroid or bicontinuous. 21

Figure 2.3: Spherical PDMS domain in multiblock copolymers based on Meier's model of an AB-block copolymer domain and triblock copolymer. 22

Figure 2.4: Schematic of the ideal chain unfolding and extension in a semi-crystalline polymer (from (a) and (b) to (c)), under tensile drawing (reproduced from Ref. 108). 26

Figure 2.5: Ps localization in the free volume holes of a polymer before its annihilation. 27

Figure 3.1: Chemical structure of PDMS-PES copolymers: (a) aliphatic polyester segment (PDMS-s-PBA), (b) cycloaliphatic polyester segment (PDMS-s-PBCH), (c) cycloaliphatic perfectly alternating polyester segment (PDMS-s-PBCH) and (d) randomly branched PDMS-cycloaliphatic copolymer (PDMS-br-PBCH). 45

Figure 3.2: Chemical structures of the monomers and agent used in PDMS oligomers synthesis and characterization. 47

Figure 3.3: Chemical structures of the monomers and branching agent used in polymers synthesis. 48

Figure 3.4: Gradient elution profile that was used in HPLC to fractionate the PDMS-PES copolymers (Stationary phase: Nucleosil C18 5 μm, mobile phase: THF/hexane; ELSD detector). *The gradient was started at 10:90 of (THF/hexane, (v/v)), held constant for 5 min, then changed linearly within 3 min to 61:39 of (THF/hexane, (v/v)), and held constant for 7.5 min and then changed linearly within 3 min to 90:10 of (THF/hexane, (v/v)), and held constant for 6 min and then changed linearly within 4.5 min to 10:90 of (THF/hexane, (v/v)). The flow rate was 1 mL/min.* 61

Figure 3.5: Typical ^{1}H-NMR spectrum of a PDMS oligomer terminated with an amine group (PDMS-NH_2). 62

Figure 3.6: Typical ^{1}H-NMR spectrum of a PDMS oligomer terminated with an ester group (PDMS-$COOCH_3$). 63

Figure 3.7: Typical ^{13}C-NMR spectrum of a PDMS oligomer terminated with an amine group (PDMS-NH_2). 64

Figure 3.8: Typical ^{13}C-NMR spectrum of a PDMS oligomer terminated with an ester group (PDMS-$COOCH_3$). 65

Figure 3.9: Typical ^{1}H-NMR spectrum of a PBCH terminated with a hydroxyl group (PBCH-OH). 65

Figure 3.10: Typical ^{13}C-NMR spectrum of a PBCH terminated with a hydroxyl group (PBCH-OH). 66

Figure 3.11: FTIR spectra of PDMS oligomers terminated with amine end groups of two different M_n (1000 and 7000 g/mol). 67

Figure 3.12: FTIR spectra of PDMS terminated with amine and ester end groups, respectively (M_n 1000 g/mol). 67

Figure 3.13: HPLC results of the undistilled and distilled PDMS oligomers of (a) 1000 g/mol target molar mass and (b) 7000 g/mol target molar mass. 70

Figure 3.14: SEC results of PDMS oligomers of various molar masses. 71

Figure 3.15: ^{1}H-NMR spectra of PDMS-s-PBA with different PDMS content (series A). 73

Figure 3.16: ^{1}H-NMR spectra of PDMS-s-PBA with different PDMS content (series B). 73

Figure 3.17: ^{13}C-NMR analysis of PDMS-s-PBA copolymers A-3 and B-3. 74

Figure 3.18: SEC results, obtained using a RI detector, for PDMS-s-PBA copolymers: (a) series A and (b) series B. 75

Figure 3.19: Typical SEC results of (a) A-3 and (b) B-3 copolymers, obtained using a RI detector and UV detector at 310 nm. 76

Figure 3.20: Typical gradient elution analysis chromatogram of a PDMS-PBA segmented copolymers (B-5), (see Section 3.2.5.5). 77

Figure 3.21: Typical gradient analysis results for PDMS-PBA multiblock copolymers of series B (see Section 3.2.5.5). 78

Figure 3.22: Typical ^{1}H-NMR spectra of PDMS-s-PBCH copolymers (C-2, D-1, E-1 and E-2) after extraction of homopolymers. 80

Figure 3.23: A typical ^{13}C-NMR spectrum of PDMS-s-PBCH copolymer (C-1). 82

Figure 3.24: Typical SEC results for PDMS-s-PBCH copolymers: (a) series C, and (b) series E. 82

Figure 3.25: SEC results of PDMS-PBCH copolymers, obtained using a RI detector and UV detector at 310 nm: (a) C-2, (b) E-2, (c) D-1, and (d) E-4. 84

Figure 3.26: Typical examples of GEC results of PDMS-s-PBCH copolymers (C-1), and PDMS and PBCH homopolymers (see Section 3.2.5.5). 85

Figure 3.27: Typical examples of GEC results of PDMS-s-PBCH copolymers (see Section 3.2.5.5). 86

Figure 3.28: Typical example of a ^{1}H-NMR spectrum of PDMS-br-PBCH with 0.5% branching agent content. 88

Figure 3.29: Typical ^{13}C-NMR spectrum of PDMS-br-PBCH with 0.5% branching agent content. 89

Figure 3.30: Typical SEC results for F-3 copolymers obtained using RI detector and UV detector at 310 nm.....90

Figure 3.31: GEC results of PDMS-br-PBCH copolymers (Series F) with 10 wt % PDMS content, 2000 g/mol PDMS M_n, and various degrees of branching (see Section 3.2.5.5)...90

Figure 4.1: WAXD profiles of (a) PDMS and PBA homopolymers and PDMS-s-PBA copolymers with different PDMS content, including magnification of the region from 2θ = 6° to 18°, and (b) PDMS and PBCH homopolymers and PDMS-s-PBCH copolymers with different PDMS content.....105

Figure 4.2: Topography and phase AFM images of thin films of polyester homopolymers: (a and b) aliphatic polyester (PBA) and (c and d) cycloaliphatic polyester (PBCH). 107

Figure 4.3: Topography and phase AFM images of thin films of polydimethysiloxane–polyester copolymers with 5 wt % PDMS (M_n PDMS segment 2000): (a and b) PDMS-s-PBA and (c and d) PDMS-s-PBCH. 108

Figure 4.4: AFM phase images of higher resolution of thin films of polyester homopolymers and polydimethysiloxane–polyester copolymers with 5 wt % PDMS: (a) PBA, (b) PDMS-s-PBA copoylmer, (c) PBCH and (d) PDMS-s-PBCH copolymer.....110

Figure 4.5: Schematic illustration of the PDMS segregations in-between the lamellae arrangements in the polydimethysiloxane–polyester copolymers.....111

Figure 4.6: Topography and phase AFM images of thin films of polydimethysiloxane–polyester copolymers with 10% PDMS (M_n PDMS segment 2000): (a and b) PDMS-s-PBA and (c and d) PDMS-s-PBCH. 111

Figure 4.7: AFM phase images of thin films of PDMS-s-PBA and PDMS-s-PBCH copolymers with 25 wt % (a and b), 40 wt % (c and d) and 60 wt % (e and f) PDMS content, respectively.....113

Figure 4.8: TEM micrographs of polydimethysiloxane–polyester copolymers: (a and c) PDMS-s-PBCH 5 wt % and 10 wt % PDMS content, respectivly, and (b and d) PDMS-s-PBA 5 wt % and 10 wt % PDMS content, respectivly. 116

Figure 4.9: TEM micrographs of polydimethysiloxane–polyester copolymers: (a, c and e) PDMS-s-PBCH 25, 40 and 60 wt % PDMS content, respectivly, and (b, d and f) PDMS-s-PBA 25, 40 and 60 wt % PDMS content, respectivly.....118

Figure 4.10: Adhesive force measurements for (a) PDMS-s-PBA and (b) PDMS-s-PBCH copolymers. 119

Figure 4.11: Surface roughness measurements for (a) PDMS-s-PBA and (b) PDMS-s-PBCH copolymers. 120

Figure 5.1: Tan δ profile of DMA results of: (a) PBCH homopolymer (D) and PDMS-s-PBCH copolymers, and (b) PDMS-br-PBCH copolymers. 132

Figure 5.2: DSC thermograms of: (a) PBCH homopolymer (D) and PDMS-s-PBCH copolymers, and (b) PDMS-br-PBCH copolymers. 133

Figure 5.3: WAXD profiles of: (a) PBCH homopolymer (D), PDMS-s-PBCH copolymers and (b) D-1 (F) PDMS-s-PBCH copolymers and PDMS-br-PBCH copolymers. The profile of PDMS homopolymer is included in both diagrams (a and b). 134

Figure 5.4: AFM images of thin films of (a and b) PBCH homopolymer and (c and d) PDMS-s-PBCH with 10 wt % PDMS content and PDMS M_n 1000 g/mol. 136

Figure 5.5: AFM images of thin films of PDMS-s-PBCH copolymers with 10 wt % PDMS and segment of PDMS of different M_n: (a) PDMS M_n 2000, (b) PDMS M_n 4000, (c) PDMS M_n 7000 and (d) PDMS M_n 10000 g/ mol. 138

Figure 5.6: Analysis section of AFM phase images of thin films of PDMS-s-PBCH copolymers with 10 wt % PDMS and PDMS segments with different M_n values: (a) PDMS M_n 4000, and (b) PDMS M_n 10000 g/mol. 139

Figure 5.7: TEM micrograph of PDMS-s-PBCH copolymer with 10 wt % PDMS content and M_n 1000 g/mol. 139

Figure 5.8: TEM micrograph of PDMS-s-PBCH copolymers with 10 wt % PDMS content and varying M_n: (a) 2000, (b) 4000, (c) 7000 and (d) 10000 g/mol. 141

Figure 5.9: AFM phase images of the PDMS-PBCH branched copolymer with 10 wt % PDMS and (a) 0.1 wt % branching agent, (b) 0.2 wt % branching agent, (c) 0.5 wt % branching agent (d) 1 wt % branching agent (e) 2 wt % branching agent. 143

Figure 5.10: TEM micrograph of PDMS-PBCH segmented (a) and branched copolymer with 10 wt % PDMS, and (b) 0.1 wt % branching agent, (c) 0.2 wt % branching agent, (d) 0.5 wt % branching agent, (e) 1 wt % branching agent, and (f) 2 wt % branching agent. 145

Figure 5.11: Adhesive force measurement of: (a) PBCH homopolymer (D), PDMS-s-PBCH copolymers and (b) D-1 (F) PDMS-s-PBCH copolymers and PDMS-br-PBCH copolymers. 147

Figure 5.12: Surface roughness of: (a) PBCH homopolymer (D), PDMS-s-PBCH copolymers and (b) D-1 (F) PDMS-s-PBCH copolymers and PDMS-br-PBCH copolymers.....148

Figure 6.1: The radioactive source placed between the two copolymer samples.....159

Figure 6.2: The three-components fit to the LT spectrum of PBCH. 160

Figure 6.3: The four-components fit to the LT spectrum of PBCH.....161

Figure 6.4: Dependence of (a) o-Ps lifetime (τ) and (b) intensity (I) on the PDMS content in PDMS-PBCH copolymers (series C).....165

Figure 6.5: Effect of the PDMS content on the radius (R) of the free volume holes in series C.166

Figure 6.6: Dependence of (a) o-Ps lifetime (τ) and (b) intensity (I) on the PDMS segment length in PDMS-PBCH copolymers (series D). 168

Figure 6.7: Effect of the PDMS segment length on the radius of the free volume holes in series D.....169

Figure 6.8: Visual representation of the total fraction of the free volume in the copolymer series C, D and F, and PBCH and PDMS homopolymers, calculated as a sum of fraction of the free volumes obtained from the two long-lived components. 170

Figure 6.9: Dependence of (a) o-Ps lifetime and (b) intensity on the branching agent content in PDMS-PBCH copolymers (series F). 171

Figure 6.10: Effect of the branching agent content on the radius (R) of the free volume holes in series F.....172

Figure 6.11: The effects of the PDMS content, PDMS M_n and the branching agent content on the o-Ps lifetime and the T_g values of the PDMS and PBCH segments in the PDMS-PBCH copolymers. 173

Figure 7.1: Typical example of the AFM adhesive force image of a PDMS-PBCH copolymer and the corresponding voltage distribution histogram.....183

Figure 7.2: AFM phase images of thin films of PDMS-PBCH alternating multiblock copolymers: (a) 5 wt % PDMS (PDMS M_n 2000 g/mol) (b) 10 wt % PDMS (PDMS M_n 2000 g/mol) (c) 25 wt % PDMS (PDMS M_n 2000 g/mol) (d) 10 wt % PDMS (PDMS M_n 1000 g/mol).....185

Figure 7.3: A Gram-Schmidt plot overlaid with the ratio of Si–O/C=O FTIR bands and AFM images for each assigned fraction of a random PDMS-PBCH multiblock copolymer with 10 wt % PDMS content.....187

Figure 7.4: GEC result for PDMS, PBCH homopolymers and a random PDMS-PBCH multiblock copolymer with 10 wt % PDMS content and AFM images for each assigned fraction of the copolymer (Chapter 3).....188

Figure 7.5: A Gram-Schmidt plot overlaid with the ratio of C=O/Si–O FTIR bands and AFM images for each assigned fraction of alternating PDMS-PBCH multiblock copolymer with 10 wt % PDMS content.....189

Figure 7.6: GEC results and AFM images for each assigned fraction of alternating PDMS-PBCH multiblock copolymer with 10 wt % PDMS content (Chapter 3). 190

Figure 7.7: Schematic representation of the fringed-micelle model, showing the crystallinity of PBCH segments in the PDMS-PBCH copolymers.....191

Figure 7.8: A Gram-Schmidt plot overlaid with the ratio of Si–O/C=O FTIR bands and AFM images each assigned fraction of a random PDMS-PBCH multiblock copolymer with 25 wt % PDMS content.....192

Figure 7.9: GEC results and AFM images for each assigned fraction of a random PDMS-PBCH multiblock copolymer with 25 wt % PDMS content (Chapter 3). 193

Figure 7.10: A Gram-Schmidt plot overlaid with the ratio of Si–O/C=O FTIR bands and AFM images for each assigned fraction of an alternating PDMS-PBCH multiblock copolymer with 25 wt % PDMS content.....194

Figure 7.11: GEC results and AFM images taken for each assigned fraction of an alternating PDMS-PBCH multiblock copolymer with 25 wt % PDMS content (Chapter 3).....195

Figure 7.12: GEC-DPFM-AFM results for a PDMS-PBCH random multiblock copolymer with 10 wt % PDMS content. 196

Figure 7. 13: Adhesive force distribution of the PDMS and PBCH homopolymers and six fractions of PDMS-PBCH random multiblock copolymer with 10 wt % PDMS content obtained from the SEC-DPFM-AFM.....197

Figure 7.14: 2D plot of the GEC-DPFM-AFM results of sample C-2 associated with both homopolymers. 198

Figure 7.15: SEC-DPFM-AFM results for a PDMS-PBCH random multiblock copolymer with 10 wt % PDMS content. 199

Figure 7.16: Adhesive force distribution of nine fractions of PDMS-PBCH random multiblock copolymer with 10 wt % PDMS content obtained from the SEC-DPFM-AFM. 199

List of Schemes

Scheme 2.1: Chemical structure of polydimethylsiloxane. 10

Scheme 2.2: Chemical structure of hexamethylcyclotrisiloxane (D_3) and octamethylcyclotrisiloxane (D_4). 12

Scheme 2.3: Redistribution reaction of linear and cyclic chains of polysiloxanes..... 12

Scheme 2.4: Synthesis of randomly alternating segmented copolymers of PDMS in the polymer-monomer condensation. 14

Scheme 2.5: Synthesis of perfectly alternating segmented copolymers of PDMS in the polymer-polymer condensation. 16

Scheme 3.1: Synthesis of the tetramethylammonium siloxanolate catalyst..... 49

Scheme 3.2: Synthesis of PDMS oligomers via equilibrium ring-opening polymerization. 49

Scheme 3.3: Amino end group deactivation reaction (at either 125 °C or 140 °C, and for 12 to 15 h). 51

Scheme 3.4: Conversion of the amino end groups in the PDMS prepolymer to ester end group. 51

Scheme 3.5: Synthesis of random segmented PDMS-PBA copolymers. 53

Scheme 3.6: Synthesis of randomly segmented PDMS-PBCH copolymers..... 55

Scheme 3.7: Synthesis of randomly branched PDMS-PBCH copolymers. 56

Scheme 3.8: Synthesis of linear polybutylenescyclohexanedicarboxylate with OH end groups. 57

Scheme 3.9: Synthesis of alternating segmented PDMS-PBCH copolymers. 58

Scheme 3.10: Scission side reaction in polyester chains. 83

Scheme 5.1: Chemical structures of PDMS-PBCH copolymers: (a) PDMS-s-PBCH and (b) PDMS-br-PBCH. 129

List of Tables

Table 3.1: Quantities of D_4 and bis(3-aminopropyl) tetramethyldisiloxane required to obtain PDMS (10 g) with various target molar masses 50

Table 3.2: Infrared assignments for PDMS-NH_2 and PDMS-$COOCH_3$ 68

Table 3.3: Comparison of the target and the determined molar masses of PDMS oligomers 69

Table 3.4: Data for the two series of PDMS-s-PBA copolymers prepared using different PDMS concentrations and two different synthesis conditions, (A and B series), by the one-prepolymer method 72

Table 3.5: Data for the three series of PDMS-s-PBCH copolymers prepared using different PDMS concentrations and PDMS molar mass 79

Table 3.6: Characteristics of the PDMS-br-PBCH copolymers (F-1 to F-5), prepared using the one-prepolymer method 87

Table 4.1: Chemical compositions and average molar masses of PBA and PBCH homopolymers, and PDMS-s-PBA and PDMS-s-PBCH copolymers, prepared using various concentrations of PDMS (2000 g/mol) 100

Table 4.2: Glass transition temperature (T_g), melting temperature (T_m) and the degree of crystallinity of PBA and PBCH hompolymers, and PDMS-s-PBA and PDMS-s-PBCH copolymers, with different polyester content 104

Table 5.1: Chemical compositions and average molar masses of two series of PDMS-PBCH copolymers: PDMS-s-PBCH copolymer and PDMS-br-PBCH copolymer 130

Table 5.2: Glass transition temperature (T_g), melting temperature (T_m) and the degree of crystallinity (area under the melting peak) of PDMS-s-PBCH and PDMS-br-PBCH copolymers 131

Table 5.3: Domain sizes (diameters) of segmented PDMS-PBCH copolymers 142

Table 5.4: Domain sizes (diameter) of branched PDMS-PBCH copolymers 146

Table 6.1: Characteristics of three series of PDMS-PBCH copolymers (C, D, and F) investigated 158

Table 6.2: The o-Ps characteristics of PDMS and PBCH homopolymers determined using the three- components fit 162

Table 6.3: Free volume holes and free volume factions of the holes in three different PDMS-PBCH copolymer series based on the four-components fit 167

Table 7.1: The characteristics of the PDMS-s-PBCH copolymers with 2000 g/mol PDMS M_n 181

Table 7.2: FWHM of the PDMS the PBCH homopolymers and the C-2 copolymer as well as the HPLC-DPFM-AFM fractions adhesive force distribution peaks 197

Chapter One

Introduction and Objectives

1.1 Introduction

Multiphase copolymers are of great importance and much has been written in the literature concerning these materials.[1-6] This is because the covalent bonding of two different polymeric blocks displaying very different properties allows for specific tailoring of the ultimate performance of a two- or more-phase system. In spite of the large amount of reported information in this area of polymer science, there is still much to be learnt about these copolymers, properties, morphologies, and possible applications. The morphology of these multiphase copolymer systems has attracted particularly wide interest among many researchers, who have tried to elucidate the detailed micro- and superstructure using a variety of techniques.[7-13] Over the past decade the number of investigations dealing with the synthesis and characterization of multiblock copolymers, such as polydimethylsiloxane-organic copolymers with an organic crystallisable segment, has increased rapidly.[9,14-22] The synthesis of these copolymers is made possible because of the many organic reactive end groups that can be placed onto the PDMS segment. These can include carboxyl, hydroxyl, amino, epoxy, as well as other types of end groups.

As a result of PDMS's unique combination of properties; such as a very low glass transition, high thermal and thermo-oxidative stability, good biocompatibility, low surface energy, ultraviolet resistance and high permeability to many gases,[3] PDMS-organic block or segmented copolymers have received particular attention for many applications, such as biomaterials, photoresists, gas separation membranes, protective coatings, elastomers and emulsifiers.[3] The copolymerizations of PDMS with organic polymers are also of particular interest since small bulk concentrations of PDMS oligomers can result in rather dramatic surface enrichment.[4] The unique surface behaviour made by the addition of the low surface energy PDMS component is a direct result of the structural properties of the polymer. Such materials are promising for sophisticated applications in many nanotechnology industries, as nanofibers, nanowires, nanomembranes and optical materials, as well as in surface patterning, lithography, and templating applications for the fabrication of information storage devices.[4]

PDMS-polyester (PES) multiblock copolymers are one of the limited studied copolymers that consist of both amorphous and crystalline components. These multiblock copolymers can be synthesized via a polycondensation reaction in the melt state under vacuum conditions.[14,23-25] However, due to the complexity of the structure of the PDMS-PES multiblock copolymers and the large difference in the solubility parameters of the PDMS and PES segments, and

other physical phenomena such as crystallization of the PES segment, there has not been much focus on studying the morphology of these copolymers.[15] The morphology of PDMS-PES copolymers is expected to display nanophase or microphase separation due to the presence of chemical incompatibility between the constituent blocks or segments of the siloxane and the ester. The understanding and controlling of such nanophase and microphase separation is an increasingly important requirement for obtaining specific desirable properties of the copolymers so that they can be used for particular applications. This fact has been the chief motivation for the present study.

The extent to which microphase separation occurs to form supermolecular structures in multiblock copolymers such as PDMS copolymers depends on four features. First is the chemical composition dissimilarity, which leads to a difference in solubility parameters and chain interactions. Second is the segment molar mass of the copolymer components; third, the crystallinity of one or both segments, and fourth, the molecular architecture of the segment or the copolymer.[26-32] Furthermore, the morphology of multiblock copolymers also depends on the way in which the materials are synthesized and the method of the film preparation. For example, different morphologies can result when copolymer are solution cast from different solvents.[33,34] The periodicity of those morphological structures for block copolymers is determined by molar mass of the components and chemical composition of the copolymers.

In multiblock PDMS-copolymers, the bulk compositions have a major influence on the surface composition and surface morphology. The effects of block length, architecture[35] and crystallinity[36,37] of block copolymers on the surface compositions are also very important. It has been proven for several PDMS-copolymers that PDMS segments tend to segregate on the copolymer surface.[35,37] In the light of the above, special emphasis was placed on the surface segregation of the PDMS segments in the present study.

Moreover PDMS-PES copolymers resulting from polycondensation are expected to have a very complex chemical microstructure, and thus morphology. This is because the incorporation of both PDMS oligomers and PES monomers into the copolymer backbone is completely random process. In the polycondensation reaction it is also possible that PES homopolymer will be formed.[38]

These products can be determined by gradient elution chromatography (GEC) techniques, which are based on the differences in the solubility of the polymers present in the copolymerization products. By combing chromatography and spectroscopy (Fourier-transform infrared, FTIR), the chemical composition variation through the molar mass distribution of the copolymers can be quickly and easily determined. In this study the chromatography fractionation technique was taken a step further: it was used as a preparative fractionation tool, using LC-transform. For each copolymer sample, several fractions were collected and morphological investigation of each fraction carried out using atomic force microscopy (AFM) in order to better understand the complex morphology of these copolymers.

1.2 Objectives

The objectives of this study can be summarized as follows:

1. Synthesize PDMS oligomers of five different molar masses using equilibrium ring-opening polymerizations.

2. Synthesize various systematic series of polydimethylsiloxane-polyester segmented (PDMS-s-PES) copolymers via condensation polymerization under different experimental conditions, namely:

- Polydimethylsiloxane-polybutyleneadipate segmented (PDMS-s-PBA) copolymers with different PDMS contents, either in bulk polymerization (series A) or in partial solution polymerization (series B), using a one-prepolymer method.

- Polydimethylsiloxane-polybutylenecyclohexanedicarboxylate segmented (PDMS-s-PBCH) copolymers with both different PDMS contents (series C), and with different PDMS segment lengths (series D), using a one-prepolymer method.

- Polydimethylsiloxane-polybutylenecyclohexanedicarboxylate segmented (PDMS-s-PBCH) copolymers with both different PDMS contents and with different PDMS segment lengths (series E), using a two-prepolymer method.

3. Synthesize a systematic series of multiblock polydimethylsiloxane-polybutylenecyclohexanedicarboxylate branched (PDMS-br-PBCH) copolymers (series F) via condensation polymerization, under vacuum and at high temperature, using a one-

prepolymer method, in the presence of a small percentage of branching agent (multifunctional monomer).

4. Conduct a study of two different synthesis methods of PDMS-s-PBCH copolymer by developing and optimizing the working conditions of the two chromatography technique; size exclusion chromatography (SEC) and GEC.

5. Investigate the morphology of the PDMS-PES copolymers in terms of:

- The effect of PES type, PDMS molar mass, chemical composition and chain branching degree, on the PDMS-PES copolymer morphology.
- The effect of PDMS molar mass, chemical composition and chain branching degree on the copolymer properties, mainly copolymer crystallinity, adhesive force (surface energy) and free volume.

6. Develop new hyphenated techniques with high performance liquid chromatography (HPLC) and AFM. Such a technique should provide more detailed analytical information about the morphology of the PDMS-s-PBCH copolymers.

7. Explore a new type of two dimensional separation using the hyphenated technique of HPLC-digital pulsed force mode of AFM (HPLC-DPFM-AFM), in which the adhesive force distribution determined for each single copolymer fraction collected from the HPLC by the LC-transform.

1.3 Layout of the thesis

A general introduction to, and the objectives of the study are given in Chapter 1. In Chapter 2 the theoretical background of several synthetic preparation methods of PDMS and PDMS copolymers is presented and discussed, with special focus on methods used in this work. A discussion of the PDMS copolymer morphology and chromatography fractionation techniques is included. The experimental work is divided into five chapters as follows; Chapter 3 describes the syntheses of the PDMS oligomer and six series of PDMS-PES copolymers. Chapter 4 and 5 describe the investigations of the morphology of four of the six copolymer series that were synthesized (in Chapter 3). The free volumes of three of copolymers series were investigated by positron annihilation lifetime spectroscopy and are explained in Chapter 6. Chapter 7 describes the investigation of copolymer fractionation and

morphology investigation (of the copolymers fractions). This chapter also includes discussion of the new proposed hyphenated techniques of HPLC-AFM and HPLC-DPFM-AFM. Finally, in Chapter 8, conclusions are drawn from the results that are described in the previous chapters, and recommendations for future research are given. Several calculations and pilot studies that are related to the five experimental chapters are included in the Appendixes.

1.4 References

1. Wang, L.; Gong, W.; Zheng, S. *Polymer International* 2009, 58(2), 124-132.
2. Luo, Z-h.; He, T-y. *Reactive and Functional Polymers* 2008, 68(5), 931-942.
3. Yilgör, I.; McGrath, J., Polysiloxane containing copolymers: A survey of recent developments. In *Polysiloxane Copolymers/Anionic Polymerization*, Springer, Berlin / Heidelberg, 1988; Vol. 86, pp 1-86.
4. Chang-sik, H.; Gardella Jr, J. A. *Journal of Macromolecular Science: Polymer Reviews* 2005, 45(1), 1-18.
5. Pticek, A.; Hrnjak-Murgic, Z.; Jelencic, J.; Kovacic, T. *Polymer Degradation and Stability* 2005, 90(2), 319-325.
6. Xie, H.-Q.; Xie, D. *Progress in Polymer Science* 1999, 24(2), 275-313.
7. Wu, N.; Zheng, A.; Huang, Y.; Liu, H. *Journal of Applied Polymer Science* 2007, 104(2), 1010-1018.
8. Fang, H.; Feng, L.; You, B.; Wu, L. *Journal of Polymer Science, Part B: Polymer Physics* 2007, 45(2), 208-217.
9. Ku, C.-K.; Lee, Y.-D. *Polymer* 2007, 48(12), 3565-3573.
10. Spontak, R. J.; Smith, S. D.; Ashraf, A. *Microscopy Research and Technique* 1994, 27(5), 412-419.
11. Dai, L.; White, J. W. *Polymer* 1997, 38(4), 775-783.
12. Xiang, H.; Shin, K.; Kim, T.; Moon, S.; Mccarthy, T. J.; Russell, T. P. *Journal of Polymer Science, Part B: Polymer Physics* 2005, 43(23), 3377-3383.
13. Castelletto, V.; Hamley, I. W. *Current Opinion in Solid State and Materials Science* 2004, 8(6), 426-438.
14. Kiefer, L. A.; Yoon, T. H.; Glass, T. E.; Jayaraman, S. K.; McGrath, J. E. *Journal of Polymer Science, Part A: Polymer Chemistry* 1997, 35(16), 3495-3506.
15. Miroslawa, E. F. *Designed Monomers and Polymers* 2000, 3(3), 325-337.
16. Antic, V. V.; Balaban, M. R.; Djonlagic, J. *Polymer International* 2001, 50(11), 1201-1208.
17. Dojcinovic, B. P.; Antic, V. V.; Vuckovic, M. V.; Djonlagic, J. *Journal of the Serbian Chemical Society* 2005, 70(12), 1469-1485.
18. Vuckovic, M. V.; Antic, V. V.; Dojcinovic, B. P.; Govedarica, M. N.; Djonlagic, J. *Polymer International* 2006, 55(11), 1304-1314.

19. van Aert, H. A. M.; Nelissen, L.; Lemstra, P. J.; Brunelle, D. J. *Polymer* 2001, 42(5), 1781-1788.
20. Stanciu, A.; Airinei, A.; Timpu, D.; Ioanid, A.; Ioan, C.; Bulacovschi, V. *European Polymer Journal* 1999, 35(11), 1959-1965.
21. Rochery, M.; Vroman, I.; Lam, T. *Journal of Macromolecular Science: Pure and Applied Chemistry* 2003, 40(3), 321-333.
22. Yilgör, E.; Yilgör, I. *Polymer* 2001, 42(19), 7953-7959.
23. Dahrouch, M.; Schmidt, A.; Leemans, L.; Linssen, H.; Götz, H. *Macromolecular Symposia* 2003, 199(1), 147-162.
24. Miroslawa El F.; Volker A. *Macromolecular Symposia* 2003, 199(1), 125-134.
25. Antic, V. V.; Vuckovic, M. V.; Djonlagic, J. *Journal of the Serbian Chemical Society* 2007, 72(2), 139-150.
26. Schmidt, J. J.; Gardella, J. A.; Salvati, L. *Macromolecules* 1989, 22(12), 4489-4495.
27. Liu, L.; Jiang, B.; Zhou, E. *Polymer* 1996, 37(17), 3937-3943.
28. Sheth, J. P.; Aneja, A.; Wilkes, G. L.; Yilgor, E.; Atilla, G. E.; Yilgor, I.; Beyer, F. L. *Polymer* 2004, 45(20), 6919-6932.
29. Zhang, Y.; Feng, Z.; Feng, Q.; Cui, F. *European Polymer Journal* 2004, 40(7), 1297-1308.
30. Prisacariu, C.; Olley, R. H.; Caraculacu, A. A.; Bassett, D. C.; Martin, C. *Polymer* 2003, 44(18), 5407-5421.
31. Luo, N.; Wang, D.-N.; Ying, S.-K. *Polymer* 1996, 37(16), 3577-3583.
32. Weidong, L.; Baotong, H. *Journal of Polymer Science, Part B: Polymer Physics* 1992, 30(7), 727-732.
33. R.G., C., Surface morphlogies od styrene-ethylene oxide block copolymers. In *Colloidal and Morphological Behavior of Block and Graft Copolymers* First ed.; Molau, G. E. (Ed.), Plenum Press, New York, 1971; pp 279-293.
34. Guan, R.; Dai, H.; Li, C.; Liu, J.; Xu, J. *Journal of Membrane Science* 2006, 277(1-2), 148-156.
35. Chen, X.; Gardella, J. A.; Kumler, P. L. *Macromolecules* 1992, 25(24), 6621-6630.
36. Schmitt, R. L.; Gardella Jr, J. A.; Magill, J. H.; Chin, R. L. *Polymer* 1987, 28(9), 1462-1466.
37. Chen, X.; Gardella, J. A.; Cohen, R. E. *Macromolecules* 1994, 27(8), 2206-2210.
38. Elvers, B.; Hawkins, S.; Schulz, G., Polyesters. In *Ullmann's Encyclopaedia of Industrial Chemistry*, Fifth ed.; Köpnick, H.; Schmidt, M.; Brügging, W.; Rüter, J.; Kaminsky, W. (Eds), VCH Verlagsgesellschaft Weinheim, Germany, 1992; Vol. A21, pp 227-251.

Chapter Two

Literature Review and Background

Abstract

Over the years, there have been many studies on the theoretical and phenomenological aspects of block (diblock, triblock and multiblock) and branched copolymer systems. However, in many real multiblock systems, the effect of such variables as chemical composition distribution, molar mass distribution and block architecture, among others, are not very well understood. This chapter is mainly devoted to review the literature that is relevant to this study. It includes the PDMS properties and the PDMS synthesis. It also includes a discussion of multiblock PDMS copolymers synthesis with an emphasis on PDMS-polyester multiblock copolymers. This is followed by reviewing PDMS copolymer morphology, focusing on several aspects of semicrystalline PDMS copolymer morphology namely microphase separation, crystallization, free volume and PDMS surface segregation. Furthermore a brief discussion on chromatography fractionation techniques used in this study are included at the end of the review.

Keywords: Polydimethylsiloxane, PDMS multiblock copolymers, PDMS copolymers morphology, chromatography fractionation systems.

2.1 Introduction

Polymeric hybrid materials continue to be the object of intensive research in the field of polymer science. PDMS copolymers have become one of the most important and versatile classes of such hybrid polymeric material. The increasing interest in multiphase copolymers of PDMS is mainly due to the unique combination of properties that are obtained from the PDMS segment (inorganic segment) and from the organic segment of the copolymer. These types of copolymers are attractive candidates for microelectronic, coating, membrane, biological and medical applications.[1-9]

Incorporation of the flexible PDMS segment into a hard organic segment such as polyester has been shown to yield several attractive properties while many of the excellent properties of the corresponding polyester homopolymer are retained.[10-12] PDMS-polyester multiblock copolymers possess good processability, low surface energy and excellent mechanical and adhesion properties. These properties are directly related to their chemical structure, macromolecular architecture and copolymer morphology.[13,14] Reports of investigations of the morphology of the multiblock PDMS-polyester copolymers in the open literature are extremely limited. This is quite the opposite to the extensive studies reports about PDMS-polyester copolymer synthesis.[11,15-19]

2.2 Polydimethylsiloxane properties and synthesis

Polysiloxanes can be regarded as derivative of inorganic silicates by partial substitution with organic groups. These materials are considered to be the most widely studied polymers with an inorganic backbone.[20,21] Historically, polysiloxanes were first synthesized in 1872, however, they did not gain commercial importance until decades later. They were introduced to the market in 1940s.[20,21] One of these polysiloxanes that is found in a wide range of commercial applications nowadays due to its excellent properties, is a linear polydimethylsiloxane (PDMS) Scheme 2.1.[22]

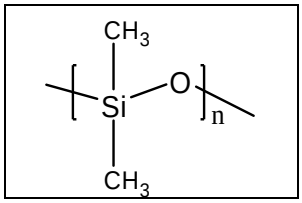

Scheme 2.1: Chemical structure of polydimethylsiloxane.

Its properties include an extremely low glass transition temperature (–123 °C), high thermal and oxidative stability, high UV resistance, low surface energy and hydrophobicity, low toxicity, good electrical properties, high permeability to many gases, and relatively low flammability.[22] In order to take advantage of the unique properties of the PDMS, a very high molar mass is required to achieve good mechanical properties, due to the low glass transition temperature. In addition, high levels of fillers are typically used to enhance the desirable physical properties.[23] Other means used to enhance the described properties include chemical modifications using crosslinking,[24] or copolymerization of the PDMS with other polymers such as polystyrene,[25,26] polycarbonate[27] and polyester.[10-12]

PDMS homopolymer is synthesized commercially by the hydrolysis and subsequent condensation of organohalosilanes, or by the acid- or base-catalyzed ring opening polymerization of cyclic siloxane monomers, particularly octamethylcyclotrisiloxane (D_4). The polymer molar mass is controlled by introducing a chain transfer agent.[21,28] The polycondensation process is often applied to the synthesis of both linear siloxane polymers and cyclic siloxane oligomers. The cyclic siloxane oligomers are further used as substrates in ring opening polymerizations. Another method of PDMS synthesis with controlled molar mass is the living anionic polymerization of hexamethylcyclotrisiloxane (D_3) using an alkyl lithium initiator.[29]

Ring opening polymerization allows control over molar mass by adjusting the stoichiometry of cyclics to the end group reactants (the monofunctional initiators agent). An example of these end group agents is bis(3-aminopropyl)tetramethyldisiloxane, which will be used in this work, under anionic conditions.

The ring opening polymerization reactions can be carried out under anionic or cationic conditions and they are usually classified as either kinetically or thermodynamically controlled processes. Protic acids are, the most common initiating species used in cationic ring opening polymerizations. In the thermodynamically controlled route, D_4 is the appropriate monomer used, whereas in the kinetically controlled route, D_3 is commonly used (see Scheme 2.2).[22]

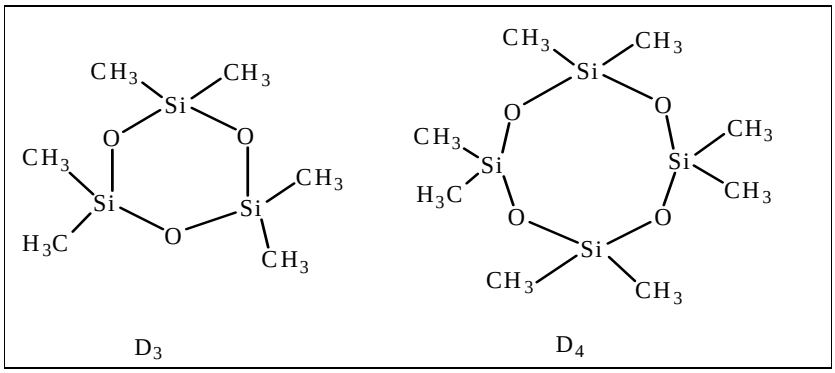

Scheme 2.2: Chemical structures of hexamethylcyclotrisiloxane (D_3) and octamethylcyclotrisiloxane (D_4).

Thermodynamically controlled reactions occur when the system is allowed to reach equilibrium conditions. This result in a redistribution of both linear and cyclic chains of polysiloxanes (see Scheme 2.3).

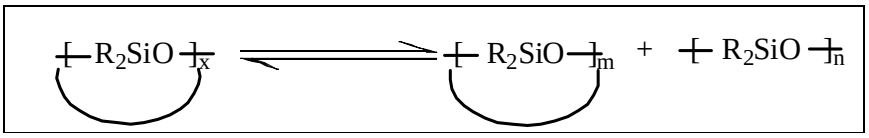

Scheme 2.3: Redistribution reaction of linear and cyclic chains of polysiloxanes.

The most popular synthetic method used in industry for polysiloxanes preparation is the ring opening equilibration polymerization of D_4 under anionic conditions.[14] This method comprises three general steps:

(1) Initiation step, during which the base catalyst attacks the silicon to afford the silanolate end-group,

(2) Propagation-depropagation steps, during which the molar mass of linear and cyclic oligomers increases, and

(3) Chain equilibration step, during which the oligomers molar mass becomes constant and the cyclic chains represent 10–15 wt % of the produced oligomers.[30]

Equilibration of the base catalyzed initiator species with D_4 results in the formation of linear chains and various cyclic species. Upon heating the reaction to 145 °C, the anions couple and by-products of trimethylamine and dimethylether are evolved, to produce a neutralized, stable material.[31] The remaining cyclic components can be easily distilled away under vacuum.

During ring opening polymerization, the growing polymer chain can perform a so-called backbiting reaction, during which it can break the Si-O bond present along the linear backbone, resulting in the production of cyclic components. Studies on this phenomenon have revealed that the equilibrium between the linear chains and cyclic components determines the polymer yield, molar mass and molar mass distribution.[32] The concentration of the equilibrium cyclic components and the linear polymer is independent of the initial monomer concentration. As a consequence, dilution of the system with a solvent results in a decrease in the linear chain yield.[30] Therefore, the equilibration reaction in this work was carried out effectively in bulk to ensure that PDMS of specific molar mass and in the best yield is achieved.

2.3 PDMS multiblock copolymers synthesis

PDMS multiblock copolymers can be classified in two ways: the first is according to the nature of the chemical link between the PDMS segment and the organic polymer segment, and the second is according to the synthetic procedure used to prepare them.

Using the first classification method, multiblock PDMS copolymers can be divided into two groups, multiblock copolymers with Si-O-C linkages and multiblock copolymers with Si-C linkages.[14] Multiblock copolymers with Si-O-C were synthesized earlier than multiblock copolymers with Si-C because copolymers containing Si-O-C are obtained from very reactive functional groups attached to the terminal silicon atom, such as chlorosilane or silylamine. On the other hand, copolymers containing Si-C links depend on the synthesis of organofunctional polysiloxanes of controlled functionality. This organofunctionality is generally much less reactive.[20]

The second classification method, which is based on the experimental procedure, divides the PDMS copolymers into random multiblock copolymer and perfectly alternating multiblock copolymers. The random multiblock copolymers are synthesized by polymer–monomer condensation or the one-prepolymer method,[10] and the alternating multiblock copolymers are synthesized by polymer–polymer condensation or two-prepolymers method.[28,33] In the following sections (2.3.1 and 2.3.2), the second method of classification is used when reviewing multiblock (segmented) PDMS copolymer synthesis.

2.3.1 Polymer–monomer condensation

Polymer–monomer condensation, or the one-prepolymer method, yields randomly segmented block copolymers. In general, the polymerization reaction comprises of a difunctional oligomer of known size and two difunctional monomers, where the oligomer usually possesses the same end groups as one of the monomers. Scheme 2.4 illustrates the general steps in the polymer–monomer condensation reaction. A two-step procedure is often preferred in this method. In the first step the PDMS end groups are reacted with an excess of one reactant and in the second step the second reactant is added to adjust the stoichiometric balance. The reactivity of the difunctional PDMS oligomers is assumed to be the same as that of organic polymer molecules (in this study the organic polymer is polyester) as they have similar functionality. The PDMS segments are, therefore, inserted randomly in the copolymer. In this method, the PDMS oligomer size and composition control the average block length of the second block. This method is commonly used in the synthesis of commercially important PDMS copolymers. By using various difunctional PDMS oligomers, a large variety of random block copolymers can be formed, including PDMS-polyester,[10,11,16-19] PDMS-polycarbonate,[27,34,35] PDMS-polyamide,[36] PDMS-polyurethane,[37,38] PDMS-polyurea,[39,40] PDMS-polysulfone[41] and PDMS-polyimide.[42]

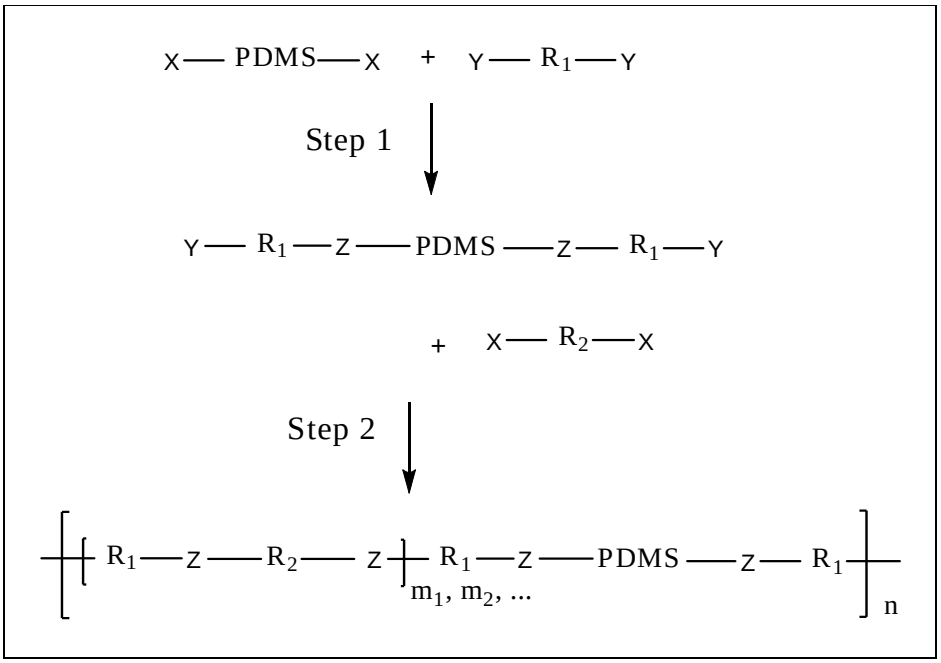

Scheme 2.4: Synthesis of randomly alternating segmented copolymers of PDMS in the polymer-monomer condensation.

The earliest PDMS copolymer that was synthesized using this method is the PDMS-polycarbonate multiblock copolymer, which was synthesized by Vaughn in 1969.[43] Synthesis involved phosgenation of a mixture of bisphenol-A and dichloro-PDMS oligomer in the presence of pyridine. The obtained multiblock copolymer contains the Si-O-C linkage. Multiblock PDMS-polyesters copolymers, in this work and as described elsewhere,[10] have been prepared using the one-prepolymer method, in a two-step reaction. In the first step PDMS with an amino alkyl end group was end-capped with ester groups by reaction with an excess of a cycloaliphatic diester. In the second step 1,4-butanediol was added, with titanium tetraisopropoxide as a catalyst. Recently, the synthesis of PDMS-aromatic polyester copolymers has also been reported.[11,15-19] Other synthesis methods of PDMS-polyester copolymers are described in Section 2.3.3.

Peebles developed a theoretical treatment to compare the effect of one-step polymerization with two-step polymerization on the hard segment length distribution in multi-block copolymers.[44] He showed that a narrower distribution of the hard segment lengths resulted when a two-stage polymerization was utilized instead of the one-stage procedure. Later, Abouzahr and Wilkes[45] compared the effect of one- and two-step polymerization on the properties of polyether or polyester (polytetramethyleneadipate) based segmented polyurethanes. They found that the polyester based polyurethanes polymerized in the one-stage process exhibited slightly poorer physical properties than their two-stage process counterparts. A greater hard–soft segmental mixing in the former, owing to their greater hard segment length distribution, was proposed as the reason for such behaviour.

2.3.2 Polymer–polymer condensation

The polymer–polymer condensation method is also called the two-prepolymer method. It involves polymerization of two different oligomers via reaction of their end groups to produce true multiblock copolymers or perfectly alternating segmented copolymers (Scheme 2.5). Polycondensation of difunctional PDMS with difunctional organic polymers constitutes a large class of reactions yielding multiblock copolymers. Synthesis of PDMS-polyester, in which chloro-terminated PDMS reacts with hydroxyl-terminated aliphatic polyester, is a typical example in this category. However, the degree of chain extension for these copolymers appears to be low.[33] Other examples of polymer-polymer condensation methods include the reaction of dimethylamino-terminated PDMS with hydroxyl-terminated-polysulfone,[46] or with dihydroxypolycarbonate[47] or with dihydroxypoly(α-methylstyrene).[48]

A low degree of polymerization was obtained for PDMS-polysulphone multiblock copolymers synthesized from diallyloligosulphones.[49]

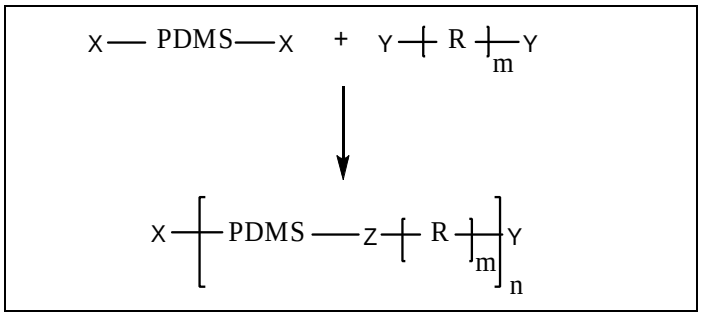

Scheme 2.5: Synthesis of perfectly alternating segmented copolymers of PDMS in the polymer-polymer condensation.

The difficulty in finding a common solvent for hydrosilylation is the main obstacle in the use of this technique. It has been shown for PDMS-polysulfone multiblock copolymers synthesized using this method that allowing the reaction to commence in a very dilute medium and then increasing the concentration progressively to maintain homogeneous conditions leads to products with higher molar masses.[50] This method is called the dilution–concentration method.

Multiblock PDMS-polystyrene and PDMS-poly(α-methylstyrene) copolymers can also be obtained from polystyrene and poly(α-methylstyrene) end-capped with vinylsilane functionality.[51] Other coupling reactions that afford many types of multiblock PDMS copolymers have been investigated.[52-55] The final molar mass depends on the extent of reaction, on the molar ratio between both functional groups, and also on side-reactions.

2.3.3 PDMS-polyester copolymer synthesis

The history of PDMS-polyester copolymer synthesis goes back to the early 1970s, when the synthesis of aromatic polyester-polyorganosiloxane block copolymers was reported in 1973.[47] However, these copolymers have Si-O-C bonds between the aromatic polyester segment and the polyorganosiloxane segment. This bond is claimed to be readily hydrolysable,[20] and hence these block copolymers are inferior in terms of hydrolysis resistance and weather resistance. The synthesis of the aromatic polyester-polyorganosiloxane block copolymers was reported a few years later.[56,57] These copolymers have an amide bond between the aromatic polyester segment and polyorganosiloxane segment. These types of aromatic polyester-polyorganosiloxane block copolymers have the disadvantage that they decompose (below

their melting points) at high temperatures without fusion and therefore they are un-mouldable. In 1990 Yamamoto et al.[16] found that a copolymer prepared by copolymerizing an aromatic polyester and a terminal diol type polyorganosiloxane, so that the bond forms an ester linkage, had excellent hydrolysis resistance, weather resistance and mouldability in addition to its excellent heat resistance, cold resistance and impact resistance. Antic et al.[17] replaced diol (silanol)-terminated-PDMS with methyl diesters of carboxypropyl-terminated PDMS to produce PDMS-polyester multiblock copolymer with polybutyleneterephthalate (PBT), as the hard segment. The same research group successfully performed the copolymerization reaction in the presence of the high-boiling solvent 1,2,4-trichlorobenzene. This was done in order to increase the mixing between the extremely non-polar siloxane prepolymer and the polar reactants of the PBT segment and, thereby, avoided phase separation during synthesis.[18]

Although the above mentioned methods were successfully used to prepare PDMS-polyester copolymers, the lack of compatibility between the polar PBT monomers (diol and diacid) and the non-polar PDMS block resulted in a significant amount of the PDMS not being incorporated into the polyester backbone. In addition, a loss in the mechanical properties has been reported for PDMS-PBT segmented copolymer when the PDMS content increases to 15 wt % and the polymer showed a lack of cohesiveness due to the incompatibility between the PBT and PDMS phases.[58] In order to improve the compatibility between the PDMS segment and the polar polyester monomers, a large variety of ABA-triblock prepolymers of PDMS terminated with different polymer segments have been used. Several examples of these are polyether,[15] polyethylene oxide PEO–PDMS–PEO,[12,58] polypropylene oxide (PPO–PDMS–PPO)[19] and polycaprolactone (PCL–PDMS–PCL).[12] The reactive functionality that was used in all the above mentioned ABA-triblock prepolymers is the hydroxyl group. A very good feature article discussing the polymers with alternating organo-silicon and π-conjugated units was published in 1998 by Ohshita and Kunai.[59]

In 1997 Kiefer et al.[10] revisited the use of PDMS terminated with amino difunctionality to produce relatively high molar mass PDMS-semicrystalline cycloaliphatic polyester segmented block copolymers based on dimethyl-1,4-cyclohexane dicarboxylate. The PDMS segment was efficiently incorporated into the copolymers via an amide link. Taking advantage of the low T_g of the PDMS segment, the copolymers demonstrated good mechanical properties and, as a result of the relatively low T_m of the polyester segment of the copolymers, they were easily compression moulded into films. These materials are expected to be potentially useful in outdoor applications due to the UV stability of both segments and

the hydrophobicity of the PDMS segment (they have, however, not been test yet toward aging and weather effects). Moreover, Miroslawa[11] used α,ω-diamino-terminated PDMS to synthesize PDMS-polyester multiblock copolymers based on PBT as a hard polyester block or segment. The soft PDMS segment was reacted with an excess of dimerized fatty acid to afford a dicarboxy-terminated oligomer containing stable amide links. Thus multiblock copolymers were obtained in a three-stage process: oligomer preparation, transesterification, and polycondensation from the melt. A magnesium-titanate catalyst was used for transesterification and polymer formation (polycondensation). The surface morphology of the obtained copolymers was studied using polarized optical microscopy (POM) and the results showed spherulitic ordering.[11] The obtained PDMS-PBT multiblock copolymers were also proven to have highly hydrophobic properties.[60]

Other polymerization methods can be used for the production of PDMS-polyester copolymers with predetermined degrees of polymerization and low polydispersities.[61] An example of one of these methods is the use of living polymerization. Polycaprolactone-b-PDMS copolymers of the ABA type have been prepared via ring opening polymerization of caprolactone, using a hydroxyalkyl terminated siloxane oligomer as initiator and macromonomer in the presence of stannous octoate as catalyst. The reactions were conducted either in bulk or in butyrolactone solution, depending on the required molar mass of the final product. Another method for the synthesis of poly(caprolactone)-b-PDMS ABA block copolymers is reported by Ekin and Wesbster.[62]

Figure 2.1 shows some examples of various copolymers architecture that can also be synthesized. In the case of the polycaprolactone-b-PDMS ABA block copolymers mentioned above, multifunctional initiators or multifunctional linking agents can be used in the living polymerization reactions to yield well-defined star-branched polymers. Alkyllithium initiators are particularly efficient types of multifunctional initiators, and polyfunctional silyl halides are highly efficient multifunctional linking agents.[63]

Comb polymers, which contain extensive branching along the polymer backbone, are synthesized in the presence of a polyfunctional coupling agent.[64] Polyfunctional or multifunctional monomers with a functionality greater than two result in randomly branched polymers. Randomly branched polymers are often prepared by step-growth or chain polymerization in the presence of a multifunctional comonomer. Low concentrations of

multifunctional comonomers are usually used at low conversions to obtain long chain branching, and this method has yielded low molar mass polymers.[63]

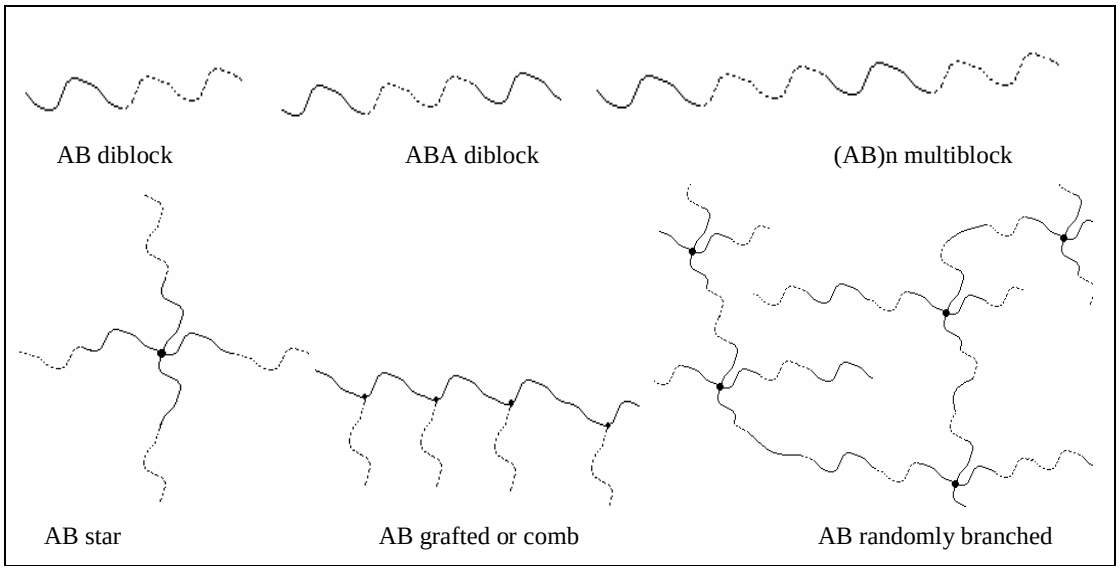

Figure 2.1: Various diblock copolymer architectures.

Branched polymers are characterized by the presence of branch points or the presence of more than two end groups, and they comprise a class of polymers between linear polymers and polymer networks.[65] Part of the present study is devoted to investigating the ability to obtain statistically branched or randomly branched PDMS-polyester copolymers using low concentrations of a multifunctional branching agent and by using a commercial route used for polyester synthesis, namely melt transesterification.

2.4 PDMS copolymer morphology

Polymer morphology can be defined as the study of the arrangement of polymer molecules into crystalline and amorphous regions, the form and structure of these regions, and the manner in which they are organized, if at all, into larger and more complex structures.[66] The morphology of multiphase copolymers plays an important role in determining the final properties of the polymers. By controlled variation of the polymer morphology the desired properties can be obtained for such polymers. The properties of copolymers that comprise hard and soft polymer segments are determined by their relative compositions. For example, copolymers with small domains of the soft segment embedded throughout the continuous hard phase behave as toughened glassy polymers. The inverted morphology behaves as a thermoplastic elastomer.[67]

The primary structure of a segmented PDMS-polyester copolymer includes its chemical composition, type of polyester, molar mass, distribution of the hard and soft segments, block length distribution (distribution of segment size), and degree of branching or crosslinking.[68] The primary structure determines the secondary structure, such as three- dimensional chain orientations, crystallinity and, consequently, the morphology of the PDMS copolymer. Both primary and secondary structures contribute to the final properties of the copolymers. The primary structure can be well controlled by synthetic conditions. For example, varying the ratio of the soft and hard segments can control the composition. The distribution of segment size is also closely related to the synthetic method. Moreover, the type of soft and hard segment can be chosen from an array of compounds and the molar masses can be varied.

Investigations of the morphology of multiblock PDMS-polyester copolymers described in literature are extremely limited. In order to complete the picture on this copolymer morphology (which is the main scope of this dissertation) the morphology of a few other multiblock or segmented PDMS copolymeric systems are discussed here, with particular emphasis on the microphase separation, crystallization and surface morphology of the copolymers. Furthermore, the morphology of the diblock PDMS copolymers is briefly considered, with focus on the diblock PDMS copolymers with a crystalline segment. For more information about this topic the following references are recommended.[14, 20, 69, 70]

2.4.1 Microphase separation in PDMS copolymers

As noted in Section 2.3, the block copolymers are composed of two chemically dissimilar bonded polymer segments. The sequential arrangement of the blocks in the copolymer results in six basic architectures: A-B diblock copolymers, A-B-A triblock copolymers, $(A\text{-}B)_n$ multiblock copolymers, star block copolymers, graft or comb copolymers, and randomly branched copolymers (Figure 2.1). At a critical molar mass of each segment in the copolymer the incompatible copolymer segments phase separate, similar to the behaviour occurring in incompatible blends. The covalent bonds between the copolymer segments prevent them from macroscopically separating. This restricts the size of the phases to the microscopic scale.[71-73] Typically the pattern in the phase separation in multiblock PDMS copolymers is exhibited only in the short range of spatial extent due to the high polydispersity of the polymers[74] and due to the variation in the segment lengths in random copolymers. In contrast to the multiblock PDMS copolymers, phase separation in the PDMS diblock copolymer systems creates well defined periodic structures on the sub-micrometer scale. When phase separation

occurs, microphases of well defined size and shape are typically formed. A variety of ordered morphologies can be achieved depending on many different variables, including copolymer composition, segment length, copolymer architecture and film preparation conditions, such as temperature, solvent, and so forth. Figure 2.2 illustrates these morphologies, which include spheres, rods, lamellae, bicontinuous, as well as inverted rods, and inverted spheres.[73]

The effect of the copolymer composition on the polyimide-PDMS copolymers morphology was reported by Rogers et al..[55] They found that block copolymers prepared with 20 wt % PDMS (M_n = 1000 g/mol) exhibit a very fine microphase separated structure. Increasing the PDMS concentration to 50 wt % and its M_n to 4500 g/mol afforded a co-continuous type of morphology.[55]

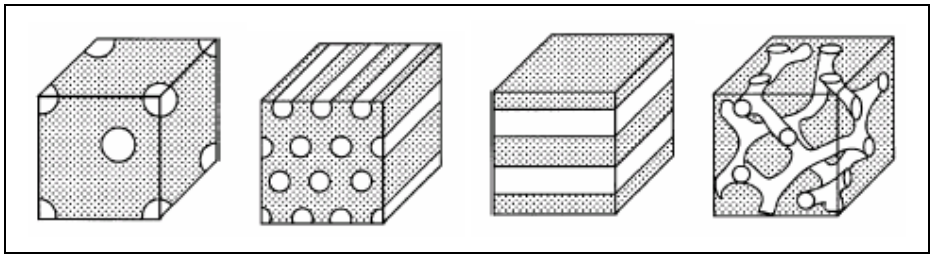

Figure 2.2: Schematic illustration of the four different types of copolymer morphology: spheres, cylinder, lamellae and gyroid or bicontinuous.

Furthermore Samseth and coworkers showed that solution cast polyimide-PDMS block copolymer films containing at least 40 wt % PDMS exhibited a siloxane continuous phase.[75,76] Another investigation showed that increasing the PDMS oligomer molar mass in polyimide-PDMS block copolymer from 2000 to 10 000 g/mol yielded larger PDMS domains and the PDMS spherical domains became more defined, indicating a higher degree of phase separation with an increasing PDMS molar mass.[77] The method of film preparation can also lead to different types of morphology. Morphological investigations carried out for *compression moulded* polyimide-PDMS copolymers revealed a semi-continuous or rod-like morphology for a 15 wt % siloxane sample. *Solution cast* films of the same copolymer showed spherical siloxane in a continuous polyimide matrix.[78] The shift in type of morphology was attributed to the casting solvent acting as a preferential solvent. Spherical siloxane phases in a continuous polyimide matrix were also observed for compression moulded copolymers prepared with a less polar polyimide and analogous copolymer compositions. This suggested that decreasing the polarity of the polyimide phase favours the more discrete microdomain structure with a higher surface to volume ratio.

Many statistical thermodynamic theories have been proposed to predict the domain size (a domain is a discrete region of space occupied by one phase and surrounded by another phase) of the copolymer morphology.[79] Theoretical consideration has been mostly restricted to amorphous monodisperse AB-block copolymers[80] although limited development of the theoretical aspects of multi-block copolymers and also theories that take into account the polydispersity of the blocks can be found in the literature.[81,82] Meier[72] was the first to identify the important elements of a statistical thermodynamic theory of linear block copolymers. An illustration of the formation of a spherical domain is shown in Figure 2.3

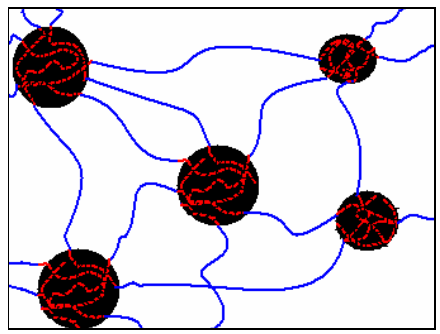

Figure 2.3: Spherical PDMS domain in multiblock copolymers based on Meier's model of an AB-block copolymer domain and triblock copolymer.[79]

The size of these microphase separated structures is in the order of magnitude of the radius of gyration of the macromolecules. The actual size of the spherical domains can be related to molar mass by the following equation:

$$R = 1.33\ \alpha\ kM_n^{1/2} \qquad \text{[Eq 2.1]}$$

where R is the domain radius (in Angströms) for a spherical domain, α and k are constants for each respective polymer (for PDMS $\alpha = 1.2$ and $k = 880 \times 10^{-3}$), and M_n is the molar mass of the spherical domain forming segment.[79]

More recently, a theory for the prediction of the phase diagrams of non-linear (star architecture) block copolymers has also been developed.[83,84] For high molar mass segments in copolymers the entropy of mixing per unit volume is low. Thus, in the case of a symmetric diblock copolymer in the disordered state, when the overall degree of polymerization (N) is sufficiently large, a reduction in temperature gives rise to excess free energy, which is minimized by the local compositional ordering or segregation of the constituent blocks.

$$\chi = A + (B/T) \qquad \text{[Eq 2.2]}$$

where χ is interaction parameter, A and B are constant for each polymer and T is the temperature.

In the case of diblock copolymers and from Eq 2.2, microphase separation in diblock copolymers can be achieved, either by decreasing the temperature at a constant degree of polymerization, and therefore increasing χ or by increasing the degree of polymerization with χ kept constant. It may be noted that χ is also dependent on thermodynamic changes, such as crystallization, in addition to the temperature.[80] Competition between phase separation and crystallization has been reported for the PDMS-polyamide (PDMS-nylon 6) block copolymer. This competition can be controlled by using mixed solvents and, eventually, the surface composition of the solution-cast films can be adjusted.[69]

In the case of a series of related block PDMS-polyurethane copolymers,[85,86] a linear dependence has been found between the extent of microphase separation and the difference in the solubility parameter. This, however, seems difficult to extend to copolymers of different structures. For instance, when the organic blocks can easily crystallize, a large difference in the solubility parameter is not necessarily required in order to observe phase-separation. Moreover, if films are prepared by solvent casting, the effect of preferential solubilisation for one block may greatly influence the morphology and, consequently, the physical and mechanical properties of the materials.[37]

While χN is also an important parameter governing the order–disorder transition in segmented copolymers, accurate application of the theories noted above is difficult in copolymers such PDMS-polyester copolymers that are found in this study. Furthermore, possible crystallizability of the hard segment also affects the extent of microphase separation, which prevents direct application of theories developed for amorphous A-B diblock copolymers. The large polydispersity of these segmented copolymers produced via step-growth polymerization, the greatly increased number of junction points (or covalent links) between the soft and the hard segments in segmented copolymer (compared to those in block copolymers of comparable overall molecular mass), and the considerable variation of χ along the segmented copolymer chain are considered to be other factors that make the development of a exact theoretical treatment difficult in multiblock copolymers. The research described and presented in the subsequent chapters clearly demonstrates that microphase separation in

PDMS-polyester copolymers (segmented and branched) is not only effected by the PDMS content and molar mass, but is also influenced by the backbone symmetry and chain architecture. However, Meier's equation [Eq 2.1] is used in some cases in this work only to demonstrate the variation in the domain size, and as an indication for the additional work that is required to be done in this area of polymer science, on both the experimental and the theoretical sides.

2.4.2 Crystallization of PDMS copolymers

In semicrystalline block copolymers the presence of a noncrystalline block enables modification of the mechanical and structural properties compared to the crystalline homopolymer. The introduction of a rubbery or glassy component usually leads to a change of the crystal type and crystallization arrangement mechanism. Crystallization in homopolymers leads to an extended conformation, or to kinetically controlled chain folding. In semicrystalline copolymers, on the other hand, equilibrium chain folding can also occur, but the equilibrium number of folds in this case is controlled by the size of the second, noncrystallisable block.[87]

Structural changes in semicrystalline copolymers in the chain-folding result from crystallization competing with microphase separation. Thus, the morphology in solution-cast films of semicrystalline copolymers is determined by two processes, crystallization and microphase separation. The surface composition of these copolymers is also subject to the competition between crystallization and microphase separation. Experiments suggest that the final morphology after crystallization depends on whether the sample is cooled from a microphase-separated melt or crystallizes from a homogeneous melt or solution.[88-90] This path dependence is a general feature of crystallization in block copolymers. Solvents that are selective for the amorphous block can lead to non-equilibrium morphologies because the crystallisable block can precipitate from solution and crystallize within microphase-separated domains of the crystallisable polymer whereas an irregular structure results when solvent is removed at temperature below T_m.[89]

Several researchers have investigated the crystallization of block PDMS-polyester copolymers.[11,19,91] In particular, Childs et al. have investigated the surface morphology of PCL-PDMS-PCL copolymer using AFM. The obtained AFM phase images showed that PCL-PDMS-PCL copolymer form very clear semicrystalline spherulites structure, the authors also

attributed the dark regions in several AFM phase images to PDMS segments.[91] The degree of crystallinity of PDMS-PBT multiblock copolymers was also measured using DSC[19] by Vuckovic et al.. It was found that the degree of crystallinity decreases as the PDMS content increases[92] and as the PDMS M_n increases.[93] Furthermore spherulitic crystal structure was observed for this copolymer using POM by Miroslawa.[11]

It has been firmly established that confinement of crystalline stems has a profound influence on crystallization in block copolymers.[94-97] Confinement can result from the presence of glassy domains or simply strong segregation between domains. In contrast, crystallization can overwhelm microphase separation when a sample is cooled from a weakly segregated or homogeneous melt. The lamellar crystallites can then nucleate and grow heterogeneously to produce spherulites, whereas these are not observed when crystallization is confined to spheres or cylinders.[94-97] Crystallization confined by glassy blocks leads to a drastic reduce in crystallization rate and a reduction in the corresponding Avrami exponent.[98,99] Crystallization of the crystallisable polymer matrix, such as polyethylene, in a phase containing rubbery or glassy cylinders can occur without disrupting the spherulitic microstructure.[74,100] On the other hand, crystallization of the polyferrocene block for PDMS-polyferrocene block copolymer was shown to be the driving force for the formation of rod-like structures in this copolymer.[70]

Crystallization and melting of the PDMS phase is observed in some of PDMS copolymers, [46,50,101-103] which indicates the PDMS phase purity. Moreover, in PEO-PDMS-PEO triblock copolymers containing crystallisable PEO blocks, the crystallinity of PDMS was described to be much higher for the copolymers than for the PDMS precursors.[104] This unusual behaviour was attributed to the extension of PDMS chains induced by phase separation and not to the crystallization of PEO on the basis of results obtained for blends of the copolymers with poly(acry1ic acid), which is miscible with PEO. In contrast to the behaviour of the central PDMS block, PEO blocks have significantly lower crystallinity than the corresponding homopolymers. The crystalline form of the hard segments in the copolymers depends on their structure, as well as on the crystallization conditions. For example, it is well known that aliphatic polyesters have greater ability to crystallize than cycloaliphatic polyesters and pure trans-isomers polyesters crystallize better than cis-isomers, in terms of both arrangements and crystallization degrees.[105] In the present work two different types of polyesters are investigated. One consequence of chain folding is that the crystallized chains in the copolymer are often not sufficiently strong for certain applications. Therefore, rearrangement of the chain order to force the strong covalent bond is usually required.[106,107]

This can be achieved by stretching the chains or aligning them in one direction and then pulling in the directions of alignment: in other words unfolding the copolymer chain in the randomly oriented spherulites to make a material where the chains have a more elongated form (see Figure 2.4). This is exactly what is expected to happen during fibre formation.

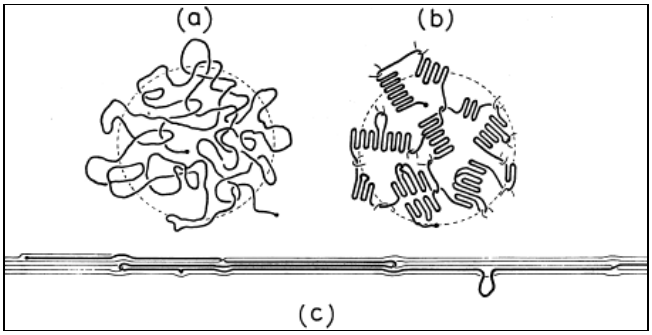

Figure 2.4: Schematic of the ideal chain unfolding and extension in a semi-crystalline polymer (from (a) and (b) to (c)), under tensile drawing (reproduced from Ref. 108[108]).

In general, for many synthetic polymers, completely extended copolymers chains are not achieved using ordinary processing methods. However, there are two routes that allow fibres to be formed with much more extended structures. The first route is by the synthesis of a polymer with a very stiff backbone. These types of polymers have liquid crystalline properties, where they become aligned in solution at a critical concentration.[106] The second route is a new processing method, based on drawing polymers from a concentrated solution or a gel, which leads to minimization of the effect of chain entanglements during the orientation process. This route has resulted in extremely high strength and high modulus fibres for polyethylene.[109] Attempts of electrospinning of PDMS-polyester copolymers from solution to achieve a similar effect are illustrated in Appendix D in this study.

2.4.3 Free volume of PDMS copolymers

Free volume is a very important characteristic of the PDMS copolymers that is directly related to the morphology, which is also affected by the chemistry of the molecules. The free volume also affects the molecular packing, thus a study of the free volume can indicate the mechanisms of aging, plasticization, gas diffusion, and other processes that are morphologically controlled in disordered materials.[110] Furthermore the mechanical properties are directly related to the free volume and the T_g of the polymer.[111] This morphological aspect has long been proposed to explain both the molecular motion and the physical behaviour of polymers.[79] A key problem in this sense is the relationship between the macroscopic

properties of the polymers and the 'holes' of free volume present in these polymers at an atomic scale of just a few angstroms.[112] Despite many efforts over the past decade to understand the physical and chemical properties of free volume, limited information of the hole sizes, concentration of the free volume and its form has emerged.

Among the techniques that have been used to investigate the free volume properties is Positronium Annihilation Lifetime Spectroscopy (PALS).[113,114] The use of PALS in the free volume characterization is unique, since it is a non-destructive technique and is sensitive to free volume at a molecular level. However, PALS has been scarcely exploited as a powerful technique for characterizing complicated polymeric systems, such as copolymers and polymer blends that are of technological interest.[115]

Although the positron was discovered in 1933,[116] the principal experiment using PALS to examine the free volume hole size was developed by Kobayashi and co-workers after six decades, in early 1990's.[117] The positron is an anti-electron, which can be generated via nuclear reactions. The positron can either annihilate as a free positron with an electron or form a metastable state, called Positronium, together with an electron. There are two states of positronium atoms: para-positronium (p-Ps) and ortho-positronium (o-Ps), which form an anti-parallel spin and parallel spin combination, respectively. This leads to different lifetime and annihilation events between these atoms; p-Ps has a shorter lifetime than o-Ps.

The Ps is only stable if thermalized within a void of molecular dimensions, where it can be localized in these holes, as is shown in Figure 2.5, e.g. the Ps is formed only in areas with low electron density.[114] The p-Ps can undergo spin allowed annihilate with the generation of energy. The o-Ps does not have the correct spin and will usually annihilate through spin exchange with the electrons from the walls of the cavity in which it resides.[110,118] The process allows determination of the size of the molecular cavity through the lifetime of the o-Ps annihilation and the o-Ps intensity is directly proportional to the number density of the events.

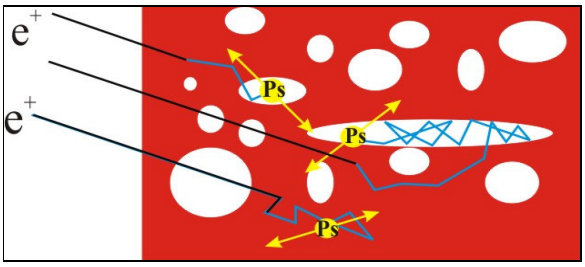

Figure 2.5: Ps localization in the free volume holes of a polymer before its annihilation.

PALS analysis typically gives three lifetime components in amorphous polymers[119] such as PDMS homopolymer: τ_1 is attributed to p-Ps self-annihilation, τ_2 is attributed to free positron and positron molecular species annihilation, and τ_3 is attributed to o-Ps pick off annihilation that occurs when the positron is localized in free volume cavities and annihilates with an electron of opposite spin from the surrounding cavity wall.[116] Thus the o-Ps pick off annihilation lifetime is sensitive to the free volume hole size in polymer materials and as the hole size increases so the lifetime of the o-Ps also increases. The following equation shows the relationship between o-Ps lifetime (τ_3) and free volume radius.

$$\tau = (1/2)\{1-(R/R_o) + [\sin(2\pi R/R_o)]/ 2\pi\}^{-1} \qquad \text{[Eq 2.3]}$$

where R is the hole radius and R_o is the infinite spherical potential radius, and $R_o = R + \Delta R$, where ΔR is an empirical parameter. The average free volume size (V_f) is calculated assuming spherical cavity shape using the following equation:

$$V_f = 4\pi R^3/3 \qquad \text{[Eq 2.4]}$$

The free volume fraction (fv), which is related to the polymer mechanical properties, is calculated as the average of the hole size and the hole concentration, as shown in the following equation.

$$f\text{v} = CI_3\,[V_f\,(\tau_3)] \qquad \text{[Eq 2.5]}$$

where fv is the free volume fraction, C is an empirical scaling constant, I_3 is the total fraction of o-Ps formed in the polymer, $V_f\,(\tau_3)$ is the mean hole volume in $Å^3$.

Similar lifetime events that are found in the amorphous polymers were reported for several semicrystalline polymers such as polyetheretherkethone, polyethyleneterephthalate and polypropylene.[118,120] However for other semicrystalline polymers such as PDMS-polypropylene oxide urethane/urea copolymer, polyethylene, polyamides, polytetrafluoroanethylene, four lifetime events were reported.[118,121-123] In PDMS-polypropylene oxide membranes the two long-lived components, τ_3 and τ_4, were attributed to two Ps states decaying in different regions in the membrane; polypropylene oxide region and PDMS region, respectively. However, for other semicrystalline polymers such as PE, the τ_3 was attributed to the free volume holes in the crystalline region and the τ_4 to the free volume

holes in the amorphous region.[123] This issue is elaborated on and investigated for the PDMS-PBCH copolymer as described in Chapter 6.

2.4.4 Surface morphology of PDMS copolymers

In addition to the bulk morphology of the PDMS copolymers, the surface morphology and property are another important characteristic in these copolymers. As a consequence of the very low cohesive energy density (intermolecular interaction) between the methyl groups, and high flexibility (low T_g) of the PDMS segment, the PDMS copolymers have extremely low surface energy.[124,125] Thus, the surfaces of PDMS copolymers, as well as their polymer blends, are significantly enriched with PDMS segments. The combined effect of the low intermolecular forces and the flexibility of the PDMS backbone have been used as the basis for understanding the surface properties. The flexibility of the backbone allows the chain to adopt various polymer configurations and therefore allows the methyl groups to be positioned on the surface. Since the surface tension of PDMS is very low, compared to most organic polymers, the PDMS segments in the PDMS-polyester copolymers are expected to flip or migrate to the more hydrophobic top (air) surface to form a silicon enriched layer.[126] This layer yields such properties as reduced friction, improved gloss and feel, and provide easier release from moulds.

It has been reported that the bulk composition has a very important effect on the surface composition of PDMS copolymers. For PDMS-bisphenol, a polycarbonate (PDMS-BPAC) random multiblock copolymers,[127] the bulk composition can determine the domain structures (mainly domain shape) in the bulk of the block copolymers and it also affects the surface morphology and the composition. Block length is the major factor determining the domain size of the block. It is also reported that the PDMS-BPAC multiblock copolymers with longer PDMS blocks or with higher PDMS bulk concentrations have higher PDMS surface concentration than the shorter or the less PDMS bulk concentrations.[127]

A study involving the surface segregation of PDMS segments in cast films of PDMS-polymethylstyrene multiblock copolymers revealed that the PDMS surface segregation extended to a depth of 210 Å. PDMS-polymethylstyrene copolymers with high PDMS bulk concentrations (60 wt %) were found to have a highly oriented lamellar morphology in the near air surface region, and the top-most air surface region (27 Å) was exclusively composed of PDMS.[69] Furukawa and coworkers[128] investigated the surface topography of PDMS-polyimide copolymers and found that the surface topography was clearly influenced by the

copolymer composition and molar mass of the PDMS segments. It was also noted that the surface of the polyimide homopolymer film was flat and smooth, while the surfaces of the copolymers differed from each other in terms of roughness. The PDMS segments segregated from the polyimide phase to form larger domains, called islands, in a sea-island structure. The study also revealed that upon the addition of 10 wt % of PDMS the contact angle increased by 25° over the homopolymer.

A quantitative surface study of PDMS-polyamide copolymer by angle-dependent X-ray photoelectron spectroscopy (XPS) revealed PDMS segregation in the free surface region. The surface composition of these amorphous–semicrystalline block copolymers depends on both their polymer structure and the way in which the films are prepared.[69] The surface region of the cast PDMS-polyamide copolymer films consists of PDMS at substantially higher concentrations than the overall bulk concentration, due to the predominant existence of the PDMS-rich microdomains separated before crystallization. It was also observed that annealing treatments could further enhance the PDMS surface segregation, yet without disturbing the large scale morphology. Furthermore in general, use of any good solvent for PDMS segments yields higher PDMS surface concentrations compared to the use of poor solvents.[69]

2.4.5 Morphology characterizations of PDMS copolymers

The morphology of PDMS copolymers can be studied at three different structural levels, according to the morphology size. The smallest structural level is the molecular structure, such as the block sequence, sequence distribution and crystal structure, which can be investigated by NMR and IR spectroscopy. The second level of structure is the nanodomain structure. A complete description of sample morphology at this level consists of the determination of the volume fraction, size, shape, orientation, and interfacial thickness of the separated phase as a function of segment content or concentration, and sample history.[129] This structural level can be directly observed by TEM, which has proven to be an efficient method for bulk morphology analysis of phase separated block copolymers.[77,130] This structural level also can be observed mainly on the copolymer surface by atomic force microscopy or more quantitatively investigated by small angle X-ray scattering. This level also includes investigation of the interdomain spacing and the morphological structure of microphase separated block copolymers. The third level of morphology includes spherulitic texture, and when size considerations are in the micron range. This type of morphology can be

investigated using small angle light scattering, electron microscopy, atomic force microscopy as well as polarized light microscopy. These methods of copolymer morphology investigation can be complemented by the use of thermal analysis methods such as differential scanning calorimetry (DSC), and dynamic mechanical analysis (DMA) to investigate the crystallinity, and phase separation, and by PALS to provide additional information about the changes in the free volume, mainly in the amorphous region.

DSC is analytical technique mainly used for the analysis of phase separation in PDMS copolymers, but DMA can also be used to some extent in phase separation investigations. In principle, in phase separated block copolymers the thermal properties are similar to properties of physical blends of the same polymer segments. Phase separation is shown by the observation of two separate glass transitions, characterized by their temperatures (T_gs). For the phase separated materials, the copolymer composition and degree of phase separation govern the shape of the modulus curve. If phase mixing of one segment occurs there will be an observable shift in the T_g of that phase toward the T_g of the other phase. The magnitude of the shift correlates with the level of phase mixing. Unfortunately, in most cases this information is lacking, particularly for the hard phase, and the domain size may affect the T_g values.[131,132]

DMA of PDMS-s-PBCH, $(AB)_n$ type copolymers, showed the glass transition of the PDMS segments as well defined, sharp tan δ loss peak around –125 to –115 ^oC, depending on the copolymer chemical composition.[10] DMA results also showed a smaller, broader peak around –50 ^oC, which is attributed to the secondary transition of polyester segments, or to the crystalline melting point of the PDMS segments.[133,134] Another strong tan δ loss peak was detected at around –2 to 15 ^oC, due to the glass transition of the amorphous region of the polyester segments. Spherulitic crystal order was also reported by Miroslawa for PDMS-polybutyleneterephthalate segmented copolymers using thin quenched cold films from the melt. The morphology investigation was done using POM.[11] The surface morphology of polycaprolactone-b-polydimethylsiloxane-b-polycaprolactone block copolymer was investigated by Childs et al., using AFM. They also reported that crystal spherulites structure could clearly observed using the phase images of the AFM.[91]

2.5 Fractionation process using chromatographic systems

Polymers normally do not consist of a particular molecule with unique chemical composition and molar mass, but rather are a mixture of molecules with a range of distributed molar

masses, the molar mass of the polymer is distributive in nature.[106] When it comes to copolymers, this complexity growths further because now there will be other distributive properties such as, chemical composition, sequence length and functionality. Thus in order to better characterize polymeric materials, a fractionation process based on one or two distributive properties is needed.[135] Without doubt, fractionation by chromatography systems is the most important fractionation technique in the field of polymer science.[136]

The chromatography process may be defined as a process by which the solute is transferred between two phases, one of which is stationary and the other moving, often traversing a long tube called a column.[66] Three main forms of liquid chromatography (LC) have been used to fractionate polymers and, in some cases, to determine average molar masses. These are size exclusion chromatography (SEC), liquid chromatography at critical conditions (LC-CC) and gradient elution chromatography (GEC).[137-139] Two of these techniques will be used in this study and are therefore now discussed in Sections 2.5.1 and 2.5.2, respectively.

2.5.1 Size exclusion chromatography

In SEC both phases are the same liquid (solvent), they differ only in that the stationary phase is part of the solvent, which is inside the porous gel particle, while the mobile phase is outside.[66] Polymer molecules are separated by size in the SEC column because of their ability to penetrate part of the internal volume of the gel particles, that is, the stationary phase. As the sample moves along the column with the mobile phase, the largest molecules are almost entirely excluded from the stationary phase, while the smallest ones find almost all the stationary phase accessible. The smaller the molecule, the more of the stationary phase volume is accessible to it and the longer the molecule stays in that phase. Small molecules thus fall behind larger ones, and are eluted from the column later.[138,139]

At this point account must be taken of the true nature of the separation, which is based on hydrodynamic volume (the volume of a polymer coil that the chain appears to occupy when it is in solution)[111] and not molar mass. The hydrodynamic volume can vary for a polymer depending on how well it interacts with the solvent, and the polymer's molar mass. Note that to obtain an absolute molar mass value of a sample, standards with known molar masses must be used to obtain a suitable calibration curve. SEC analysis provides the number average of molar mass of the polymer (M_n), the weight average of molar mass of the polymer (M_w), as well as the polydispersity index (PDI) (the molar mass distribution).[137,138]

It is, however, also necessary to separate copolymers, not into unique molecules each with a particular molar mass, but into a series of narrower molar mass distribution fractions. The separated fractions are usually required for further analysis by a wide range of analytical techniques, such as FTIR,[140,141] NMR[142] (to investigate the chemical composition or the microstructure for each fraction), TEM and AFM (to investigate the copolymer morphology for each fraction) (see Chapter 7). Subjection of the fractions obtained from SEC to analysis via FTIR yields not only molar mass distribution data, but also provides the relationship between the molar mass distribution and the type of functionality and the chemical composition in the copolymers.[140,141] Furthermore, useful information about the chemical composition of the eluate can be obtained by combining results obtained from two different detectors, especially if one detector is sensitive to an absorption band specific to one of the species in a copolymer.[143]

2.5.2 Gradient elution chromatography

The accurate determination of the chemical composition distribution of copolymers is very important for the characterization of copolymers. Among the several techniques available to measure chemical composition distribution, GEC is considered to be the most important and prominent technique.[137,143,144] When polymer mixtures of homopolymers and their copolymers are analyzed by SEC, the similarity in the hydrodynamic volume of different polymers leads to overlapping in the molar mass distributions. This usually leads to the elution of the homopolymers and their copolymers from the SEC column at the same retention times. Therefore, in the analysis of heterogeneous polymers, analysis by GEC can give much better interpretations of the chemical composition distribution (CCD) of the polymer mixtures than analysis by a normal SEC column.[145]

The GEC principal is based on precipitation and re-dissolution by changing the polymer solubility or polarity, using a gradient of solvents and concentrations. The difference in solubility or polarity between the building blocks of a copolymer and the copolymer itself creates the opportunity to analyze the chemical composition distribution of the polymers. First a dissolved polymer is injected into a column filled with a non-solvent or a weak solvent, and thus the polymer precipitates and adsorb to the stationary phase. By increasing the eluent and solvent strength the precipitated polymer gradually dissolves and desorbs, and thus starts eluting. Elution therefore depends on the chemical composition of the polymer backbone, functional groups, etc; thus each fraction will elute independent of molecular

mass.[146] In GEC there are two modes of separation. The first mode is reversed-phase (RP) chromatography. In this mode of GEC the stationary phase is non-polar and the mobile phase is polar. The second mode of separation is normal phase (NP) chromatography. In this mode polar stationary phases and non-polar mobile phases are used. Here the solute is retained by the interaction of its polar functional groups with the polar groups on the surface of the stationary phase.[146-149]

2.6 Conclusion

The literature review presented in this chapter shows the great interest that has been placed on the PDMS copolymers, in terms of their synthesis and morphology characterizations. It is clear that much has been achieved particularly in the field of PDMS copolymers synthesis. Several copolymerization methods were used in the synthesis of various architectures of these copolymers. However, the traditional melt polycondensation under vacuum and at high temperature is the most applicable synthetic method. Therefore, in this study the syntheses of six series of PDMS-PES copolymers are carried out using this method (see Chapter 3).

Although the syntheses of PDMS copolymers are investigated in numerous scientific studies, there is not much data in the open literature concerning the morphology of these copolymers, particular for PDMS-copolymers with organic crystallisable segment. It also follows from the literature review that certain aspects concerning the morphology of the multiblock copolymers remain unsolved. The various types of morphology that can be obtained from these copolymers and the effect of the competition between the crystallinity and the phase separations on these types of morphology are only examples of the unsolved aspects. Other examples are: the effects of the organic segments, PDMS molar masses, chemical composition and chain branching degree on the copolymers morphology as well as on the copolymer properties mainly copolymer crystallinity, surface energy and free volume. In the subsequent chapters most of these ambiguous morphological aspects for several types of PDMS-PES copolymers will be studied, and a great clarity as to the role and effect of these aspects have will be unfold.

2.7 References

1. McGrath, J.; Dunson, D.; Mecham, S.; Hedrick, J., Synthesis and characterization of segmented polyimide-polyorganosiloxane copolymers. In *Progress in Polyimide Chemistry I* Springer, Berlin / Heidelberg, 1999; Vol. 140, pp 61-105.
2. Lin Chen, J. R. R. B. D. C. *Electrophoresis* 2004, 25(6), 914-921.

3. Clemens, L. M.; Kantner, S. S.; Mazurek, M. Polysiloxane-grafted copolymer release coating sheets and adhesive tapes. Application Number: 06/757278, United States, 1988.

4. Qiu Dai; Zhicheng Zhang; Feng Wang; Liu, J. *Journal of Applied Polymer Science* 2003, 88(12), 2732-2736.

5. Takeo, M.; Toshiro, U.; Akio, K.; Tsutomu, F.; Ikuro, M.; Mitsuru, A. *Journal of Applied Polymer Science* 1997, 64(6), 1153-1159.

6. Mishima, S.; Kaneoka, H.; Nakagawa, T. *Journal of Applied Polymer Science* 1999, 71(2), 273-287.

7. Suresh, K. J.; Gabor, E.; Joseph, P. K.; Daniel, E.; Gail, D.; Shannon, B.; Flavius, P. *Journal of Biomedical Materials Research, Part A* 2008, 87A(1), 69-77.

8. Min-Hsien, W. *Surface and Interface Analysis* 2009, 41(1), 11-16.

9. Patrito, N.; McCague, C.; Norton, P. R.; Petersen, N. O. *Langmuir* 2007, 23(2), 715-719.

10. Kiefer, L. A.; Yoon, T. H.; Glass, T. E.; Jayaraman, S. K.; McGrath, J. E. *Journal of Polymer Science, Part A: Polymer Chemistry* 1997, 35(16), 3495-3506.

11. Miroslawa, E. F. *Designed Monomers and Polymers* 2000, 3(3), 325-337.

12. Antic, V. V.; Vuckovic, M. V.; Djonlagic, J. *Journal of the Serbian Chemical Society* 2007, 72(2), 139-150.

13. Bates, F. S.; Schulz, M. F.; Khandpur, A. K.; Förster, S.; Rosedale, J. H.; Almdal, K.; Mortensen, K. *Faraday Discussions* 1994, 98, 7-18.

14. Yilgör, I.; McGrath, J., Polysiloxane containing copolymers: A survey of recent developments. In *Polysiloxane Copolymers/Anionic Polymerization*, Springer, Berlin / Heidelberg, 1988; Vol. 86, pp 1-86.

15. DeYoung, D. J.; Murphy, G. J. Hydrophilic silicone-modified polyester resin and fibers and films. Application Number: 07/813024, United States, 1992.

16. Yamamoto, N.; Mori, H.; Nakata, A.; Suehiro, M. Aromatic polyester-polyorganosiloxane block copolymer. Application Number: 4894427, United States, 1990.

17. Antic, V. V.; Balaban, M. R.; Djonlagic, J. *Polymer International* 2001, 50(11), 1201-1208.

18. Dojcinovic, B. P.; Antic, V. V.; Vuckovic, M. V.; Djonlagic, J. *Journal of the Serbian Chemical Society* 2005, 70(12), 1469-1485

19. Vuckovic, M. V.; Antic, V. V.; Dojcinovic, B. P.; Govedarica, M. N.; Djonlagic, J. *Polymer International* 2006, 55(11), 1304-1314.

20. Jones, R. G.; Ando, W.; Chojnowski, J., *Silicon-Containing Polymers. The Science and Technology of their Synthesis and Applications*. First ed.; Kluwer Academic Publishers, Netherlands, 2000.

21. Hardman, B., Silicones. In *Encyclopedia of Polymer Science and Engineering*, Second ed.; Kroschwitz, J. I. (Ed.), John Wiley and Sons., United States, 1989; Vol. 15, pp 234-251.

22. Brook M.A., *Silicon in Organic, Organometallic, and Polymer Chemistry*. First ed.; John Wiley and Sons, Inc., United States 2000; pp 256-274.
23. Enikolopyan, N.; Fridman, M.; Stalnova, I.; Popov, V., Filled polymers: Mechanical properties and processability. In *Filled Polymers I Science and Technology* Springer, Berlin / Heidelberg, 1990; Vol. 96, pp 1-67.
24. Hill, D. J. T.; Preston, C. M. L.; Salisbury, D. J.; Whittaker, A. K. *Radiation Physics and Chemistry* 2001, 62(1), 11-17.
25. Hui Peng, S. C. L. F. Z. F. *Polymer International* 2004, 53(7), 833-837.
26. Mesut, A.; Sennur, D.; Nil, B.; Nimet, I. U.; Nalan, A. A.; Salih, D. *Polymer International* 2005, 54(2), 374-380.
27. Ma, C.-C. M.; Gu, J.-T.; Fang, W.-C.; Yang, J.-C.; Tsai, L.-D. *Journal of Applied Polymer Science* 1997, 66(1), 67-75.
28. Odian, G., *Principles of Polymerization*. Fourth ed.; John Wiley and Sons, United States, 2004; pp 139-143, 595-597.
29. DeSimone, J. M.; York, G. A.; McGrath, J. E.; Gozdz, A. S.; Bowden, M. J. *Macromolecules* 1991, 24(19), 5330-5339.
30. Kendrik, T. C.; Parbhoo, B. M.; White, J. W., *Chain Polymerization Part II: Polymerization of Cyclosiloxanes*. First ed.; Pregamon Press, Oxford, 1989; Vol. 4, pp 459-492.
31. Gilbert, A. R.; Kantor, S. W. *Journal of Polymer Science* 1959, 40(136), 35-58.
32. Morton, M.; Bostick, E. E. *Journal of Polymer Science, Part A: General Papers* 1964, 2(2), 523-538.
33. O'Malley, J.; Pacansky, T. J.; Stauffer, W. *Macromolecules* 1977, 10(6), 1197-1199.
34. van Aert, H. A. M.; Nelissen, L.; Lemstra, P. J.; Brunelle, D. J. *Polymer* 2001, 42(5), 1781-1788.
35. Akio, N.; Toshitaka, K. *Journal of Applied Polymer Science* 2006, 100(1), 565-575.
36. Yilgör, E.; Yilgör, I.; Süzer, S. *Polymer* 2003, 44(24), 7271-7279.
37. Stanciu, A.; Airinei, A.; Timpu, D.; Ioanid, A.; Ioan, C.; Bulacovschi, V. *European Polymer Journal* 1999, 35(11), 1959-1965.
38. Rochery, M.; Vroman, I.; Lam, T. *Journal of Macromolecular Science: Pure and Applied Chemistry* 2003, 40(3), 321.
39. YíIgör, Ì.; Sha'aban, A. K.; Steckle Jr, W. P.; Tyagi, D.; Wilkes, G. L.; McGrath, J. E. *Polymer* 1984, 25(12), 1800-1806.
40. Yilgör, E.; Yilgör, I. *Polymer* 2001, 42(19), 7953-7959.
41. Pospiech, D.; Häubler, L.; Komber, H.; Voigt, D.; Jehnichen, D.; Janke, A.; Baier, A.; Eckstein, K.; Böhme, F. *Journal of Applied Polymer Science* 1996, 62(11), 1819-1833.
42. Ku, C.-K.; Lee, Y.-D. *Polymer* 2007, 48(12), 3565-3573.
43. Vaughn, H. A. *Journal of Polymer Science, Part B: Polymer Letters* 1969, 7(8), 569-572.
44. Peebles, L. H. *Macromolecules* 1974, 7(6), 872-882.

45. Abouzahr, S.; Wilkes, G. L. *Journal of Applied Polymer Science* 1984, 29(9), 2695-2711.

46. Tyagi, D.; Hedrick, J. L.; Webster, D. C.; McGrath, J. E.; Wilkes, G. L. *Polymer* 1988, 29(5), 833-844.

47. Matzner, M.; Noshay, A.; Robenson, L. M.; Merriam, C. N.; Barclay, J. R.; McGrath J.E. *Applied Polymer Symposium* 1973, 22, 143-156.

48. Noshay, A.; Matzner, M.; Karoly, G.; Stampa, G. B. *Journal of Applied Polymer Science* 1973, 17(2), 619-628.

49. Gagnebien, D.; Madec, P. J.; Maréchal, E. *European Polymer Journal* 1985, 21(3), 301-308.

50. Auman, B. C.; Percec, V.; Schneider, H. A.; Cantow, H.-J. *Polymer* 1987, 28(8), 1407-1417.

51. Chaumont, P.; Beinert, G.; Herz, J.; Rempp, P. *Polymer* 1981, 22(5), 663-666.

52. Kajiyama, M.; Kakimoto, M.; Imai, Y. *Macromolecules* 1990, 23(5), 1244-1248.

53. Nagasaki, Y.; Matsukura, F.; Kato, M.; Aoki, H.; Tokuda, T. *Macromolecules* 1996, 29(18), 5859-5863.

54. Risch, B. G.; Rodrigues, D. E.; Lyon, K.; McGrath, J. E.; Wilkes, G. L. *Polymer* 1996, 37(7), 1229-1242.

55. Rogers, M. E.; Glass, T. E.; Mecham, S. J.; Rodrigues, D.; Wilkes, G. L.; McGrath, J. E. *Journal of Polymer Science, Part A: Polymer Chemistry* 1994, 32(14), 2663-2675.

56. Ginnings, P. R. High slip polyester films containing siloxane units. Application Number: 06/472514 United States, 1985.

57. Yamamoto, N.; Mori, H.; Nakata, A.; Suehiro, M. Thermoplastic resin composition. Application Number: 07/475793, Tokyo, JP, 1992.

58. Dahrouch, M.; Schmidt, A.; Leemans, L.; Linssen, H.; Götz, H. *Macromolecular Symposia* 2003, 199(1), 147-162.

59. Ohshita, J.; Kunai, A. *Acta Polymerica* 1998, 49(8), 379-403.

60. Miroslawa, E. F.; Volker, A. *Macromolecular Symposia* 2003, 199(1), 125-134.

61. Stoenescu, R. Asymmetric amphiphilic triblock copolymers, synthesis, characterization and self-assembly. PhD, University of Basel, Switzerland, 2004.

62. Abdullah E.; Dean C.W. *Journal of Polymer Science, Part A: Polymer Chemistry* 2006, 44(16), 4880-4894.

63. McKee, M. G.; Unal, S.; Wilkes, G. L.; Long, T. E. *Progress in Polymer Science* 2005, 30(5), 507-539.

64. Costello, P. A.; Martin, I. K.; Slark, A. T.; Sherrington, D. C.; Titterton, A. *Polymer* 2002, 43(2), 245-254.

65. Roovers, J., Branched Polymers. In *Encyclopaedia of Polymer Science and Technology*, Second ed.; Kroschwitz, J. I. (Ed.), John Wiley and Sons, United States, 1985; Vol. 2, pp 478-479.

66. Collins, E. A.; Bares, J.; Billmeyer Jr., F. W., *Experiments in Polymer Science*. First ed.; John Wiley and Sons, United States, 1973; pp 154-167.

67. Molau, G. E., *Colloidal and Morphological Behaviour of Block and Graft Copolymers* Plenum Press, New York, 1971; pp 75-84.

68. van Aert, H. A. M.; Sijbesma, R. P.; Fischer, H.; de Waal, B. F. M.; Gilberts, J.; Maas, J. H.; Broer, D.; Meijer, E. W. *Acta Polymerica* 1998, 49(1), 18-26.

69. Chang-sik, H.; Gardella Jr, J. A. *Journal of Macromolecular Science: Polymer Reviews* 2005, 45(1), 1-18.

70. Abetz, V.; Simon, P., Phase behaviour and morphologies of block copolymers. In *Block Copolymers I*, Springer, Berlin / Heidelberg, 2005; Vol. 189, pp 125-212.

71. Kambour, R. P. *Journal of Polymer Science, Part B: Polymer Letters* 1969, 7(8), 573-577.

72. Meier, D. J. *Journal of Polymer Science, Part C: Polymer Symposia* 1969, 26, 81-98.

73. Brown, R. A.; Masters, A. J.; Price, C.; Yuan, X. F., *Polymer Properties: Chain Segregation in Block Copolymers*. First ed.; Pregamon Press, Oxford, 1989; Vol. 2, pp 155-170.

74. Hamley, I. W., *Developments in Block Copolymer Science and Technology, Introduction to Block Copolymers*. University of Leeds, UK, 2004; pp 1-29.

75. Samseth, J.; Spontak, R. J.; Mortensen, K. *Journal of Polymer Science, Part B: Polymer Physics* 1993, 31(4), 467-474.

76. Samseth, J.; Mortensen, K.; Burns, J. L.; Spontak, R. J. *Journal of Applied Polymer Science* 1992, 44(7), 1245-1256.

77. Fitzgerald, J. J.; Tunney, S. E.; Landry, M. R. *Polymer* 1993, 34(9), 1823-1832.

78. Andrea D. B. Synthesis and Characterization of Poly (Siloxane Imide) Block Copolymers and End-Functional Polyimides for Interphase Applications. PhD, Virginia Polytechnic Institute and State University Virginia, United States, 1999.

79. Sperling, L. H., *Introduction to Physical Polymer Science*. Wiley-Interscience and Sons, United States, 2006; pp 115-116, 169-171, 390.

80. Miles, I. S.; Rostai, S., *Multicomponent Polymer Systems*. Second ed.; Longman Singapore Publishers, Singapore, 1994; pp 103-147.

81. Angerman, H.; ten Brinke, G.; Erukhimovich, I. *Macromolecules* 1996, 29(9), 3255-3262.

82. Angerman, H.; ten Brinke, G.; Erukhimovich, I. *Macromolecules* 1998, 31(6), 1958-1971.

83. Floudas, G.; Hadjichristidis, N.; Tselikas, Y.; Erukhimovich, I. *Macromolecules* 1997, 30(10), 3090-3096.

84. Floudas, G.; Pispas, S.; Hadjichristidis, N.; Pakula, T.; Erukhimovich, I. *Macromolecules* 1996, 29(11), 4142-4154.

85. Jonquières, A.; Clément, R.; Lochon, P. *Progress in Polymer Science* 2002, 27(9), 1803-1877.

86. Sheth, J. P.; Yilgor, E.; Erenturk, B.; Ozhalici, H.; Yilgor, I.; Wilkes, G. L. *Polymer* 2005, 46(19), 8185-8193.

87. Hamley, I., Crystallization in block copolymers. In *Interfaces Crystallization Viscoelasticity*, Springer, Berlin / Heidelberg, 1999; Vol. 148, pp 113-137.

88. Séguéla, R.; Prud'homme, J. *Polymer* 1989, 30(8), 1446-1455.

89. Cohen, R. E.; Cheng, P. L.; Douzinas, K.; Kofinas, P.; Berney, C. V. *Macromolecules* 1990, 23(1), 324-327.

90. Veith, C. A.; Cohen, R. E.; Argon, A. S. *Polymer* 1991, 32(9), 1545-1554.

91. Childs, M. A.; Matlock, D. D.; Dorgan, J. R.; Ohno, T. R. *Biomacromolecules* 2001, 2(2), 526-537.

92. Antic, V. V.; Govedarica, M. N.; Djonlagic, J. *Polymer International* 2004, 53(11), 1786-1794.

93. Antic, V. V.; Govedarica, M. N.; Djonlagic, J. *Polymer International* 2003, 52(7), 1188-1197.

94. Rangarajan, P.; Register, R. A.; Fetters, L. J. *Macromolecules* 1993, 26(17), 4640-4645.

95. Rangarajan, P.; Register, R. A.; Adamson, D. H.; Fetters, L. J.; Bras, W.; Naylor, S.; Ryan, A. J. *Macromolecules* 1995, 28(5), 1422-1428.

96. Ryan, A. J.; Hamley, I. W.; Bras, W.; Bates, F. S. *Macromolecules* 1995, 28(11), 3860-3868.

97. Balsamo, V.; Gil, G.; Urbina de Navarro, C.; Hamley, I. W.; von Gyldenfeldt, F.; Abetz, V.; Canizales, E. *Macromolecules* 2003, 36(12), 4515-4525.

98. Hamley, I. W.; Fairclough, J. P. A.; Bates, F. S.; Ryan, A. J. *Polymer* 1998, 39(6-7), 1429-1437.

99. Shiomi, T.; Tsukada, H.; Takeshita, H.; Takenaka, K.; Tezuka, Y. *Polymer* 2001, 42(11), 4997-5004.

100. Loo, Y.-L.; Register, R. A.; Adamson, D. H. *Macromolecules* 2000, 33(22), 8361-8366.

101. Abdelkrim, B.; Georges, B.; Gérard, H.; Georges, S. *Macromolecular Chemistry and Physics* 1995, 196(1), 411-428.

102. Chu, J. H.; Rangarajan, P.; Adams, J. L.; Register, R. A. *Polymer* 1995, 36(8), 1569-1575.

103. Auman, B. C.; Percec, V.; Schneider, H. A.; Jishan, W.; Cantow, H.-J. *Polymer* 1987, 28(1), 119-131.

104. Kuo, W. F.; Tong S.N.; Pearce, E. M.; Kwei, T. K. *Journal of Applied Polymer Science* 1993, 48(7), 1297-1301.

105. East, A. J., Polyester fibres. In *Synthetic Fibres: Nylon, Polyester, Acrylic, Polyolefin*, First ed.; McIntyre, J. E. (Ed.), Woodhead Publishing Limited and CRC press LLC: Cambridge, England, 2005; pp 111-115.

106. Painter, P. C.; Coleman, M. M., *Fundamentals of Polymer Science*. Second ed.; CRC Press, United States, 1997.

107. Powell, P. C.; Housz, A. J. I., *Engineering with Polymers*. Second ed.; Stanley Thornes (Publishers) Ltd, Britain, 1998; pp 19-31.

108. Seymour, R. B., *Introduction to Polymer Chemistry*. First ed.; McGraw-Hill, Inc., New York, 1971; pp 28-42.

109. Givens, S. R.; Gardner, K. H.; Rabolt, J. F.; Chase, D. B. *Macromolecules* 2007, 40(3), 608-610.

110. Pethrick, R. A., Characterization of polymers In *Encyclopaedia of Polymer Science and Technology*, Third ed.; Kroschwitz, J. I. (Ed.), John Wiley and Sons Inc, United States, 2004; Vol. 9, p 178.

111. Miller, M. L., *The Structure of Polymers*. Second ed.; Reinhold Publishing Co., United States, 1968; pp 181, 278-309.

112. Fucugauchi, L. A.; Lopez, R.; Millan, S.; Alvarez, J.; Fendler, J. H. *Molecular Crystals and Liquid Crystals* 1989, 177, 101-112.

113. Jean, Y. C.; Mallon, P. E.; Schrader, D. M., *Principles and Applications of Positron and Positronium Chemistry*. First ed.; World Scientific Publishing Co., Singapore, 2003; pp 253-280.

114. Pethrick, R. A. *Progress in Polymer Science* 1997, 22(1), 1-47.

115. López-castañares, R.; Olea-cardoso, O.; Vázquez-moreno, F.; Lizama-soberanis, B.; Camps-carvajal, E.; Angeles-anguiano, E.; Castaño, V. *Bulgarian Journal of Physics* 2002, 29(3-4), 155-178.

116. Brandt, W.; Berko, S.; Walker, W. W. *Physical Review* 1960, 120(4), 1289-1295.

117. Kobayashi, Y. *Journal of the Chemical Society, Faraday Transactions* 1991, 87(22), 3641-3645.

118. Sánchez, V.; López, R.; Fucugauchi, L. A.; Ito, Y. *Journal of Applied Polymer Science* 1995, 56(7), 779-791.

119. Mallon, P. E.; Greyling, C. J.; Vosloo, W.; Jean, Y. C. *Radiation Physics and Chemistry* 2003, 68(3-4), 453-456.

120. Li, X.; Gidley, D. W.; Hristov, H. A.; Yee, A. F. *Polymer* 1994, 35(1), 14-17.

121. Adam, D.; Wojciech, O.; Franz, S. *European Polymer Journal* 2003, 39(10), 2051-2058.

122. Dutta, D.; Bhattacharyya, A.; Ganguly, B. N. *Journal of Membrane Science* 2003, 224(1-2), 127-135.

123. Ferreira Marques, M. F.; Gordo, P. M.; Kajcsos, Zs.; Lopes Gil, C.; de Lima, A. P.; Queiroz, D. P.; de Pinho, M. N. *Radiation Physics and Chemistry* 2007, 76 (2), 129–133.

124. Fang, H.; Zhou, S.; Wu, L. *Applied Surface Science* 2006, 253(5), 2978-2983.

125. Luo, Z.-h.; He, T.-y. *Reactive and Functional Polymers* 2008, 68(5), 931-942.

126. Huang, W.; Yao, Y.; Huang, Y.; Yu, Y. *Polymer* 2001, 42(4), 1763-1766.

127. Zhuang, H.; Gardella, J. A. *Macromolecules* 1997, 30(12), 3632-3639.

128. Furukawa, N.; Yamada, Y.; Furukawa, M.; Yuasa, M.; Kimura, Y. *Journal of Polymer Science, Part A: Polymer Chemistry* 1997, 35(11), 2239-2251.

129. Petrovic, Z. S.; Ferguson, J. *Progress in Polymer Science* 1991, 16(5), 695-836.

130. Chen, X.; Gardella, J. A.; Kumler, P. L. *Macromolecules* 1993, 26(15), 3778-3783.

131. Bares, J. *Macromolecules* 1975, 8(2), 244-246.

132. Lind, A. C. *Macromolecules* 1984, 17(3), 300-307.

133. Yang, H.; Nguyen, Q. T.; Ding, Y.-D.; Long, Y.-C.; Ping, Z. *Journal of Membrane Science* 2000, 164(1-2), 37-43.

134. Aranguren, M. I. *Polymer* 1998, 39(20), 4897-4903.

135. Koningsveld, R.; Stockmayer, W. H.; Nies, E., *Polymer Phase Diagrams*. Oxford University Press in the UK, Oxford and New York, 2001; pp 193-200.

136. Nikos, H.; Stergios, P.; George, F., *Block Copolymers: Synthetic Strategies, Physical Properties, and Application*. First ed.; John Wiley and Sons, United States, 2003; pp 175-179.

137. Pasch, H., Analysis of complex polymers by interaction chromatography. In *Polymer Analysis, Polymer Physics*, Springer, Berlin / Heidelberg, 1997; Vol. 128, pp 1-45.

138. Crompton, T. R., *Practical Polymer Analysis*. First ed.; Plenum Press, New York, 1993; pp 256-321.

139. Crompton T.R., *Polymer Reference Book*. First ed.; Rapra Technology Limited, UK, 2006; pp 263-281.

140. Somsen, G. W.; Gooijer, C.; Brinkman, U. A. T. *Journal of Chromatography A* 1999, 856(1-2), 213-242.

141. Kok, S. J.; Arentsen, N. C.; Cools, P. J. C. H.; Hankemeier, T.; Schoenmakers, P. J. *Journal of Chromatography A* 2002, 948(1-2), 257-265.

142. Krämer, I.; Hiller, W.; Pasch, H. *Macromolecular Chemistry and Physics* 2000, 201(14), 1662-1666.

143. Kawai, T.; Teramachi, S.; Tanaka, S.; Maeda, S. *International Journal of Polymer Analysis and Characterization* 2000, 5(4), 381-399.

144. Isemura, T.; Sato, T.; Kawahara, K.; Otsuka, K. *International Journal of Polymer Analysis and Characterization* 2008, 13(2), 119-135.

145. Glöckner, G.; van den Berg, J. H. M. *Journal of Chromatography A* 1987, 384, 135-144.

146. Philipsen, H. J. A. *Journal of Chromatography A* 2004, 1037(1-2), 329-350.

147. Jandera, P.; Holcapek, M.; Kolárová, L. *International Journal of Polymer Analysis and Characterization* 2001, 6(3), 261-294.

148. Falkenhagen, J.; Much, H.; Stauf, W.; Muller, A. H. E. *Macromolecules* 2000, 33(10), 3687-3693.

149. Jandera, P.; Holcapek, M.; Kolárová, L. *Journal of Chromatography A* 2000, 869(1-2), 65-84.

Chapter Three

Synthesis of Multiblock PDMS-PES Copolymers via Melt Polycondensation and their Characterization

Abstract

Polydimethylsiloxane (PDMS) oligomers with five different molar masses were synthesized via equilibrium ring-opening polymerization of octamethylcyclotetrasiloxane (D_4). The obtained PDMS oligomers were used to synthesize six series of semicrystalline multiblock polydimethylsiloxane-polyester (PDMS-PES) copolymers via a melt transesterification process under vacuum conditions. Two of these series were synthesized using a one-prepolymer reaction method, in which difunctional PDMS oligomer (prepolymer) was reacted with 1,4-butanediol (BD) and adipic acid (AA) under different reaction conditions. In the first series (series A) the PDMS oligomer was reacted, in bulk polymerization, with BD and AA to obtain polydimethylsiloxane-butyleneadipate segmented (PDMS-s-PBA) copolymers with various PDMS contents. In the second series (series B) the first stage of the previous reaction was carried out in toluene. Furthermore, two series of polydimethylsiloxane-polybutylenecyclohexanedicarboxylate segmented (PDMS-s-PBCH) copolymers were synthesized via a one-prepolymer reaction method by reacting BD and 1,4-dimethylcyclohexanedicarboxylate (DMCH) in bulk with either PDMS of varying content (PDMS M_n 2000 g/mol) (series C) or with PDMS of different segment length (PDMS content 10 wt %) (series D). The fifth series (series E) was synthesized using the two-prepolymer method for PDMS with a constant segment length (M_n 1000 g/mol) and PBCH with a hydroxyl end group (M_n 940 g/mol). In addition, various quantities of branching agent were added to the reaction vessel containing the 10 wt % PDMS content copolymers with PDMS of molar mass 1000 g/mol in series D, to prepare multiblock randomly branched polydimethylsiloxane-polybutylencyclohexanedicarboxylate (PDMS-br-PBCH) copolymers (series F). The obtained polymers were characterized using FTIR, NMR, viscometery and SEC to determine the chemical composition, molar mass and polydispersity index. Size exclusion chromatography-multi angle laser light scattering was used to determine the degree of branching in series F. The formation of the copolymers was also verified using gradient elution chromatography (GEC). These synthesized copolymers series, were further investigated as described in the subsequent chapters.

Keywords: polydimethylsiloxane synthesis, polydimethylsiloxane–polyester segmented copolymer, polydimethylsiloxane–polyester randomly branched copolymer.

3.1 Introduction

Thermoplastic polyesters are widely used because of their excellent heat resistance and high mechanical strength.[1] However, the crystalline polyesters that are largely used today are inferior in terms of weather resistance and impact resistance, though they have high mechanical strengths. Thus, in efforts to overcome these disadvantages, a copolymer containing PDMS as a soft segment is used to improve polyester properties. PDMS is one of the most important and versatile classes of high performance polymers due to its excellent flexibility weather resistance, hydrophobicity recovery and thermal properties.[2-5]

Melt transesterification is a major commercial route for the synthesis of polyesters. This route involves high temperatures and relatively long reaction times, and reduced pressures in the final step.[6-8] Catalysts (e.g. titanium alkoxide) are required to reduce the reaction times. In the polyesterification, not only do monomeric units add to the growing chains, but individual chains also react with one other. The esterification conditions also permit constant transesterification within the chain itself. Consequently, the copolymer obtained is expected to exhibit relatively broad molar mass distributions. Transesterification also accounts for the fact that if more than two starting materials are used they become incorporated into the polyesters in a statistical way, regardless of their time of introduction.[1]

A synthetic procedure for obtaining PDMS-semicrystalline cycloaliphatic polyester segmented block copolymers based on DMCH was introduced by Kiefer and coworkers.[9] They used a one-prepolymer method in a two steps reaction. In the first step, PDMS with an amino alkyl end groups is end-capped with an ester group by reaction with an excess of a cycloaliphatic diester. In the second step, 1,4-butanediol is added, together with titanium tetraisopropoxide as a catalyst. Thus the PDMS segment was efficiently incorporated into the copolymer via an amide link. PDMS-s-PBCH copolymers of high molar mass were prepared and characterized. The major advantage of this method is that traditional melt polymerization techniques that are used for polyester synthesis were used to form segmented PDMS-PES copolymers.

This chapter describes how the method mentioned above was extended and used to prepare polydimethylsiloxane-butyleneadipate segmented (PDMS-s-PBA) copolymers (aliphatic polyester segment) and randomly branched segmented polydimethylsiloxane–polybutylenecyclohexanedicarboxylate (PDMS-br-PBCH) copolymers, in addition to the

random segmented polydimethylsiloxane–polybutylenecyclohexanedicarboxylate (PDMS-s-PBCH) copolymers. Furthermore, the two-prepolymer method was used to prepare perfectly alternating PDMS-s-PBCH copolymers. The method used to prepare perfectly alternating PDMS-s-PBCH copolymers is based on the method developed by O'Malley et al. to synthesize an alternating block PDMS–polysulphone copolymer.[10] The chemical structures of the copolymers synthesized in this study are illustrated in Figure 3.1.

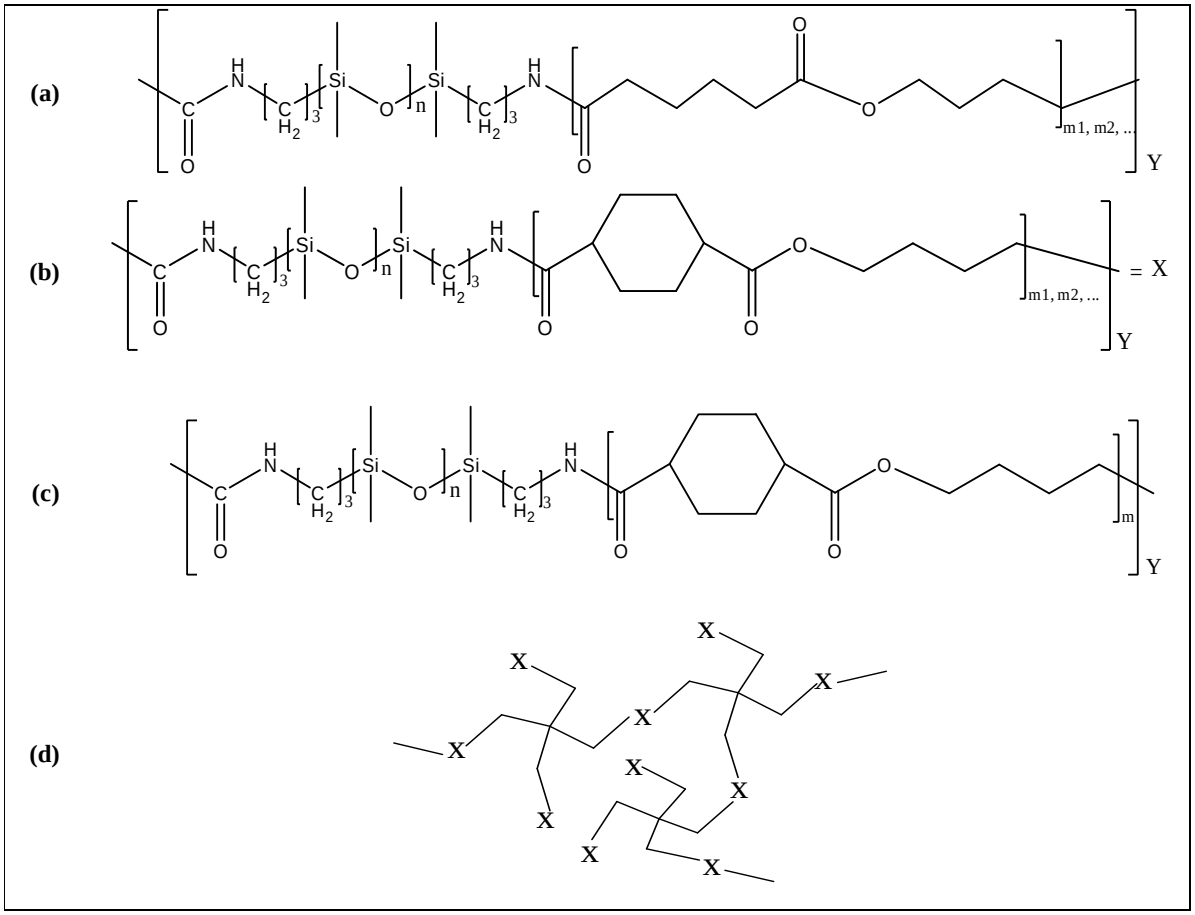

Figure 3.1: Chemical structure of PDMS-PES copolymers: (a) aliphatic polyester segment (PDMS-s-PBA), (b) cycloaliphatic polyester segment (PDMS-s-PBCH), (c) cycloaliphatic perfectly alternating polyester segment (PDMS-s-PBCH) and (d) randomly branched PDMS-cycloaliphatic copolymer (PDMS-br-PBCH).

In this study PBA and PBCH systems (aliphatic and cycloaliphatic polyesters) were selected because they afford well defined high molar mass segmented copolymers that are soluble in common solvents and hence allow for molar mass and other solution characterization methodologies. Furthermore, the dimethylcylohexanedicarboxylate (DMCH) based monomers have the added advantage of having relatively low polarity (7.94 $(cal/cm)^{1/2}$,

calculated using the group contributions method),[11] compared to adipic acid (AA) for the aliphatic polyester (8.84 $(cal/cm)^{1/2}$). PDMS is a very non-polar polymer (7.34 $(cal/cm)^{1/2}$) and therefore it was hoped that by using a low polarity polyester monomer (cycloaliphatic), miscibility would be maintained throughout the melt reaction.

Two series of aliphatic polyester copolymers were prepared with varying compositions under different experimental conditions. On the other hand, four series of cycloaliphatic polyester copolymers were prepared with varying PDMS segment lengths and architectures, in addition to varying the PDMS content. The weight percent of PDMS was varied with respect to the polyester segment. This affords a systematic copolymer series with differing compositions. A branching agent with four functional sites was also used to produce randomly branched copolymers. All the copolymerizations were carried out in bulk, except in the first stage of the copolymerization for the second series of PDMS-s-PBA copolymers synthesized (series B), in order to obtain high conversions.

3.2 Experimental

3.2.1 Materials

Octamethylcyclotetrasiloxane (D_4, +99% purity, Figure 3.2) was purchased from Fluka Company (Sigma-Aldrich). It was dried by stirring over calcium hydride over night under nitrogen. A vacuum distillation of the D_4 was carried out at 60–70°C, using a short path distillation apparatus. The dried D_4 was stored under a nitrogen atmosphere in a round bottom flask sealed with a rubber septum and adhesive tape.

Bis(3-aminopropyl)tetramethyldisiloxane (+97% purity, Figure 3.2) was purchased from Industrial Analytical Company. It was used as received and stored in desiccators over calcium hydride.

Tetramethylammonium hydroxide pentahydrate (+97% purity, Figure 3.2) was purchased from Sigma-Aldrich. It was used as a catalyst for equilibrium ring-opening polymerization.

Benzophenone (99% purity, Figure 3.2) was purchased from Sigma-Aldrich; and used as received. It was used to deactivate the amine end group of the PDMS oligomers.

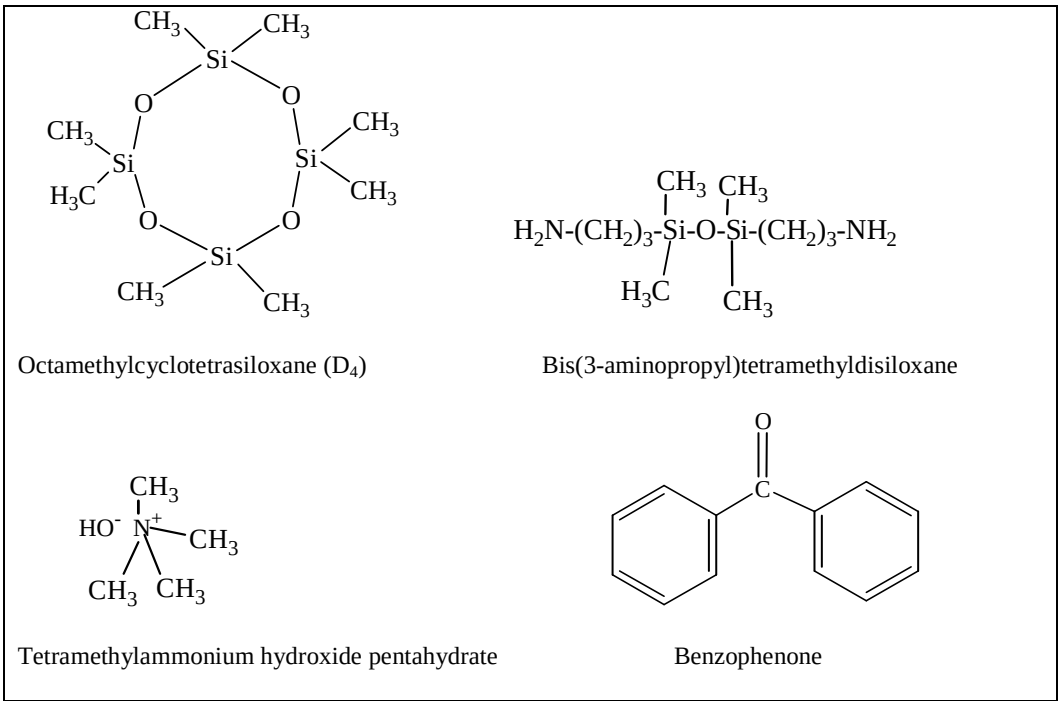

Figure 3.2: Chemical structures of the monomers and agent used in PDMS oligomers synthesis and characterization.

1,4-dimethylcyclohexanedicarboxylate (DMCH, ≥99% purity, 90% cis isomer, Figure 3.3) was purchased from Sigma-Aldrich and used as received.

Adipic acid (AA, ≥99% purity, HPLC, Figure 3.3) was purchased from Sigma-Aldrich and used without further purification.

1,4-butanediol (BD, +99% purity, Figure 3.3) was purchased from Sigma-Aldrich, dried over molecular sieve overnight, and distilled under reduced pressure. It was used with AA or DMCH to synthesize polyester segment in the PDMS-PES copolymers.

Pentaerythritol (98% purity, Figure 3.3) was purchased from Sigma-Aldrich and used as a branching agent to obtain randomly branched PDMS-PBCH copolymers.

Titanium tetraisopropoxide (TIP, 99.99% purity) was purchased from Labchem and used as a polycondensation catalyst. It was diluted in freshly distilled toluene to approximately 0.005 g/mL concentration. The solution was stored under a nitrogen atmosphere and molecular sieve until required for polymerization.

Chloroform, methanol, isopropanol, tetrahydrofuran (THF), toluene, hexane, and d-chloroform solvents were purchased from Sigma-Aldrich. These solvents were used as

received in the polymer synthesis or characterization, except the toluene, which was distilled over small pieces of sodium and benzophenone, under an argon atmosphere.[12] The distilled solvent was storaged under an argon atmosphere.

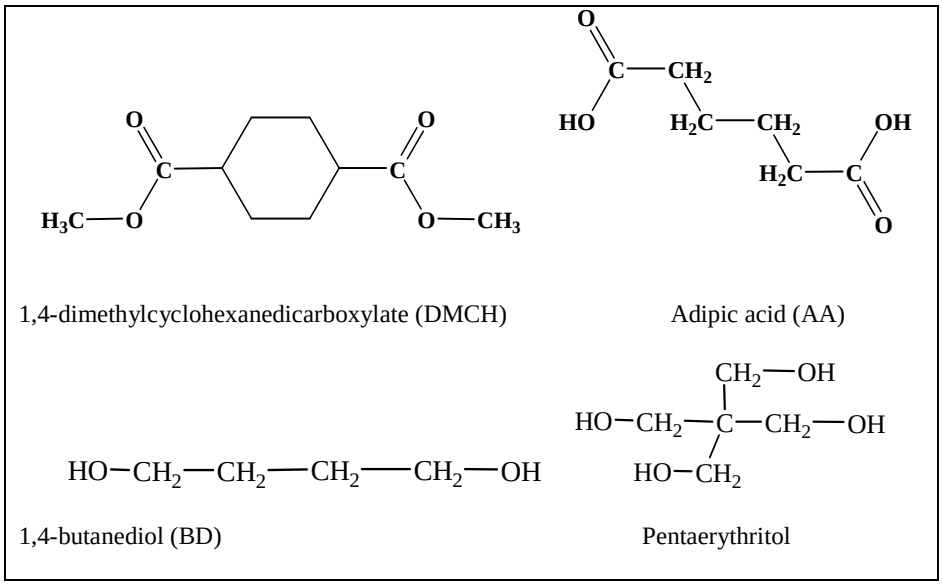

Figure 3.3: Chemical structures of the monomers and branching agent used in polymers synthesis.

3.2.2 Synthesis of PDMS oligomers

Five PDMS oligomers with amino functional groups, and different molar masses of (1000, 2000, 4000, 7000, 10000 g/mol), were synthesized, using equilibrium ring-opening polymerization based on the method reported in literature using D_4.[13] The first step in PDMS synthesis is preparing the siloxanolate catalyst, which is used in the second step to prepare the PDMS oligomers.

3.2.2.1 Preparation of tetramethylammonium hydroxide siloxanolate catalyst

The tetramethylammonium hydroxide siloxanolate catalyst synthesis was carried out by reacting tetramethylammonium hydroxide pentahydrate with D_4, as is illustrated in Scheme 3.1. Tetramethylammonium hydroxide pentahydrate (0.25 g) was added to the reaction vessel, followed by the addition of D_4 (5 mL), via syringe. The reaction mixture was stirred with nitrogen bubbling through it for 40 h at 80 °C. The nitrogen flow was high enough to aid in the removal of water. Following the reaction, the mixture was cooled to room temperature and diluted with D_4 (5 mL) to reduce the viscosity of the mixture. The catalyst was added almost immediately, to avoid moisture absorption of atmospheric water.

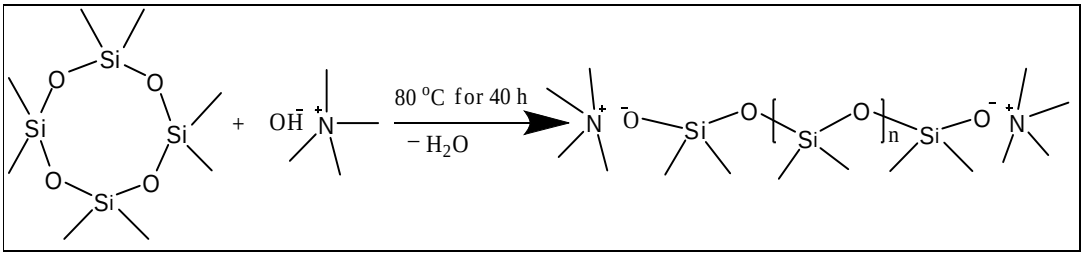

Scheme 3.1: Synthesis of the tetramethylammonium siloxanolate catalyst.

3.2.2.2 Synthesis of PDMS oligomers terminated with an aminopropyl group

The synthetic route that was used in the study for the synthesis of the PDMS oligomers is an equilibration of the cyclic tetramer D_4 and a difunctional siloxane end-blocking reagent, i.e. bis(3-aminopropyl)tetramethyldisiloxane (Scheme 3.2).

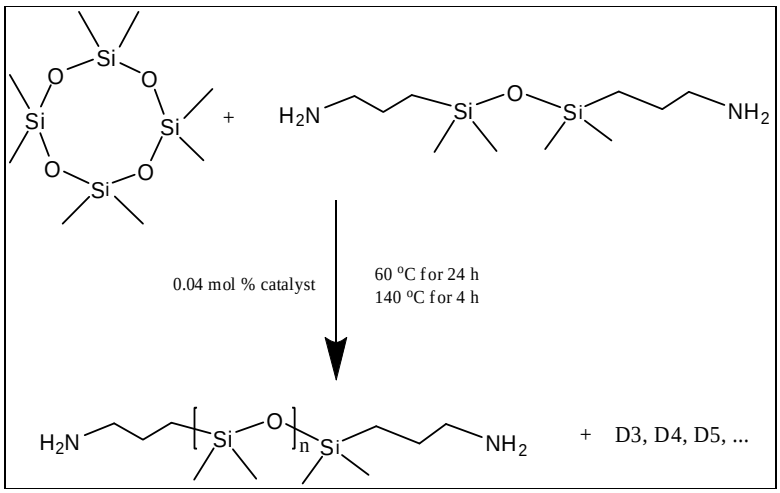

Scheme 3.2: Synthesis of PDMS oligomers via equilibrium ring-opening polymerization.

The synthetic procedure used was as follows:

1. Bis(3-aminopropyl)tetramethyldisiloxane was added to a flame dried 25 mL two-neck round bottomed flask equipped with a magnetic stir bar and rubber septum. The D_4 was added to the flask.

2. The reaction mixture was heated to 80 °C and 0.04 mole % (based on the number of moles of D_4) of the siloxanolate catalyst solution was added. The reaction temperature was maintained for 24 h to allow the mixture to equilibrate.

3. The reaction mixture was subsequently heated at 140 °C for 4 h while bubbling nitrogen through it to decompose the catalyst and remove the trimethylamine by-product.

4. The reaction mixture was heated at 125 °C under vacuum for 3–5 h to remove the cyclic compounds (D_3, D_4, D_5 ...) from the equilibrium mixture. The polymer was stored under nitrogen in a dried round bottom flask sealed with a rubber septum and adhesive tape, until required for use.

Table 3.1 shows the quantities of D_4 and bis(3-aminopropyl) tetramethyldisiloxane that were used to synthesize the PDMS oligomers of desirable molar mass. An example of the calculation used to determine the quantity of D_4 and bis(3-aminopropyl) tetramethyldisiloxane required to obtained PDMS oligomers with specific molar masses is summarized in Appendix A-1.

Table 3.1: Quantities of D_4 and bis(3-aminopropyl) tetramethyldisiloxane required to obtain PDMS (10 g) with various target molar masses

Target M_m (g/mol)	Bis(3-aminopropyl) tetramethyldisiloxane (g)	D_4 (g)
1000	2.50	8.63
2000	1.24	10.07
4000	0.62	10.78
7000	0.36	11.10
10000	0.25	11.21

5. Chromatography techniques were used to verify the removal of cyclic compounds resulting from equilibration, and to measure the molar mass of the PDMS oligomers. ^{1}H-NMR was used to verify the molar masses of the PDMS oligomers. An example of the calculation used to determine the molar mass of PDMS oligomers using ^{1}H-NMR spectra is summarized in Appendix A-2

3.2.2.3 PDMS amine end group deactivation reaction

In order to measure the PDMS molar mass using SEC, the amine end groups were first deactivated by reacting the amine groups in the PDMS oligomers with benzophenone,[14] as shown in Scheme 3.3. The amine groups were removed as a precaution, since it has been reported that it is possible that the silyl-amine linkage can undergo hydrolysis if any water is present leading to SEC column fouling. [14,15] The deactivation reaction was done based on the method reported by Bowens. The reaction was carried out at either 125 °C or at 140 °C, for 12 to 15 h. Details of experimental conditions and the obtained results are discussed in Appendix A-3.

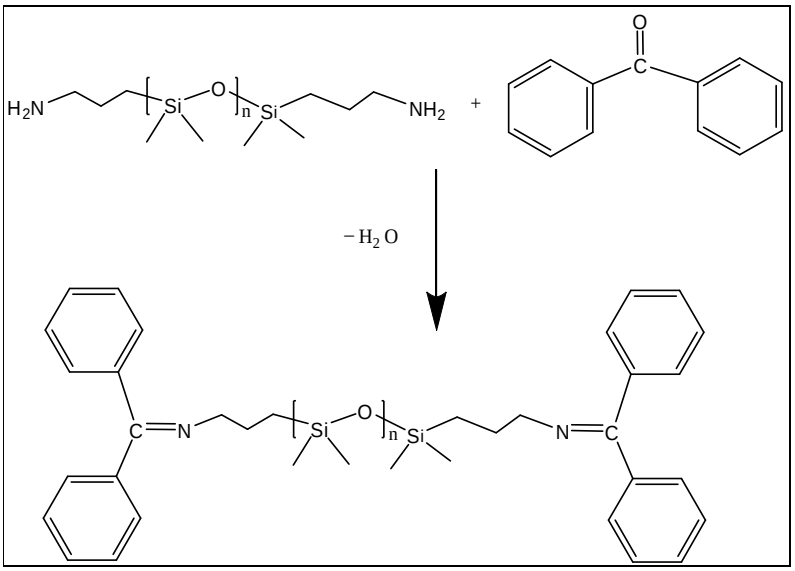

Scheme 3.3: Amino end group deactivation reaction (at either 125 °C or 140 °C, and for 12 to 15 h).

3.2.2.4 End-capping of polydimethylsiloxane

The aminopropyl terminated PDMS oligomer was reacted with a fourfold excess of DMCH to ensure that no coupling reaction could occur, and to yield an ester terminated PDMS oligomer, with an amide link at each end. This was used further in the PDMS-PBCH copolymer synthesis. The end-capping reaction was conducted in a one neck flask equipped with a condensing arm. The reactor temperature was set to 110 ℃, as shown in Scheme 3.4.

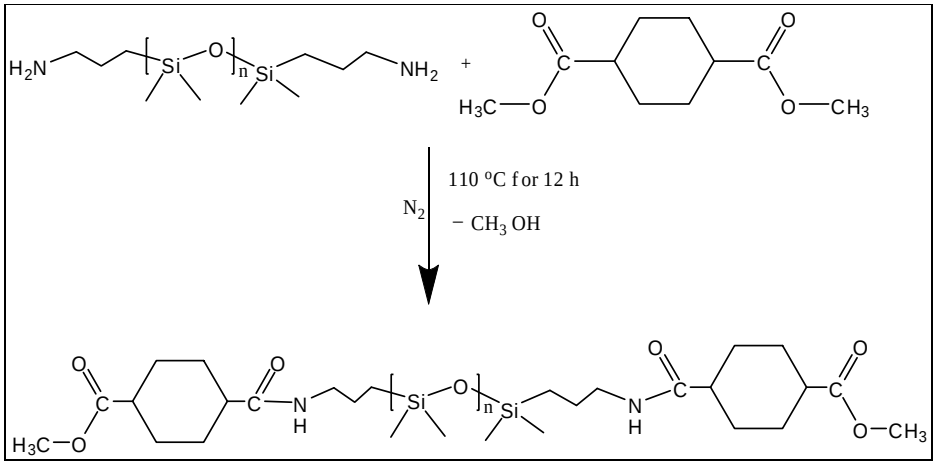

Scheme 3.4: Conversion of the amino end groups in the PDMS prepolymer to ester end group.

A magnetic stir bar was used and nitrogen was bubbled through the hot solution. As the reaction progressed, the methanol evolved and was removed from the reaction vessel. Depending on the volume charged to the flask, the actual amount of time required for the

reaction to run to completion was in the order of 6–10 h. To ensure that complete conversion was achieved, the reaction was allowed to run for 12 h.

3.2.3 Synthesis of PDMS-PES copolymers via the one-prepolymer method

Segmented copolymers of PDMS-PES can be prepared by two means: a one-prepolymer method and a two-prepolymer method. Both of these methods were used in this work. The first method is the more common: it affords random segmented PDMS-PES copolymers and can be carried out in a one-step or in a two-step reaction.

3.2.3.1 PDMS-s-PBA copolymers

Two methods for the synthesis of PDMS-s-PBA copolymers were used. Both are one-prepolymer methods, and all the reactants were introduced in one step as shown in Scheme 3.5. The first method is polycondensation in a melt in a one-step reaction. The AA and BD monomers, as well as the PDMS oligomers, were charged into a 25 mL round bottom flask. The reactor was connected with an adapter, which was also connected to a distillation arm to collect methanol and excess butanediol that was evolved during the reaction. The nitrogen inlet line could be closed and vacuum applied to the condensing arm, as needed. The reactor temperature was increased to melt the raw materials. After 30 min TIP catalyst was added to the reaction mixture. The reaction temperature was increased to 140 °C under a nitrogen gas flow, and the reaction was continued for 6 h. Half of the first added quantity of TIP catalyst was added, before the reaction temperature was raised to 220 °C, under reduced pressure, and the polymerization allowed to continue for a further 8 h.

The second method of PDMS-s-PBA copolymer synthesis is called the dilution-concentration method, which starts in solution and ends under bulk polymerization conditions.[16] First AA and BD in a 1:1.1 molar ratio were added to a two-neck round bottom reaction vessel. The reactor temperature was increased to melt the raw materials and then freshly distilled toluene was added to form a solution of 40% copolymer concentration. After approximately 30 min TIP catalyst and the PDMS oligomers were added in the required percentages to the reaction mixture. The reaction temperature was increased to 140 °C, under a nitrogen gas flow. The reaction was continued for 6 h. Half of the first added quantity of TIP catalyst was added, and then the reaction temperature was raised to 220 °C, under reduced pressure, and the polymerization allowed to continue for 8 h.

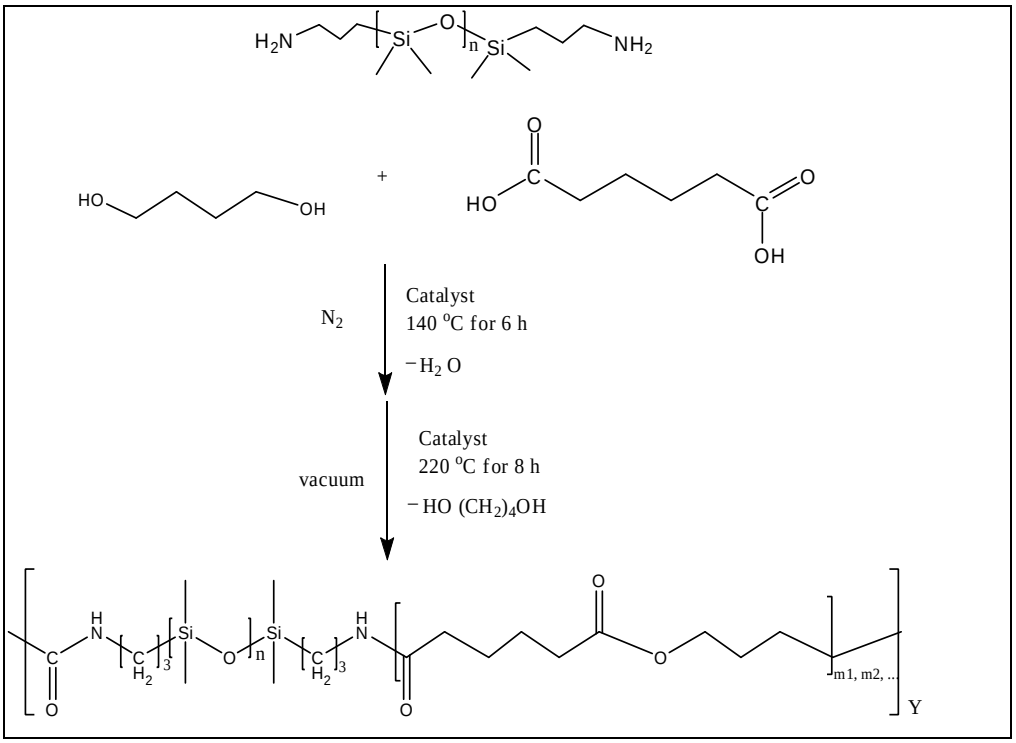

Scheme 3.5: Synthesis of random segmented PDMS-PBA copolymers.

PBA homopolymer was synthesized in the same manner, without PDMS oligomer addition. The entire series of PDMS-s-PBA copolymers was soluble in chloroform. The solutions were precipitated into a 60/40 mixture of methanol/isopropanol to remove any unreacted PDMS and PES from the final product, which were then precipitated. The copolymer was further purified from the remaining PDMS homopolymer by reprecipitation from the THF solution, into n-hexane, and then dried at 40 °C under vacuum. This allowed for the correct experimental determination of the weight percent of PDMS incorporated into the copolymer in later ^{1}H-NMR studies. The unreacted PDMS weight was measured gravimetrically as the weight of polymer before and after the extraction. The same purification procedures were carried out for all the obtained copolymers (the PDMS-s-PBCH and PDMS-br-PBCH copolymers). The structures and compositions of the synthesized PDMS-PES copolymers were verified by ^{1}H-NMR spectroscopy and GEC, while the molar masses were determined by SEC.

3.2.3.2 PDMS-s-PBCH copolymers

Two series of segmented PDMS-PBCH copolymers were prepared using a one-prepolymer method in a two-step reaction. The first step in the two steps reaction is the preparation of a

functionalized PDMS oligomer that can be utilized in a condensation polymerization with the monomers that are used in producing the hard segment (polyester segment). This was discussed in Section 3.2.2.4. Here the second step of this method is discussed. The reaction carried out in the second step is depicted in Scheme 3.6.

DMCH and BD in a 1:1.5 molar ratio were charged, into a 25 mL one-neck round bottom flask connected with an adapter, which was also connected to a distillation arm to collect methanol and excess BD that evolves during the reaction. The nitrogen inlet line could be closed and vacuum applied to the condensing arm as needed. After the addition of the monomers, PDMS with ester end groups was added. This was followed by purging the flask with nitrogen for 5 min and the vacuum was then applied for another 5 min to remove any trace of water remaining in the monomers. At this point, a slow nitrogen flow was started and the reactor vessel preheated to 110 °C, then stirring was started. After the monomers had melted, the TIP catalyst was added and the reaction allowed to proceed at 160 °C for 3 h. The final temperature reached was 220 °C and determined by the boiling point of the diol under high vacuum. An aliquot of titanium catalyst was added before taking the reaction to reduced pressure in order to achieve high conversions. The entire series of PDMS-s-PBCH copolymers was soluble in chloroform.

In order to, investigate the effect of the PDMS concentration and PDMS molar mass on the copolymers properties ten segmented copolymers of PDMS-PBCH were synthesized in two series. In the first series the PDMS oligomers that were used are of similar molar masses (2000 g/mol) and the PDMS concentration was varied, as shown in Table 3.5 (series C) (shown later in Section 3.3.2.2). In the second series of five copolymers, the copolymers contain similar concentrations of the PDMS (10 wt %), but with different PDMS molar masses as shown in Table 3.5 (series D).

Several important observations were noted, during the copolymerization reaction. In the early stages of the reaction, with PDMS oligomer, diester and diol monomers present, the reactants formed a clear colourless homogeneous mixture above the melting point of the DMCD. However, this was not the case for the PDMS-s-PBA copolymers. Here, as the temperature was increased, and throughout the ester interchange process, the mixture remained clear, a light tan colour, and homogeneous. As the vacuum was applied, after the addition of the second aliquot of catalyst, the mixture changed to an opaque tan colour, and the viscosity increased dramatically. This may be an indication of phase separation of the two segments.

Upon cooling, the entire series of PDMS-PBCH copolymers was opaque due to the semi-crystalline nature.

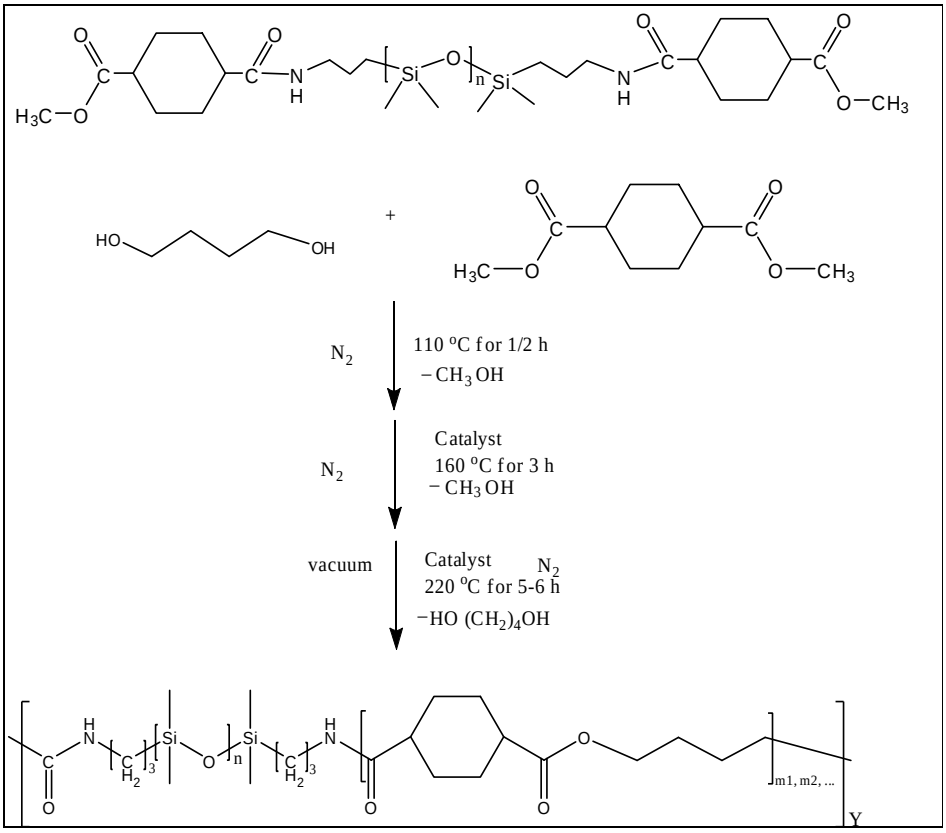

Scheme 3.6: Synthesis of randomly segmented PDMS-PBCH copolymers.

3.2.3.3 PDMS-br-PBCH copolymers

PDMS-br-PBCH copolymers were synthesized in a similar manner by a condensation reaction in the melt state between DMCH, BD and PDMS, in two stages, in the presence of TIP as a catalyst and pentaerythritol as a branching agent (Scheme 3.7). In the second stage, and after the ester end group PDMS addition, pentaerythritol was added to the reaction vessel in the required quantity. The reaction was continued for 2 h at 160 °C. Half of the first added amount of TIP catalyst was added, and then the reaction temperature was raised to 220 °C, under reduced pressure, and the polymerization was continued for 8 h.

The first four copolymers in the series of PDMS-br-PBCH copolymers were completely soluble in chloroform and THF. The last sample in the series was partially soluble in chloroform, which indicated that part of this copolymer was highly branched or even

crosslinked. However, insoluble materials were removed from the product samples during the purification step, by filtration.

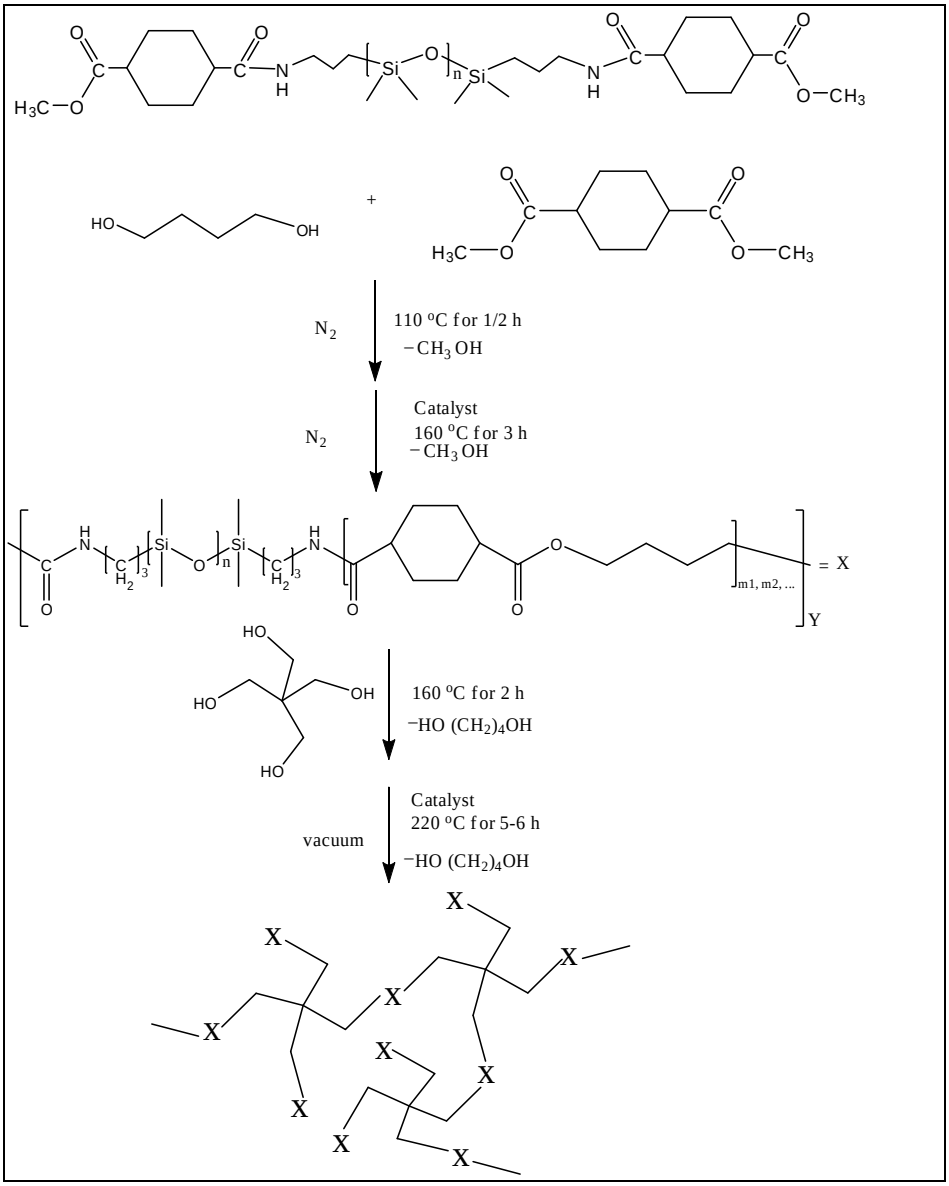

Scheme 3.7: Synthesis of randomly branched PDMS-PBCH copolymers.

3.2.4 Synthesis of PDMS-PBCH copolymers via the two-prepolymer method

In this study segmented copolymers of PDMS-PBCH were also prepared using the two-prepolymer method or polymer-polymer polycondensation method. This method is expected to afford perfectly alternating segmented PDMS-PES copolymers. The synthesis of the first segment (PDMS oligomer) is discussed in Section 3.2.2 and the synthesis of the second segment (PBCH segment) is now discussed (Section 3.2.4.1).

3.2.4.1 PBCH homopolymers

Polybutylenecyclohexanedicarboxylate was synthesized using a melt polymerization method. The reaction is depicted in Scheme 3.8. DMCH and BD, in a 1:1.5 molar ratio, were charged, into a 25 mL one-neck round bottom flask connected with a distillation arm to collect methanol and excess BD that is evolved during the reaction. After addition of the monomers, a slow nitrogen flow was started and the reactor preheated to 110 °C, with stirring. After the monomers had melted, the TIP catalyst was added and the reaction was allowed to proceed with slow nitrogen flow at 160 °C for 3 h. The second stage started when half of the first amount of the TIP catalyst was added and temperature was increased to 220 °C. The pressure within the reaction flask was then decreased to approximately 40 Pa and the reaction was allowed to proceed for approximately 2–3 h at 220 °C, and high vacuum. On completion of the reaction, the flask and its contents were allowed to cool and the crude product stored under N_2.

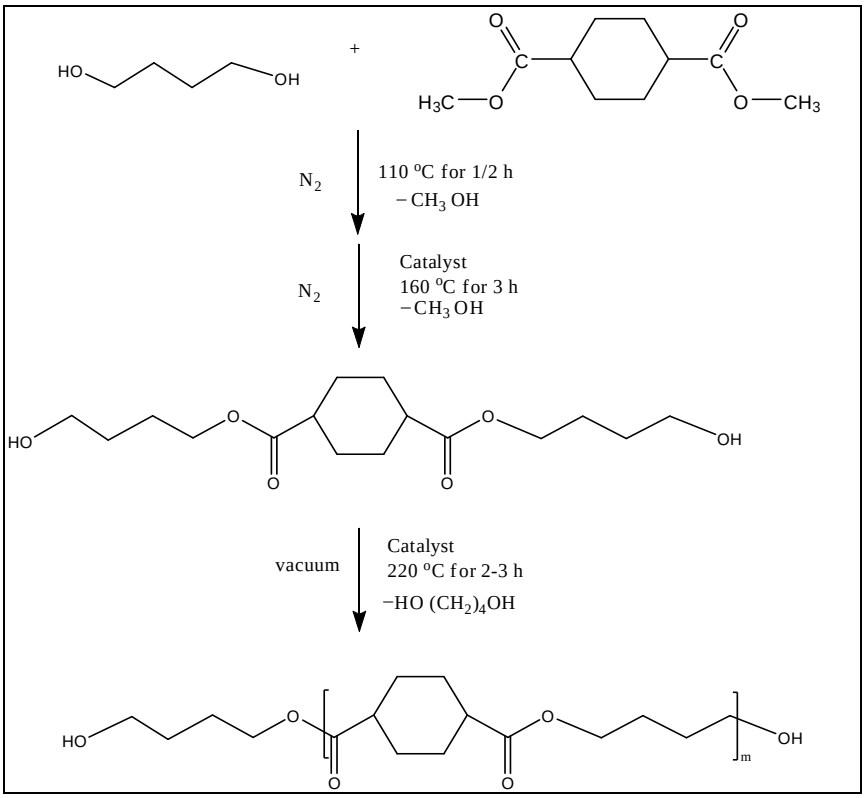

Scheme 3.8: Synthesis of linear polybutylenescyclohexanedicarboxylate with OH end groups.

3.2.4.2 PDMS-s-PBCH copolymers

The second approach used for the synthesis of the PDMS-s-PBCH copolymer involved first preparing a functionalized polyester oligomer that could be utilized in a second

transesterfication step. The obtained functionalized polyester oligomer was reacted with the ester functional PDMS oligomer to produce perfectly alternating segmented copolymers, as is outlined in Scheme 3.9. The raw materials were charged to a 25 mL round bottom flask. The reactor temperature was increased to 110 °C in order to melt the raw materials. After 30 min, TIP catalyst was added to the reaction mixture. The reaction temperature was increased to 160 °C under nitrogen gas flow. The reaction was continued for 3 h. Half the first added amount of TIP catalyst was added, before the reaction temperature was raised to 220 °C, under reduced pressure. The polymerization was continued for 5–6 h, as in the one-prepolymer method.

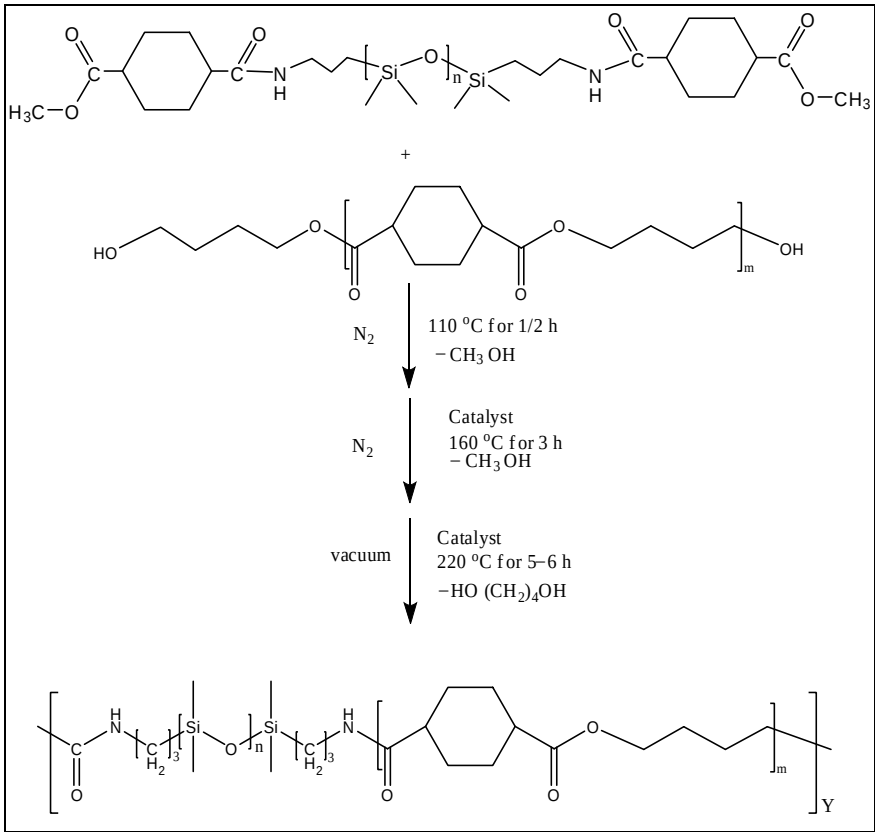

Scheme 3.9: Synthesis of alternating segmented PDMS-PBCH copolymers.

3.2.5 Characterization techniques

3.2.5.1 Nuclear magnetic resonance spectroscopy (NMR)

The chemical composition of the obtained amino and ester terminated PDMS oligomers were determined using NMR (^{1}H and ^{13}C-NMR) (a Varian Unity Inova). ^{1}H-NMR spectra were

measured on a Varian 300 MHz instrument using deuterated chloroform as solvent. All the spectra were referenced to the solvent chemical shift at δ 7.26 ppm. The absolute molar mass of the PDMS oligomer was also calculated using ^{1}H-NMR spectra (with the absence of the internal standard TMS in d-chloroform solvent). This is necessary to later avoid any confusion with the siloxane peak (chemical shifts) assignments (the signals from the methyl groups of the PDMS oligomers and copolymers would have overlapped with the TMS reference peak). ^{13}C-NMR spectra were obtained in the same manner as the ^{1}H-NMR spectra but long runs were used (overnight runs). All the ^{13}C-NMR spectra were referenced to the solvent chemical shift at δ 77.0 ppm. The chemical compositions of the resultant PDMS-s-PES copolymers were also determined from the 300 MHz ^{1}H-NMR spectra by measuring the integrals of the peaks assigned to the methene protons (δ 4.1 ppm) of the PES component, and the dimethyl protons (δ 0.07 ppm) of the PDMS component, after the purified copolymers had been dissolved in d-chloroform. All the chemical shifts in the NMR spectra were assigned to the corresponding chemical structures according to the Cambridge Soft. Chem. Office 2006, using an NMR prediction software program.

3.2.5.2 Fourier-transform infrared spectroscopy (FTIR)

The chemical composition of the obtained prepolymers (amino and ester terminated PDMS oligomers) were determined using FTIR. FTIR was used to follow, and characterize, the emergence and disappearance of the amine group (NH_2) as the molar mass of the PDMS oligomer increased. PDMS samples were prepared by placing a drop of the material between two sodium chloride discs. The infrared spectra were obtained with a Perkin Elmer 1650 Fourier-transform infrared spectrophotometer, and recorded in the range from 500 to 4000 cm^{-1}, using 32 scans.

3.2.5.3 High performance liquid chromatography (HPLC)

HPLC was used to verify the removal of cyclic compounds resulting from equilibration polymerization during PDMS synthesis. The separation was performed using a dual pump HPLC comprising the following units: a Waters 2690 separations module (Alliance), Agilent 1100 series variable wavelength detector, and PL-ELS 1000 detector, and UV detector was adjusted to 254 nm, which corresponds to the absorption of the aromatic ring.[17] Data were recorded and processed using PSS Win GPC unity (Build 2019) software. A PLgel (Polymer Laboratories) 3 μm mixed-E column was used at 30 °C. THF was used as solvent at a flow rate of 1.0 mL/min. The polymer samples were prepared by dissolving 10 mg of PDMS in 2

mL THF. The samples were filtered through a Gelman Glass Acrodisc or a Gelman GHP Acrodisc prior to introduction to the column.

3.2.5.4 Size exclusion chromatography (SEC)

SEC was used to determine the average molar masses (M_n and M_w) of the prepared PDMS oligomers and its polydispersity. The end groups of the oligomers were deactivated and the samples were run through a lab chromatography column to ensure removal of non-deactivated species. The PDMS was dried at 40 °C for 24 h under vacuum and dissolved in THF. SEC analysis was carried out using a Waters model 610 pump, Waters model WISP 717 auto-injector, and model 410 refractive index detector and 486 UV detector. Two PLgel columns 5 μm Mixed-C 300 x 7.5 mm and a pre-column (PLgel 5 μm Guard 50-7.5 mm) were used. The column oven was kept at 30 °C and the injection volume was 100 μm. THF was used as solvent at a flow rate of 1.0 ml/min, and calibration was done using polystyrene standards. Furthermore the average molar mass of the PDMS-PES (M_n and M_w) and its polydispersity were also determined by SEC. The UV detector was adjusted to 310 nm, which corresponds to the absorption of the ester group.[18] For SEC analysis, 10 mg of PDMS-PES copolymers were dissolved in 2 mL THF. The samples were filtered through a Gelman Glass Acrodisc or a Gelman GHP Acrodisc prior to introduction to the column.

3.2.5.5 Gradient elution chromatography (GEC)

GEC was successfully used to monitor the chemical composition of the PDMS-PES copolymers. In the GEC the copolymers fractionate based on the chemical composition using a mixture of THF and hexane with a flow rate of 1 mL/min. Figure 3.4 illustrates the gradient elution profile of the solvents concentration. The separation was performed using a dual pump HPLC comprising of the following units: Waters 2690 separation module (Alliance), Agilent 1100 series variable wavelength detector, and PL-ELS 1000 detector. Data were recorded and processed using PSS WinGPC unity (Build 2019) software. The separation was achieved using a bare silica column (Nucleosil C18 5 μm (250 mm x 4.6 mm)), working at 30 °C. Samples were prepared in THF at a concentration of 5 mg/mL.

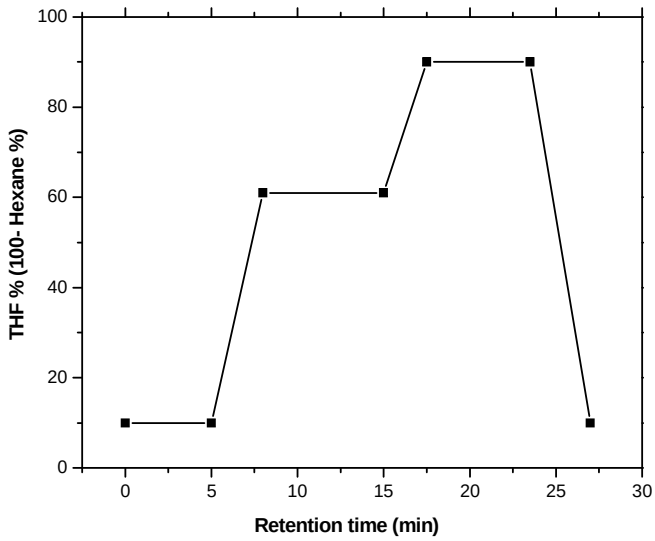

Figure 3.4: Gradient elution profile that was used in HPLC to fractionate the PDMS-PES copolymers (Stationary phase: Nucleosil C18 5 μm, mobile phase: THF/hexane; ELSD detector). ***The gradient was started at 10:90 of (THF/hexane, (v/v)), held constant for 5 min, then changed linearly within 3 min to 61:39 of (THF/hexane, (v/v)), and held constant for 7.5 min and then changed linearly within 3 min to 90:10 of (THF/hexane, (v/v)), and held constant for 6 min and then changed linearly within 4.5 min to 10:90 of (THF/hexane, (v/v)). The flow rate was 1 mL/min.***

3.2.5.6 Size exclusion chromatography-multi angle laser light scattering (SEC-MALLS)

The SEC-MALLS measurements were carried out on polymer solutions to determine the root mean square radius of gyration values in order to calculate the branching indexes (g)[19] of the PDMS-br-PBCH copolymers. The MALLS instrument is placed after the SEC column, followed by the RI detector. The SEC separates the copolymer sample with regard to hydrodynamic volume and then the samples pass through the MALLS instrument that analyzes each elution segment, and then the samples pass through the RI detector. A chromatography system here consisted of a 610 Waters pump, a 717 autosampler (Waters, Milford, MA), a laser photometer MiniDAWN (Wyatt Technology Corporation, Santa Barbara, CA) and a 410 differential refractometer (Waters). ASTRA software (Wyatt Technology Corporation) was used for data processing and collection. The same columns as used in the previous SEC analysis (Section 3.2.5.5), were used. The mean square radius of gyration ($<R^2>$) was obtained from SEC-MALLS for the PDMS-br-PBCH copolymers and their analogy of PDMS-s-PBCH copolymer. Thus the branching indexes of PDMS-br-PBCH copolymers were determined using the following equation:

$$g = <R^2>_{branched} / <R^2>_{linear} \quad \text{[Eq 3.1]}$$

3.3 Results and Discussion

3.3.1 PDMS and PBCH oligomers characterization

3.3.1.1 Chemical characterization of PDMS and PBCH oligomers

The chemical composition of the PDMS oligomers was characterized using NMR (^{1}H-NMR, ^{13}C-NMR) and FTIR. Figure 3.5 shows typical ^{1}H-NMR spectrum of a PDMS oligomer terminated with an amine group. Five different chemical shifts (δ) can be distinguished in the spectrum at δ 0.07, 1.2, 1.5, 2.0 and 2.6 ppm. The chemical shift at δ 0.07 ppm corresponds to the protons in the methyl group bonded to silicon (CH_3), and the chemical shift at δ 2.0 ppm corresponds to the protons in the end group (amine group (NH_2)). The other three chemical shifts are related to protons in the methene groups positioned between the silicone atom and the amine group.

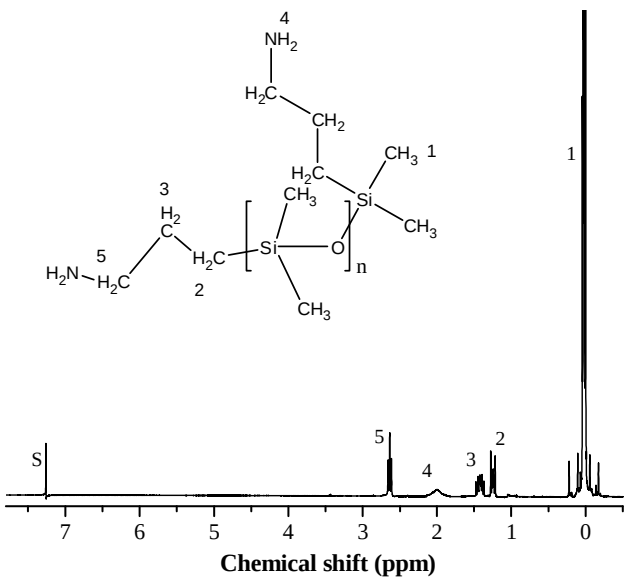

Figure 3.5: Typical ^{1}H-NMR spectrum of a PDMS oligomer terminated with an amine group (PDMS-NH_2).

Characterization of the ester end capped of PDMS was achieved using ^{1}H-NMR. Figure 3.6 shows that the chemical shift at δ 2.0 ppm for PDMS-NH_2 is shifted to δ 7.6 ppm, which corresponds to the protons in the amide group.

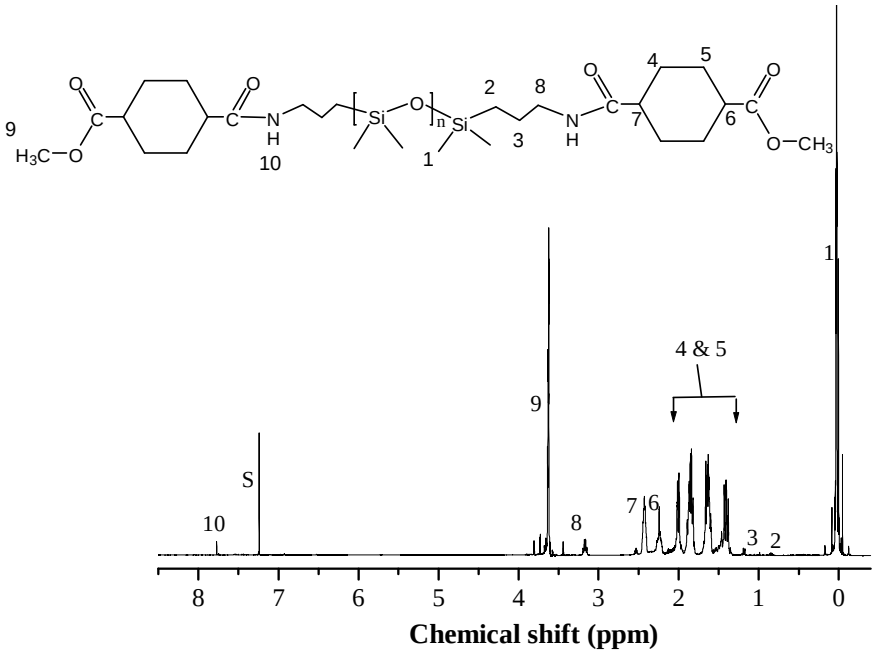

Figure 3.6: Typical ^{1}H-NMR spectrum of a PDMS oligomer terminated with an ester group (PDMS-COOCH$_3$).

Furthermore the chemical shift at δ 2.6 ppm for PDMS-NH$_2$ is shifted to δ 3.24 ppm in the PDMS-COOCH$_3$, which corresponds to the protons in the methene group attached to the amide group. This set of data gave a clear indication of complete functionalization, and that the amine terminated PDMS had been converted to an ester terminated PDMS. The spectra clearly show the presence of the methyl group attached to a silicon atom at a chemical shift of δ 0.07 ppm, whereas the chemical shifts at δ 1.4–2.4 ppm are assigned to the protons on the cyclohexane and methene units at the chain end. The large intensities of the chemical shifts that are assigned to the protons on the cyclohexane compared to that assigned to methane, is due to the fact that any excess DMCD has not been removed when the ^{1}H-NMR analysis was carried out. The remaining DMCD was reacted in the second stage with the BD to form the polyester segment in the copolymer and polyester homopolymers as by a product. This was removed after polymerisation as discussed in Section 3.2.3.1.

Figure 3.7 shows a ^{13}C-NMR spectrum of the PDMS oligomer terminated with an amine group. There are four well defined chemical shifts, at δ 0, 12, 26 and 45 ppm. The chemical shift at δ 0 ppm corresponds to the carbon atom in the methyl group bonded to silicon (CH$_3$), the chemical shift at δ 12 ppm corresponds to the carbon atom attached to the silicon atom, and the last chemical shift at δ 45 ppm corresponds to the carbon atom attached to the amine

group (NH_2) at the chain end. The chemical shift at δ 26 ppm corresponds to the carbon atom in the methene group placed between the methene attached to the silicone atom and the methene attached to the amine group. When the amine end group was converted to the ester end group in the PDMS oligomers the ^{13}C-NMR spectrum showed a new chemical shift (Figure 3.8) in the area δ 10–60 ppm, due to the carbon atoms in the cyclohexane and methyl groups at the chain end.

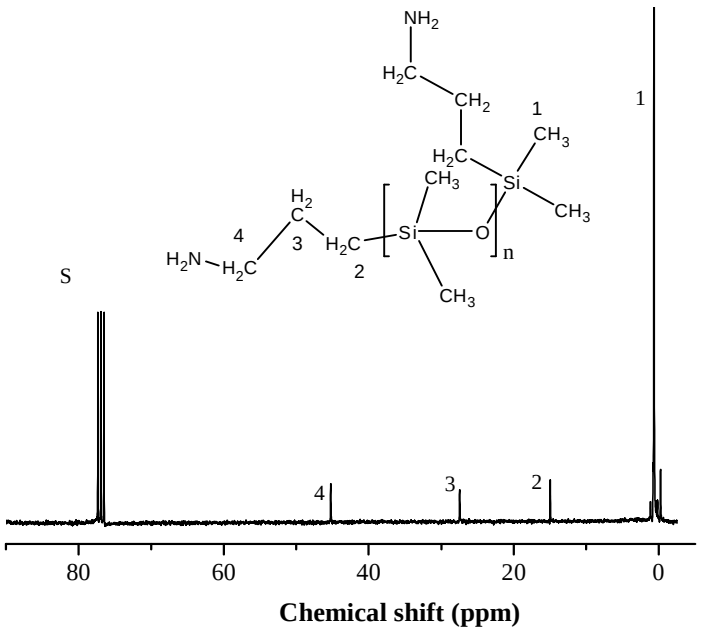

Figure 3.7: Typical ^{13}C-NMR spectrum of a PDMS oligomer terminated with an amine group (PDMS-NH_2).

The chemical shifts at δ 175–176 ppm correspond to the carbon of the carbonyl group. The shift at δ 176 ppm is related to the carbon atom in the ester's carbonyl group and that at δ 175.6 ppm is related to the carbon atom of the amide group created after the reaction between the -NH_2 end group of PDMS oligomer and the ester group. This is a further indication that the PDMS end group was converted into an ester end group, which in the second step reacts with the diol monomers.

The chemical composition of the PBCH oligomers was also characterized using ^{1}H-NMR and ^{13}C-NMR. During the synthesis of the PBCH homopolymer it was assumed that the resulting polymer would be terminated with a hydroxyl group since an excess of diol was used during the polymerization. The effect of this end group on the ^{1}H-NMR spectrum can be seen in Figure 3.9 as a chemical shift at δ 3.7 ppm.

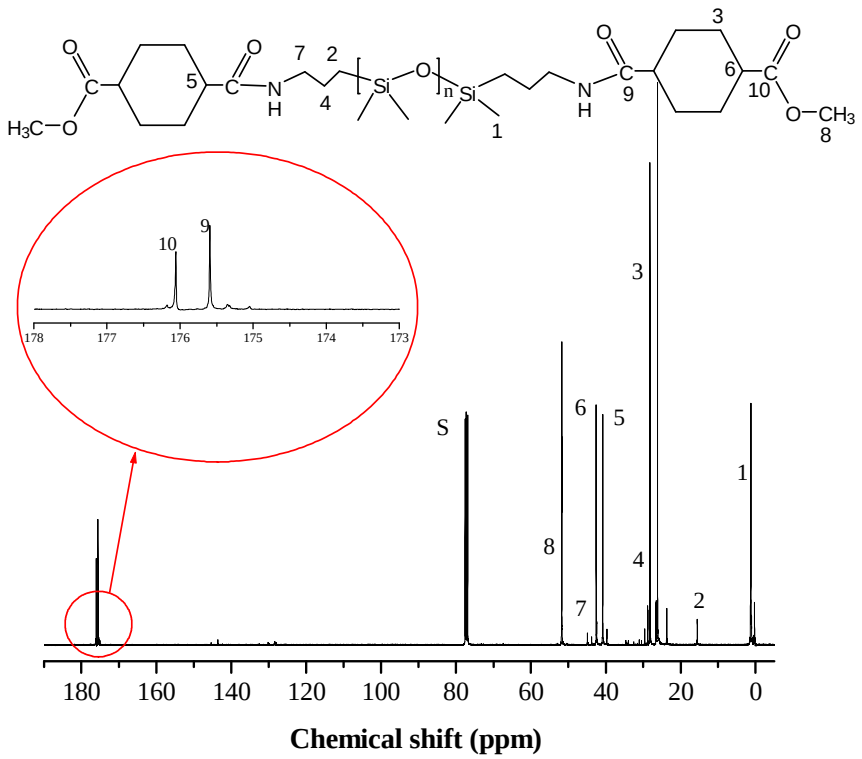

Figure 3.8: Typical ^{13}C-NMR spectrum of a PDMS oligomer terminated with an ester group (PDMS-COOCH$_3$).

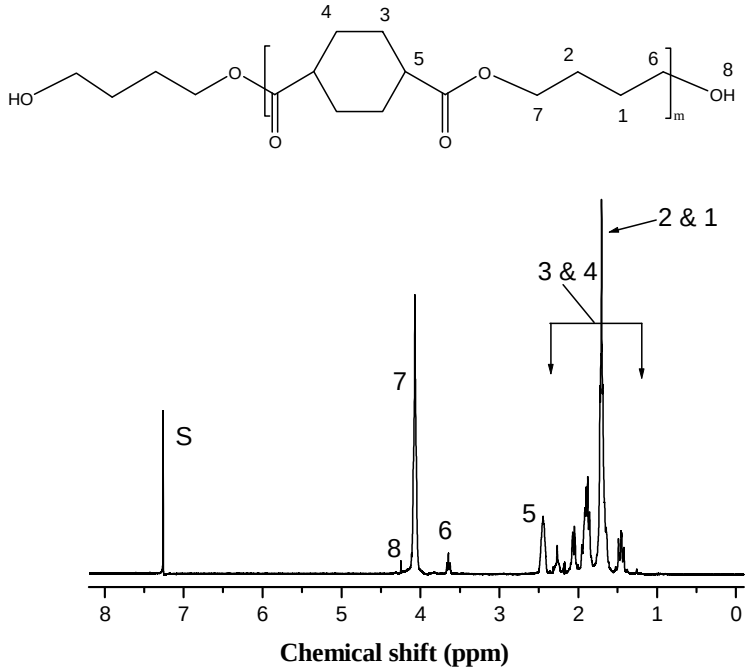

Figure 3.9: Typical ^{1}H-NMR spectrum of a PBCH terminated with a hydroxyl group (PBCH-OH).

The ^{1}H-NMR spectrum of the PBCH terminated with a hydroxyl group also shows chemical shifts at δ 1.4–2.4 ppm, which are assigned to the protons on the cyclohexane and methylene units in the main chain. The signal at δ 4.1 ppm is due to the protons in the methylene group that are attached to the carbonyl group in the polymer backbone.

Figure 3.10 shows the ^{13}C-NMR spectrum of the PBCH terminated with a hydroxyl group in which four chemical shifts can be distinguished. The chemical shifts at δ 20–67 ppm are due to the carbons in the cyclohexane and methylene groups along the backbone of the PBCH, and the chemical shift at δ 175–176 ppm corresponds to the carbon in the carbonyl group.

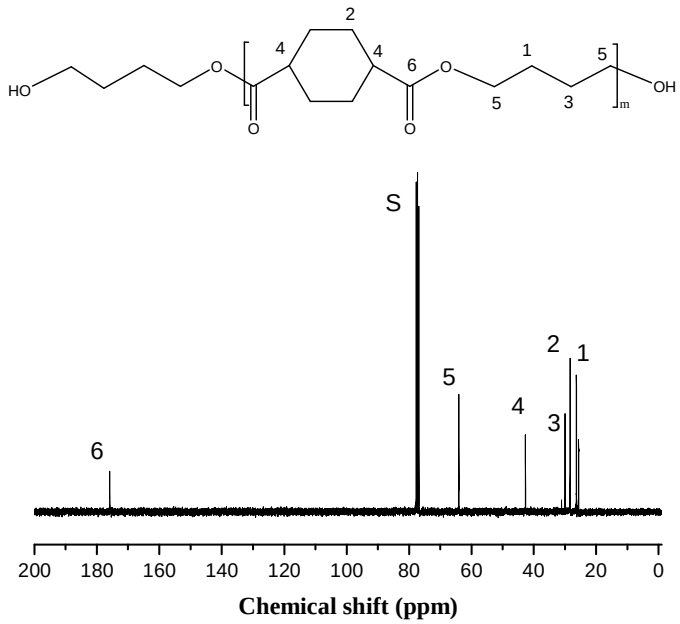

Figure 3.10: Typical ^{13}C-NMR spectrum of a PBCH terminated with a hydroxyl group (PBCH-OH).

Figure 3.11 shows the FTIR spectra of the PDMS oligomer of two different molar masses (1000 and 7000 g/mol) bands, before the esterification process. The assignments are indicated in the figure. In the case of the low molar mass PDMS oligomer the amine absorption appears more clearly than in the case of the high molar mass PDMS oligomer (dotted curve in the figure). The FTIR result confirms results that have been reported by Jeffrey,[20] for PDMS terminated with amine groups.

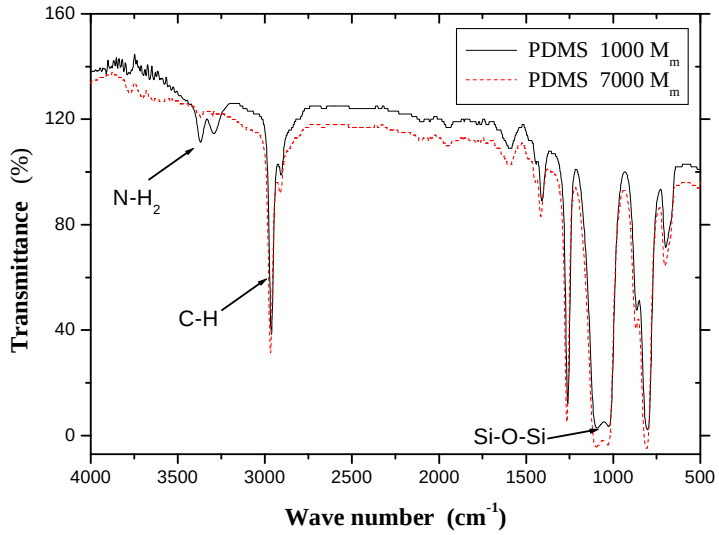

Figure 3.11: FTIR spectra of PDMS oligomers terminated with amine end groups of two different M_n (1000 and 7000 g/mol).

Figure 3.12 shows typical FTIR spectra of the PDMS oligomer (M_m 1000 g/mol) before and after the esterification process, in which the amine groups are converted to ester groups. All the bands that indicate the chemical structures of the respective PDMS oligomers with the two different end groups (PDMS-NH_2 and PDMS-$COOCH_3$ represented by the solid curve and dotted curve, respectively) are clearly defined in the figure. The spectra of the PDMS in Figure 3.12 are of low molar mass oligomer and hence the NH_2 band appears very clearly.

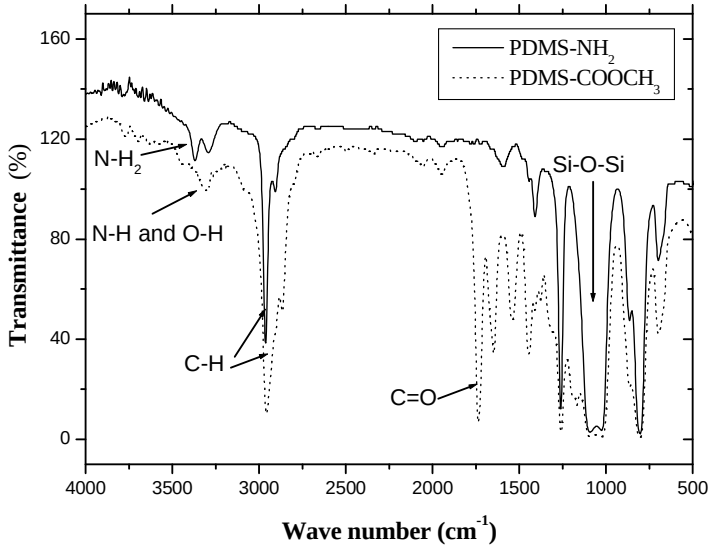

Figure 3.12: FTIR spectra of PDMS terminated with amine and ester end groups, respectively (M_n 1000 g/mol).

In addition to the Si-O-Si absorption band at 1051 cm^{-1} a strong carbonyl absorbance at 1730–1740 cm^{-1} is apparent, as well as the broad absorbance due to the C-O bond at 1100–1200 cm^{-1} in Figure 3.12. Thus functionalization of the PDMS prepolymer to the diester form was clearly confirmed via FTIR. Assignment of all the bands in the FTIR spectrum is given in Table 3.2. In the FTIR spectrum of the PDMS-$COOCH_3$ (Figures 3.12) the band at 3260 cm^{-1} may be due to the presence of hydroxyl groups from the methanol in the product or water molecules in the atmosphere. (The PDMS-NH_2 samples taken after the ring opening polymerization were stopped and the reactor was transferred to the argon box. In the argon box the FTIR samples were prepared. In the case of PDMS-$COOCH_3$, the samples were taken from the reaction vessel and put on the FTIR cell in the room atmosphere).

Table 3.2: Infrared assignments for PDMS-NH_2 and PDMS-$COOCH_3$

Wave number (cm^{-1})	Assignment
3260	N-H stretch of the amine end group
2960	C-H stretch of the methyl group
2864	alkane stretch
1730	ester carbonyl
1456	methylene bend
1257	$Si(CH_3)_2O$ symmetric deformation
1171	C-O
1051	Si-O-Si stretch
800	$Si(CH_3)_2$ stretch, CH_3 rock

3.3.1.2 Determination of PDMS molar mass and the removal of cyclic components

Molar masses for the amine-terminated PDMS oligomers were determined by ^{1}H-NMR after thermal decomposition of the siloxanolate catalyst and removal of the cyclic components by distillation. Results were confirmed by chromatographic analysis as is discussed later in this section. From equation [Eq A.1] and by the integration of the chemicals shifts in the ^{1}H-NMR spectra the molar mass can be calculated. A typical ^{1}H-NMR spectrum of PDMS with 1000 g/mol theoretical molar mass is shown in Figure 3.5. ^{1}H-NMR spectra of PDMS with other

molar masses are shown in Appendix A-2. A summary of the obtained results is tabulated in Table 3.3.

Table 3.3: Comparison of the target and the determined molar masses of PDMS oligomers

Target M_m (g/mol)	M_m [a] (g/mol)	M_w [b] (g/mol)	M_n [b] (g/mol)	M_w /M_n [b]
1000	940	1554	1213	1.28
2000	1950	2846	2194	1.30
4000	3400	5270	4250	1.24
7000	6050	9980	7120	1.41
10000	9100	12640	10195	1.24

[a] Measured by ^{1}H-NMR

[b] Measured by SEC

Table 3.3 shows that the M_m determined from ^{1}H-NMR is lower than the target M_m for all the PDMS oligomers and as the molar mass increases this difference between the target and the determined molar mass becomes larger. This may indicate that less cyclic molecules were formed during the synthesis of low molar mass PDMS than in the higher molar mass PDMS oligomer. This could be because in the case of PDMS synthesis with high molar mass the quantity of D_4 that is used in the polymerization feed is greater than in the case of PDMS with low molar mass. This can contribute to an increase in the concentration (by weight) of cyclic molecules when the polymerization reaction reaches the equilibrium stage. This is because fewer PDMS molecules were formed in the case of the higher PDMS molar mass oligomers than were formed in the case of the lower PDMS molar masses oligomers from the same weight of D_4.

HPLC with an ELSD detector was used to ensure that distillation under vacuum can successfully separate the cyclic products (cyclic compounds of siloxane) from the linear products (PDMS oligomer) after the ring opening equilibrium polymerization. This was necessary in order to ensure that the correct percentage of the required PDMS oligomer will be used in the copolymerization reaction in the later stage. Before SEC and HPLC analysis can be done it is necessary to carry out a deactivation reaction of the PDMS oligomer end group. This is done by reacting the amine end group with benzophenone (see Section 3.2.2.3 and Appendix A-3).

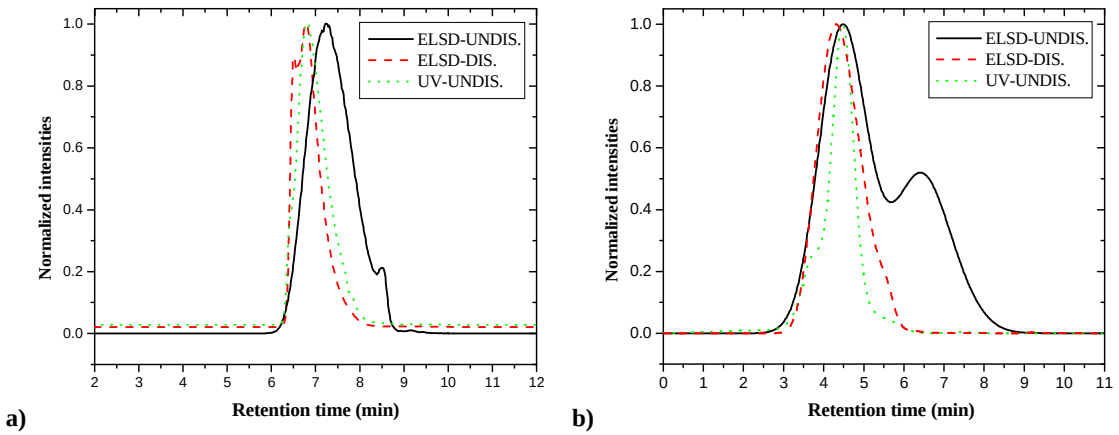

Figure 3.13: HPLC results of the undistilled and distilled PDMS oligomers of (a) 1000 g/mol target molar mass and (b) 7000 g/mol target molar mass.

Figure 3.13 shows an example of the HPLC results obtained for undistilled and distilled PDMS oligomers. It is clear that cyclic PDMS oligomers can be removed using vacuum distillation. A UV detector was also used to monitor the liner PDMS oligomers, which are terminated with benzene rings. The benzene ring has UV absorption at approximately 254 nm.[17] However, no complete overlapping was obtained for any of the PDMS oligomers; thus, even though cyclic compounds of siloxane can be removed there is no way to be completely sure that all cyclic compounds have been removed from the reaction mixture.

SEC was used to determine the average molar masses and polydispersity of the PDMS oligomers. Figure 3.14 shows five overlaid peaks from SEC results of PDMS of different molar mass after removal of the cyclic compounds of siloxane and blocking the end group. The obtained average molar mass (M_n and M_w) and polydispersity index results from SEC for these five polymers are summarized in Table 3.3. The obtained molar mass values (M_n) from the SEC are clearly greater than the values of the target molar masses, and also larger than the estimated molar mass values (M_n) by ^{1}H-NMR technique. This is due to the fact that SEC results are relative to the linear polystyrene standards and are not absolute molar masses values. In addition to the possibility of the addition hydrodynamic volume to each PDMS molecule when the end functions groups (amino) were blocked by bulky group (benzophenone group).

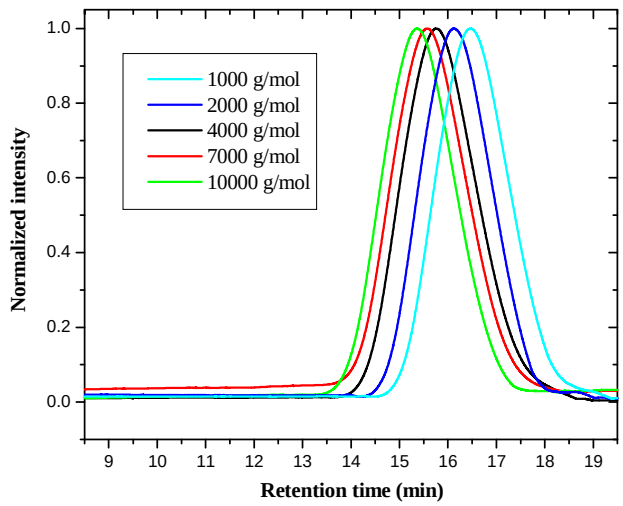

Figure 3.14: SEC results of PDMS oligomers of various molar masses.

The molar mass of the polyester homopolymers were determined in the same manner as the PDMS-PES copolymers and the results are discussed in Section 3.3.2.

3.3.2 PDMS-s-PES copolymer characterization

3.3.2.1 PDMS-s-PBA copolymer

Data pertaining to the two series of PDMS-s-PBA copolymers, synthesized using the one-prepolymer method, are tabulated in Table 3.4. The first series of the PDMS-s-PBA copolymers (series A) was prepared in bulk polymerization and the second series (series B) the first stage of the copolymer synthesis was carried out in toluene (see Section 3.2.3.1). The chemical compositions of the PDMS-s-PBA copolymers were characterized by ^{1}H-NMR after homopolymer extraction. The results obtained are shown in Figure 3.15 for series A and in Figure 3.16 for series B.

The ^{1}H-NMR spectra in both figures clearly show six distinguishable chemical shifts. The presence of the methyl groups attached to the silicon atoms in the PDMS segment appears at the chemical shift δ 0.07 ppm. The protons of the methene groups attached to the ester groups in the ester segment appear at the chemical shift δ 4.1 ppm. These chemical shifts provide confirmation of the presence of both PDMS and PBA segments. The proton of the amide group appears at the chemical shift δ 7.6 ppm, which provides confirmation of the formation of the copolymers. The PDMS and PBA contents were determined as illustrated in Appendix

B-1 by calculations based on the integration of both these peaks. Results are included in Table 3.4.

Table 3.4: Data for the two series of PDMS-s-PBA copolymers prepared using different PDMS concentrations and two different synthesis conditions, (A and B series), by the one-prepolymer method

Sample	PDMS (wt %)	PDMS[a] (wt %)	Unreacted PDMS (wt %)	M_w [b] (g/mol)	M_n [b] (g/mol)	M_w/ M_n
PBA	0	0.00	-	9650	4214	2.29
A-1	5	2.88	42.4	8288	3342	2.48
A-2	10	6.11	38.9	9905	4442	2.23
A-3	25	12.50	50.0	8153	3810	2.14
A-4	40	26.30	34.3	8617	3830	2.25
A-5	60	37.10	38.3	7989	3682	2.17
PBA	0	0.00	-	15795	8143	1.94
B-1	5	4.57	8.2	11239	6314	1.78
B-2	10	8.97	10.3	17700	9415	1.88
B-3	25	21.70	13.2	18066	9819	1.84
B-4	40	34.20	14.7	14310	8131	1.66
B-5	60	51.10	14.9	12568	7141	1.76

[a] Measured by ^{1}H-NMR

[b] Measured by SEC

The PDMS contents (wt %) calculated from the ^{1}H-NMR spectra, were somewhat lower than the theoretical values, which were estimated from the initial concentration in the copolymerization feed. The percentages of unreacted PDMS indicate that the amount of unreacted PDMS increases with an increase in the PDMS content. Nevertheless, in the case of series B, the solvent used provided a more compatible media between the PDMS and the PBA monomers and thus higher PDMS incorporation was obtained.

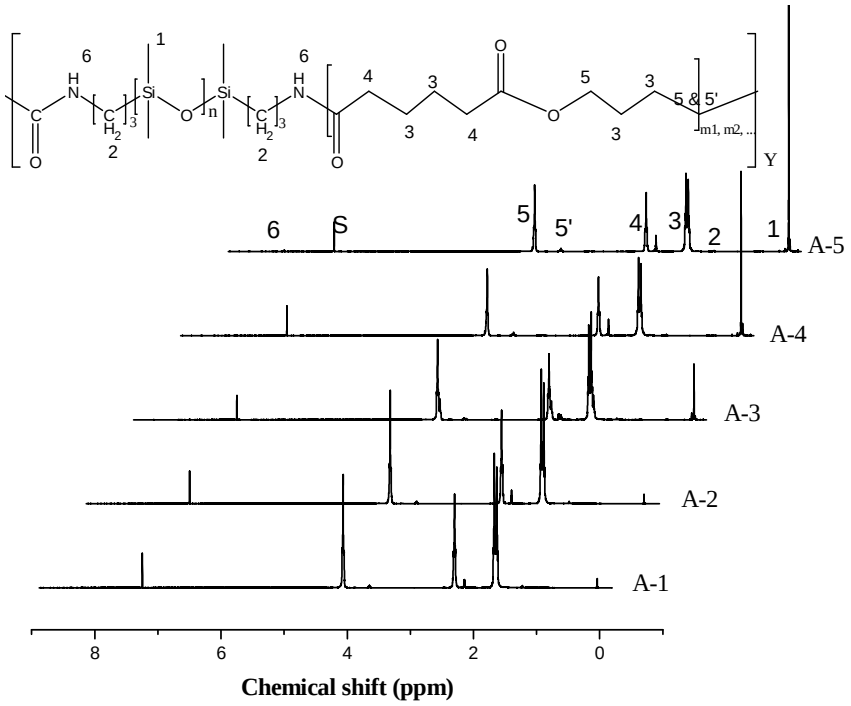

Figure 3.15: ^{1}H-NMR spectra of PDMS-s-PBA with different PDMS content (series A).

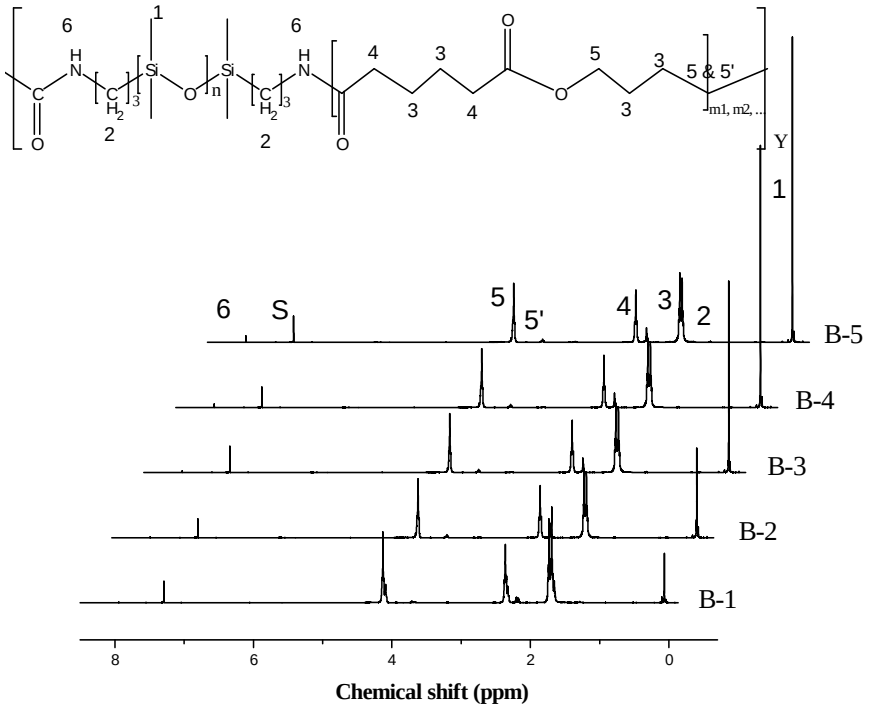

Figure 3.16: ^{1}H-NMR spectra of PDMS-s-PBA with different PDMS content (series B).

Figure 3.17 shows two typical examples of ^{13}C-NMR spectra for series A and series B of the PDMS-s-PBA copolymers.

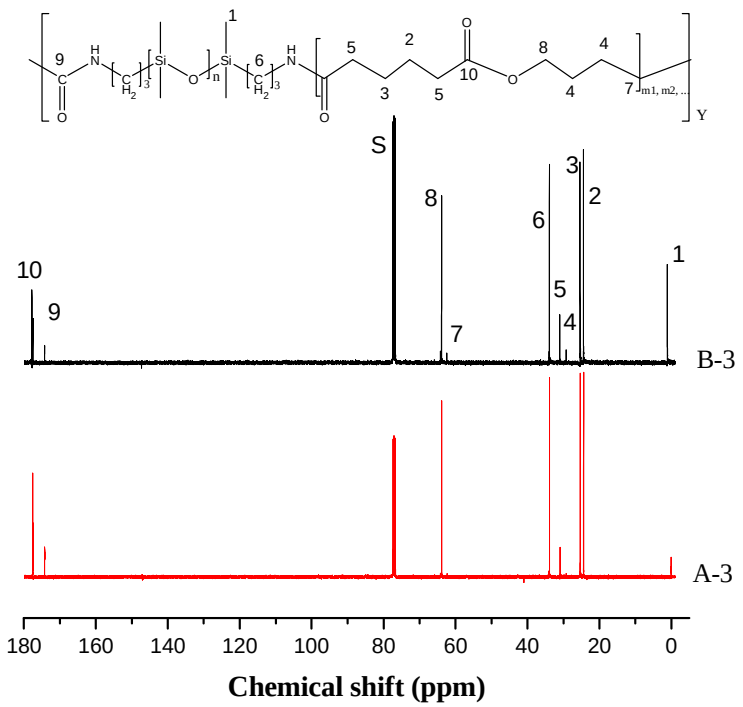

Figure 3.17: ^{13}C-NMR analysis of PDMS-s-PBA copolymers A-3 and B-3.

The chemical shift at δ 0 is due to methyl groups in the PDMS segment whereas the chemical shifts at δ 10–60 are due to the carbon atoms in the PBA segment. Each of the chemical shifts in the spectra is assigned to the respective carbon atom in the copolymer chain as clearly illustrated in the figure. The peak at δ 175.5 is related to the carbon atom in the amide group, formed by the reaction between the amine end group of the PDMS oligomer and an ester group. This is a very clear indication that the amide link was successfully created between the PDMS and PBA segments.

SEC analysis was performed on the PDMS-s-PBA copolymers to determine the molar mass of the copolymers. Figure 3.18 shows the molar mass distributions of the PDMS-s-PBA copolymers for series A (Figure 3.18(a)) and for series B (Figure 3.18(b)).

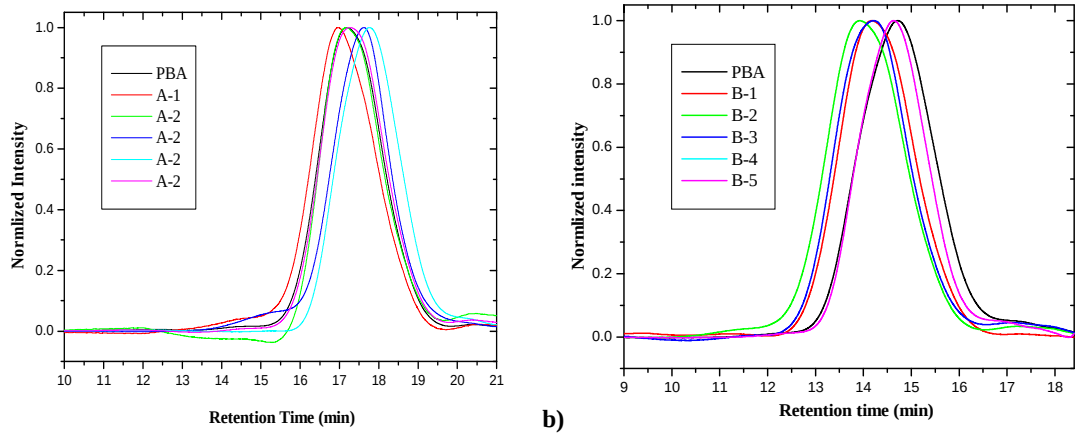

Figure 3.18: SEC results, obtained using a RI detector, for PDMS-s-PBA copolymers: (a) series A and (b) series B.

Figure 3.18 also shows the molar mass distributions of the PBA homopolymers. The SEC results are included in Table 3.4. The number average molar masses (M_n values) of PDMS-s-PBA ranged from 6314 to 9819 g/mol for series B, and for series A the maximum M_n was 4442 g/mol. The molar masses of the copolymers in series B were much higher than that in series A. This is because in series B, the first stage of the copolymerization reactions was carried out in concentrated solution. Under these conditions the reaction medium is heterogeneous, at least at the beginning of the reaction. The copolymer then starts to act as a compatibilizer and the reaction medium becomes progressively clear. Thus, for the PDMS-s-PBA copolymer, high dilution is favoured at the beginning of the reaction (to allow the reaction to start), and high concentrations are necessary to obtain high final conversions. It has been reported by Auman et al.[16] that, in the case of PDMS-polysulphone multiblock copolymers, starting in highly diluted medium and concentrating progressively to maintain homogeneous conditions leads to higher molar masses. This method is called the dilution-concentration method and has been discussed previously (see Section 2.3.2). In this study this has also proven to be the case for the PDMS-s-PBA copolymers. There is, however, no clear effect of a change in the PDMS content on the M_n of the copolymers. The polydispersity values over the entire series were less than 2.5. This demonstrates the high efficiency of extraction of the small species of either homopolymers or copolymers during the purification step.

A dual RI/UV detector system was used in the SEC analysis.[21] These detectors were used in order to determine whether more PDMS or ester was present in the lower or higher molar mass parts of the copolymers. By comparing results obtained from the different detectors

used it was possible to make assumptions on the incorporation of the PDMS in the copolymers. Figure 3.19 shows the obtained results for two selected examples of series A and B, namely A-3 and B-3.

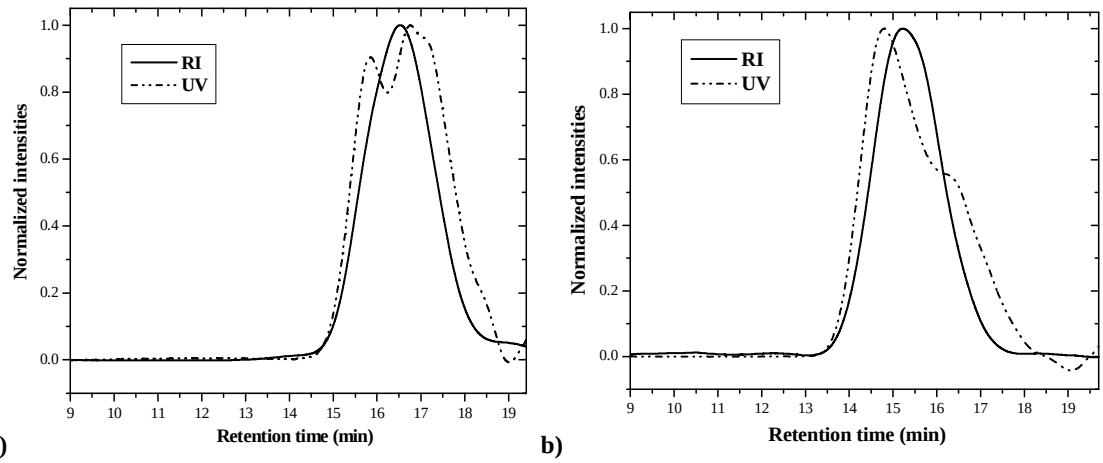

Figure 3.19: Typical SEC results of (a) A-3 and (b) B-3 copolymers, obtained using a RI detector and UV detector at 310 nm.

In SEC the RI signal is an indication of the concentration of the copolymer molecules with a particular molar mass. The intensity of the UV signal at 310 nm is a function of the quantity of ester groups (C=O) present in a sample.[18] Therefore the UV signal can be used as indication of the relative quantity of the PBA segments in the copolymer samples as a function of the molar mass distribution in the copolymers. In the case of even distributions of PBA segment along the copolymer chains the normalized detector signals are supposed to overlap with each other. However, not all the samples showed overlapping of the RI and UV. The UV peaks are slightly shifted to either the right or left of the RI peaks, as is shown in Figure 3.19. This is clear indication that random copolymers were obtained, where the ester segment is randomly distributed over the molar mass distribution of the PDMS-s-PBA copolymer. The heterogeneity of the copolymers was investigated further using GEC.

Figure 3.20 shows a typical gradient elution analysis of the PDMS-s-PBA copolymers before and after the extraction of the unreacted PDMS oligomers.

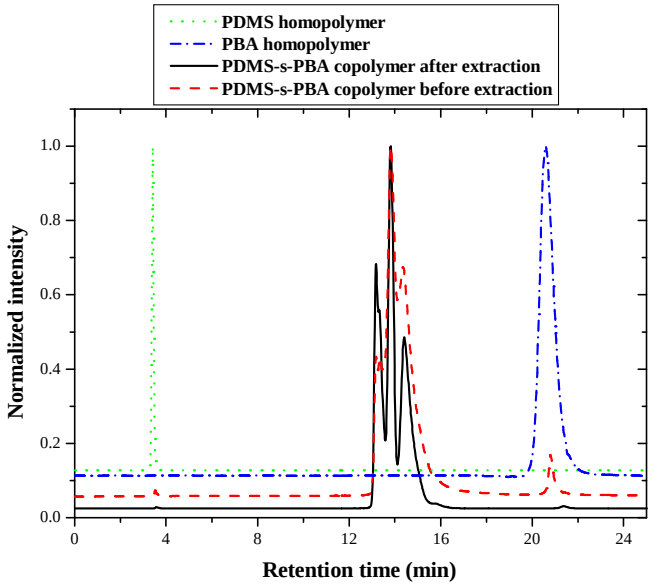

Figure 3.20: Typical gradient elution analysis chromatogram of a PDMS-PBA segmented copolymers (B-5), (see Section 3.2.5.5).

The PDMS and the PBA homopolymers also injected to identify the positions of the homopolymers that could appear in the copolymers. In the PDMS-s-PBA copolymers three grouping of peaks can be observed. The two small peaks at approximately 3 and 22 min can be attributed to the PDMS homopolymer and the PBA homopolymers, respectively. The peaks that related to the PDMS and the PBA homopolymers are extremely small in the extracted PDMS-s-PBA copolymer. The large peak at about 13 min is that of the copolymer containing both PDMS and PBA segments.

Figure 3.21 shows chromatograms of the PDMS-s-PBA copolymers of series B with different PDMS content and 2000 g/mol. Series A was not investigated by GEC due to the low PDMS incorporation and the small molar masses of the obtained copolymers. Here, in series B, it was noticed that with increasing PDMS content there was a shift in the time at which the copolymers eluted. This shift is due to the fact that separation in GEC occurs according to the chemical composition. PDMS elutes from the column after a shorter retention time compared to the PBA, and therefore the higher PDMS content copolymers (B-5) elute earlier than the lower PDMS content copolymers (B-1). In two copolymers in this series (B-1 and B-4) there was still a small quantity of PBA homopolymer present, which eluted at 22 min. Subsequent extractions did not result in its removal, due to the low molar mass of these PDMS-PBA copolymers. The small remains of the homopolymers were also observed for several PDMS-

PBCH copolymers (C-2, E-2 and most of F series), discussed later (Section 3.3.2.2 and 3.3.2.3).

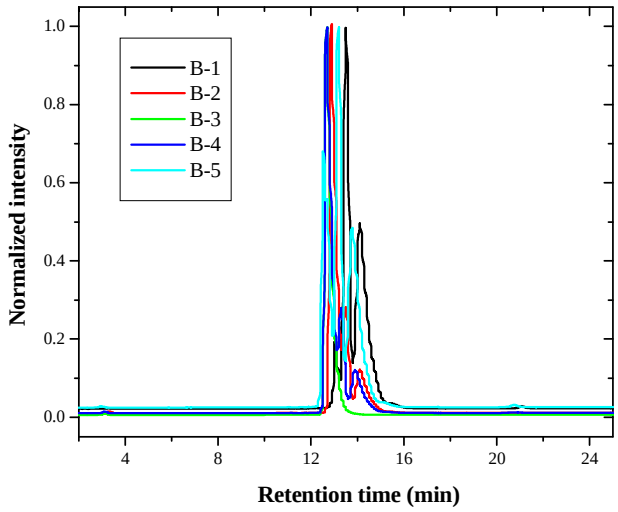

Figure 3.21: Typical gradient analysis results for PDMS-PBA multiblock copolymers of series B (see Section 3.2.5.5).

Since extremely small quantities of homopolymers were observed in several PDMS-PBA copolymers the effect of the presence of this small quantity on the surface morphology investigation was considered to be insignificant. However, the surface morphology of several copolymers from series C, D and E was investigated in Chapter 7 after complete PBCH removal by using GEC-AFM off line coupling technique.

3.3.2.2 PDMS-s-PBCH copolymer

Table 3.5 shows three series of PDMS-s-PBCH copolymers. Two of these series (series C and D) were prepared by the one-prepolymer method and one series (series E) was prepared using a two-prepolymer method. The chemical compositions of the PDMS-s-PBCH copolymers were determined using ^{1}H-NMR. Figure 3.22 shows four examples of ^{1}H-NMR spectra of PDMS-s-PBCH copolymers (C-2, D-1, E-1 and E-2). The spectra clearly show the presence of the methyl groups attached to the silicon atoms δ 0.07 ppm. The chemical shifts at δ 1.4–2.4 ppm are assigned to the protons on the cyclohexane and methene units in the main chain. The chemical shift at δ 4.1 ppm is due to the protons in the methylene group attached to the carbonyl group along the backbone of the copolymer, indicating the presence of the polyester segment. The small chemical shift at δ 4.25 ppm corresponds to the proton in a butanol unit located at the chain end. The chemical shift at δ 3.24 ppm corresponds to the

protons in the methene group attached to amide group. The proton of the amide group appears at the chemical shift δ 7.6 ppm, which provides confirmation of the formation of the copolymers. Several ^{1}H-NMR spectra of the PDMS-s-PBCH did not show chemical shifts at δ 3.24 and at δ 4.25 ppm because the concentration of amide and the chain ends was too low for detection. Similar chemical shifts were obtained for alternating PDMS-s-PBCH copolymers, as is illustrated for examples E-1 and E-2.

Table 3.5: Data for the three series of PDMS-s-PBCH copolymers prepared using different PDMS concentrations and PDMS molar mass

Sample	PDMS M_n (g/mol)	PDMS (wt %)	PDMS[a] (wt %)	Unreacted PDMS (wt %)	M_w [b] (g/mol)	M_n [b] (g/mol)	M_w/ M_n
PBCH	-	0	0.00	-	27719	17171	1.66
C-1	2000	5	4.74	5.2	25990	16665	1.76
C-2	2000	10	9.20	8.0	27719	17171	1.62
C-3	2000	25	22.70	9.2	34502	20239	1.71
C-4	2000	40	35.76	10.7	32720	18568	1.70
C-5	2000	60	52.10	13.2	31204	16860	1.85
D-1	1000	10	9.35	6.5	29981	15142	1.98
D-2	2000	10	9.20	8.0	27719	17171	1.62
D-3	4000	10	8.90	11.0	31712	17816	1.78
D-4	7000	10	9.10	10.0	37770	16862	2.24
D-5	10000	10	8.60	14.0	39915	18828	2.12
E-1	2000	5	6.74	3.4	27720	14904	1.86
E-2	2000	10	13.10	6.2	33917	18235	1.86
E-3	2000	25	27.21	9.9	29266	17420	1.68
E-4	1000	10	12.42	6.8	35043	18640	1.88

[a] Measured by ^{1}H-NMR

[b] Measured by SEC

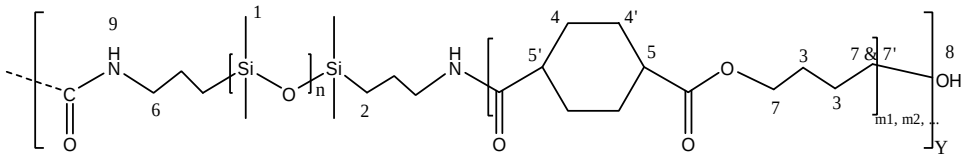

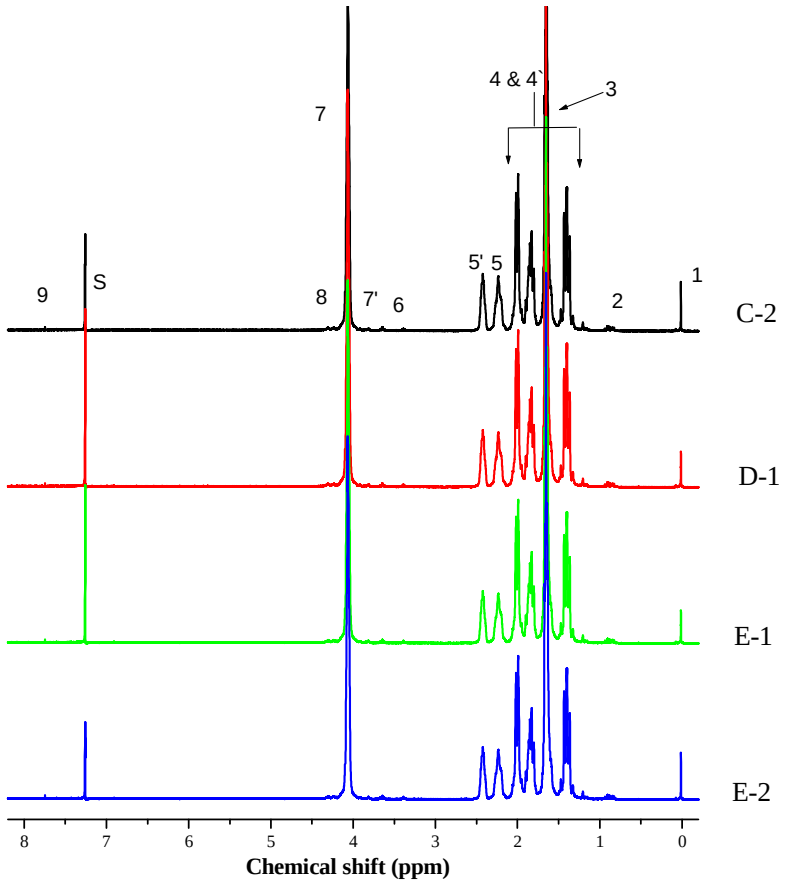

Figure 3.22: Typical ^{1}H-NMR spectra of PDMS-s-PBCH copolymers (C-2, D-1, E-1 and E-2) after extraction of homopolymers.

^{1}H-NMR spectra of PDMS-s-PBCH copolymers, prepared using the one-prepolymer method, were also used to determine the chemical composition of these copolymers by integrating the peaks at δ 0.07 and at δ 4.1 ppm and using the equations shown in Appendix B (Eq B-1 and Eq B-2). Results are included in Table 3.5.

The experimental value of the PDMS content calculated from the ^{1}H-NMR spectra, were somewhat lower than the theoretical values, which were determined from the initial concentration in the copolymerization feed. This is similar to the results obtained for the PBA-s-PDMS copolymers. The percentages of unreacted PDMS increase with an increase in the PDMS content for series C and with an increase in the PDMS segment length for series

D. This might be as a result of fewer functional groups on the PDMS chain available to react as the PDMS content increases in series C and as the molar mass of the PDMS increases for the same PDMS weight present in series D. Furthermore, when series C is compared with series B, the percentage of unreacted PDMS for the aliphatic polyester (PBA), (series B in Table 3.4), is higher than for cycloaliphatic polyester (PBCH) (series C in Table 3.5). This is due to the fact that the cycloaliphatic polyester is more compatible with PDMS than the aliphatic polyester. All the copolymers in the series did, however, show good PDMS incorporation with a higher PDMS feed ratio. All the PDMS-s-PBCH copolymers prepared using the two-prepolymer method, show relatively high PDMS incorporation greater than that obtained from the one-prepolymer method. This is due to the restriction of the incorporation of the PBCH long segment, due to the low concentration of the reactive group when it compared with the reactive groups in the monomers that are used in the one-prepolymer method (DMCH). The net result of that is high PDMS content obtained in the copolymer chains obtained from two-prepolymer method, after the extraction of the unreacted prepolymers. In series E two important points must be emphasized: firstly, although the amounts of unreacted PDMS are very low (Table 3. 6) the copolymer yield was very little. Second, at the end of the reaction, in E series, when the vacuum is applied the presence of large quantity of unreacted PBCH segments can cause two segments of PBCH to react and form longer PBCH segment. The longer PBCH segment can also react with the PDMS-PBCH copolymers. This may lead to the formation of random length of PBCH segment in the end of the copolymers chains.

Figure 3.23 shows the ^{13}C-NMR spectrum of a PDMS-s-PBCH copolymer. There are three regions of chemical shifts. The first region is at δ 0 ppm, which is related to the methyl groups in the PDMS segment. The second region is from δ 10–60 ppm, which is due to the carbons in the cyclohexane and methene groups along the backbone of the PBCH segment. The third region is at δ 175–176 ppm, which is related to the carbon in the carbonyl group. The chemical shift at δ176 ppm is due to the actual carbon atom in the ester carbonyl group and the chemical shift at δ 175.5 ppm is related to the carbon atom in the amide group, formed by the reaction between the amine end group of PDMS oligomer and an ester group of the diester monomer.

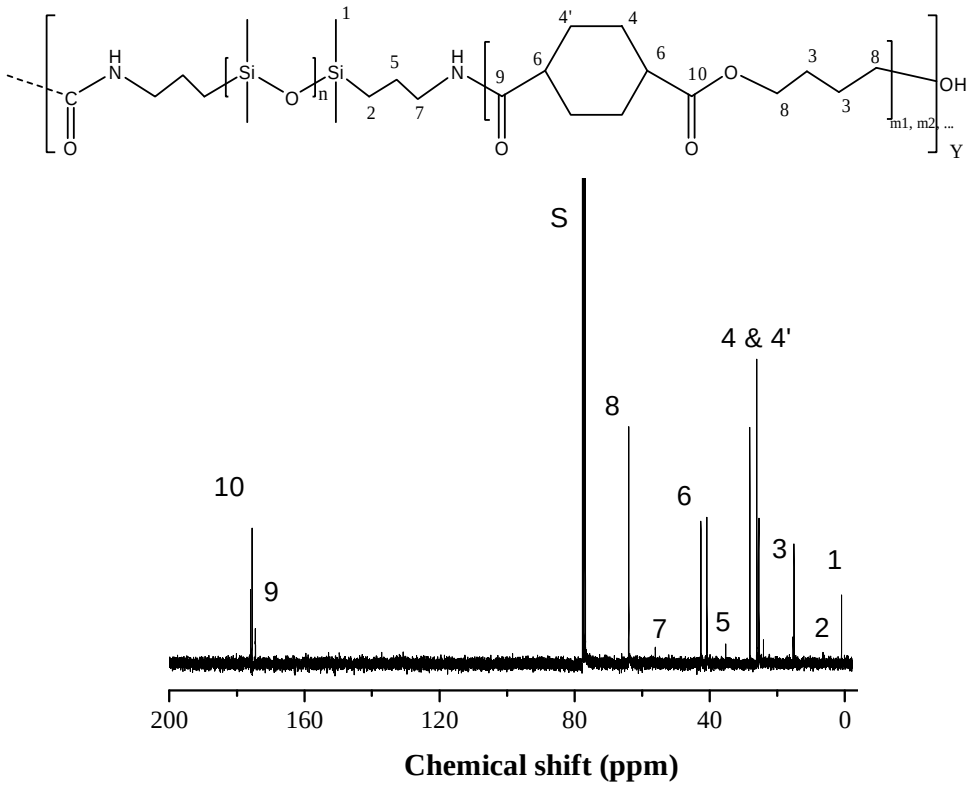

Figure 3.23: A typical ^{13}C-NMR spectrum of PDMS-s-PBCH copolymer (C-1).

Figure 3.24 shows SEC traces of the PDMS-s-PBCH copolymers with different PDMS concentrations or different PDMS block lengths. All have mono-modal peaks, with relatively narrow distributions. In some cases there is small broad peak at the low molar mass side, which might be due to low molar mass fractions of the copolymer, it could not be due to PDMS oligomers because unreacted PDMS oligomers were extracted twice immediately after the copolymerization as described in experimental section (Section 3.2).

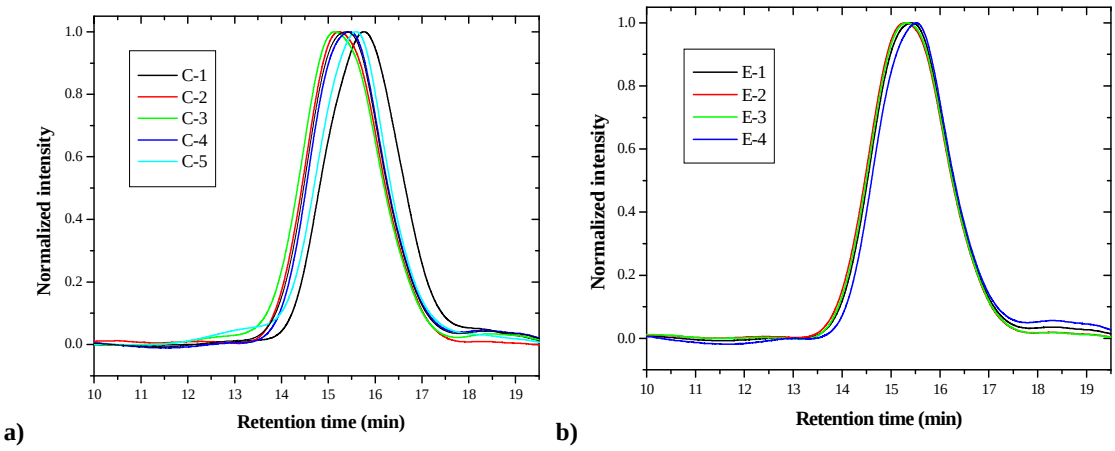

Figure 3.24: Typical SEC results for PDMS-s-PBCH copolymers: (a) series C, and (b) series E.

In Figure 3.24(a), in some cases there is also a small peak or shoulder at the high molar mass side, indicating high molar mass fraction of the copolymer. These fractions could be generated by the chain ester link scission (side reaction) that can occur during polycondensation reactions, as is shown in Scheme 3.10.

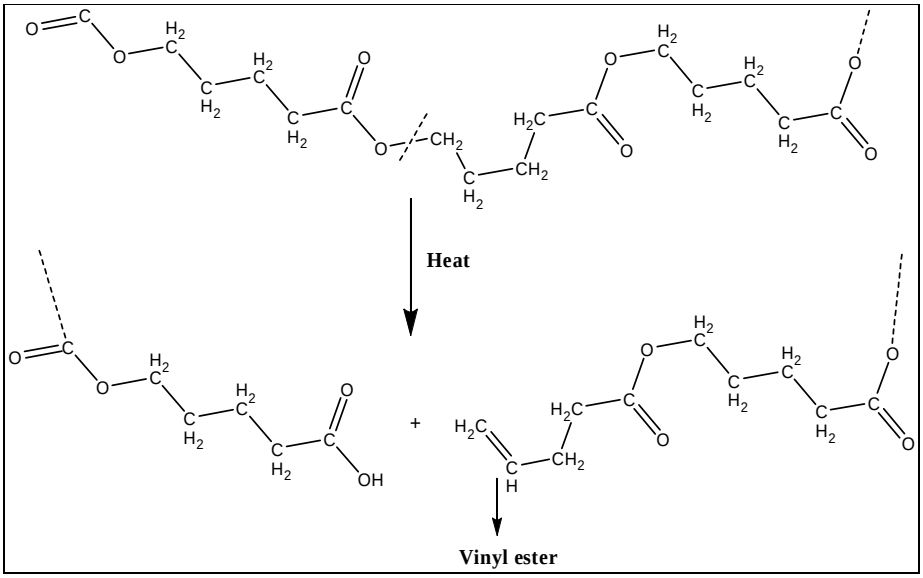

Scheme 3.10: Scission side reaction in polyester chains.

The polyester chain segment breaking reaction occurs to form the vinyl ester (-COO-CH=CH_2), which can react with other chain ends to reform ester links or to form acetaldehyde (anhydride link) (-CO-O-CO-).[22,23] Vinyl esters can also form complexes with metals such as titanium, which is present in the catalyst structure. This complex has a yellow brownish colour, and thus all those samples show brown colours.[22,23]

Table 3.5 shows a summary of the SEC results. The number average molar mass of PDMS-s-PBCH copolymers ranged from about 20239 to 16665 g/mol for series C, from 18828 to 15142 g/mol for series D, and from 18640 to 14904 g/mol for series E. There is, however, no clear effect on the M_n of the copolymers due to using different copolymerization methods, or different PDMS content, or different PDMS of different molar mass. The polydispersity values for the entire C and E series were < 2, but for D-4 in series D it was as high as 2.24. This range of polydispersity values for the products of polycondensation reactions is considered to be extremely good,[24] and demonstrates the high efficiency of the extraction of the small species of either homopolymers or copolymers during the purification step.

Two detectors (RI and UV) were used for SEC analysis to obtain a clear picture of the chemical composition of the copolymers and their molar mass distributions. Four examples of the results obtained are shown in Figure 3.25; in all the samples the UV peaks were shifted to either the right or left of the RI peaks.

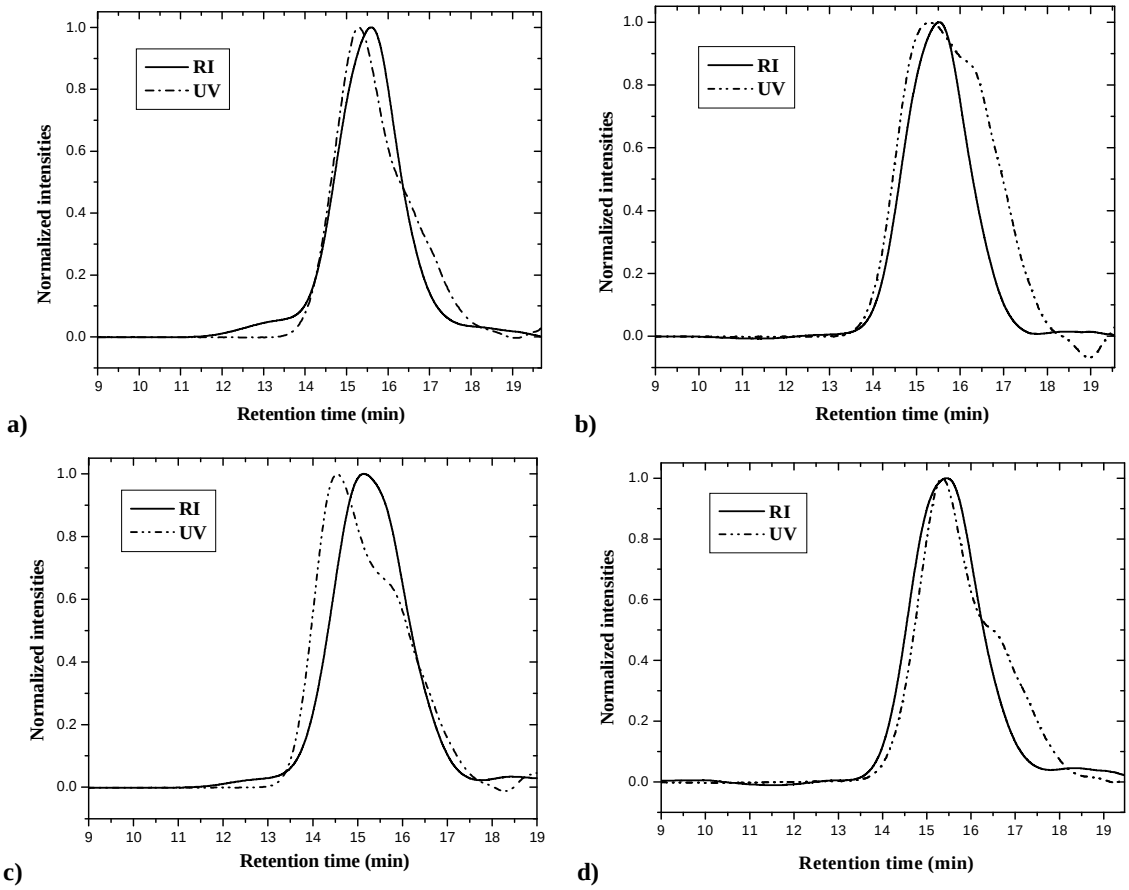

Figure 3.25: SEC results of PDMS-PBCH copolymers, obtained using a RI detector and UV detector at 310 nm: (a) C-2, (b) E-2, (c) D-1, and (d) E-4.

The UV signal at 310 nm was also used as an indication of the concentration of the PBCH (ester group (C=O)) segments in the copolymer samples as a function of the molar mass distribution in the copolymers, which was detected from the RI response. The copolymers C-2, E-2 and E-4 show UV peaks shifted to the right of the RI peak. This could be an indication that there is more PBCH present in the lower molar mass copolymer molecules than in the higher molar mass copolymer molecules. On the hand, copolymer D-1 shows the UV peak shifted to the left, which indicates that there is less PBCH present in the lower molar mass copolymer molecules. In the case of both copolymers obtained using the one-prepolymer method (C-2 and D-1), small shoulders at high molar mass were observed in the RI response that were not detected using the UV detector. The shoulders indicate that the high molar mass

copolymer chains consist of very small PBCH segment lengths (m = 1) (as the ester group is not detected by the UV detector at 310 nm).[18] This type of randomness is not observed for a perfectly alternating copolymer (E-2 and E-4). Not observing such randomness could be due to the large segment lengths of both PDMS and PBCH that were incorporated into the copolymer chain using the two-prepolymer copolymerization method. This explanation was confirmed from the GEC results, as illustrated in Figures 3.26 and 3.27.

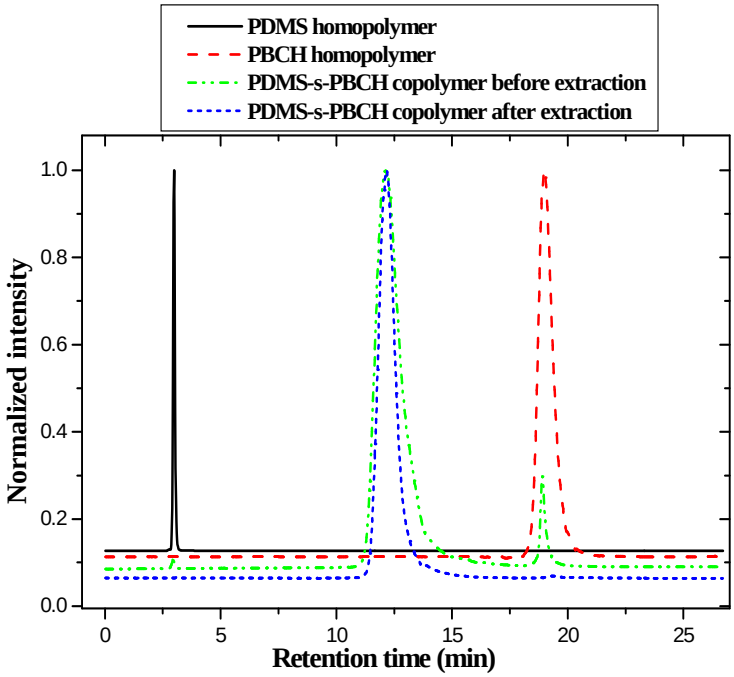

Figure 3.26: Typical examples of GEC results of PDMS-s-PBCH copolymers (C-1), and PDMS and PBCH homopolymers (see Section 3.2.5.5).

Figure 3.26 shows a typical example of the GEC results for C-1 before and after copolymer purification, and PDMS and PBCH homopolymers, using a mixture of hexane and THF solvents with a gradient profile as shown in Section 3.2.5.5. GEC analyses of PDMS and PBCH homopolymers were run separately. It was found that, the PDMS sample eluted between 2.5 and 3 min. On the other hand, a PBCH sample eluted at 18–21 min retention time. Two GEC chromatograms were recorded for the C-1 copolymer: the first before purification and the second after the PDMS and PBCH homopolymers were extracted from the C-1 copolymer. The GEC chromatogram of the copolymer before homopolymers extraction shows a very good separation into three fractions, based on the chromatographic behaviour of the PDMS and PBCH homopolymers discussed above. These fractions can be easily assigned as follows: the first fraction, at 2.8 min, is unreacted PDMS homopolymer, the second fraction, at 18 min, is PBCH homopolymer and the large fraction, which start

eluting at 12 min is clearly copolymer chains that consist of both PDMS and PBCH segments. The GEC chromatogram of the purified copolymer shows one large fraction at about 12–15 min for the copolymer. The complete absence of the homopolymer fractions proves the successful removal of the PDMS homopolymers.

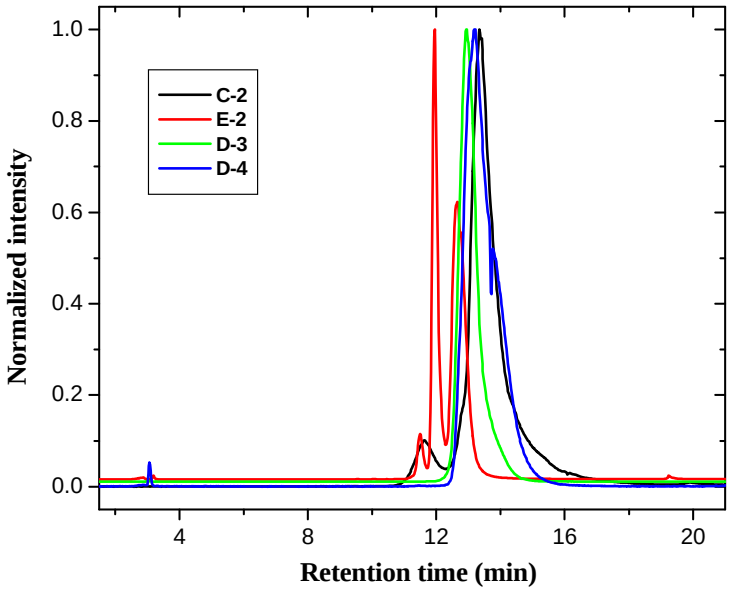

Figure 3.27: Typical examples of GEC results of PDMS-s-PBCH copolymers (see Section 3.2.5.5).

Figure 3.27 shows four examples of the GEC results form series C, D and E after copolymer purification. Two copolymers in this series (C-2 and E-2) show, in addition to the main eluted peak, small peaks, which could be due to the variation in the PDMS content in the copolymer chains. There was also a very small shift in the time at which the copolymers eluted, which corresponds to the increasing PDMS molar mass in the copolymer chains for D-3 and D-4. However, from C-2 and E-2 results one can conclude that the shift does not correspond to the increasing PDMS molar mass alone, but it is indeed corresponding to small changes in the PDMS content in the copolymers, as revealed from ^{1}H-NMR results (see Table 3.5). The separation in GEC occurs according to chemical composition, the higher PDMS content copolymer chains elute earlier than the lower PDMS content chains. However, the shift in the eluting time in Figure 3.27 could be also attributed to the variation in the PBCH segment length in the random copolymers, which can also affect the peak shape and position.

3.3.2.3 PDMS-br-PBCH copolymer

Characterisation of the PDMS-br-PBCH copolymer series, prepared using the one-prepolymer method are tabulated Table 3.6.

Table 3.7: Characteristics of the PDMS-br-PBCH copolymers (F-1 to F-5), prepared using the one-prepolymer method

Sample	PDMS M_n (g/mol)	Branching agent (wt %)	PDMS [a] (wt %)	Unreacted PDMS (wt %)	M_w [b] (g/mol)	M_n [b] (g/mol)	M_w/ M_n	g [c]
F(D-1)	1000	0	9.35	6.50	29981	15142	1.98	1
F-1	1000	0.1	9.10	10.00	27208	14717	1.84	0.94
F-2	1000	0.2	9.51	4.90	33950	14634	2.32	0.75
F-3	1000	0.5	9.32	6.80	35147	15832	2.22	0.62
F-4	1000	1	8.90	11.00	33573	16141	2.08	0.52
F-5	1000	2	9.44	5.60	35632	16345	2.18	0.47

[a] Measured by ^{1}H-NMR

[b] Measured by SEC

[c] Measured by SEC-MALLS

Figure 3.28 shows a typical ^{1}H-NMR spectrum of a PDMS-br-PBCH copolymer. The spectrum shows similar chemical shifts to those obtained for the PDMS-s-PBCH copolymer namely δ 0.07, 1.4–2.4, and 4.1 ppm. The proton of the amide group appears at the chemical shift δ 7.6 ppm, which provides confirmation of the formation of the copolymers. There is also a small chemical shift at δ 3.7 ppm, which corresponds to the protons that are attached to methylene units in the branching agent. This chemical shift provides proof that the obtained copolymer is a branched copolymer. ^{1}H-NMR spectra of PDMS-br-PBCH copolymers were also used to determine the chemical compositions of these copolymers. The results are also included in Table 3.6.

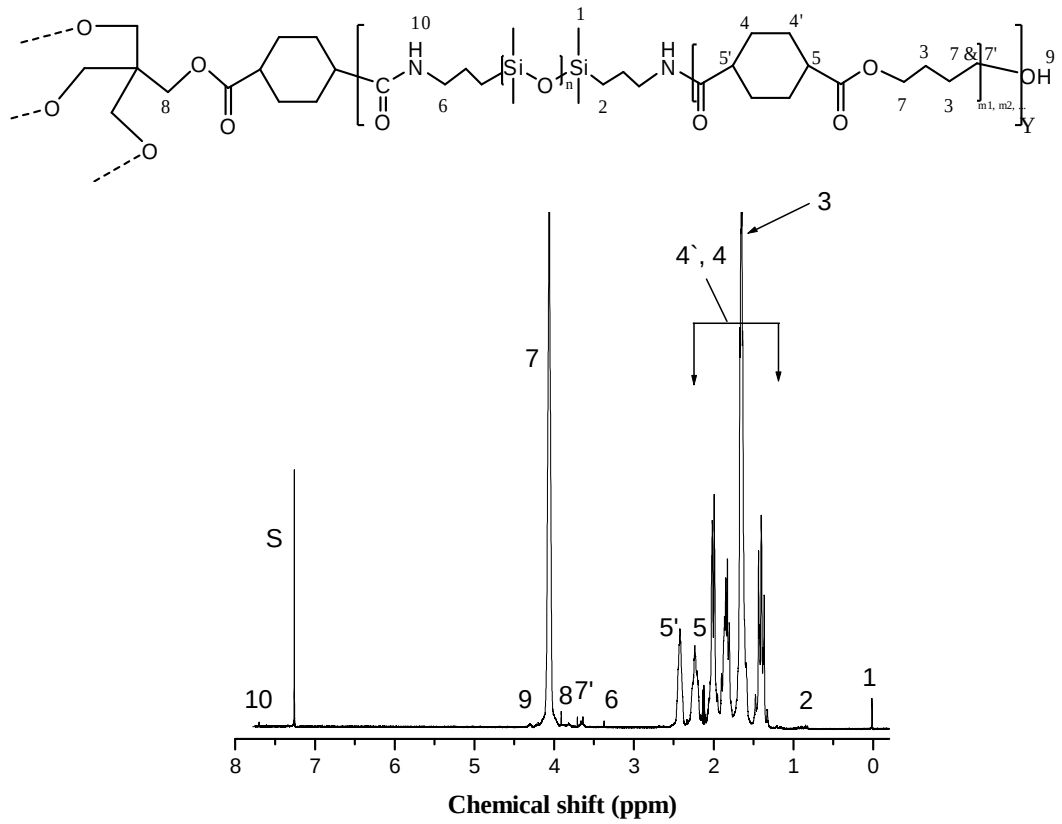

Figure 3.28: Typical example of a ^{1}H-NMR spectrum of PDMS-br-PBCH with 0.5% branching agent content.

Figure 3.29 shows the ^{13}C-NMR spectrum of the PDMS-br-PBCH copolymer. It also shows similar chemical shifts to that observed for PDMS-s-PBCH copolymers (Figure 3.23), in addition to the important chemical shifts (enlarged in the same figure) at δ 42.7 ppm, which corresponds to the carbon at the branching point. The copolymer compositions of the synthesized PDMS-br-PBCH copolymers are summarized in Table 3.6. The initial PDMS content in the copolymerization feed in the entire series was 10 wt %, however, the PDMS content values in the copolymers calculated from ^{1}H-NMR spectra of the PDMS-br-PBCH were lower than the theoretical values. The content of the branching agent in the branched copolymers had no clear effect on the percentages of unreacted PDMS.

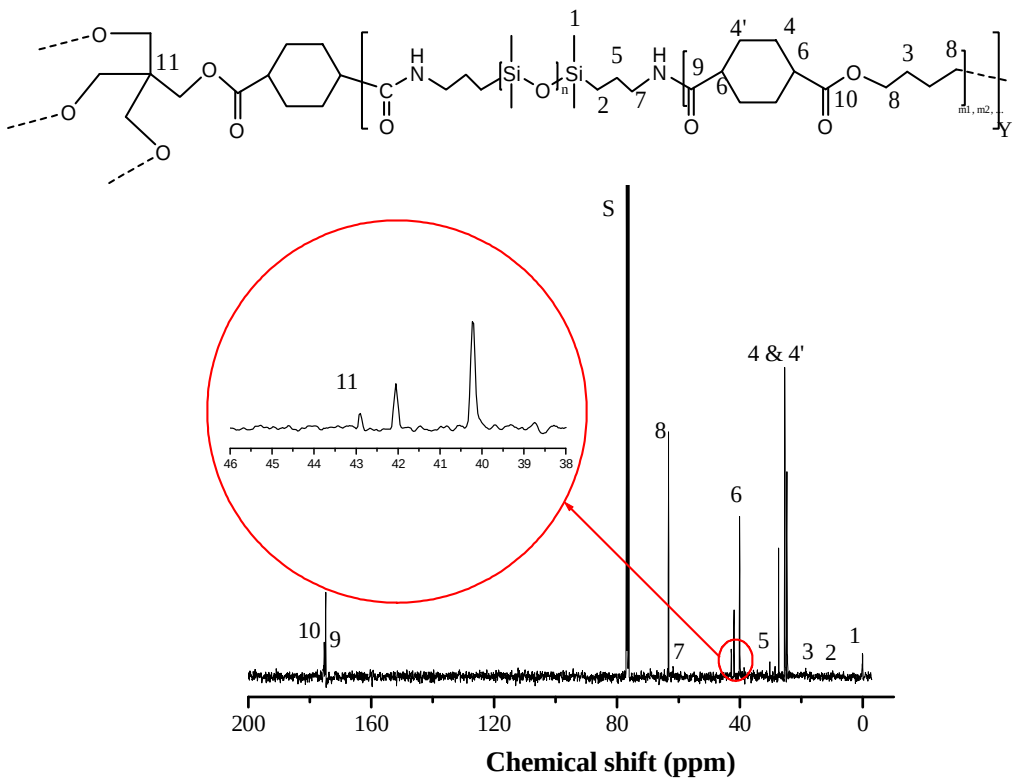

Figure 3.29: Typical ^{13}C-NMR spectrum of PDMS-br-PBCH with 0.5% branching agent content.

SEC was applied to PDMS-br-PBCH copolymers to evaluate the molar masses of the copolymers using an IR detector. The number average molar masses (M_n and M_w) and the polydispersity values (M_n/M_w) obtained for the branched copolymers are summarized in Table 3.6. It was found that PDMS-br-PBCH copolymers can be obtained with relatively high molar mass using melting polycondensation under the same condition as the PDMS-s-PBCH copolymers. Table 3.6 shows that the number average molar masses of the copolymers in the PDMS-br-PBCH series ranged from 16345 to 14171 g/mol. However, a change in the percentages of branching agent used had no clear effect on the M_n of the copolymers. The polydispersity values for the entire series were less than three, which is considered to be fairly low for a condensation polymerization reaction when compared to the polydispersity of products of a typical condensation polymerization.[25]

Figure 3.30 shows a typical example of the SEC results obtained using a dual RI and UV detector system for F-3 copolymers. The UV peak is shifted to the left of the RI peak similar to in the cases of the C-2, E-2 and E-4 copolymers. This shows that the PBCH segment is not well dispersed over the molar mass distribution of the copolymers.

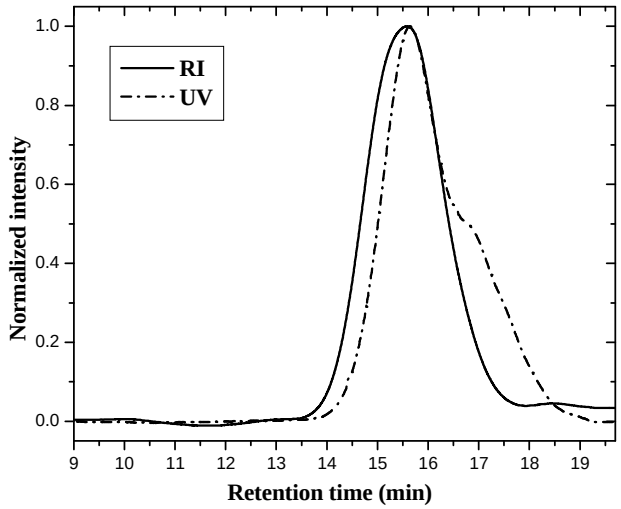

Figure 3.30: Typical SEC results for F-3 copolymers obtained using RI detector and UV detector at 310 nm.

Figure 3.31 shows the GEC results of the PDMS-br-PBCH copolymers (series F) after copolymer purification.

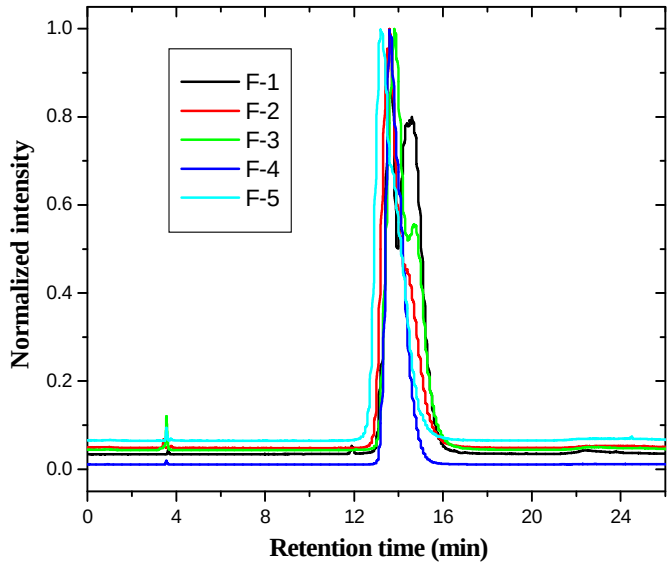

Figure 3.31: GEC results of PDMS-br-PBCH copolymers (Series F) with 10 wt % PDMS content, 2000 g/mol PDMS M_n, and various degrees of branching (see Section 3.2.5.5).

The GEC results show, in addition to the small shift between the copolymers peaks, each single copolymer eluted peak seems to consist of several overlapping peaks. The overlapping (multiple) peaks become more recognized as the branching degree increases. These multiple peaks are due the difference in the PDMS content in the copolymer chains and possibly also

as a result of the branching point and the end group effect (mainly OH). Both the branching point and the end group effect increases as the branching degree increases, leading to an increase in the polarity of the copolymer and thus a shift in the elution time of the copolymer to higher values. Any branching PBCH homopolymers formed must elute after liner PBCH homopolymer (after 18 min). The elution peak of the branched copolymer in the GEC chromatogram shows broader distribution than that for both the PDMS-s-PBCH copolymers series (series C and series D). There are very small amounts of PBCH residual present at about 18 min, which can be considered negligible in comparison to the copolymer present. The broadness in the copolymer peak could be attributed to the branching effect and the end group in the branches, in addition to the large polydispersity of the copolymers in this series when compared with the polydispersity of the copolymers in the C series.

3.4 Conclusions

Five different molar masses of PDMS oligomers terminated with amine groups were successful synthesized via equilibrium ring-opening polymerization of D_4. The chemical structure of the PDMS oligomers was confirmed by both ^{1}H-NMR and FTIR. The PDMS oligomers were successful used in polycondensation in the melt state to prepare PDMS-PES copolymers with relatively high molar masses. The syntheses of PDMS-PES copolymers was carried out using a one-prepolymer method in a one-step reaction, to prepare PDMS-PBA segmented copolymers, and a two-step reaction to prepare PDMS-PBCH segmented and branched copolymers. The PDMS-PBCH segmented and branched copolymer synthesis using a one-prepolymer method, involves, first, end capping the PDMS oligomer with an excess of ester end groups, followed by reacting with an excess diol. The end capping reaction was confirmed using FTIR. A two-prepolymer method also successfully used to prepare alternating PDMS-s-PBCH copolymer, using PDMS and PBCH as prepolymers. Copolymer molar masses had a great dependency on the ability to achieve high vacuum in the final step of the reaction sequence, to enable removal of the excess diol. This forced the reaction to completion and, with carefully controlled stirring rates and high temperatures, high molar masses were achieved. Any unreacted PDMS in the soluble segmented and the branched copolymers were removed by precipitation techniques. The copolymer formation and the homopolymers extraction were confirmed by developing a gradient solvent profile using GEC techniques.

The chemical composition of the obtained copolymers was estimated by ^{1}H-NMR, and the average molar masses for all the copolymers and the contraction factor for the branched copolymers were measured by SEC and SEC-MALLS respectively. The results showed that the percentage of unreacted PDMS increases with an increase the PDMS feed content, for both types of polyester, with higher unreacted PDMS for the PDMS-s-PBA series than for the PDMS-s-PBCH series. The unreacted PDMS also increases with an increase in the molar mass of the PDMS segment. It was also found that the contraction factor decreases with an increase the branching agent content in the feed, but no clear effect on the PDMS incorporation can be observed. All the copolymer series did, however, show good PDMS incorporation with a higher PDMS feed ratio. Although the copolymer molar mass depends greatly on the ability to achieve high vacuum in the final step of the reaction, the M_n for PDMS-s-PBCH was larger than that for PDMS-s-PBA copolymer; however, no clear effect or change in the M_n of the copolymers was detected due to a change in the PDMS content or the molar mass of the PDMS segment or the branching agent content.

The polyester content along the molar mass distribution of the copolymers was monitored by SEC using a combined a UV and RI detectors. The copolymers showed random distribution for the PES segment over the entire molar mass distribution. The distribution of the chemical composition was further investigated using GEC, for all the copolymers series (A–F) in this chapter. Selected samples from series C, D and E were investigated using SEC-LC-transform and the results presented in Chapter 7.

3.5 References

1. Elvers, B.; Hawkins, S.; Schulz, G., Polyesters. In *Ullmann's Encyclopaedia of Industrial Chemistry*, Fifth ed.; Köpnick, H.; Schmidt, M.; Brügging, W.; Rüter, J.; Kaminsky, W. (Eds), VCH Verlagsgesellschaft Weinheim, Germany, 1992; Vol. A21, pp 227-251.

2. Cai, D. K.; Neyer, A.; Kuckuk, R.; Heise, H. M. *Optical Materials* 2008, 30(7), 1157-1161.

3. Brown, D. A.; Price, G. J. *Polymer* 2001, 42(10), 4767-4771.

4. Mazurek, M. H.; Robert, H. C.; Michael, D.; Mingos, P., Silicones. In *Comprehensive Organometallic Chemistry III*, First ed.; Elsevier, Oxford, 2007; pp 651-697.

5. Ehsani, M.; Borsi, H.; Gockenbach, E.; Morshedian, J.; Bakhshandeh, G. R. *European Polymer Journal* 2004, 40(11), 2495-2503.

6. Goodman, I., Polyester. In *Encyclopaedia of Polymer Science and Engineering*, Second ed.; Kroschwitz, J. I. (Ed.), John Wiley and Sons, United States, 1989; Vol. 12, pp 1-75.

7. McKee, M. G.; Unal, S.; Wilkes, G. L.; Long, T. E. *Progress in Polymer Science* 2005, 30(5), 507-539.

8. Pang, K.; Kotek, R.; Tonelli, A. *Progress in Polymer Science* 2006, 31(11), 1009-1037.

9. Kiefer, L. A.; Yoon, T. H.; Glass, T. E.; Jayaraman, S. K.; McGrath, J. E. *Journal of Polymer Science, Part A: Polymer Chemistry* 1997, 35(16), 3495-3506.

10. O'Malley, J.; Pacansky, T. J.; Stauffer, W. *Macromolecules* 1977, 10(6), 1197-1199.

11. Grulke, A. E., Solubility parameter values. In *Polymer Handbook*, Fourth ed.; Brandrup, J.; Immergut, E. H.; Grulke, E. A. (Eds), John Wiley and Sons, New York, 1999; Vol. VII, pp 682-683.

12. Armarego, W. L. F.; Perrin, D. D., *Purification of Laboratory Chemicals*, Fourth ed.; Reed Educational and Professional Publishing, Oxford, 2000; p 16.

13. Yilgör, I.; McGrath, J., Polysiloxane containing copolymers: A survey of recent developments. In *Polysiloxane Copolymers/Anionic Polymerization*, Springer, Berlin / Heidelberg, 1988; Vol. 86, pp 1-86.

14. Bowens, A. D. Synthesis and characterization of poly(siloxane imide) block copolymers and end-functional polyimides for interphase applications. PhD in Chemistry, State University Virginia, United States, 1999, p 97.

15. David, P. W. Polydimethylsiloxane containing block copolymers: synthesis and characterization of alternating poly(arylene ether phosphine oxide)-b-siloxane and segmented nylon 6,6-b-siloxane copolymers. PhD in Chemistry, State University Virginia, United States, 2001, pp 129-133.

16. Auman, B. C.; Percec, V.; Schneider, H. A.; Cantow, H.-J. *Polymer* 1987, 28(8), 1407-1417.

17. Thomas, M. J. K., Ultraviolet and visible spectroscopy In *Analytical Chemistry by Open Learning*, Second ed.; Ando J.D (Ed.), John Wiley and Sons, New York, 1996; pp 172-175.

18. Günther, K., *Characterization of Plastics by Physical Methods: Experimental Techniques and Practical Application* First ed.; Handser Publishers, New York, 1986; p 173.

19. Honeycutt, J. D. *Computational and Theoretical Polymer Science* 1998, 8(1-2), 1-8.

20. Jeffrey, M. Synthesis and characterization of cycloaliphatic and aromatic polyester-polydimethylsiloxane segmented copolymers. MSc in Chemistry, State University Virginia, United States, 1997, p 77.

21. Trathnigg, B.; Feichtenhofer, S.; Kollroser, M. *Journal of Chromatography A* 1997, 786(1), 75-84.

22. East, A. J., Polyester fibres. In *Synthetic Fibres: Nylon, Polyester, Acrylic, Polyolefin*, First ed.; McIntyre, J. E. (Ed.), Woodhead Publishing Limited and CRC press LLC, Cambridge, England, 2005; pp 103-108.

23. Riechmann, T.; Völker, S., Poly(ethylene terephthalate) polymerization mechanism, catalysis, kinetics, mass transfer and reactor design In *Modern Polyesters: Chemistry and Technology of Polyester and Copolyesters*, Scheirs, J.; Long, E. T. (Eds), John Wiley and Sons, England, 2003; pp 48-65.

24. Billmeyer Jr, W. F., The size and weight of polymer molecules. In *Introduction to Polymer Science and Technology: an SPE Textbook*, First ed.; Kaufman S.H.; Falcetta J.J. (Eds), John Wiley and Sons, New York, 1977; pp 175-176.

25. Kricheldorf, H. R. *Macromolecular Symposia* 2003, 199(1), 1-14.

Chapter Four

Morphology of Semi-crystalline Polydimethylsiloxane-Polyester Copolymers: 1 Effect of the PDMS Content and the Polyester Type

Abstract

The morphology of two series of semicrystalline polydimethylsiloxane-polyester segmented (PDMS-s-PES) copolymers with varying polydimethylsiloxane (PDMS) content was investigated. One series was based on polybutyleneadipate (PBA) as the polyester segment and the other was based on a polybutylenecyclohexanedicarboxylate ester (PBCH) segment. The copolymers were characterized using DMA, DSC and WAXD. The microscopic surface morphology and the microscopic bulk morphology were investigated using AFM and TEM, respectively. The effects of the polyester type and the PDMS content on the crystallinity degree as well as the copolymer surface and bulk morphology at room temperature were investigated for each series. DSC and WAXD results showed the ability of the copolymers to crystallize, to various degrees, depending on the polyester type and the PDMS content. The results showed that the PDMS content had a greater influence on the crystallinity degree in the PDMS-s-PBCH (cycloaliphatic) copolymers series than in the PDMS-s-PBA (aliphatic) copolymers series. In the copolymers with a low PDMS content the AFM images showed spherulitic crystal morphology and evidence of PDMS nano-domains in between the crystal lamellae of the ester phase on the copolymer surface. A heterogeneous distribution of the PDMS domains was also observed for these copolymers in the bulk morphology as a result of this segregation between the polyester lamellae. All the copolymers, in both series, showed microphase separation as a result of the incompatibility between the PDMS segment and the polyester segment. Three types of surfaces and bulk morphologies were observed: spherical microdomains of PDMS in a matrix of polyester, bicontinuous double diamond type morphology, and spherical microdomains of polyester in a matrix of PDMS as the PDMS content increases. Furthermore, the adhesive force and surface roughness of the copolymers were measured using the pulsed-force mode of the AFM. Results correlated to the composition of the copolymers.

Keywords: segmented copolymer morphology; microphase separation; AFM; TEM.

4.1 Introduction

The morphology of a multiphase polymer system plays an important role in determining the final properties of the polymers. This area of polymer science has attracted wide interest among many researchers who have tried to elucidate the details of microstructure and superstructure using a variety of techniques. The number of investigations dealing with the synthesis and characterization of multiblock copolymers with crystalline and amorphous segments has rapidly increased during the last years.[1-7]

Semicrystalline copolymer morphology has recently received much attention largely because of the ability of these copolymers to exhibit considerable morphological richness.[8-11] This richness of morphology arises from two main factors. The first is the driving force for microphase separation between unlike segments, especially in the melt. This favours the formation of nano-scale domains such as lamellae, spheres and cylinders. The second factor is the driving force for crystallization of one segment. This favours the formation of alternating amorphous and crystalline layers.[12] When the noncrystallisable segment is glassy during crystallization ($T_g > T_c$) the crystallization occurs within the nano-scale domains as a result of the microphase separation.[12] On the other hand, when the amorphous matrix is soft or rubbery during crystallization ($T_g < T_c$) these two forces compete and, in this case, crystallization often occurs with little morphological constraint. This enables the crystallisable segment to "breakout" and the crystallization overrides any previous melt structure, usually forming lamellar structures and (in many cases) spherulites, depending on the composition. However, if the strength of the microphase separation is more than the strength of the crystallization, then the crystallization can be only confined to within spherical, cylindrical or lamellar nano-scale domains. This is mainly observed in strongly segregated systems with a rubbery block.[12-15]

PDMS-s-PES copolymers are semicrystalline copolymer systems that consist of amorphous–crystalline multi-blocks, where the T_g of the PDMS amorphous segment is lower than the T_c of the crystalline polyester segment.[3] These materials can be regarded as thermoplastic elastomers due to the microphase separation of the soft siloxane blocks and the hard polyester blocks. The copolymers demonstrate good mechanical properties, such as impact shock resistance, even in low temperature environments, as a result of the low T_g of the PDMS segment. In addition, the films are easily compression moulded as a result of the relatively low T_m of the copolymer. Moreover, these materials are expected to be potentially useful in

outdoor applications due to their UV stability and the hydrophobicity of the PDMS segment.[1,2] These copolymers have, however, not yet been tested for durability towards ageing and weather effects.

The extremely non-polar nature of the PDMS structure combined with its weak intermolecular interaction leads to the creation of a polymer phase that is both thermodynamically and mechanically incompatible,[16] not only with the polyester segment but also with virtually all other polymeric systems. This leads to the formation of a multiphase morphology, regardless of whether the other segment is amorphous or semicrystalline. Another important factor to be considered in PDMS copolymers is that the glass transition temperature of the PDMS segment in the copolymer is extremely low. PDMS should behave like a non-polar viscous liquid at room temperature (at which most characterizations are conducted).[17] Therefore, the low glass transition temperature also provides ideal conditions for the formation of phase-segregated polymer morphologies. The degree of phase segregation between the hard and soft segments depends on their molar masses, and the interaction of the segments with themselves and with each other. Moreover, the interaction between the hard segments depends on the symmetry of the monomer in the polyester segment. Therefore, a chain extender having a more symmetrical structure will enhance the formation of organized structures, resulting in a more complete phase separated morphology.[18] The morphology of segmented PDMS-PES copolymers is, therefore, very complicated, not only because of their multiphase structure but also because of other physical phenomena, such as crystallization of the polyester segment.

Only a few studies of the morphology of amorphous–crystalline multi-block copolymers have been reported. Most of these studies have been confined to the use of visual inspection of the copolymers using various microscopic techniques. Among the few copolymers that have been studied are the PDMS-PES segmented copolymers.[3,18] Miroslawa[3] recently reported on the spherulitic crystal order of polydimethylsiloxane-polybutyleneterephthalate segmented copolymers. He used thin, quenched cooled films from the melt, and investigated the morphology using polarizing optical microscopy (POM). More recently, Childs et al.[18] used atomic force microscopy (AFM) to investigate the surface morphology of polycaprolactone-b-polydimethylsiloxane-b-polycaprolactone block copolymers. They reported that crystal spherulite structures could be very clearly observed using the AFM phase images of the surface. Although the surface morphology of polybutyleneadipate (PBA) aliphatic

homopolyester has been studied using POM[19] and AFM,[20] as recently reported in literature, to date no reports of a systematic investigation of the morphology of PDMS-PES copolymers with either cycloaliphatic or aliphatic polyester segments have been found. A study of a systematic series of these copolymers will contribute to an understanding of the interrelationship between the phase separation and crystallization of the polyester segments.

The aim of the research described in this chapter is, therefore, to systematically investigate the surface and bulk morphology of two series of PDMS-PES segmented copolymers: polydimethylsiloxane-polybutyleneadipate (PDMS-s-PBA) and polydimethylsiloxane-polybutylenecyclohexanedicarboxylate (PDMS-s-PBCH) segmented copolymers. This will allow for a study of the effect of an aliphatic and cycloaliphatic polyester segment on the copolymer morphology. Thus, two series of PDMS-s-PBA and PDMS-s-PBCH copolymers with a constant PDMS segment length (2000 g/mol) and varying PDMS content, and the homopolymers PBA and PBCH, were synthesized via a transesterification reaction under vacuum conditions following the general procedure proposed by Kiefer and coworkers[2] (described and discussed in Chapter 2).

The copolymers were characterized using DMA, DSC and WAXD to determine their glass transition temperatures (T_g), melting points (T_m) and, degree of crystallinity. The effects of the PDMS content and polyester type on the copolymers, surface morphology of thin films as well as the bulk morphology of both copolymer series were investigated using AFM and TEM, respectively.

4.2 Experimental

4.2.1 Copolymers

Two series of copolymers, PDMS-s-PBA and PDMS-s-PBCH, were synthesized via a condensation reaction in the melt state. The chemical and the molar mass characteristics of these copolymers are determined as described in Sections 3.3.2.1 and 3.3.2.2 and summarized in Table 4.1. The purity of the copolymers was also confirmed by gradient elution chromatography (see Chapter 3).

Table 4.1: Chemical compositions and average molar masses of PBA and PBCH homopolymers, and PDMS-s-PBA and PDMS-s-PBCH copolymers, prepared using various concentrations of PDMS (2000 g/mol)

Sample	PDMS in feed (wt %)	PDMS in the copolymer[a] (wt %)	Mw[b] (g/mol)	Mn[b] (g/mol)	Mw/Mn
PBA	0	0.00	15795	8143	1.94
B-1	5	4.57	11239	6314	1.78
B-2	10	8.97	17700	9415	1.88
B-3	25	21.70	18066	9819	1.84
B-4	40	34.20	14310	8131	1.66
B-5	60	51.10	12568	7141	1.76
PBCH	0	0.00	27719	17171	1.66
C-1	5	4.74	25990	16665	1.76
C-2	10	9.20	27719	17171	1.62
C-3	25	22.70	34502	20239	1.71
C-4	40	35.76	32720	18568	1.70
C-5	60	52.10	31204	16860	1.85

[a] Measured by ^{1}H-NMR

[b] Measured by SEC

4.2.2 Characterization

4.2.2.1 Dynamic mechanical analysis (DMA)

DMA analysis of the copolymers was carried out on a Perkin Elmer 7e using the thin-film extension mode. Liquid nitrogen was used to cool the samples to –150 °C. The frequency was 1 Hz and the heating rate was 5 °C/min. The polymer samples were prepared by casting 10 wt % copolymer solutions in THF solvent on mica substrates. The thickness of the samples was about 0.5 mm.

4.2.2.2 Differential scanning calorimetry (DSC)

DSC analyses of the various copolymers were carried out with a TA Instruments Q100 DSC system. The DSC apparatus was calibrated by measuring the melting temperature of indium metal according to a standard procedure. All measurements were conducted under a nitrogen atmosphere flow, and at a purge gas flow rate of 50 mL/min. Polymer samples of 1.0–2.0 mg were cooled in aluminum pans from 25 to –30 °C at a rate of 10 °C/min, held isothermally at –30 °C for 5 min, and then heated further at 10 °C/min. The melting curve was recorded. The melting temperature (T_m) was determined from the obtained curve, and the area under the crystalline melting peak (ΔH_m) was estimated. The ΔH_m is related to the degree of crystallinity.

4.2.2.3 Wide-angle X-ray diffraction (WAXD)

WAXD was performed at iThemba LABS (South Africa) on a Bruker AXS D8 ADVANCE diffractometer at room temperature, with filtered CuKα radiation, using a LynxEye position sensitive detector. All samples were scanned at diffraction angles (2θ), ranging from 5° to 50°, with a step size of 0.02°. The samples were prepared by casting films of 10 wt % copolymer solutions in THF on mica substrates to form thin films with a thickness of about 0.5 mm. From the WAXS data, the percentage of crystallinity was calculated by peak deconvolution and subsequent determination of the relative areas under the amorphous halo and the crystalline peaks of the X-ray diffraction scan. The ratio of the area under the crystalline peaks (I_c) to the total (amorphous + crystalline) area (I_{tot}) gave the degree of crystallinity (ω_m).

4.2.2.4 Atomic force microscopy (AFM)

AFM images were obtained on a multimode AFM model no. MMAFMLN, with a Nanoscope IIIa controller from Veeco, operating in non-contact mode, and using a low resonance frequency silicon cantilever with a resonance frequency of about 60 kHz and a spring constant of k = 50 N/m. The substrate containing the polymer samples was attached to the sample holder with double-sided adhesive tape. All experiments were carried out under ambient conditions. The scan rate was set in the range of 0.5 to 0.7 Hz. Topography and phase images were captured simultaneously for the tapping mode.

All AFM images were enhanced in the Veeco imaging software program and subjected to a plane fitting and flattening procedure, which eliminates the image bow resulting from non-linear scanner movement. Additionally, digital filtering was carried out to remove noise and clarify the structures present in the image. Since the filtering is a very sensitive process that can generate unreal features or remove existing features, the filtering was kept to a minimum. Only noise and image artifacts were eliminated. The typical sequence of digital filtering applied was: auto-flattening, planefit, and lowpass filtering. Auto-flattening eliminates the image bow by calculating a least square fitted, second-order polynom for each scan line, and subtracting it from the scan line. The planefit removes the effect of a skew sample by calculating a best, second-order polynomial planefit and subtracting it from the image. Lowpass filtering is used to remove high frequency noise, such as spikes, by replacing each data point in the image with a weighted average of the points in a 3 x 3 matrix surrounding the point.

AFM samples were prepared as ultra-thin films by the solution casting method on mica wafers (1 x 1 cm^2). One drop of 0.5 wt % copolymer in THF was placed on the mica plate and then covered with another mica plate to spread the solution between the two mica plates. The two mica plates were slid against each other in opposite directions to form an ultra-thin film of 10 to 5 μm. The films were dried at room temperature for 24 h.

The pulsed-force mode of the AFM[21] was used to measure the surface energy by measuring the adhesive force between the AFM tip and the copolymer surfaces. In this case the AFM was operated in contact mode, and at the same time a sinusoidal modulation was applied to its Z-piezo. Each image was recorded for a scan size of 2 x 2 μm^2. The same tip was used to measure all the adhesive forces in order to avoid inconsistencies due to a variation in tip radii or spring constants. The adhesive force (F) was calculated using the following equation:

$$F = V \times k \times S \qquad \text{[Eq 4.1]}$$

where V is the average voltage value from the adhesion images, k is the spring constant (= 2.8 N/m) of the cantilever and S (= 500 nm/V) is the sensitivity of the photodiode. The adhesive force was determined as an average of five adhesion images; each image of these images consists of 256 x 256 single measurements in the observed areas, and all the measurements were carried out under the same conditions.

The surface roughness was measured from the topography images associated with the adhesion images in the pulsed force mode. The mean roughness (Ra) is the arithmetic average of the surface height deviation from the mean plane.[22] Ra was calculated according to the following equation:

$$Ra = 1/n \left(\sum_{i=1}^{n} | Zi | \right) \qquad \text{[Eq 4.2]}$$

The surface roughness of the copolymers was measured as an average of five values taken at different places on the surface of each segmented copolymer, over an area of 2 x 2 μm^2.

4.2.2.5 Transmission electron microscopy (TEM)

TEM experiments were performed on the ultra-thin films of PDMS-PES copolymers using a JEOL 200 CX instrument (University of Cape Town). The copolymer films were prepared, using a solvent casting technique, from 10 wt % copolymer in THF, followed by cryo ultra-microtoming of very thin slices, cut at –100 °C to a thickness of about 40–60 nm.

4.3 Results and discussion

4.3.1 Copolymer characterization

Multicomponent PDMS-PES copolymers are expected to show a multiphase structure of a soft amorphous phase of PDMS and relatively less soft phase of polyester, in addition to the PES crystalline hard phase. DMA was used to determine the T_g values of both amorphous phases. Table 4.2 shows the T_g values of the PDMS-PES copolymers with different PDMS content. Two glass transition temperatures were observed for all the copolymers. The fact that the T_g values of the PBA and PBCH homopolymers are –50 °C[23] and 15 °C,[2] respectively, and the T_g value of the PDMS homopolymer is –123 °C,[17] suggests that the higher T_g (T_gH) in the copolymer is due to the PES segments and the lower T_g (T_gL) due to the PDMS segment. In the PDMS-s-PBCH series a secondary transition was observed at about –50 °C. This was very clear for copolymers with a low PDMS content. A secondary transition was also observed for the PBCH homopolymers. This transition is related to the polyester segment, as reported by Kiefer and coworkers.[2] The presence of two T_g values implies a segregated morphology on the micro or nano-scale. The low T_g values of the PDMS-PES copolymers (except for B-1 and C-1, Table 4.2) remained more or less constant. The independence of the T_g values indicated that the PDMS-PES copolymers exhibited a

high degree of phase separation. The nature of the phase separated morphology was investigated further using TEM and AFM.

Table 4.2: Glass transition temperature (T_g), melting temperature (T_m) and the degree of crystallinity of PBA and PBCH hompolymers, and PDMS-s-PBA and PDMS-s-PBCH copolymers, with different polyester content

Sample	Polyester (wt %)	T_gL^a (°C)	T_gH^b (°C)	T_m (°C)	ΔH_m (J/g)	ΔH_{mPES} (J/g)	Crystallinity $\omega_m{}^c$ (%)	Crystallinity ω_{mPES} (%)
PBA	100.00	-	–66	58.1	53.4	53.4	43.6	43.6
B-1	95.43	-	–68	57.7	50.4	52.8	39.5	41.4
B-2	91.03	–118	–73	56.7	43.2	47.5	35.8	39.3
B-3	78.30	–119	–73	55.9	21.9	27.9	30.9	39.5
B-4	65.80	–123	–79	54.7	18.8	28.6	23.9	36.3
B-5	48.90	–123	–82	54.2	4.5	9.2	16.2	33.1
PBCH	100.00	-	15	67.7	79.1	79.1	31.4	31.4
C-1	95.26	–94	12	62.2	42.3	44.4	23.4	24.6
C-2	90.80	–115	5	61.1	28.4	31.3	16.4	18.0
C-3	77.30	–118	–5	60.9	15.1	19.5	14.1	18.2
C-4	64.24	–123	–3	57.2	12.2	18.9	9.6	14.9
C-5	47.90	–121	–7	55.7	1.5	3.1	6.1	12.7

[a] The lowest glass transition temperature measured from the tan δ curve

[b] The highest glass transition temperature measured from the tan δ curve

[c] The degree of crystallinity measured from WAXD data

Table 4.2 also shows the results of the DSC analyses of both copolymer series. Analyses were carried out in order to determine the effect of the PDMS content on the melting temperature and the degree of crystallinity in the samples. The degree of crystallinity is related to the enthalpy of melting (ΔH_m), which is determined from the area under the melt peak in the DSC thermogram. Table 4.2 shows that the polymer crystallinity decreases with an increase in the weight fraction of PDMS in the copolymer. Similar results were obtained

for the melting point. The enthalpy of melting based on the polyester content (ΔH_{mPES}) was calculated using the weight fraction of the polyester in the copolymers and the enthalpies of melting (ΔH_m). The results are included in Table 4.2. It is clear that for both series of copolymers the crystallizability of the polyester decreased as the PDMS content increased.

WAXD analysis was also used to determine the actual crystallinity degree, and to provide more information about the changes in the copolymer crystal regions and in the crystallinity types. These results are illustrated in Figure 4.1 and summarized in Table 4.2.

Figure 4.1 shows the WAXD spectra for the PDMS and homopolymers of the polyesters as well as for the PDMS-s-PBA and PDMS-s-PBCH copolymers series. Copolymer samples with a PDMS content of more than 10% showed a characteristic amorphous halo (small shoulder) at 2θ = 12.5°. This is related to the PDMS amorphous region. It is clearly observed for the PDMS homopolymer in Figure 4.1(b) and the insert in Figure 4.1(a). The position of this halo does not change in the copolymers, confirming the formation of relatively pure PDMS micro-domains. This phenomenon has been reported for other PDMS copolymers such as PDMS–polyurethane segmented copolymers.[24]

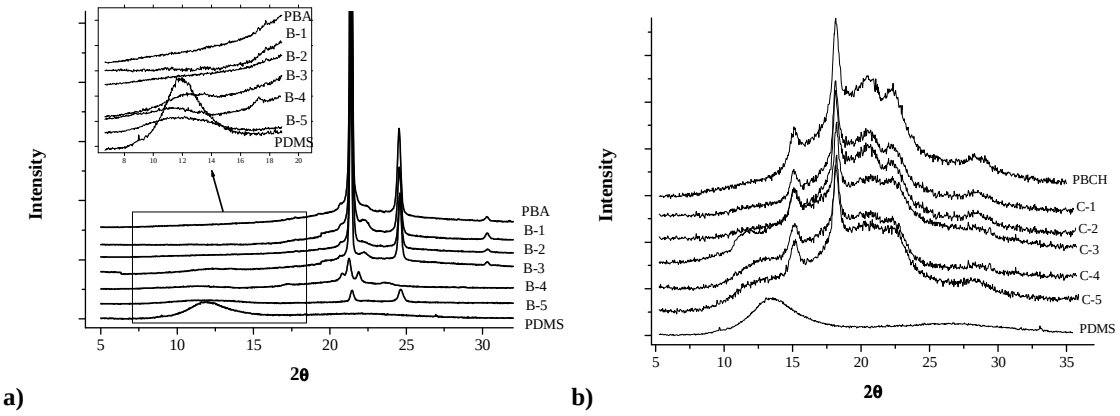

Figure 4.1: WAXD profiles of (a) PDMS and PBA homopolymers and PDMS-s-PBA copolymers with different PDMS content, including magnification of the region from 2θ = 6° to 18°, and (b) PDMS and PBCH homopolymers and PDMS-s-PBCH copolymers with different PDMS content.

Figure 4.1(a) shows that the WAXD spectra of PBA and the PDMS-s-PBA copolymers have very sharp peaks at 21.8, 24.5 and 30.3°. On the other hand, no very sharp peaks were observed in Figure 4.1(b) for PBCH and the PDMS-s-PBCH copolymers, at 15.3, 18.2, 20.5, 22.1 and 28.6°. The fact that the same peaks were observed within each series indicates that the polyester segments have more or less the same crystalline structure in the homopolymers

as in the respective copolymers. The decrease in intensity of crystallinity peaks as the PDMS content increases indicates that the total degree of crystallinity decreases for the copolymers. The percentage crystallinity (ω_m) was calculated by peak deconvolution, and the subsequent ratio of the area under the crystalline peaks (I_c) to the total (amorphous + crystalline) area (I_{tot}) gave the degree of crystallinity (ω_m), according to the following equation:

$$\omega_m(\%) = (I_c / I_{tot}) \times 100 \qquad \text{[Eq 4.3]}$$

Results of calculations from the WAXD data of the thin films of the copolymers are tabulated in Table 4.2. There was a significant reduction in crystallinity of the copolymers as the PDMS content increased in both copolymer series. This is similar to what was revealed by the DSC data. The degree of the crystallinity based on the polyester content (ω_{mPES}) was calculated using the degree of crystallinity (ω_m) and the polyester weight fraction. The obtained values are tabulated in Table 4.2. It is clear from the ω_{mPES} values that there was a decrease in crystallinity of the polyester segments from 43.60% for PBA to 33.12% for the B-5 copolymer and from 31.40% for PBCH to 12.73% for the C-5 copolymer. In all cases, for the copolymers with similar PDMS content, the PDMS-s-PBCH copolymer series showed a greater decrease in polyester crystallinity degree relative to the PDMS-s-PBA copolymer series. The PDMS content, therefore, has a greater influence on the polyester crystallinity in the cycloaliphatic series compared to the aliphatic series. This may be attributed to one of the following reasons, or a combination of both. First the low T_g (–66 °C) of the PBA segment allows more PBA segments to arrange in the crystalline phase than the higher T_g PBCH segment (15 °C). This large difference in chain mobility can result in decreased PBCH segment crystallinity. Second, the large difference in polarity (calculated using the group contributions method)[25] between the PDMS segment (7.34 $(cal/cm)^{1/2}$) and the PBA segment (8.84 $(cal/cm)^{1/2}$), compared with the PBCH segment (7.94 $(cal/cm)^{1/2}$), could, during the copolymerization, lead to a broader PBCH segment distribution in the copolymer chains and therefore a higher degree of mixing in the PDMS-s-PBCH copolymers series than that in the PDMS-s-PBA copolymers series.

4.3.2 Microscopic surface morphology of the copolymers

The surfaces of thin films of the homopolymers and the segmented copolymers (prepared by the casting method) were imaged via tapping mode AFM at ambient temperature. The resulting topography, or height images and phase images, are shown in Figures 4.2–4.4 and

Figures 4.6–4.7. For the sake of the simplicity of discussion, the starting PDMS content is used in the text and, the actual copolymer content is given in Table 4.1. Figure 4.2 shows the topography (left images) and phase images (right images) for the PBA (a, b) and PBCH (c, d) homopolymers (notice the scale in the AFM images are chosen to best represent to the observed morphology).

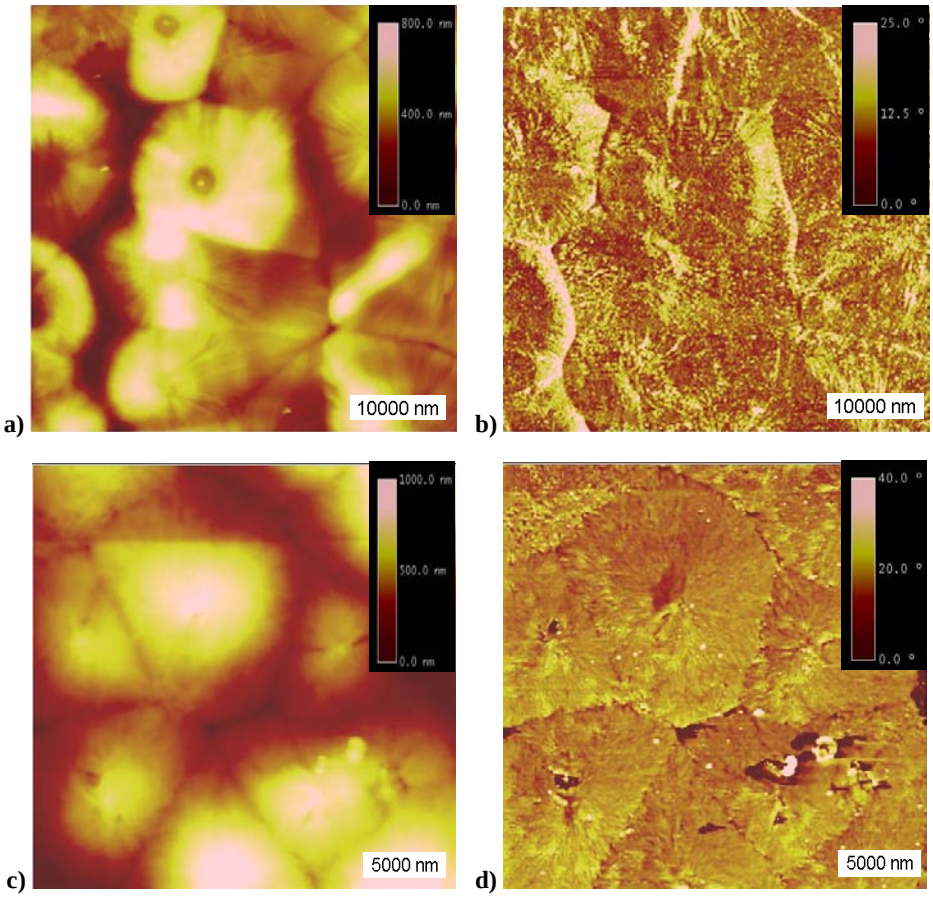

Figure 4.2: Topography and phase AFM images of thin films of polyester homopolymers: (a and b) aliphatic polyester (PBA) and (c and d) cycloaliphatic polyester (PBCH).

Both polymers show clear semicrystalline spherulitic morphology. Although it is possible to distinguish the spherulitic structures from the height images, it is clear that the phase images provide more detailed information about the spherulitic crystal structure than the height images. This is especially true in the case of the PBCH homopolymer. The height images obtained using the tapping mode are not 100% reliable for copolymers with different segments or blocks because the relative contrast of the different blocks depends sensitively on the driving frequency in the height images, which does not exist in the phase images.[26, 27] However, the information obtained from the phase images complements the information

obtained from the height images. Most of the discussion will therefore focus on the phase images. Similar types of spherulitic crystal structure to those observed in this study for the PBA homopolymer have been reported by Frömsdorf et al..[20]

The surface morphologies of the PDMS-s-PBA and PDMS-s-PBCH copolymers with 5 wt % PDMS content are shown in Figure 4.3.

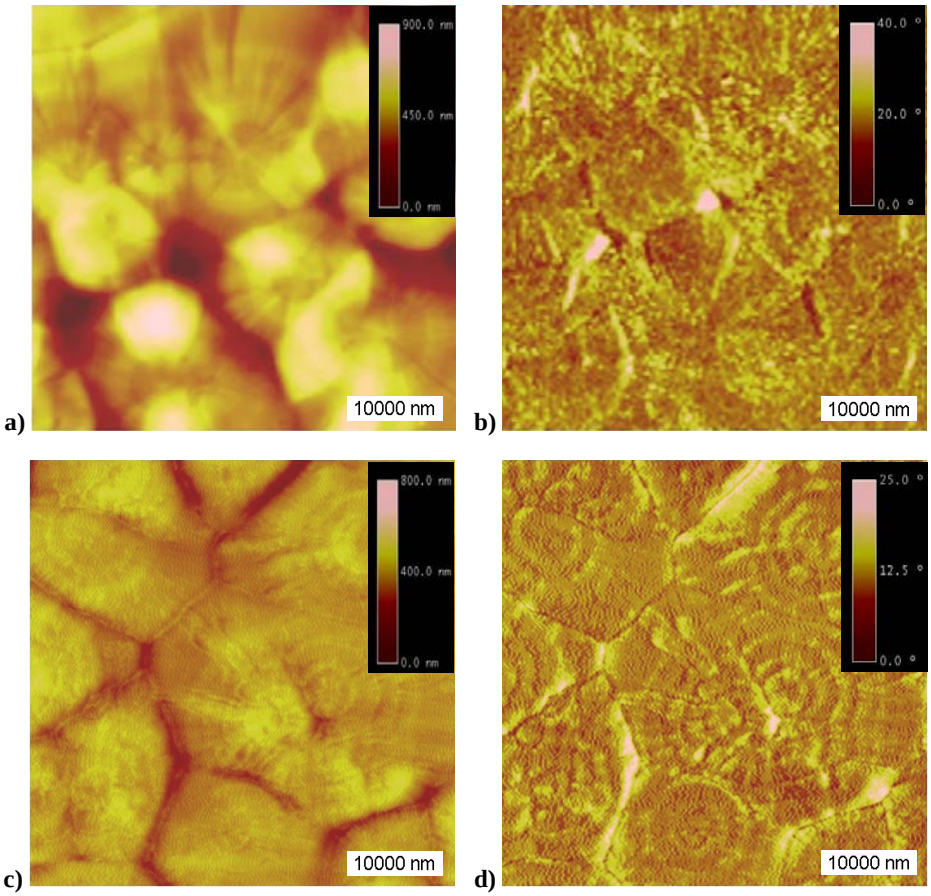

Figure 4.3: Topography and phase AFM images of thin films of polydimethysiloxane–polyester copolymers with 5 wt % PDMS (M_n PDMS segment 2000): (a and b) PDMS-s-PBA and (c and d) PDMS-s-PBCH.

The AFM phase images show well-defined spherulitic crystal morphology for both the PDMS-s-PBA (B-1) and the PDMS-s-PBCH (C-1) copolymers. These spherulites seem to grow from primary nuclei and then develop as globular aggregates. The size of the spherulites is relatively large: the diameters of the spherulites for both copolymers are in the range 20–30 μm. This variation in the spherulites size (or diameter) and the particular curvature of the frontier between neighbouring spherulites indicates that the spherulites are not nucleated simultaneously.[28] The appearance of the spherulite crystal structure for these

copolymers is probably due to a low PDMS content. The longer polyester segments in the copolymers allow the chain to fold, forming a lamella crystal structure. A similar type of morphology to that observed for PDMS-PES copolymers in this study has been reported by Miroslawa for polydimethylsiloxane–polybutyleneterephthalate segmented copolymers, using POM.[3]

Figure 4.4 shows the AFM phase images obtained for the homopolymer and the copolymer surfaces using a high AFM resolution or higher magnification. This figure shows that the spherulites comprise close-packed lamellae. The slight variation in the brightness of bright region (polyester phase) can be attributed either to the changes in the height of the lamellae or due to the presence of both crystalline and amorphous areas in the spherulitic crystal structure. By comparing the lamellae arrangement and thickness for PBA and PBCH (Figures 4.4(a) and (c), respectively) one can see that PBCH has a larger lamella thickness than PBA. This difference in the lamella thickness is believed to be kinetically selected as a result of the differences between the PBA and the PBCH polyesters in terms of the crystallization rate, state of entanglement, molar masses and the interfacial energy.

In the case of the PDMS-s-PBA and PDMS-s-PBCH copolymers small spherical domains were detected in-between the lamellae inside the spherulitic crystal structure, as shown in Figure 4.4(b) and (d). The average size or diameter of these domains is approximately 25 ± 5 nm for PDMS-s-PBA copolymers and 30 ± 5 nm for PDMS-s-PBCH copolymers. On the other hand, in Figure 4.4(a) and (c) no domains are seen for PBA and PBCH homopolymers. Therefore, it is believed that these domains in the copolymer are PDMS segments segregated to form PDMS domains or islands (dark spots in the phase images) in the polyester matrix (the bright region in the phase images). In literature, two different theories have been suggested to interpret phase images in terms of sample properties. The first[27-30] relates the contrast of the phase images to surface stiffness and the second[31-33] relates the contrast of the phase images to the energy dissipation at the AFM tip and the sample surface interface. However, both of these theories agree that different components in a heterogeneous material or system, such as PDMS-PES copolymer systems, can be distinguished from the phase images. PDMS and polyester are different both chemically and mechanically, and a combination of both these types of differences leads to variations between the PDMS regions and polyester regions in terms of the elasticity or viscoelasticity properties, as well as in the energy dissipation between the sample surface and the AFM tip interface.

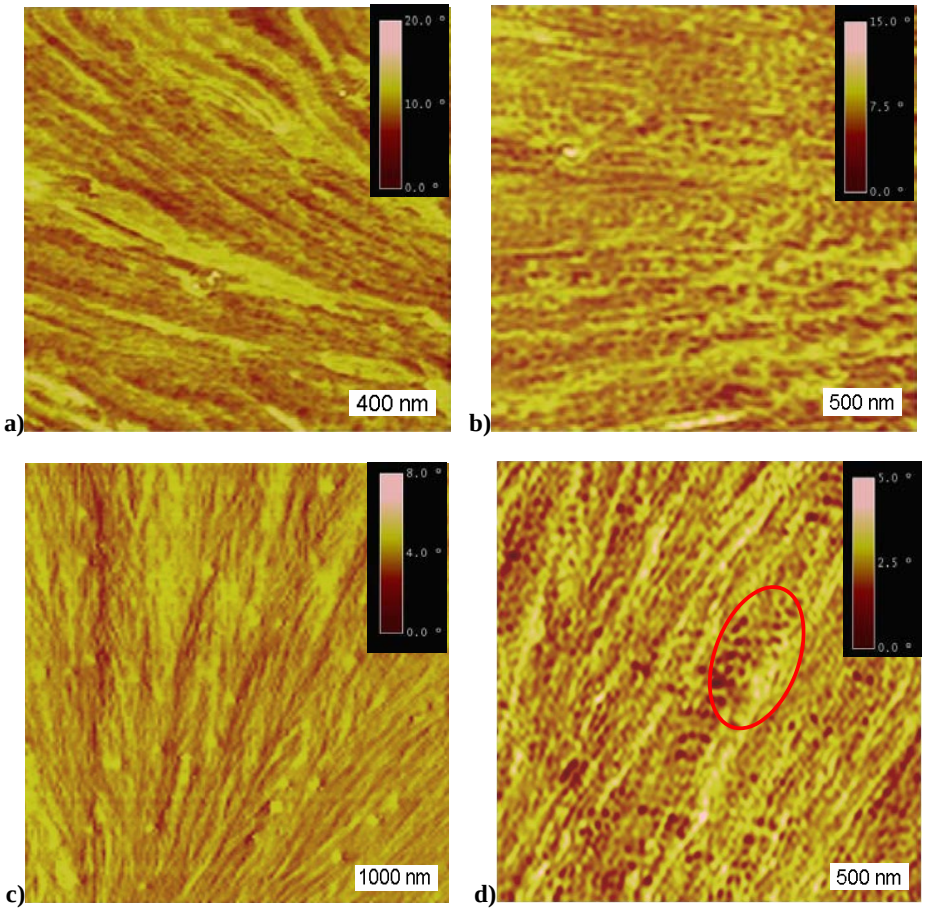

Figure 4.4: AFM phase images of higher resolution of thin films of polyester homopolymers and polydimethysiloxane–polyester copolymers with 5 wt % PDMS: (a) PBA, (b) PDMS-s-PBA copoylmer, (c) PBCH and (d) PDMS-s-PBCH copolymer.

Figure 4.5 is a schematic illustration demonstrating how the PDMS domains form between the lamellae structures in the PDMS-PES copolymers. The fact that spherulites as well as small amounts of spherical domains were observed in these copolymers suggests that liquid–liquid demixing had occurred, where the major part of the phase-separated PDMS segments seem to be present as spheres in-between the crystalline phases of the polyester.

Figure 4.6 shows AFM images of the 10 wt % PDMS content PDMS-PES copolymers. A slightly different morphology to the 5 wt % PDMS content copolymer morphology was observed for these higher content copolymers (B-2 and C-2). Firstly, in the case of the PDMS-s-PBA copolymers (Figure 4.6(a)), the dominant type of surface morphology is a spherulitic crystal structure. Once again, spheres of PDMS domains appear in the phase images.

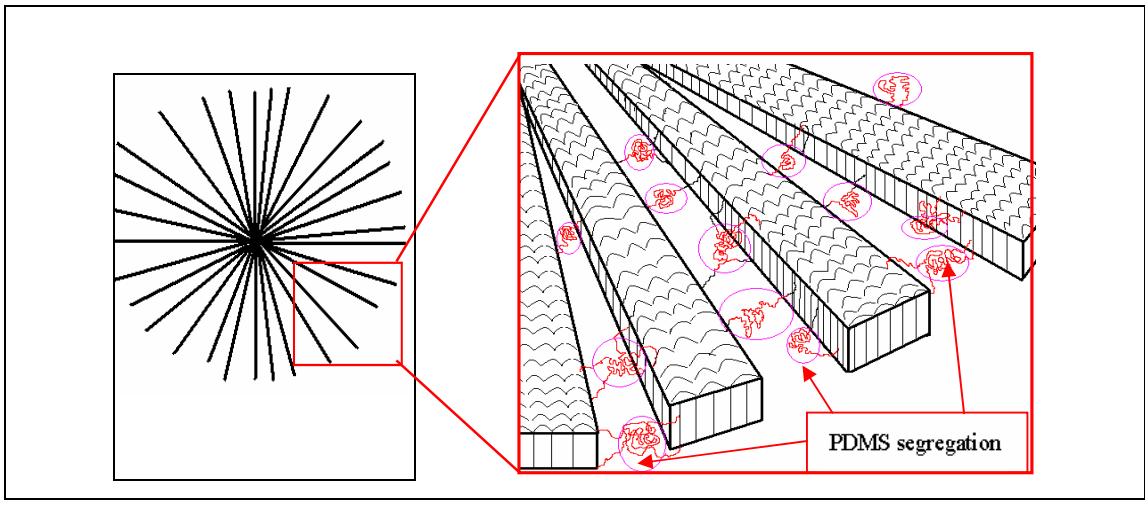

Figure 4.5: Schematic illustration of the PDMS segregations in-between the lamellae arrangements in the polydimethysiloxane–polyester copolymers.

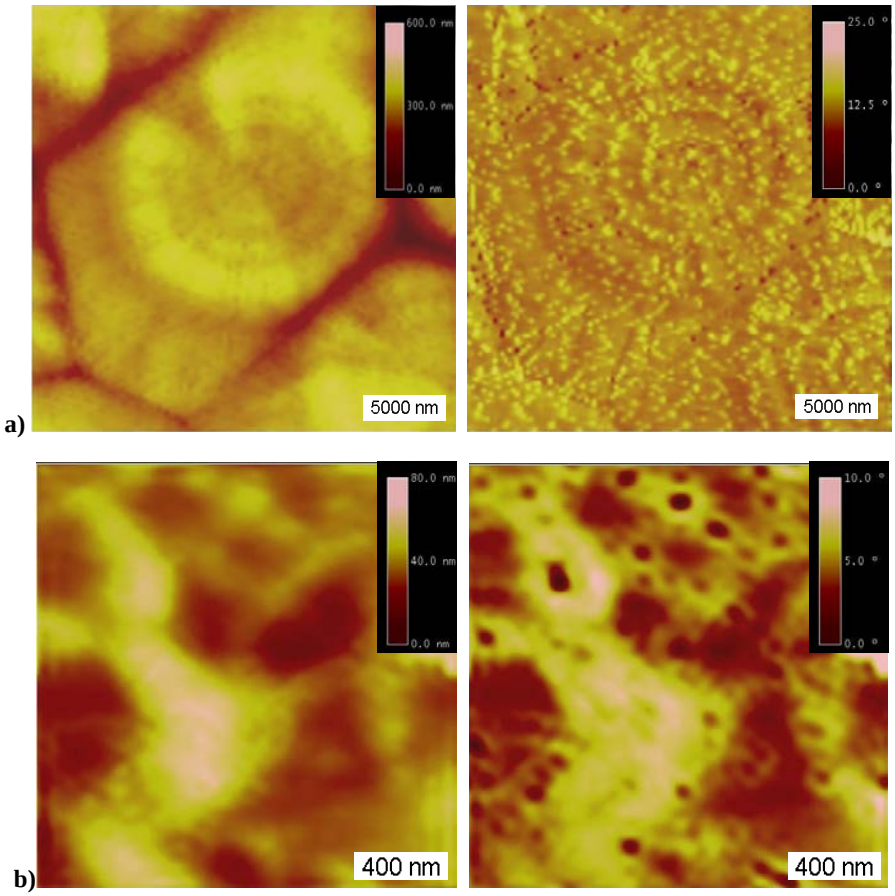

Figure 4.6: Topography and phase AFM images of thin films of polydimethysiloxane–polyester copolymers with 10% PDMS (M_n PDMS segment 2000): (a and b) PDMS-s-PBA and (c and d) PDMS-s-PBCH.

However, the PDMS domains appear larger and concentrated around (or more noticeable around) the boundaries of the spherulites. In the case of the 10 wt % PDMS content PDMS-s-PBCH copolymer (Figure 4.6(b)) spheres of the PDMS domains are also observed in the AFM phase images, but no spherulitic crystal structures are observed, even in AFM images of smaller magnification (larger images size 50 μm x 50 μm). In this case the diameters of the PDMS spheres are greater than 50 nm, which is about twice as large as the diameter measured for the 5 wt % PDMS in PDMS-s-PBCH copolymers series. This might be due to the increase in PDMS content, which leads to shorter polyester segments and the incorporation of more PDMS segments in the copolymer chain. There is also the possibility that a very small percentage of short polyester segments may be trapped inside the PDMS domains. The absence of an observable crystal structure on the surface of the PDMS-s-PBCH copolymer is also reflected by the dramatic decrease (13.34% decrease) in the polyester crystallinity (ω_{mPES}) in the copolymer relative to that for the PDMS-s-PBA copolymer with a 10 wt % PDMS content (4.28% decrease).

Attempt of observing the PDMS domains between the spherulitic crystal structures for sample C-2, using the HCl vapour treatment, is described in Appendix B, Section B.2.4. The C-2 copolymer morphology was further investigated (on fractions of the copolymer), to determine whether it is possible to observe the same type of crystal structure as that seen for PDMS-s-PBA copolymer. This is performed using a new hyphenated HPLC-LC-transform-AFM technique, which is described in Chapter 7.

When the PDMS contents increased to 25 wt % (Figure 4.7), no spherulites are detected by AFM on the surface for either type of copolymer. This is most probably due to the presence of relatively smaller amounts of crystallinity in these copolymers, as detected by DSC and WAXD, and the decreased probability of the formation of crystals at the interface. In the bright phase very bright areas can be distinguished. This bright spots can be either the result of the height effect or an evidence of PBCH crystalline domains in C-3 copolymers. This phenomenon will be discussed further in Chapter 7. The PDMS domains on the surface of both B-3 and C-3 copolymers increase in number as well as in size. The average diameter of the PDMS domains in the PDMS-s-PBA copolymers (B-3) (Figure 4.7(a)) is more than 70 ± 10 nm and in the PDMS-s-PBCH copolymers (C-3) (Figure 4.7(b)) more than 60 ± 10 nm.

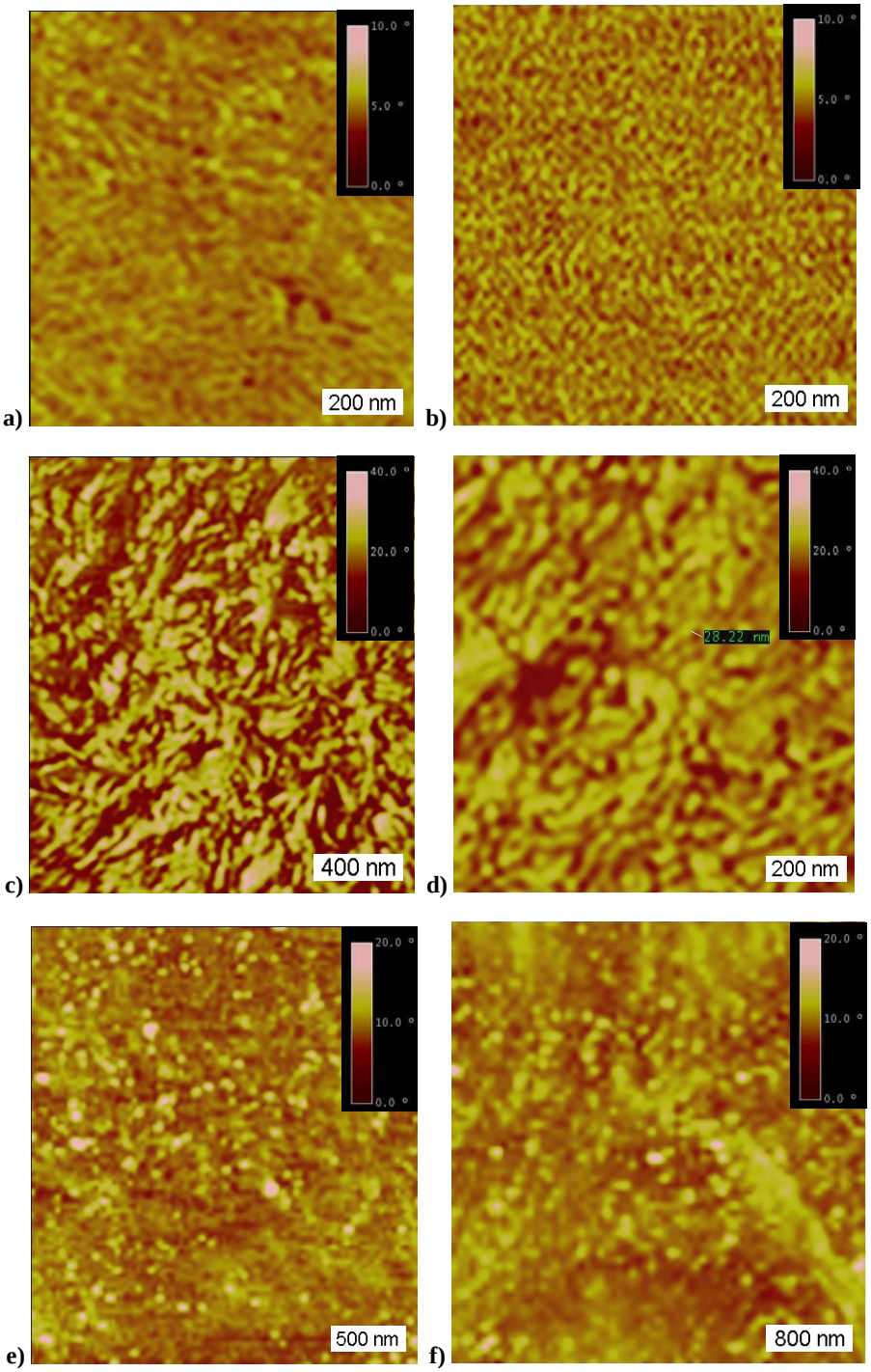

Figure 4.7: AFM phase images of thin films of PDMS-s-PBA and PDMS-s-PBCH copolymers with 25 wt % (a and b), 40 wt % (c and d) and 60 wt % (e and f) PDMS content, respectively.

As the concentration of the PDMS increases to 40 wt % (B-4 and C-4) (Figure 4.7(c) and (d)), the spherical PDMS domains start connecting with each other and a bicontinuous double diamond type of morphology appears on the surface. Upon a further increase in PDMS

content to 60 wt % (B-5 and C-5) (Figure 4.7(e) and (f)) this type of morphology changes to spheres of polyester surrounded by rubbery phases of PDMS.

The results of the WAXD, DSC and AFM analyses show that the crystallization of the polyester segments in the PDMS-PES copolymers is commonly affected by the PDMS component. A high PDMS content has a stronger inhibition effect on the crystallization of the polyester component for the PDMS-s-PBCH copolymers series than for the PDMS-s-PBA copolymers series. The inhibition of the crystallization of the polyester segment makes the observation of the crystallization at the surface increasingly difficult upon increasing PDMS content. This factor, combined with the strong preferential surface segregation of the PDMS components, means that no crystal morphology is observed via AFM in the higher content PDMS copolymers (above a 10 wt % PDMS content). In the case of the cycloaliphatic series no crystal morphology is observed for copolymers above a 5 wt % PDMS content due to the greater inhibition of crystallization by the PDMS in this series.

The high-content PDMS copolymers showed spherical domains of the PDMS phase embedded in a matrix of the polyester phase. This type of morphology changes from spherical domains to bicontinuous double diamond to a PDMS dominant phase. Unlike in the lower content PDMS copolymers, there was no indication of PDMS domains between the crystal structure, and any crystallinity in the high-content PDMS copolymers was confined within the spherical microdomains of the polyester that are prescribed by microphase separation. A similar observation has been reported for other block copolymers such as poly(ethylene)-b-poly(styrene-r-ethylene-r-butene) by Loo et al..[29]

4.3.3 Microscopic bulk morphology of the copolymers

TEM images, illustrated in Figures 4.8 and 4.9, clearly show that all the polydimethylsiloxane–polyester copolymers had distinct microphase separation (notice the scale in the TEM images are chosen to best represent to the observed morphology). This supports the results of the T_g measurements that were obtained by DMA. Figure 4.8 shows TEM micrographs of a cross-section of the PDMS-s-PBA and PDMS-s-PBCH copolymers with different PDMS contents. One can distinguish dark areas, which are related to the PDMS phase, due to its higher electron density relative to the polyester. Thus, the polyester homopolymer is essentially featureless. At 5 wt % PDMS content (Figure 4.8(a) and (b)) very fine microphase domains in spherical shapes are observed for both types of copolymers.

These spheres are believed to be due to the segregation of PDMS segments. A similar type of morphology was detected for the 10 wt % PDMS content copolymers (Figure 4.8(c) and (d)). The TEM micrograph of a 5 wt % PDMS content copolymer suggests that the sub-micron domains do not seem to be homogenously distributed (see the ovals in Figure 4.8(a) and (b)), when compared with the TEM micrograph of a 10 wt % PDMS content segmented copolymer. In the case of the 5 wt % PDMS content copolymers this could be as a result of the PDMS segregating between or around the lamella crystal structure, as has been shown for the thin film surfaces of the PDMS-s-PBA and PDMS-s-PBCH copolymers in Figure 4.4(b) and (d). In contrast to the 5 wt % PDMS content copolymers, the PDMS domains in the 10 wt % PDMS content copolymers appear to be more evenly distributed in the polyester matrix. This is due to the lower degree of crystallinity in these copolymers compared with that for the 5 wt % PDMS content copolymers. Similar results of microdomain phase separation have been reported by Van der Schuur et al. for poly(propyleneoxide) based polyether(ester-amide)s with non-crystallisable amide segments.[30]

The bulk morphology of the PDMS-s-PBA copolymer series was similar to the PDMS-s-PBCH copolymer series, as shown by TEM. However, the average size of the PDMS domains of copolymer B-1 (Figure 4.8(a)) is 10 ± 3 nm, which is smaller than that of copolymer B-1 (approximately 25 ± 5 nm, Figure 4.8(b)). This could be because less PDMS was incorporated into the B-1 copolymer, and hence fewer PDMS segments segregated to each other, forming smaller spherical PDMS domains (compared to the C-1 copolymer). On the other hand, in the case of the B-2 copolymer (Figure 4.8(c)) the average diameter of the PDMS domains was 200 ± 50 nm. This value is much larger than that of the C-2 copolymers (40 ± 10 nm, Figure 4.8(d)), even though the actual PDMS content for B-2 copolymer (8.97 wt %) was less than that for the C-2 copolymer (9.20 wt %). This suggests that decreasing the polarity of the polyester phase (an aliphatic polyester has higher polarity than a cycloaliphatic polyester) favours the more discrete microdomain structure (PDMS segregations), with a higher surface to volume ratio.

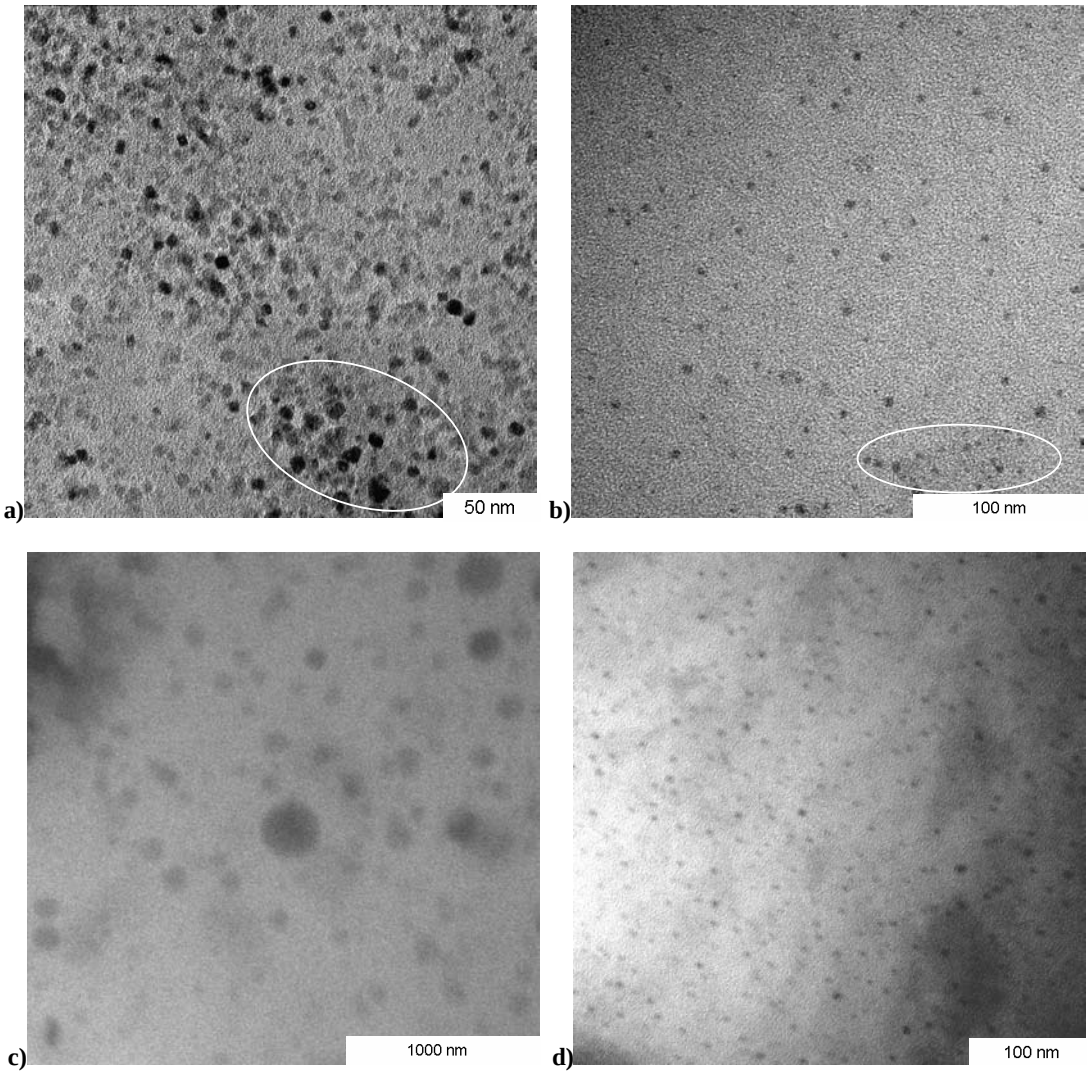

Figure 4.8: TEM micrographs of polydimethysiloxane–polyester copolymers: (a and c) PDMS-s-PBCH 5 wt % and 10 wt % PDMS content, respectivly, and (b and d) PDMS-s-PBA 5 wt % and 10 wt % PDMS content, respectivly.

The average diameter of the nano-spherical domain of the 5 wt % PDMS content copolymers, as measured from the TEM images, is smaller than that measured from AFM images on the thin film surfaces. This may be due to one or all of the following three reasons. First, when measuring very small objects using the AFM, the actual size of the AFM tip cannot be neglected; the measured profile is in fact a convolution of the actual profile and the tip shape. However, correction procedures have been developed that can be applied.[31] Second, flattening can occur,[32] especially when the surface consists of soft material such as PDMS segments. This problem can be minimized by using the tapping mode of AFM. The third reason arises from the affinity of the PDMS segments to diffuse to the copolymer surface.[33]

The PDMS at the surface is expected to have a substantially higher concentration than the overall bulk concentration, which might lead to the formation of larger microdomains of the PDMS on the surface than in the bulk.

The difference in the samples preparation conditions for the AFM and TEM analyses was expected to lead to significantly different bulk and surface morphologies, where samples of higher polymer concentrations were used for TEM analysis. In addition, the PDMS component will segregate on the copolymer surface. This has been reported for various copolymers with one PDMS segment or block.[34,35] Surprisingly, however, there was a high degree of similarity in the type of morphology of the copolymers determined by AFM and TEM. This might be a result of using very thin films for the copolymers in the surface analyses.

As the PDMS content in the PDMS-s-PBA and PDMS-s-PBCH copolymers increased, a different bulk morphology started to form: in the 25 wt % PDMS content copolymers the PDMS spheres started connecting to each other (Figure 4.9(a) and (b)). This indicates that the copolymer morphology or the type of microphase separation is dependent on the PDMS content. This is clearly seen when the spheres completely disappear in the 40 wt % PDMS content copolymers and the morphology changes to bicontinuous or co-continuous phases, as can be seen in Figure 4.9(c) and (d). In this micrograph the PDMS phase and polyester phase are both represented as being continuous and interpenetrating. This requires a sufficient amount of hard segments (about 60 wt % polyester). Any crystallinity in the copolymer would be limited to the polyester domains.

In the 60 wt % PDMS content copolymers (Figure 4.9(e) and (f)) the PDMS phase forms the dominant phase and the polyester segments segregate to form spheres. As expected, the size of these spheres varies, as a result of the copolymer synthesis method, where the polyester segments have various lengths and are randomly distributed in the copolymers. DSC results showed that the 60 wt % PDMS content copolymers had a very low percentage of crystallinity, and that is confined within the spherical domains.

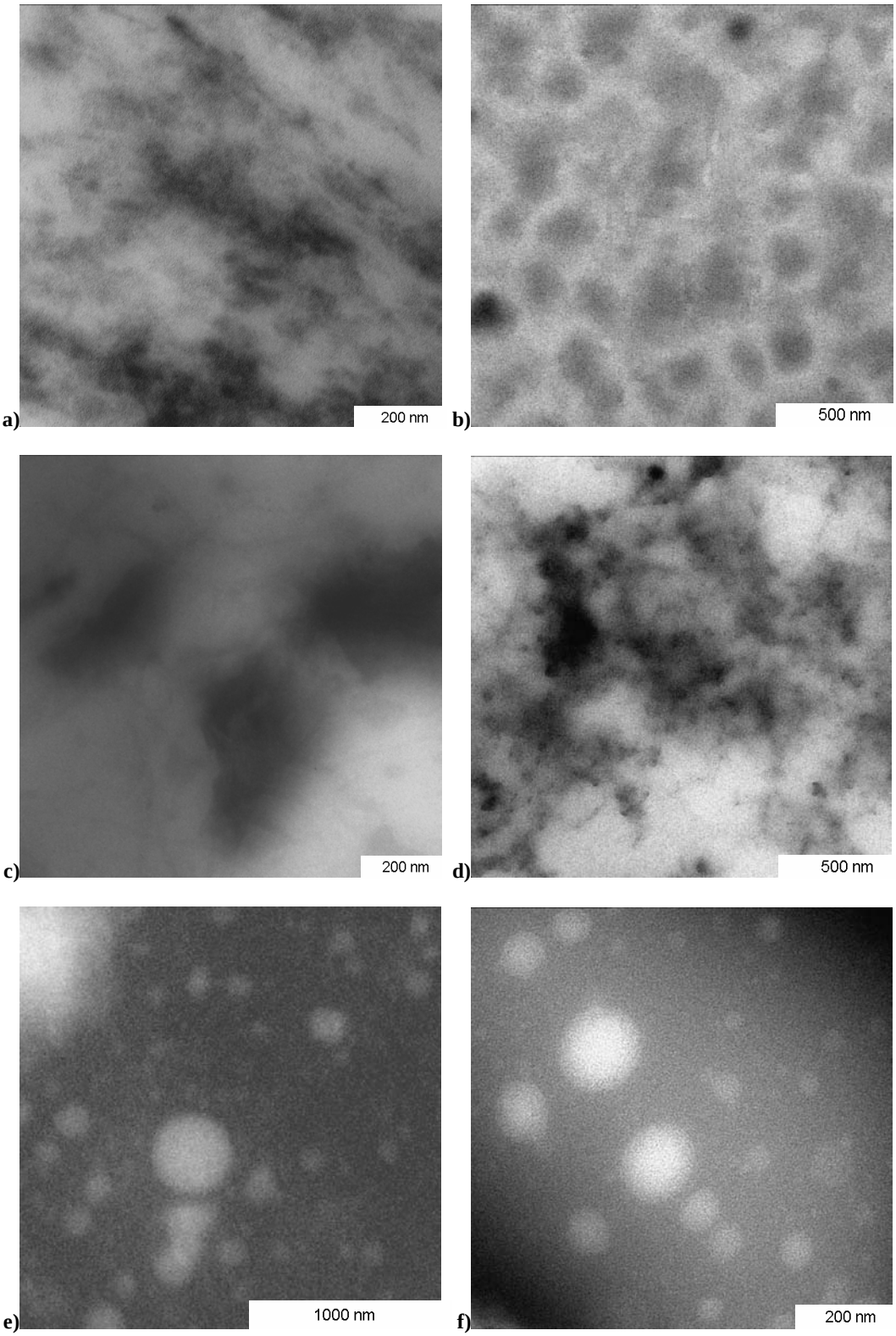

Figure 4.9: TEM micrographs of polydimethysiloxane–polyester copolymers: (a, c and e) PDMS-s-PBCH 25, 40 and 60 wt % PDMS content, respectivly, and (b, d and f) PDMS-s-PBA 25, 40 and 60 wt % PDMS content, respectivly.

4.3.4 Adhesive force and surface roughness measurements

PDMS has a very low surface energy, and hence microphase-separated PDMS-s-PES copolymers are expected to have a low surface energy due to the PDMS surface segregation. The surface energy (adhesive force) of these copolymers was measured using digital pulsed-force mode AFM (DPFM-AFM). The average of the adhesive force was calculated and plotted against the PDMS content, as shown in Figure 4.10. Several adhesive force images are included to illustrate the clear difference between the two series.

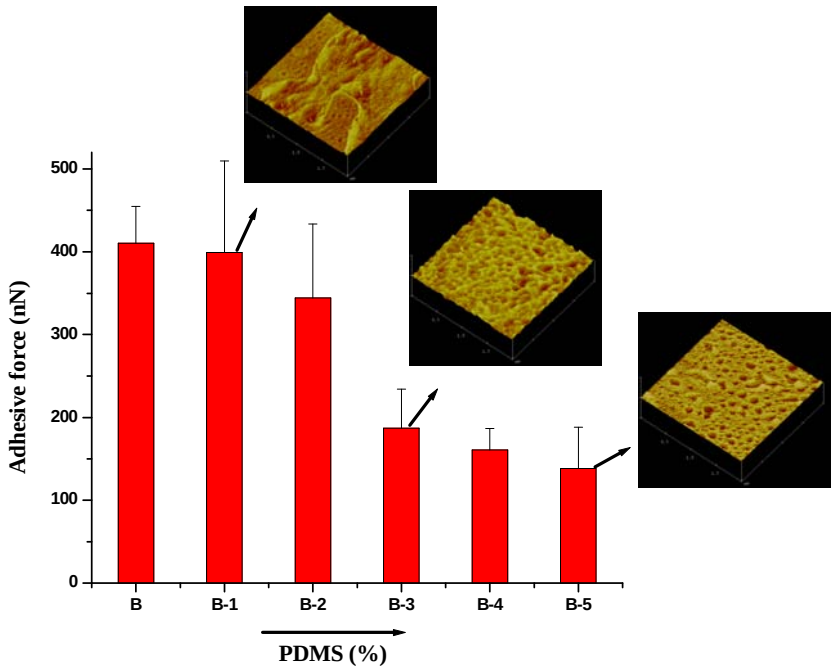

a)

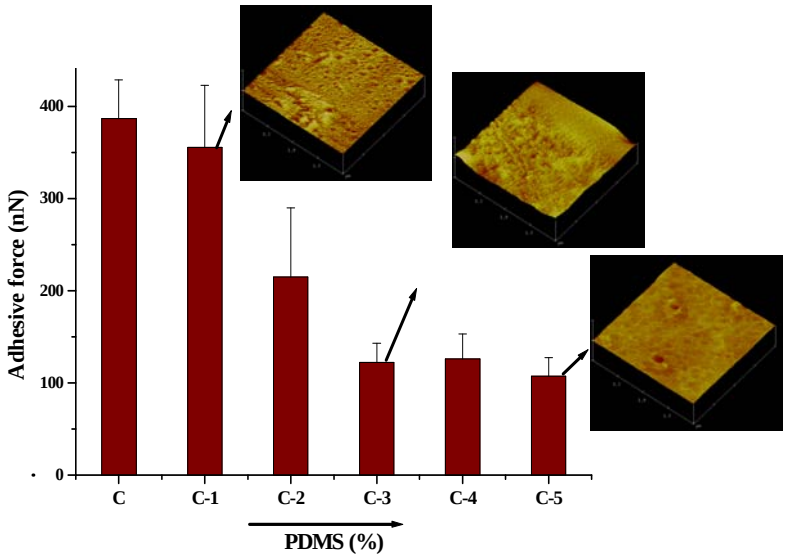

b)

Figure 4.10: Adhesive force measurements for (a) PDMS-s-PBA and (b) PDMS-s-PBCH copolymers.

This figure shows that as the PDMS content increases so the adhesive force decreases in both copolymers. For the lowest PDMS content samples (B-1) and (C-2), significant changes in the adhesive force of more than a 15% decrease are seen, whereas there are only small changes in the high PDMS content samples (B-3, B-4 and B-5) and (C-3, C-4 and C-5). Additionally, minimization of the adhesive force in both series is a result of an enrichment of the surface with PDMS segment. This was also observed from the AFM phase images. This result is consistent with results reported in literature for other PDMS copolymers.[33-36]

The large standard deviation in both copolymers series refers to the diversity in the surface composition or in the functional groups on the surface (such as CH_3, CH_2, C=O and OH), which might be used as an indication that no complete monolayer of PDMS was formed on the copolymer surface. This confirms results obtained for perfectly alternating copolymers with bis-A sulphone, aromatic ester, urea and imide structures.[37] The authors reported that a PDMS with M_n of between 6800 and 12000 g/mol was required to form a complete siloxane monolayer.[37]

Figure 4.11 shows the influence of varying the PDMS content on the surface roughness of the PDMS-s-PBA and PDMS-s-PBCH copolymers. The surface roughness values for B, B-1, B-2, C and C-1 are quite large, which might be due to the spherulitic crystal structure in these polymers.

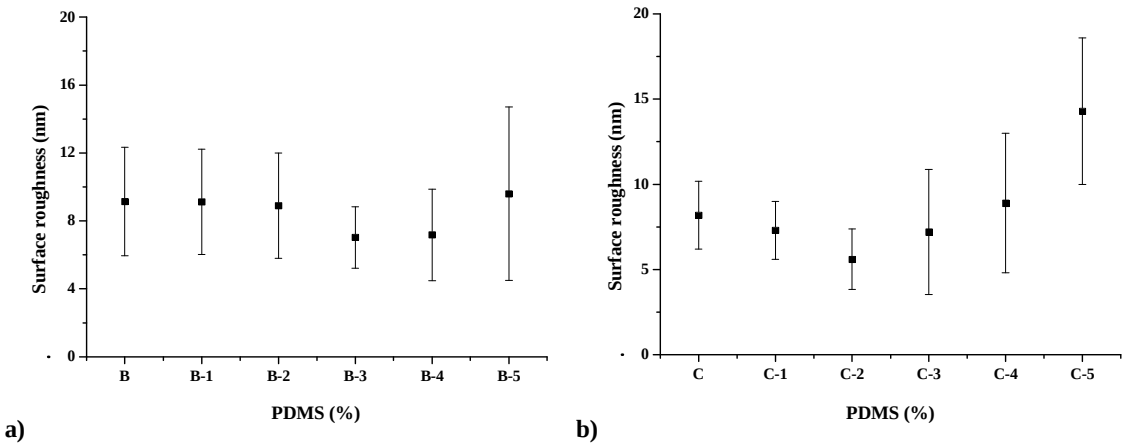

Figure 4.11: Surface roughness measurements for (a) PDMS-s-PBA and (b) PDMS-s-PBCH copolymers.

However, in the other copolymers the surface roughness values increase with increasing PDMS content. This could be related to an increase in the phase separation on the surface as the PDMS content increases, where the PDMS segments or domains form islands on the

surface, and the size and the height of these islands increase as the PDMS concentration on the surface of the copolymers increases. Because the surface composition of these copolymers seems to depend on PDMS content and polyester type, the spherulitic crystal morphology changed to a spherical PDMS microdomain morphology when PDMS increases to a specific degree (in the case of PDMS-s-PBA 25 wt % and in the case of PDMS-s-PBCH to 10 wt %). This change in the surface morphology affects the adhesive force, as well as the surface roughness. The relationship between the segmented copolymer composition and surface roughness, shown in Figure 4.11, shows a non-linear relationship between the average surface roughness and the weight percent of PDMS content.

4.4 Conclusions

The morphology of two series of hybrid PDMS-s-PBA and PDMS-s-PBCH copolymers were investigated. A significant reduction in crystallinity of the copolymers in both copolymer series was observed as the PDMS content increased, as determined by WAXD and DSC. Moreover, the effect of the PDMS on the crystallinity degree was greater in the PDMS-s-PBCH copolymers series than in the PDMS-s-PBA copolymers series. This was attributed to either the higher chain mobility of the PBA segment compared to the PBCH segment or to the large difference in the polarity between the PDMS segment and the PBA segment, when compared with the PBCH segment, which led to a higher degree of mixing in the PDMS-s-PBCH copolymers series than that in the PDMS-s-PBA copolymers series.

An investigation of the microscopic surface morphology of the copolymers, using AFM, showed that the PBA and PBCH homopolymers exhibited spherulite morphology. Both the PDMS-s-PBA and PDMS-s-PBCH copolymers with a 5 wt % PDMS content showed spherulite morphology despite the ability of PDMS segments to segregate at the surface. The PDMS domains were observed between the lamella crystal structures on the surface of these copolymers. This leads to a heterogeneous distribution of the PDMS domain within the polyester matrix. As the content of PDMS increased to 10 wt %, the PDMS nano-domain distribution became more homogeneous for both copolymer series. In the case of the PDMS-s-PBA copolymer, however, the PDMS domains were clearly observed around the boundaries of the spherulites. The PDMS-s-PBCH copolymers showed clear microphase separation, in which the PDMS formed spherical domains in a matrix of PBCH and, in contrast to PDMS-s-PBA, no spherulites crystal structure was observed for PDMS-s-PBCH copolymers in AFM images. In the PDMS-s-PBA and PDMS-s-PBCH copolymers with 10

wt % PDMS content the diameters of the PDMS spheres were larger than the diameters measured for PDMS-s-PBA and PDMS-s-PBCH copolymers with 5 wt % PDMS content. This was attributed to the increase in PDMS content and consequent increase in the PDMS segment lengths.

AFM images also showed that in both types of polyester copolymers the copolymer surface morphology or the type of microphase separation is dependent on the PDMS content: when the PDMS content increased to 40 wt % the PDMS spheres completely disappeared and the morphology changed to a bicontinuous or co-continuous morphology. As the PDMS content increased above 50 wt % the PDMS phase formed the dominant phase and the polyester segments segregated to form spheres. The phase separation in segmented copolymers with random polyester segment length, and for low PDMS content, probably occurs by liquid–liquid demixing in combination with crystallization. The PDMS segments were able to segregate in between the lamella structure without destroying the spherulitic structure. This only occurs in the case of the low content PDMS copolymers. On the other hand, the high PDMS contents copolymers showed that crystallization was confined mainly within spherical, nano-scale domains in the bulk of the sample.

Furthermore, TEM results confirmed the multiphase bulk morphology that was detected by DMA and AFM for both copolymers series. Three types of morphologies were observed. Copolymers with a 5 wt % PDMS content showed heterogeneously distributed spherical microdomains of PDMS in a matrix of polyester. As the content of the PDMS increased to 10% the PDMS domain distribution became more homogeneous. At a PDMS content of 40 wt %, a bicontinuous double diamond type of morphology was observed in the TEM images, and when the PDMS content increased to 60 wt %, spherical microdomains of polyester in a matrix of PDMS was observed for both copolymers.

The adhesive force measurements were correlated to the PDMS content and the surfaces of the PDMS-s-PES copolymers showed very low surface energy. The relationship between the segmented copolymer composition and surface roughness generally increases with increasing the PDMS content, and it shows a non-linear relationship with the weight percent of PDMS content.

4.5 References

1. Yamamoto, N.; Mori, H.; Nakata, A.; Suehiro, M. Aromatic polyester-polyorganosiloxane block copolymer. Application Number: 250859 Tokyo, JP, 1990.

2. Kiefer, L. A.; Yoon, T. H.; Glass, T. E.; Jayaraman, S. K.; McGrath, J. E. *Journal of Polymer Science, Part A: Polymer Chemistry* 1997, 35(16), 3495-3506.

3. Miroslawa, E. F. *Designed Monomers and Polymers* 2000, 3(3), 325-337.

4. Antic, V. V.; Balaban, M. R.; Djonlagic, J. *Polymer International* 2001, 50(11), 1201-1208.

5. Dojcinovic, B. P.; Vesna, V. A.; Vuckovic, M. V.; Jasna, D. *Journal of the Serbian Chemical Society* 2005, 70(12), 1469-1485.

6. Vuckovic, M. V.; Antic V. V.; Dojcinovic B. P.; Govedarica M. N.; Djonlagic J. *Polymer International* 2006, 55(11), 1304-1314.

7. Yilgör, İ.; McGrath, J., Polysiloxane containing copolymers: A survey of recent developments. In *Polysiloxane Copolymers/Anionic Polymerization*, Springer, Berlin / Heidelberg, 1988; pp 1-86.

8. Ekin, A.; Webster, D. C. *Journal of Polymer Science, Part A: Polymer Chemistry* 2006, 44(16), 4880-4894.

9. Rangarajan, P.; Register, R. A.; Adamson, D. H.; Fetters, L. J.; Bras, W.; Naylor, S.; Ryan, A. J. *Macromolecules* 1995, 28(5), 1422-1428.

10. Ryan, A. J.; Hamley, I. W.; Bras, W.; Bates, F. S. *Macromolecules* 1995, 28(11), 3860-3868.

11. Loo, Y.-L.; Register, R. A.; Ryan, A. J. *Macromolecules* 2002, 35(6), 2365-2374.

12. Müller, A.; Balsamo, V.; Arnal, M., Nucleation and crystallization in diblock and triblock copolymers. In *Block Copolymers II*, Springer, Berlin / Heidelberg, 2005; pp 1-63.

13. Zhang, F.; Chen, Y.; Huang, H.; Hu, Z.; He, T. *Longmuir* 2003, 19(14), 5563-5566.

14. Douzinas, K. C.; Cohen, R. E.; Halasa, A. F. *Macromolecules* 1991, 24(15), 4457-4459.

15. Hamley, I. W.; Fairclough, J. P. A.; Terrill, N. J.; Ryan, A. J.; Lipic, P. M.; Bates, F. S.; Towns-Andrews, E. *Macromolecules* 1996, 29(27), 8835-8843.

16. Stanciu, A.; Airinei, A.; Timpu, D.; Ioanid, A.; Ioan, C.; Bulacovschi, V. *European Polymer Journal* 1999, 35(11), 1959-1965.

17. Higuchi, A.; Nakagawa, T. *Journal of Polymer Science, Part B: Polymer Physics* 1994, 32(1), 149-157.

18. Childs, M. A.; Matlock, D. D.; Dorgan, J. R.; Ohno, T. R. *Biomacromolecules* 2001, 2(2), 526-537.

19. Dong, T.; Kai, W.; Inoue, Y. *Macromolecules* 2007, 40(23), 8285-8290.

20. Frömsdorf, A.; Woo, E. M.; Lee, L.-T.; Chen, Y.-F.; Förster, S. *Macromolecular Rapid Communications* 2008, 29(15), 1322-1328.

21. Krotil, H.-U.; Stifter T.; Waschipky, H.; Weishaupt, K.; Hild, S.; Marti, O. *Surface and Interface Analysis* 1999, 27(5-6), 336-340.

22. *Veeco Metrology Group, Digital Instruments, Nanoscope Command Reference Manual*. Digital Instruments /Veeco Metrology Group Inc., United States 2001; pp 14-25.

23. Chang, S.-J.; Tsai, H.-B. *Journal of Applied Polymer Science* 1994, 51(6), 999-1004.

24. Hernandez, R.; Weksler, J.; Padsalgikar, A.; Runt, J. *Macromolecules* 2007, 40(15), 5441-5449.

25. Grulke, A. E., Solubility parameter values. In *Polymer Handbook*, Fourth ed.; Barandrup, J.; Immergut, E. H.; Grulke, E. A. (Eds), John Wiley and Sons, Inc., New York, 1999; Vol. VII, pp 682-683.

26. Leclère, P.; Hennebicq, E.; Calderone, A.; Brocorens, P.; Grimsdale, A. C.; Müllen, K.; Brédas, J. L.; Lazzaroni, R. *Progress in Polymer Science* 2003, 28(1), 55-81.

27. Daniels, R.; Magonov, S. Method and system for increasing the accuracy of a probe-based instrument measuring a heated sample. Application Number: 354448 Plainview, NY, 2001.

28. Villers, D.; Dosière, M.; Paternostre, L. *Polymer* 1994, 35(8), 1586-1592.

29. Loo, Y.-L.; Register, R. A.; Ryan, A. J. *Physical Review Letters* 2000, 84(18), 4120-4123.

30. Van der Schuur, M.; Van der Heide, E.; Feijen, J.; Gaymans, R. J. *Polymer* 2005, 46(11), 3616-3627.

31. Samorí, P.; Francke, V.; Mangel, T.; Müllen, K.; Rabe, J. P. *Optical Materials* 1998, 9(1-4), 390-393.

32. Rivetti, C.; Guthold, M.; Bustamante, C. *Journal of Molecular Biology* 1996, 264(5), 919-932.

33. Mahoney, C. M.; Gardella, J. A.; Rosenfeld, J. C. *Macromolecules* 2002, 35(13), 5256-5266.

34. Chen, X.; Gardella Jr, J. A.; Kumler, P. L. *Macromolecules* 1992, 25(24), 6631-6637.

35. Liu, Y.; Zhao, W.; Zheng, X.; King, A.; Singh, A.; Rafailovich, M. H.; Sokolov, J.; Dai, K. H.; Kramer, E. J. *Macromolecules* 1994, 27(14), 4000-4010.

36. Jin Z.; Sergio R.R.; Jiaxing C.; Mingzhu Xu.; Joseph A.G.J. *Macromolecules* 1999, 32(2), 455-461.

37. Andrea, D. B. Synthesis and characterization of poly(siloxane imide) block copolymers and end-functional polyimides for interphase applications. PhD, Virginia Polytechnic Institute and State University Virginia, United States, 1999, p 54.

Chapter Five

Morphology of Semi-crystalline Polydimethylsiloxane-Polyester Copolymers: 2 Effect of the PDMS Molar Mass and the Branching Degree

Abstract

The morphology of two series of semicrystalline polydimethylsiloxane–polybutylenecyclohexanedicarboxylate copolymers, segmented (PDMS-s-PBCH) and randomly branched (PDMS-br-PBCH), with relatively low PDMS content (10 wt %), was characterized via indirect methods and via direct observation (microscopic investigations). The indirect methods was achieved using DMA, DSC and WAXD techniques, to determine the glass transition temperatures (T_g) values, melting point (T_m), and degree of crystallinity. The direct observation of the copolymer morphology was achieved by applying AFM and TEM techniques. The effects of the PDMS segment length and the branching degree on the copolymer morphology were investigated using both methods. DSC and WAXD results revealed the ability of the copolymers to crystallize to various degrees, depending on the PDMS segment length and the degree of branching. The segmented copolymers with a short PDMS length had a spherulitic morphology as detected by AFM. Because of incompatibility between the PDMS and PBCH segments both series showed microphase separation. This microphase separation was detected by the two T_g values in the DMA results and also visualized on the copolymer surface using AFM and in the copolymer bulk using TEM. The phase separation manifested in mainly two types of morphologies: spherulitic crystal morphology and spherical micro-domains of PDMS.

Keywords: segmented copolymer morphology, branched copolymer morphology, AFM and TEM.

5.1 Introduction

PDMS copolymers derive their unusual properties from the thermodynamic incompatibility and resultant phase separation (domain formation) of the component polymer segments. In many cases both domains are amorphous,[1,2] but in other cases, as it was discussed in Chapter 4, one of the components may crystallize to further enhance the mechanical properties, where the hard segment domains act as physical crosslinks in the system.[3-7] The complex behaviour of the multiblock copolymers with semicrystalline components is due to the richness of morphology, which arises from the interplay between microphase separation and self-organizing processes that take place as a consequence of the thermodynamic immiscibility of the covalently linked blocks and their crystallization.[8-11]

Semicrystalline PDMS-PES copolymers are among the few amorphous–crystalline multiblock copolymers that crystallize above the glass transition temperature of the non-crystallisable segment. The presence of noncrystalline segments in the semicrystalline copolymer enables modification of the morphology and eventually affects the copolymer's properties (compared to the PDMS homopolymer's properties).[3,12] Furthermore, generally speaking, crystallization in homopolymers leads to an extended conformation in which the chain folding is kinetically controlled, whereas in the copolymer the chain folding is controlled by the amount or the size of the second noncrystallisable segment.[12] Thus, through the introduction of a rubbery component such as PDMS in crystalline polyesters, changes in the polymer morphology, and the chemical changes results in desirable properties for such copolymers.

The most obvious and direct methods that can be used for investigating the copolymer morphology and identifying phase separation is visual inspection, using microscopic instruments such as POM, SEM, TEM and AFM. Recently, Miroslawa[4] reported that polydimethylsiloxane-polybutyleneterephthalate segmented copolymers showed semicrystalline morphology of spherulite using POM technique, but the details of the morphology were not presented. More recently Childs and coworkers[13] investigated the surface morphology of polycarpolactone-b-polydimethylsiloxane-b-polycarpolactone copolymers using more advanced techniques, (e.g. AFM), and also detected semicrystalline spherulitic morphology. Microscopic methods are usually complemented by other analytical techniques, such as DSC, DMA and X-ray diffraction. Kiefer and co-workers[3] studied the effect of different PDMS content and molar mass on several thermal and mechanical

properties of PDMS-PBCH copolymers. However, to the best of the author's knowledge the morphology of segmented or branched PDMS-PBCH copolymers has not been systematically investigated. The study of these copolymers is considered a challenging task, and could contribute to the understanding of the interrelationship between phase separation and crystallization. This chapter describes a systematic morphology investigation that was carried out into PDMS-s-PBCH copolymers with a constant PDMS content (10 wt %), but with various PDMS segment lengths. The morphology of statistical or randomly branched PDMS-br-PBCH copolymers for a PDMS segment length of 1000 g/mol and 10 wt % PDMS content, but with different branching degrees was also investigated.

5.2 Experimental

5.2.1 Copolymers

Two series of copolymers, PDMS-s-PBCH and PDMS-br-PBCH, were synthesized via a condensation reaction in the melt state.[3] The resulting segmented and branched copolymers were purified using five different solvents, as reported in Chapter 3. The copolymer formation and the purity of the copolymers were confirmed by GEC. The copolymer compositions and the average molar masses are tabulated in the Table 5.1.

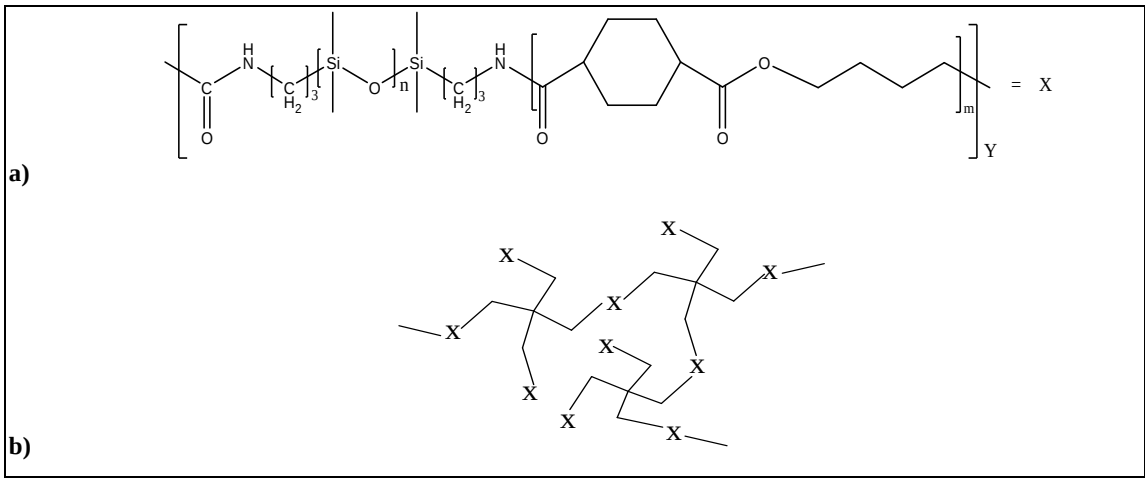

Scheme 5.1: Chemical structures of PDMS-PBCH copolymers: (a) PDMS-s-PBCH and (b) PDMS-br-PBCH.

Table 5.1: Chemical compositions and average molar masses of two series of PDMS-PBCH copolymers: PDMS-s-PBCH copolymer and PDMS-br-PBCH copolymer

Sample	PDMS M_n (g/mol)	Branching agent (wt %)	PDMS in copolymer [a] (wt %)	M_w [b] (g/mol)	M_n [b] (g/mol)	M_w/ M_n	g [c]
D -1	1000	0	9.35	29981	15142	1.98	1.00
D -2	2000	0	9.20	27719	17171	1.62	-
D-3	4000	0	8.90	31712	17816	1.78	-
D -4	7000	0	9.10	37770	16862	2.24	-
D -5	10000	0	8.60	39915	18828	2.12	-
F-1	1000	0.1	9.10	27208	14717	1.84	0.94
F-2	1000	0.2	9.51	33950	14634	2.32	0.75
F-3	1000	0.5	9.32	35147	15832	2.22	0.62
F-4	1000	1.0	8.90	33573	16141	2.08	0.52
F-5	1000	2.0	9.44	35632	16345	2.18	0.47

[a] Measured by ^{1}H-NMR

[b] Measured by SEC

[c] Measured by SEC-MALLS

5.2.2 Characterization

Details of the characterization techniques and procedures used for DMA, DSC, WAXD, AFM and TEM are described in Section 4.2.2.

5.3 Results and discussion

5.3.1 Copolymer characterization

DMA was used to determine the T_g values of the multicomponent PDMS-PBCH copolymers. Table 5.2 shows the T_g values of PDMS-s-PBCH with various PDMS molar masses (series D) and PDMS-br-PBCH with various branching degrees (series F). Two glass transition temperatures were observed for all the copolymers in both series. The T_g values of the PDMS and PBCH homopolymers are –123 °C and 15 °C, respectively.[3,14] Hence the higher T_g in the copolymer is due to the PBCH segment: it occurs between 3 and 12 °C for the PDMS-s-

PBCH copolymer, and between 6 and 10 °C for the PDMS-br-PBCH copolymer. In contrast, the lower T_g is due to the PDMS segment; this value varies as the PDMS segment length changes from 1000 to 10000 g/mol in series D, but does not change much with an increase in the degree of branching in series F. However, a secondary transition was observed at about –50 °C in both series, as shown in Figure 5.1. This is related to the PBCH segment, as reported by Kiefer and coworkers.[3] Simultaneously, and for longer PDMS segments (more that 2200 g/mol), the PDMS segment can also crystallize, and its T_m is also seen at approximately –50 °C.[15]

Table 5.2: Glass transition temperature (T_g), melting temperature (T_m) and the degree of crystallinity (area under the melting peak) of PDMS-s-PBCH and PDMS-br-PBCH copolymers

Sample	Polyester (wt %)	T_gL[a] (°C)	T_gH[b] (°C)	T_m (°C)	ΔH_m (J/g)	ΔH_{mPES} (J/g)	Crystallinity ω_m[c] (%)	Crystallinity ω_{mPES} (%)
D-1	90.65	–111	3	66.3	37.4	41.2	28.4	31.3
D-2	90.80	–115	7	61.1	28.4	31.2	16.4	18.0
D-3	91.10	–120	9	55.8	30.1	33.0	16.1	17.6
D-4	90.90	–122	11	56.4	27.4	30.1	13.1	14.4
D-5	91.40	–123	12	54.2	26.5	28.9	12.4	13.5
F-1	90.90	–113	10	62.2	33.3	36.6	23.5	25.9
F-2	90.49	–115	7	58.1	29.8	32.9	22.6	24.9
F-3	90.68	–114	8	55.9	31.1	34.2	21.3	23.3
F-4	91.10	–115	7	57.2	24.2	26.5	17.5	20.3
F-5	90.56	–116	6	54.3	19.5	21.5	15.5	17.1

[a] The lowest glass transition temperature from the tan δ curve

[b] The highest glass transition temperature from the tan δ curve

[c] The degree of crystallinity measured from WAXD data

The presence of two T_g values implies that each segment is segregated, to form phase separation (in the micro- or nano-scale). The low T_g values of most of these copolymers stayed more or less constant, especially those of the branched copolymers. The independence of the T_g of PDMS segments in copolymers D-4 and D-5 indicated that the PDMS segment in

the PDMS-s-PBCH copolymers has a high degree of phase separation. In contrast, the T_g of PDMS segments in D-1 and D-2 copolymers showed significant shift to a higher value, which indicated some degree of mixing for the PDMS segments in these copolymers. Slightly more revealing with respect to the thermal transition behaviour are the corresponding tan δ profiles in Figure 5.1.

Figure 5.1(a) shows that the T_g peak of PDMS clearly occurs at about –111°C for copolymer D-1 (PDMS M_n 1000 g/mol). The higher T_g for D-1 compared to that of D-5 (PDMS Mn 10000 g/mol), namely –123°C, can be explained to be a result of an increase in the number of restrictions imposed on the D-1 chains by the hard segments. The restrictions on the PDMS segment in the D-1 sample increase due to the combined effects of the higher degree of segmental mixing in the copolymer and the shorter average PDMS segment length of D-1. Furthermore, it has been reported that the T_g of aminopropyl PDMS oligomers increases with their decreasing molecular weight, from –123°C for samples with a molar mass higher than 3670 g/mol to –118°C for samples with a molar mass lower than 1000 g/mol.[16] This may contribute to the T_g shift in the copolymers with short PDMS segment length.

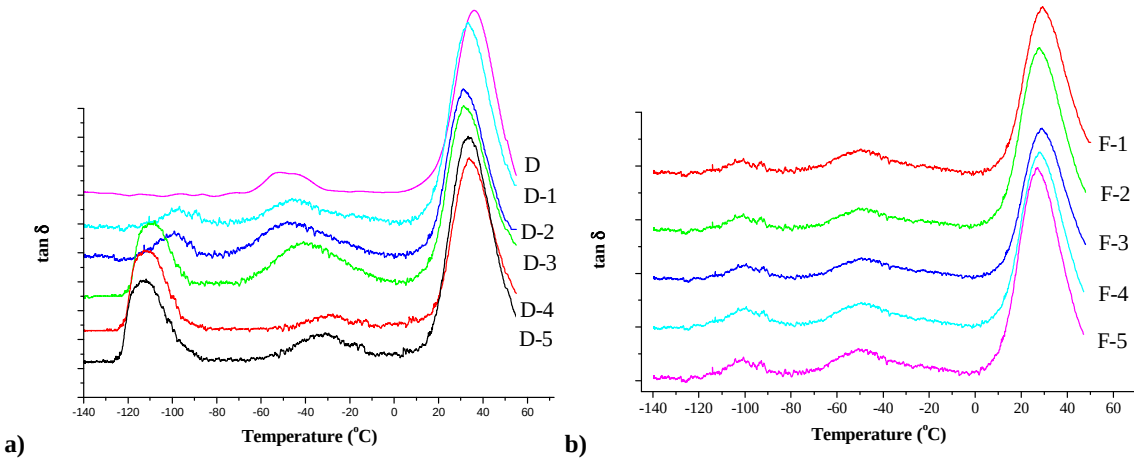

Figure 5.1: Tan δ profile of DMA results of: (a) PBCH homopolymer (D) and PDMS-s-PBCH copolymers, and (b) PDMS-br-PBCH copolymers.

In the D-1 and D-2 samples one can clearly see a broad glass transition peak (compared with the D-3, D-4 and D-5 samples). Such behaviour suggests the presence of a substantial amount of microphase mixing in the D-1 samples (as discussed above), and in the D-2 samples. This is not surprising in light of the fact that the ability of the D-1 copolymers to microphase separate is expected to be much lower than in the case of D-5 due to the lower degree of polymerization in the PDMS segment in the D-1 copolymer and thus a smaller χN (χ is the

Flory interaction parameter, which is also molar mass dependent (see Section 2.4.1)).[17] Microphase mixing would be substantial and it would be enhanced by the presence of methylene ($-CH_2-$) units in the PDMS end groups (see Scheme 5.1). There is no clear effect of the branching degree on the PDMS T_g values of the series F comparing with D-1, as illustrated in Figure 5.1.

The effect of the PDMS segment length and the branching degree on the melting temperature and the degree of crystallinity were investigated using DSC. The crystallinity degree is related to the area under the melting peak. From Table 5.2 it is clear that the area under the melting peak or the enthalpy of melting (the polymer crystallinity) decreases with an increase in the length of the PDMS segment in the copolymer (either based on the total weight of the copolymer (ΔH_m) or based on the weight of the polyester content (ΔH_{mPES})). Similarly the melting point decreases with an increase in the length of the PDMS segment in the copolymer. In the case of branched copolymers, it appears that the copolymer crystallinity degree and the melting points decrease with an increase in the branching degree in the copolymers. It was noticed that the melting peak of crystalline PBCH segments in both copolymer series is only detected in the first heating cycle using DSC. This might be due to the slow melt crystallization rates of these polyesters. The DSC thermograms of PBCH homopolymer and PDMS-s-PBCH and PDMS-br-PBCH copolymers are illustrated in Figure 5.2.

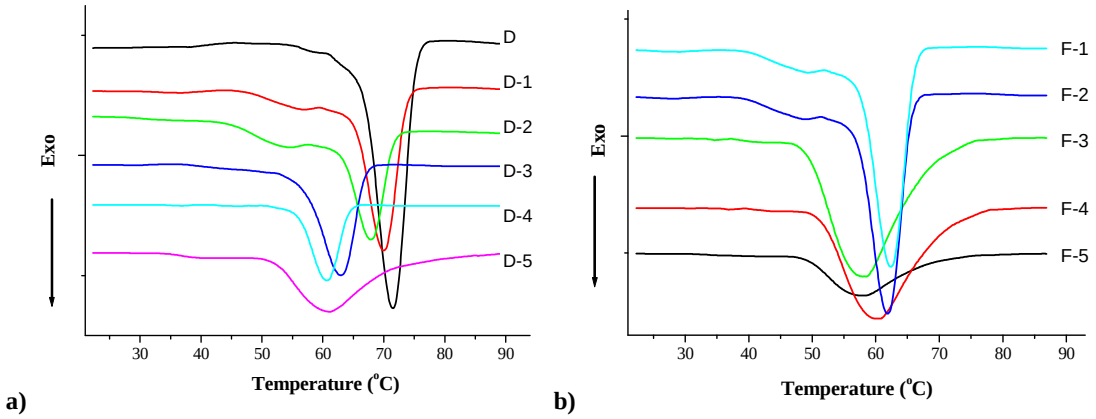

Figure 5.2: DSC thermograms of: (a) PBCH homopolymer (D) and PDMS-s-PBCH copolymers, and (b) PDMS-br-PBCH copolymers.

In the case of D-1, D-2, F-1 and F-2 copolymers, small shoulders appeared associated with the crystalline melting peaks of these copolymers in the DSC curves. These shoulders might be due to relaxation resulting from the amorphous PBCH segment or due to a lower long-

range order of the microdomains. The latter has been reported to be present in semicrystalline block copolymers when they have not been thermally annealed at high temperatures.[18] However, the shoulders here could also be an indication of the presence of crystallites of different sizes and perfection, due to the irregularity of the length of the PBCH segments or to crystal reorganization during the heating cycle in the DSC.

The effect of the PDMS segment length and the branching degree on the degree of crystallinity was also confirmed using WAXD analysis, as illustrated in Figure 5.3 and Table 5.2. Figure 5.3 (a and b) shows the intensity and WAXD pattern for PDMS and PBCH homopolymers, and PDMS-s-PBCH (a) and PDMS-br-PBCH (b) copolymers. The crystalline reflection peaks were observed at 15.3, 18.2, 20.5, 22.1, and 28.6°. This indicates that similar crystalline structures were present in the PDMS-s-PBCH and PDMS-br-PBCH copolymers as well as in the polyester homopolymers (PBCH).

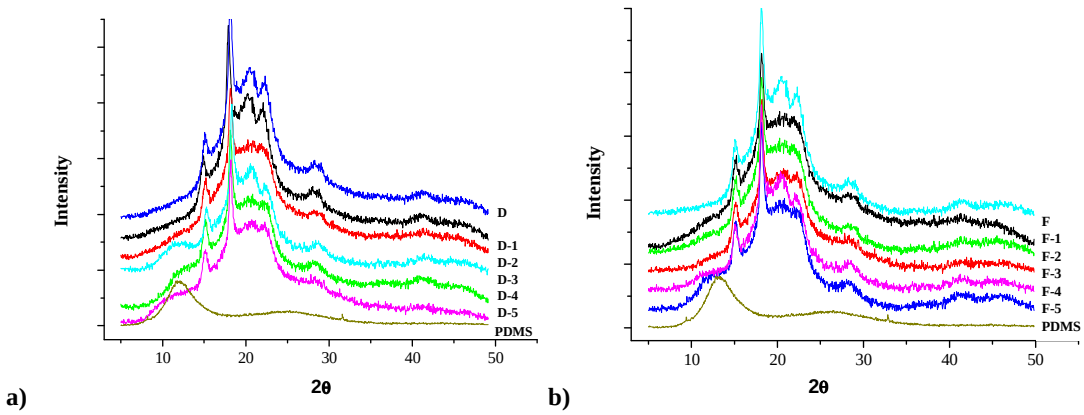

Figure 5.3: WAXD profiles of: (a) PBCH homopolymer (D), PDMS-s-PBCH copolymers and (b) D-1 (F) PDMS-s-PBCH copolymers and PDMS-br-PBCH copolymers. The profile of PDMS homopolymer is included in both diagrams (a and b).

There is a small PDMS shoulder at 2θ = 12.5°, which is related to the amorphous halo of the PDMS region. This is also observed in the PDMS homopolymer's WAXD pattern. The presence of this halo in the copolymers with long PDMS segments (D-3, D-4 and D-5) as well as the copolymers with high branching degrees (F-4 and F-5), and in the light of the fact that the position of this halo does not generally change in the copolymers, confirms the formation of a relatively pure PDMS micro or nano-segregated phases. This phenomenon has been also reported for other PDMS copolymers such as PDMS-polyurethane segmented copolymers[19] and PDMS-s-PBA copolymers (see Chapter 4).

The percentage of crystallinity was calculated from the WAXS data in Figure 5.3, by peak deconvolution. The ratio of the area under the crystalline peaks (I_c) to the total (amorphous + crystalline) area (I_{tot}) gave the degree of crystallinity (ω_m) and the crystallinity based on the polyester content (ω_{mPES}) was calculated. The results obtained are summarized in Table 5.2. The WAXD data of the thin films agree well with DSC results. WAXD results also showed that there was a significant reduction in crystallinity of the copolymers as the PDMS segment length increases in series D. There was also a clear decrease in the crystallinity of the copolymers as the branching degree increases in the branched copolymers (series F).

5.3.2 Microscopic surface and bulk morphology of the copolymers

First, the morphology of segmented copolymers with different PDMS segment lengths will be discussed, and then the effect of branching on the morphology of the PDMS-PBCH copolymers with short PDMS segment length (1000 g/mol) will be discussed (notice the scale in the AFM and the TEM images are chosen to best represent to the observed morphology).

Figure 5.4 shows the surface morphology of the PBCH homopolymer (Figure 5.4(a) and (b)), height and phase images, respectively) and PDMS-s-PBCH copolymers with 10 wt % PDMS content and PDMS M_n 1000 g/mol (Figure 5.4(c) and (d)), height and phase images, respectively), as monitored by AFM. All the AFM images show well-defined semicrystalline morphology of spherulites. The spherulites size of the polyester homopolymer (20–25 μm) is, however, much larger than that of the copolymers (10–15 μm). This indicates that incorporating PDMS segments in the polyester chains affects the crystallinity arrangement or order, as well as the melting temperature and the crystallinity degree, as has been discussed in DSC and WAXD results (see Section 5.3.2). The reduction in the melting temperature of the copolymers can be as a result of the decrease in the spherulite size.

This type of surface morphology recorded for the PDMS-s-PBCH copolymers confirms the results observed by Miroslawa[4] for the surface of polydimethylsiloxane-polybutyleneterephthalate segmented copolymers, using POM. However, the internal structure of these spherulites is better revealed in the PDMS-s-PBCH copolymers in the phase image than the height image. Additional information can be gained from the variation in the contrast in the phase image, where the PDMS domain can be clearly seen.

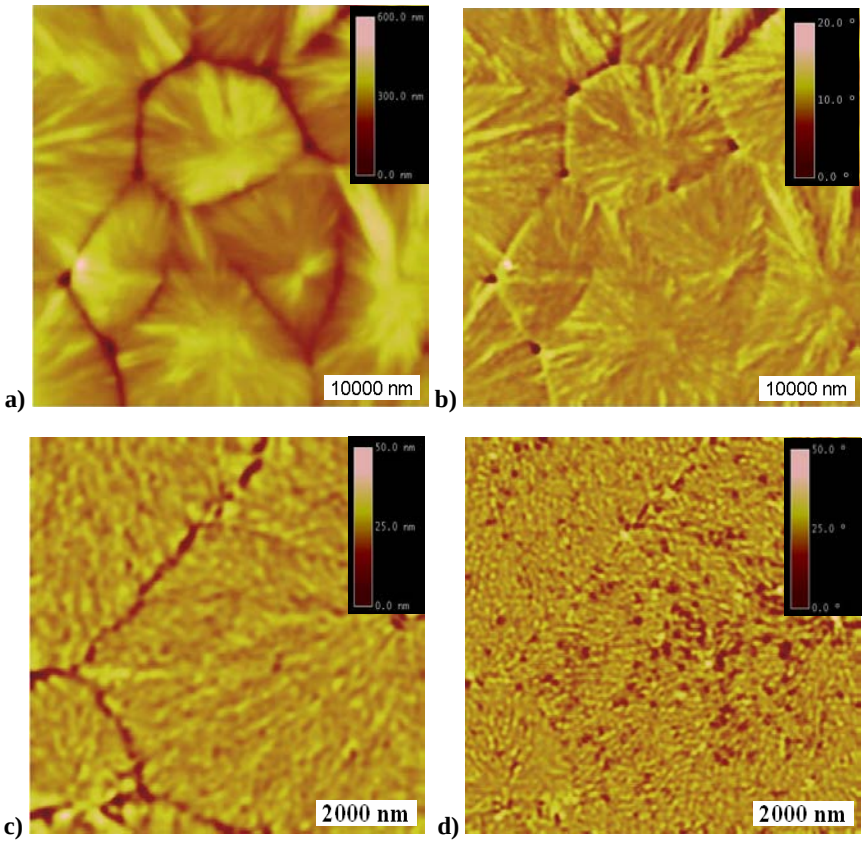

Figure 5.4: AFM images of thin films of (a and b) PBCH homopolymer and (c and d) PDMS-s-PBCH with 10 wt % PDMS content and PDMS M_n 1000 g/mol.

Two phases can be distinguished when moderate to hard tapping forces are used. Small darker spherical domains in a matrix of the continuous phase are due to the PDMS component representing the minority phase. It is proposed that these spherical domains in the copolymer are PDMS segments that segregate to form PDMS domains or islands (dark spots in the phase images) in polyester matrix (the bright region in the phase images). As has been mentioned in Chapter 4 (see Section 4.3.2), PDMS and polyester are different both chemically and mechanically, and the combination of both of these differences leads to variation between the PDMS regions and polyester regions in terms of the viscoelasticity properties as well as in the energy dissipation between the sample surface and the AFM tip interface. Thus, the siloxane containing phases appear darker than the ester containing phases in the AFM phase image micrographs. Therefore, the small dark spheres in Figure 5.4(d) are most likely related to the PDMS domain. The AFM phase image of the PDMS-s-PBCH copolymer with 10 wt % and, 1000 g/mol M_n PDMS in Figure 5.4(d) shows domains of PDMS between the crystal lamellae, similar to the ones seen for the PDMS-s-PBCH copolymers with 5 wt % and 2000 g/mol M_n PDMS segments (Figure 4.4). The size of the

PDMS domain seems to be large compared to that obtained for PDMS-s-PBCH copolymers with larger PDMS segment length and 10 wt % PDMS (see Figure 5.5). One of the possible explanations for this is that crystallization of the PBCH segment leads the PDMS segments being pushed out of the crystal structure. This continuous rejection of PDMS amorphous segment by the crystallisable PBCH segment during the crystal growth allows more PDMS segment to segregate and form larger domains of PDMS on the copolymer surface. The slight variation in the brightness of bright region (polyester phase) in Figure 5.4(d) can be attributed either to the changes in the height of the lamellae or due to the presence of both crystalline and amorphous areas in the spherulitic crystal structure.

Figure 5.5 shows the morphology of a PDMS-s-PBCH copolymer with 10 wt % PDMS content and various PDMS segment lengths. No spherulitic crystal structure was detected on the surface for the copolymer with the large PDMS segment length. This is simply because the longer PDMS segments inhibit the crystallization significantly. However bright spots were detected, which can either be due to the height effect or due to crystalline domains PBCH in the copolymers. There is still evidence of the PDMS domains between the lamellae order particularly in the phase images of copolymer samples D-2 and D-3, as shown by the circles in Figures 5.5(a) and 5.5(b). The PDMS domains are clearly observed in all cases, and when comparing the sizes of these spheres it is clear that as the PDMS segment length increases so the size of the PDMS spheres increases, it increases from 40±10 nm in diameter for D-2 to more than 200±50 nm for D-4 (see Figure 5.6(a) and 5.6(c), respectively, and Table 5.3).

In the case of the copolymers with small PDMS segments, the crystallinity and the incompatibility between the copolymer components seems to work together as driving forces for microphase separation on the copolymer surface. Therefore the phase separation occurs after the crystallization has taken place. On the other hand, when the PDMS segment is long the semicrystalline spherulites cannot be observed. This might be because the PDMS segments disrupt the crystal order of the polyester segments and therefore microphase separation occurs first, which prevents large spherical crystal structures from forming.

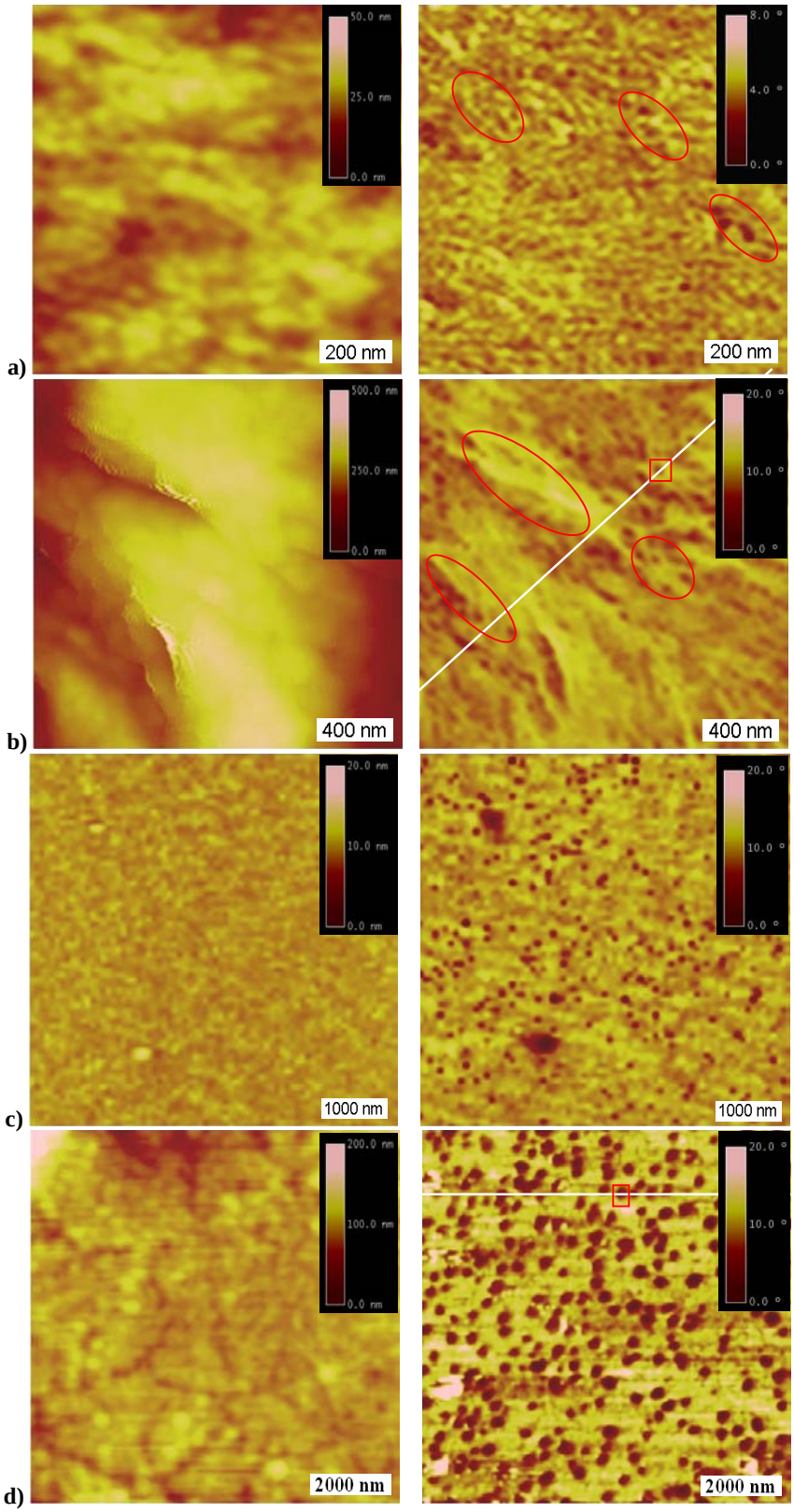

Figure 5.5: AFM images of thin films of PDMS-s-PBCH copolymers with 10 wt % PDMS and segment of PDMS of different M_n: (a) PDMS M_n 2000, (b) PDMS M_n 4000, (c) PDMS M_n 7000 and (d) PDMS M_n 10000 g/ mol.

Figure 5.6 shows examples of the measurements of the spheres diameters using the phase profile of the AFM phase images, for two PDMS-s-PBCH copolymers, with 10 wt % PDMS and different PDMS segment lengths: (a) PDMS M_n 4000 g/mol, and (b) PDMS M_n 10000 g/mol. Figures 5.6(a) and 5.6 (b) show the phase profiles along the lines drawn in the AFM phase images Figure 5.5(b) and 5.5(d), respectively across several PDMS domains in order to measure the spheres diameters. The resulting average diameter values, which are summarized in Table 5.3, were based on three images for each copolymer.

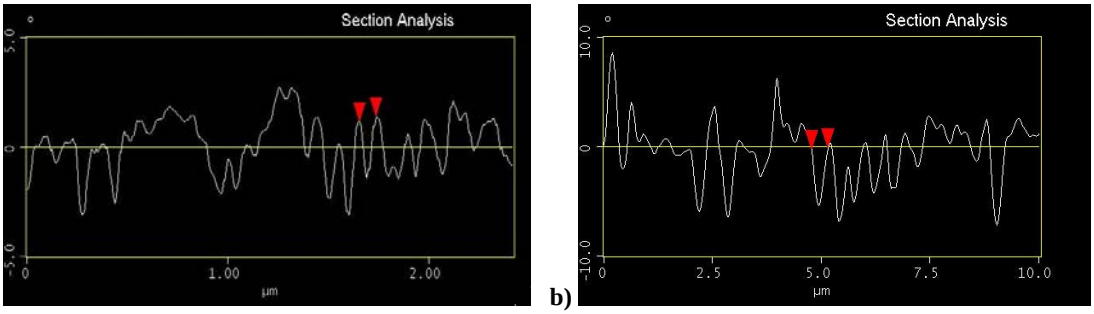

Figure 5.6: Analysis section of AFM phase images of thin films of PDMS-s-PBCH copolymers with 10 wt % PDMS and PDMS segments with different M_n values: (a) PDMS M_n 4000, and (b) PDMS M_n 10000 g/mol.

Figure 5.7 shows a TEM micrograph of a cross-section of a PDMS-s-PBCH copolymer with 10 wt % PDMS and PDMS segment of M_n 1000 g/mol. It clearly shows that the PDMS-s-PBCH copolymer had distinct microphase separation, which supports the T_g results obtained using DMA.

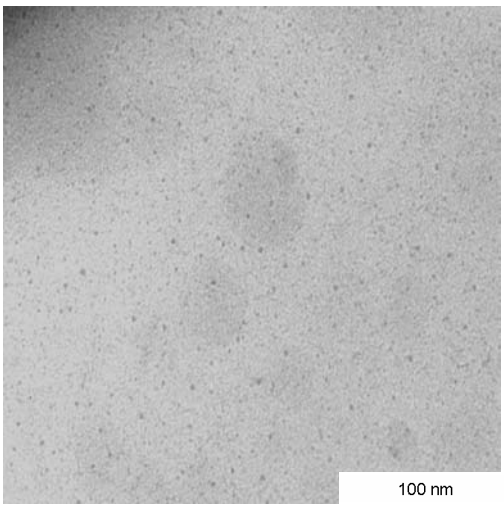

Figure 5.7: TEM micrograph of PDMS-s-PBCH copolymer with 10 wt % PDMS content and M_n 1000 g/mol.

Since the contrast in TEM images results from the difference in the electron density in silicon and carbon, the PDMS phase can be distinguished as a dark area due to the higher electron density of Si relative to the polyester segment (C and O). Therefore, the dark spots or spheres in Figure 5.7 correspond to the PDMS domains. These are surrounded by the light matrix, which is obviously the polyester phase. For the copolymers with quite short PDMS segments (M_n 1000 g/mol) (D-1) the largest spherical domains obtained from TEM images have a diameter of approximately 20 nm (Figure 5.7), this contrast to AFM results in which the diameter of the PDMS domains goes up to 300 nm (Figure 5.4(d)). This indicates, indirectly, that crystallization of the polyester segment is one of the driving forces that leads PDMS segment to segregate on the surface, where it forms bigger domains, and probably the phase separation in the bulk is more affected by the microphase separation in the solution (liquid–liquid demixing), before the crystallizations of the polyester segment commenced. On the other hand, the smallest visible spherical domains for D-1 in the Figure 5.7 have a diameter of approximately 5 nm (nano-domains). Based on that standard deviation of the measured diameters of the PDMS domains one can conclude that the PDMS segment was not distributed evenly along the copolymer chains. This is suggested by the relatively large standard deviation in the size of PDMS domains not only for D-1 but for the entire series (Table 5.3).

Figure 5.8 shows examples of TEM micrographs of PDMS-s-PBCH copolymer containing 10 wt % PDMS of various M_n. The micrographs show a very fine micro-phase separated structure with the polyester as the continuous phase and the PDMS as the included phase mostly in a spherical shape. No obvious crystal structure can be detected in these TEM pictures. However, the PDMS domains can be clearly seen in all cases. Furthermore, as the PDMS segment length increases in the copolymer chains, the diameter of the PDMS domains becomes larger. Therefore, the PDMS spherical domains become more defined as the PDMS segment length increases. This indicates a higher degree of phase separation with an increasing PDMS molar mass. This finding is consistent with results of DMA analysis, specifically for D-3, D-4 and D-5 in Figure 5.1. The average sizes of the PDMS domains were determined by TEM images analysis using Image J. exe. Software. The size of the PDMS spheres increases from 15±5 nm in D-1 to 80±40 nm (nano-domains) in D-5. See Table 5.3.

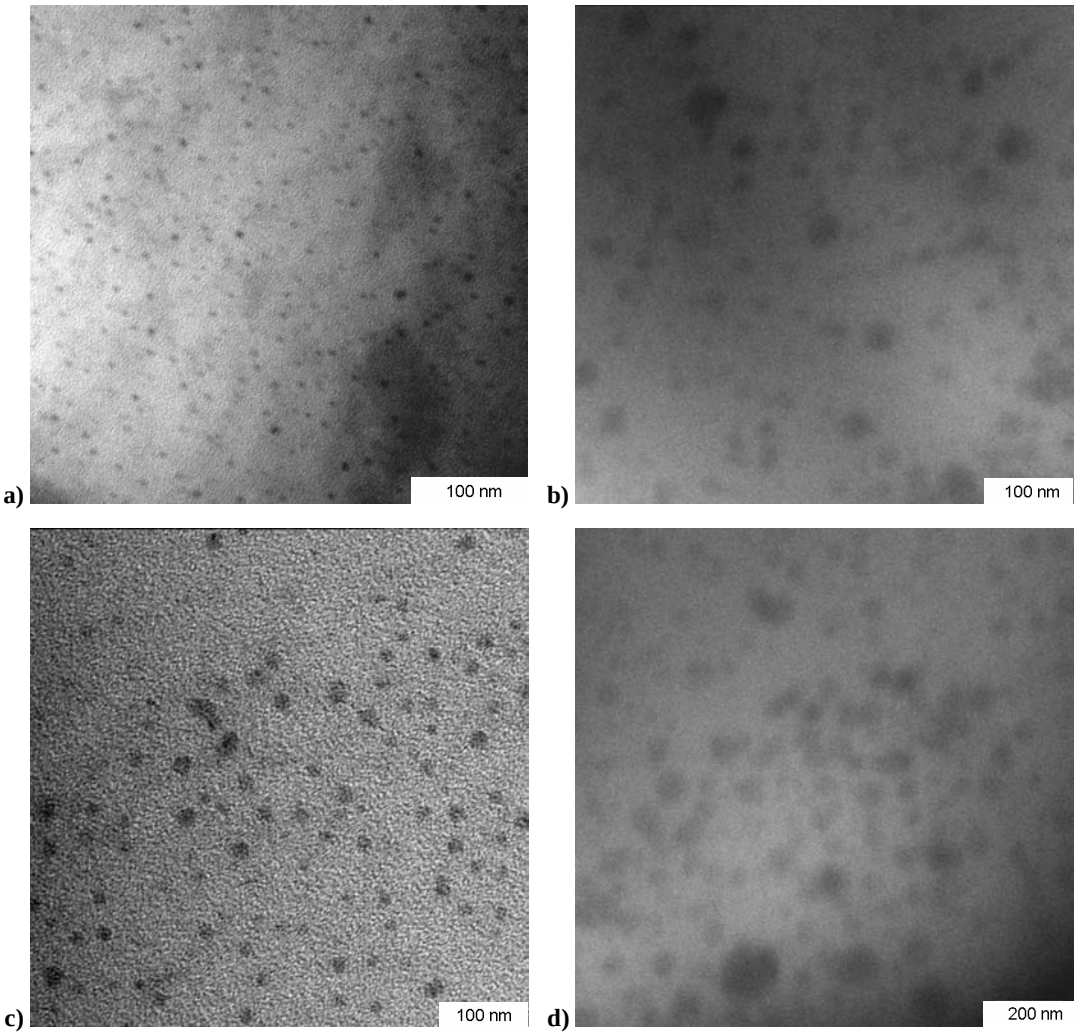

Figure 5.8: TEM micrograph of PDMS-s-PBCH copolymers with 10 wt % PDMS content and varying M_n: (a) 2000, (b) 4000, (c) 7000 and (d) 10000 g/mol.

The PDMS domain size in the spherical morphology can be related to the molar mass of the spherical domain forming segment using the Meier equation[20]

$$R = 1.33\ \alpha\ kM_n^{1/2} \qquad \text{[Eq 5.1]}$$

where R is the domain radius for a spherical domain, α and k are constants for each polymer (for PDMS α = 1.2 and k = 880×10^{-3}, for R in Angströms), and M_n is the molar mass of the spherical domain forming segment.[21] Table 5.3 shows the theoretical diameters of the domain and the experimentally diameters. The theoretical diameter was calculated based on Eq 5.1, and the experimentally diameters were obtained from AFM and TEM analyses.

Table 5.3: Domain sizes (diameters) of segmented PDMS-PBCH copolymers

Sample	Theoretical diameter (nm)	Diameter from AFM (nm)	Diameter from TEM (nm)
D-1	4.44	250±100	15±5
D-2	6.28	40±10	25±10
D-3	8.88	60±20	40±20
D-4	11.75	200±50	60±30
D-5	14.05	300±100	80±40

The largest nanospheres for the PDMS-s-PBCH copolymers with 10 wt % PDMS and PDMS M_n 10000 g/mol Figure 5.9(d) have a diameter of approximately 80±40 nm (sub-micron domains) as measured from TEM images. The size of the nanodomains consisting of just one PDMS segment is expected to be 14.1 nm, based on the PDMS molar mass and using Eq 5.1. This indicates that the nanodomains contain more than one segment of PDMS, and possibly also very short PBCH segments, which link two or more PDMS segments with each other. Although the dimensions of the spheres determined using the Meier equation do not show very good agreement with the experimentally determined dimension, the dimensions of the spherical PDMS domains (obtained by TEM), seem to obey a law proportionality with $Mn^{2/3}$ in agreement with the previous studies, when a strong separation between the copolymer components was observed.[22,23]

The average sphere diameters obtained from AFM are larger than those obtained from TEM. This could be due to one or both of the following reasons. First, due to the low surface energy of the PDMS it has a propensity to diffuse to the copolymer surface, thus more PDMS is in the surface than in the bulk. Second reason is that error could occur due to the AFM architecture error. Such an error may arise due to one or both of the following reasons. First, when measuring very small objects using AFM, the actual size of AFM tip cannot be neglected, the measured profile is in fact a convolution of the actual profile by the tip shape.[24] Second, flattening can occur,[25] especially when the surface of a soft material is measured (in this case PDMS). The flatting was minimized by using AFM in the tapping mode.

Figure 5.9 shows the AFM phase images of the thin film surface of PDMS-br-PBCH copolymer with various branching degree. The PDMS content in all the copolymers is 10 wt % and the PDMS segment length is 1000 g/mol.

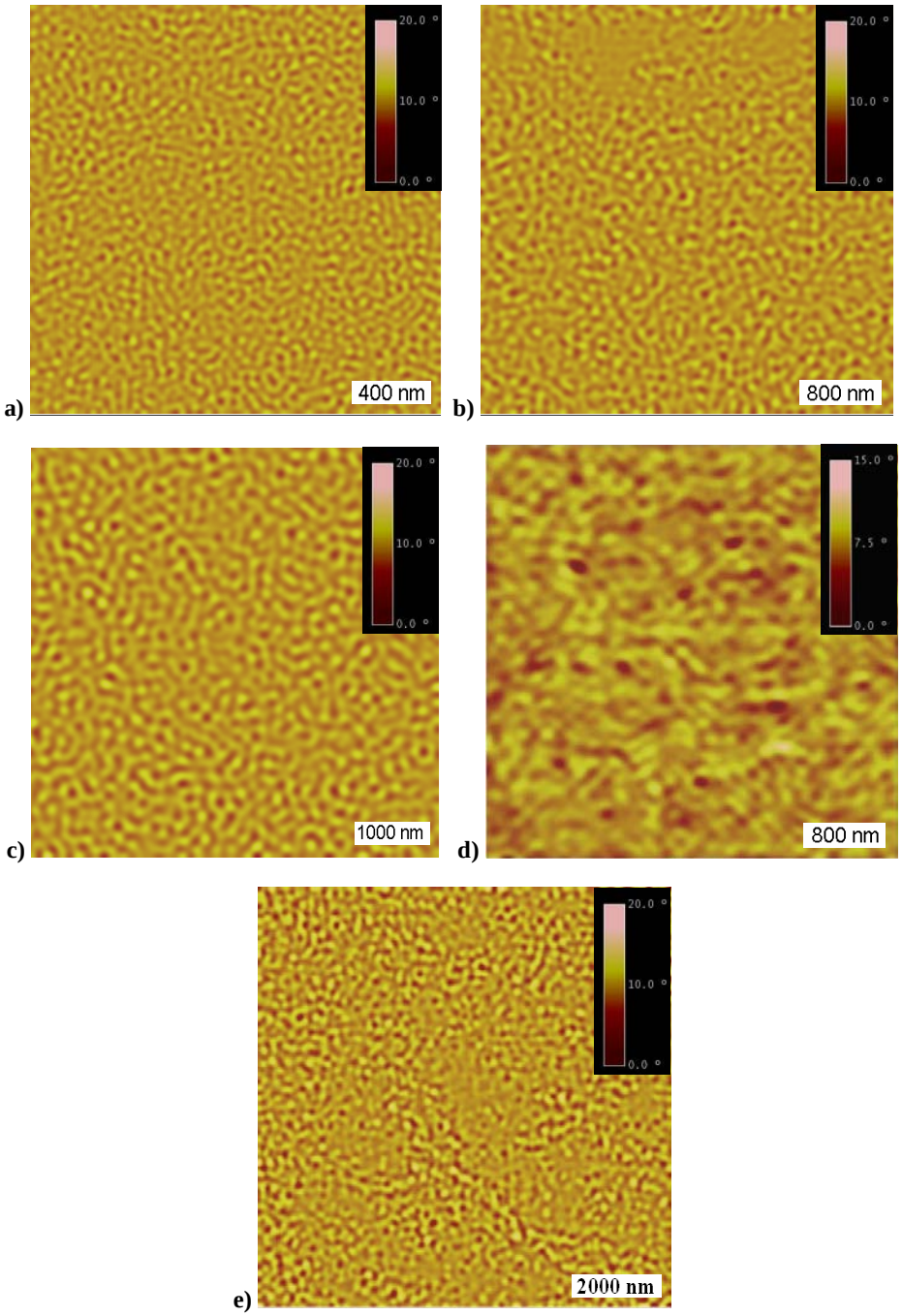

Figure 5.9: AFM phase images of the PDMS-PBCH branched copolymer with 10 wt % PDMS and (a) 0.1 wt % branching agent, (b) 0.2 wt % branching agent, (c) 0.5 wt % branching agent (d) 1 wt % branching agent (e) 2 wt % branching agent.

All the copolymers show spherical PDMS domains. However, F-5 (Figure 5.9(e)) also shows secondary morphology, where several of the PDMS spheres are connected with each other to form another phase of continuous PDMS regions. The diameters of these domains were determined from the AFM images and the results summarized in Table 5.4. The diameter of

the PDMS spheres increases as the branching degree increases. Microphase separation of the spherical hard domains for segmented and branched segmented poly(urethane urea) copolymers, has been previously reported by Sheth and coworkers[26] using only phase images of the AFM.

Although the variation in the brightness of the bright phase in Figure 5.9 can be explained as the variation in the height or the surface roughness, another explanation is possible; this is as a result of the presence of hard crystalline PBCH. However, in Figure 5.9 the semicrystalline spherulites were not observed even when a small percentage of the branching agent was used, as in F-1 (0.1 wt %), although F-1 has a relatively large degree of crystallization (see Table 5.2). This indicates the combination effect of both the random branches and the PDMS segment content. Both may disrupt the large crystal order of polyester segments, especially the spherulitic crystal structure. These factors might also be the cause of the noticeable reduction in the T_gH of the polyester segment (T_gH in Table 5.2). This reduction in the T_gH can be seen in the entire series of the branched copolymers (series F), when it is compared to segmented copolymer that has the same PDMS segment length as the branched copolymers sample D-1. The reduction in T_gH probably gives more ability to the PDMS segment to diffuse to the copolymer surface due to the increase of the copolymer chain mobility.

Figure 5.10 shows TEM micrographs of the PDMS-br-PBCH copolymers with various degrees of branching, and with 10 wt % PDMS content and 1000 g/mol PDMS segment length. In the bulk of the copolymer, as the branching degree increases in the copolymer chain, the diameters of the PDMS domains become larger.

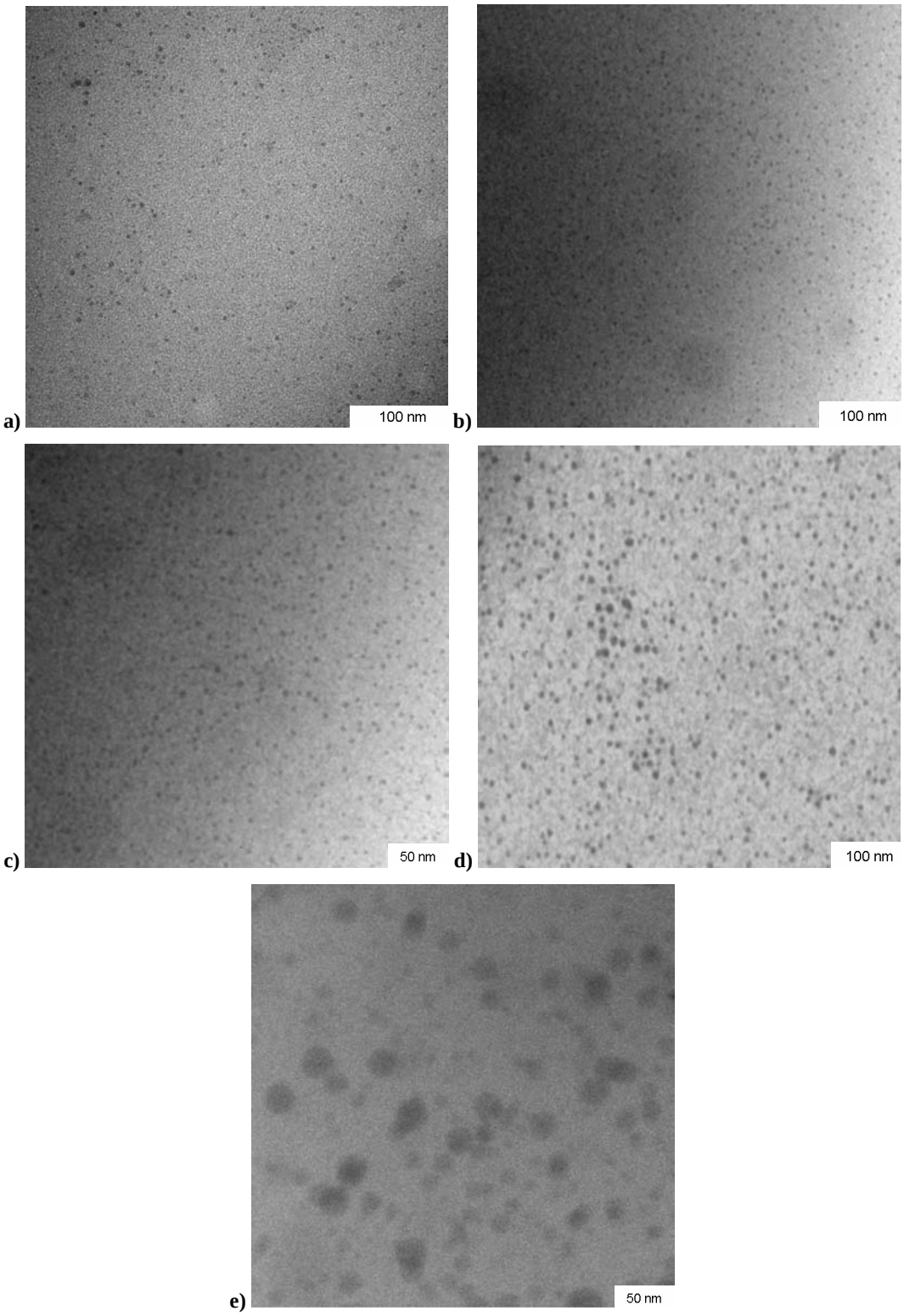

Figure 5.10: TEM micrograph of PDMS-PBCH segmented (a) and branched copolymer with 10 wt % PDMS, and (b) 0.1 wt % branching agent, (c) 0.2 wt % branching agent, (d) 0.5 wt % branching agent, (e) 1 wt % branching agent, and (f) 2 wt % branching agent.

Once again, the TEM micrographs for the PDMS-br-PES copolymers generally show similar morphologies to those obtained in the AFM images. However, the most dominant type of morphology observed in the F-5 copolymer was only spherulitic microphase-separated PDMS domains. The diameters of the PDMS domains were measured in the copolymer bulk from the TEM images and the average diameters are tabulated in Table 5.4.

Table 5.4: Domain sizes (diameter) of branched PDMS-PBCH copolymers

Sample	Diameter from AFM (nm)	Diameter from TEM (nm)
F-1	50±10	20±5
F-2	100±20	30±10
F-3	150±30	35±10
F-4	300±60	40±15
F-5	400±80	50±20

Once again it is clear that the diameter of the PDMS domains increase as the branching degree increases. This might be due to the effect of the increase in the branching degree on the degree of the crystallinity of the polyester segments (as it has been discussed in the DCS results in Section 5.3.1) and because the T_g values of the copolymer segments are below room temperature. Therefore, the PDMS segment will have much better chain mobility as the degree of the crystallinity decreases and thus the size of PDMS domains increases. For instance, it increases from 30±10 nm in diameter for D-2 to more than 50±20 nm for D-5 see Table 5.4. Similar to the case of the segmented copolymers, the average diameters obtained by AFM are larger than those obtained from TEM images, for similar reasons mentioned previously in the PDMS-s-PBCH copolymers in this section. This indicates that the branching in the copolymers does not restrict the PDMS segment movement toward the copolymers surface.

5.3.3 Adhesive force and surface roughness

PDMS has a very low surface energy,[27,28] and due to the PDMS surface segregation, the PDMS-PBCH copolymers are expected to have a low surface energy. The surface energy (adhesive force) of PDMS-PBCH segmented and branched copolymers was measured using digital pulsed-force mode AFM (DPFM-AFM). Results are shown in Figure 5.11 where the averages of the adhesive force are plotted against the PDMS segment length and the branched contents and several adhesive force images are also included.

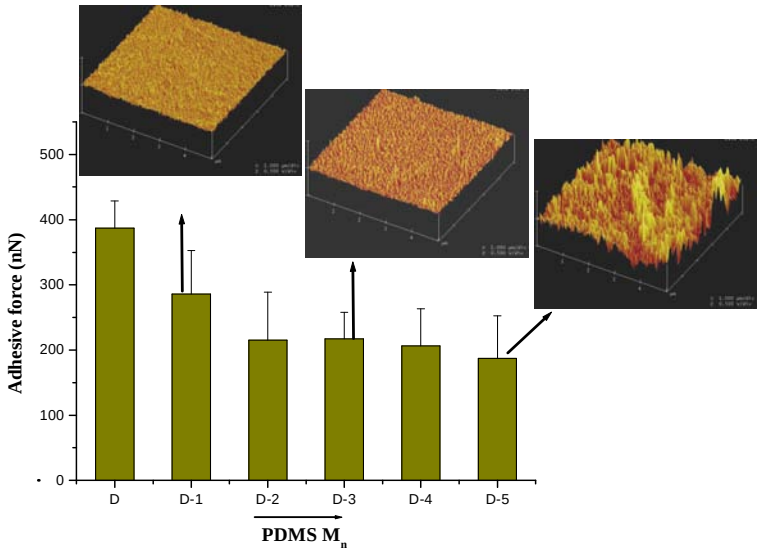

a)

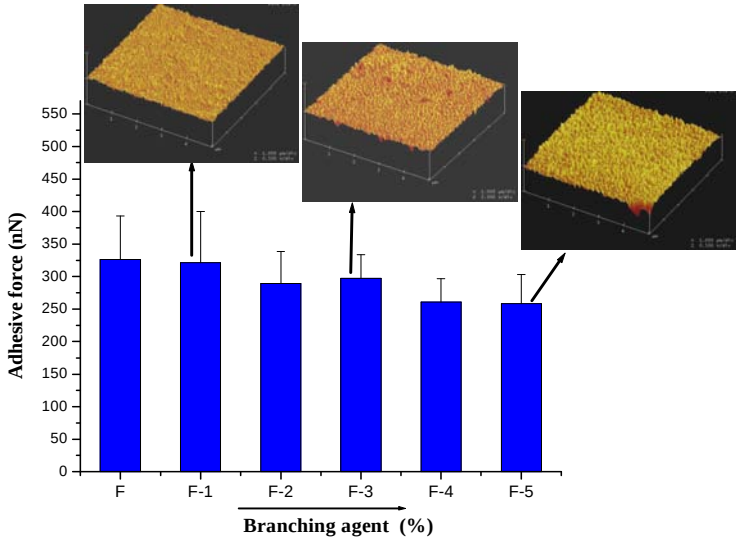

b)

Figure 5.11: Adhesive force measurement of: (a) PBCH homopolymer (D), PDMS-s-PBCH copolymers and (b) D-1 (F) PDMS-s-PBCH copolymers and PDMS-br-PBCH copolymers.

It is clear from Figure 5.11 that as the PDMS segment length increases, the adhesive force decreases. A similar effect is found for an increase in the branching degree. The dark spots in the adhesive force images indicate lower surface energy regions, which are more likely related to the PDMS domains, as it has been suggested by Jin et al. for polyimidesiloxane copolymers.[29]

The large standard deviation in both copolymers might be due to the heterogeneity of the surface composition or in the functional groups on the surface (such as CH_3, CH_2, C=O and OH). It is clear evident that no complete monolayer of PDMS has been formed on the surface

of PDMS-PBCH segmented copolymer due to the large variation in the entire D series. In case of complete formation of a monolayer the variation of the function group on the surface would be less and therefore, the standard deviation would be smaller. Similar results were obtained for PDMS-br-PBCH, where no complete PDMS monolayer is formed.

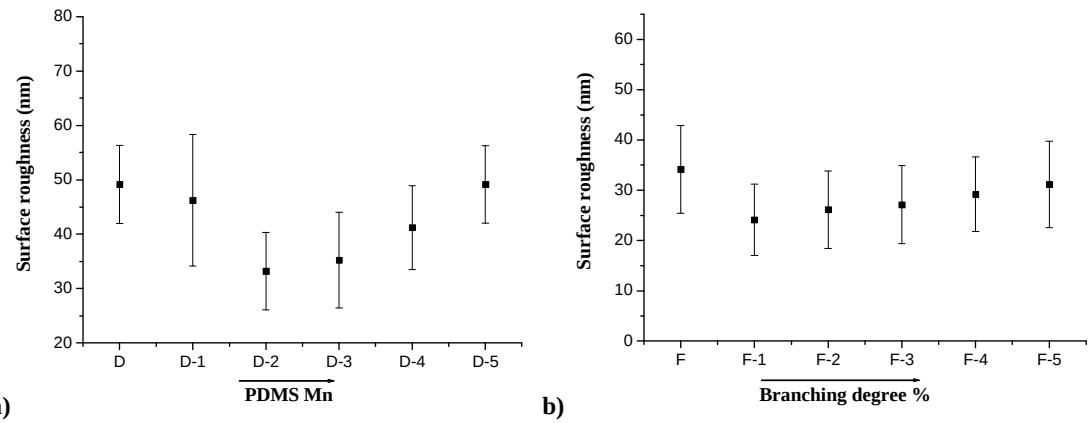

Figure 5.12: Surface roughness of: (a) PBCH homopolymer (D), PDMS-s-PBCH copolymers and (b) D-1 (F) PDMS-s-PBCH copolymers and PDMS-br-PBCH copolymers.

Figure 5.12 shows the influence of varying PDMS segment length on the surface roughness of the PDMS-PBCH as well as the influence of various degree of branching, it seems that the surface roughness value for D and D-1 (F) is quite large which might be due to the spherulitic crystal structure in these polymers. However, for the rest of the copolymers the surface roughness value increases with increasing the PDMS segment length, which could be related to increasing in the phase separation on the surface as the PDMS length increases. The PDMS length segments or domains form islands on the surface. The size and the height of these islands increase as the PDMS concentration on the copolymers surfaces increases.

The surface composition of these copolymers seems to depend on both the polymer structure PDMS segment length and degree of branching. The spherulitic crystal morphology changed to a spherical PDMS microdomain morphology when PDMS increases to a specific degree, which affects the adhesive force, as well as the surface roughness.

Figure 5.12 shows a non-linear relationship between the average surface roughness and PDMS segment length and the branched degree. The changes in the surface roughness due to varying the PDMS content in the polysiloxane-polyimides copolymers has been

reported by Furukawa and co-workers.[30,31] The change in the surface roughness was related to the degree of phase separation in the copolymer, which cannot be done in the PDMS-s-PES systems due to the fact that in addition to the phase separation effect, the crystallinity has a great effect on the surface roughness. As the crystallites were not detected for the branched (PDMS-br-PBCH) copolymers on the copolymer surface, the changes in the surface roughness could be used as an indication of the degree of phase separation in this case.

5.4 Conclusions

The morphology of two series of semicrystalline PDMS-s-PBCH copolymers and PDMS-br-PBCH copolymers, with 10 wt % PDMS content were successfully investigated using DMA, DSC, WAXD, AFM and TEM techniques. The AFM images of PBCH homopolymer and PDMS-s-PBCH copolymers with 10 wt % PDMS content and PDMS of M_n 1000 g/mol showed that the PBCH homopolymer exhibited spherulite crystal morphology whereas the PDMS-s-PBCH copolymers exhibited spherulite morphology as well as PDMS domains disrupting the lamella arrangement in the spherulites. Despite the ability of the PDMS segments to segregate on the surface the polyester segments managed to crystallize rather well, as seen in the AFM images of the copolymers with short PDMS segment lengths. This was confirmed by WAXD and DSC results. For longer PDMS segment lengths the crystalline spherulite disappeared and the morphology became more homogeneous. However, WAXD and DSC analyses revealed relatively low degrees of crystallinity for the entire segmented and branched copolymers series. This indicated that the crystallinity might be confined only in small regions. It was clear that the PDMS segment length and the branching degree had unfavourable effects on the crystallization of the PBCH segment. It was difficult for the polyester segments to form a spherulitic superstructure with PDMS of M_n 2000 or even in lower PDMS of M_n 1000 with a small degree of branching (0.1 wt % and g = 0.94).

The microphase separation in both segmented and branched PDMS-PBCH copolymers with random polyester segment lengths and 10 wt % PDMS was clearly detected in the DMA results, and visualized in AFM and TEM images. The phase separation probably occurs by liquid–liquid demixing (or microphase separation in the solution), in combination with crystallization of the polyester segment. The main type of phase separation morphology was spherical domains of PDMS in the PBCH matrix. The diameters of these domains increase in proportion to the PDMS segment length for the segmented copolymers and to the degree of

branching for the branched copolymers. In the case of branched copolymers the increase in the branching degree forces the PDMS domains to connect with each other, and this eventually leads to the formation of a type of bicontinuous phase separation on the surface. However the bicontinuous phase separation was not observed in the bulk morphology by TEM. This difference in the morphology between the bulk and the surface illustrates that there is a higher concentration of PDMS on the surface than in the bulk. This is a result of the ability of PDMS segments to diffuse or flip to the surface, due to the low surface energy of the PDMS. This is also indicated from the difference in the sizes of the PDMS domains on the surface and in the bulk of the copolymers. Furthermore, results of AFM pulsed mode for both copolymer series showed a significant change in the adhesive force, which was correlated to difference in the PDMS M_n in series D and to an increase in the branching degree in series F. The change in both the PDMS M_n and branching degree also affected the surface roughness of the samples, as observed from AFM height images, which were captured with the associated adhesive force images.

5.5 References

1. Chun-Kang, K.; Yu-Der, L. *Polymer* 2007, 48(12), 3565-3573.
2. Malhotra, L.; Bluhm, T. L.; Deslandes, Y. *European Polymer Journal* 1986, 22(5), 391-397.
3. Kiefer, L. A.; Yoon, T. H.; Glass, T. E.; Jayaraman, S. K.; McGrath, J. E. *Journal of Polymer Science, Part A: Polymer Chemistry* 1997, 35(16), 3495-3506.
4. Miroslawa, E. F. *Designed Monomers and Polymers* 2000, 3(3), 325-337.
5. Antic, V. V; Balaban, M. R.; Djonlagic, J. *Polymer International* 2001, 50(11), 1201-1208.
6. Dojcinovic, B. P.; Antic V.V.; Vuckovic, M. V.; Djonlagic J. *Journal of the Serbian Chemical Society* 2005, 70(12), 1469-1485.
7. Vuckovic, M. V.; Antic V.V.; Dojcinovic B.P.; Govedarica M.N.; Djonlagic J. *Polymer International* 2006, 55(11), 1304-1314.
8. Ekin, A.; Webster, D. C. *Journal of Polymer Science, Part A: Polymer Chemistry* 2006, 44(16), 4880-4894.
9. Rangarajan, P.; Register, R. A.; Adamson, D. H.; Fetters, L. J.; Bras, W.; Naylor, S.; Ryan, A. J. *Macromolecules* 1995, 28(5), 1422-1428.
10. Ryan, A. J.; Hamley, I. W.; Bras, W.; Bates, F. S. *Macromolecules* 1995, 28(11), 3860-3868.

11. Loo, Y.-L.; Register, R. A.; Ryan, A. J. *Macromolecules* 2002, 35(6), 2365-2374.

12. Müller, A.; Balsamo, V.; Arnal, M., Nucleation and crystallization in diblock and triblock copolymers. In *Block Copolymers II*, Springer, Berlin / Heidelberg, 2005; pp 1-63.

13. Childs, M. A.; Matlock, D. D.; Dorgan, J. R.; Ohno, T. R. *Biomacromolecules* 2001, 2(2), 526-537.

14. Higuchi, A.; Nakagawa, T. *Journal of Polymer Science, Part B: Polymer Physics* 1994, 32(1), 149-157.

15. Clarson, S. J.; Dodgson, K.; Semlyen, J. A. *Polymer* 1985, 26(6), 930-934.

16. Jignesh, P. S.; Ashish, A.; Garth, L. W.; Emel, Y.; G Ekin, A.; Iskender, Y.; Frederick, L. B. *Polymer* 2004, 45(20), 6919-6932.

17. Etxabarren, C.; Iriarte, M.; Uriarte, C.; Etxeberría, A.; Iruin, J. J. *Journal of Chromatography A* 2002, 969(1-2), 245-254.

18. Balsamo, V.; Gil , G.; Urbina de Navarro, C.; Hamley, I. W.; Gyldenfeldt, F.; Abetz V.; Cañizales, E. *Macromolecules* 2003, 36(12), 4515-4525.

19. Hernandez, R.; Weksler, J.; Padsalgikar, A.; Runt, J. *Macromolecules* 2007, 40(15), 5441-5449.

20. Meier, D. J. *Journal of Polymer Science, Part C: Polymer Symposia* 1969, 26, 81-98.

21. Sperling, L. H., *Introduction to Physical Polymer Science.* Wiley-Interscience and Sons: United States, 2006; pp 169-171.

22. Hashimoto, T.; Fujimura, M.; Kawai, H. *Macromolecules* 1980, 13(6), 1660-1669.

23. Stanciu, A.; Airinei, A.; Timpu, D.; Ioanid, A.; Ioan, C.; Bulacovschi, V. *European Polymer Journal* 1999, 35(11), 1959-1965.

24. Samorí, P.; Francke, V.; Mangel, T.; Müllen, K.; Rabe, J. P. *Optical Materials* 1998, 9(1-4), 390-393.

25. Rivetti, C.; Guthold, M.; Bustamante, C. *Journal of Molecular Biology* 1996, 264(5), 919-932.

26. Sheth, J. P.; Unal, S.; Yilgor, E.; Yilgor, I.; Beyer, F. L.; Long, T. E.; Wilkes, G. L. *Polymer* 2005, 46(23), 10180-10190.

27. Luo, Z.-h.; He, T.-y. *Reactive and Functional Polymers* 2008, 68(5), 931-942.

28. Hardman, B., Silicones. In *Encyclopaedia of Polymer Science and Engineering*, First ed.; Kroschwitz, J. I. (Ed.), John Wiley and Sons., United States, 1989; Vol. 15, pp 234-251.

29. Jin Z.; Sergio R.R.; Jiaxing C.; Mingzhu Xu.; Joseph A.G.J. *Macromolecules* 1999, 32(2), 455-461.

30. Andrea, D. B. Synthesis and characterization of poly(siloxane imide) block copolymers and end-functional polyimides for interphase applications. PhD dissertation, Virginia Polytechnic Institute and State University, United States, 1999, p 54.

31. Furukawa N; Yamada Y; Furukawa M; Yuasa M; Kimura Y. *Journal of Polymer Science, Part A: Polymer Chemistry* 1997, 35(11), 2239-2251.

Chapter Six

Measurement of Free Volume in PDMS-PBCH Copolymers Using Positron Annihilation Lifetime Spectroscopy

Abstract:

In order to obtain more information on the morphology of PDMS-PBCH semicrystalline copolymers positron annihilation lifetime spectroscopy (PALS) was used to measure the free volume in the copolymers as well as in the PDMS and PBCH homopolymers. The free volumes of the PDMS and the PBCH homopolymers were determined by analyzing the lifetime (LT) spectra using a three-components fit. In the case of the PDMS-PBCH copolymer series, where the three-components fit becomes has no physical relevance the LT spectra of the PDMS-PBCH copolymer series were analyzing using a four-components fit in addition to the three component fit. In this chapter, however the discussion is focused on determining the free volumes of three different series of PDMS-PBCH copolymers using four-components fit. The effects of the chemical composition and the molar mass of the PDMS segment, and the branching degree, on the o-Ps annihilation parameters and thus on the free volume of the PDMS-PBCH copolymers, were investigated. Results also indicated that positron annihilation characteristics (the longest lifetime components (τ_3 and τ_4) and their intensities (I_3 and I_4) are very useful for studying the effect of the morphological parameters (microphase separation and crystallinity) on the free volume in the copolymer series. Changes in the T_g values of the PDMS segment and the PBCH segment in the copolymers were related to the o-Ps lifetime, which is indicative of a change in free volume in the copolymers. Very good agreement between the DMA results and the PALS results were also observed.

Keywords: free volume, positron lifetime, phase separation.

6.1 Introduction

Positron annihilation techniques have been used extensively to determine the free volume in various semicrystalline and amorphous polymers.[1-9] The free volume can be understood as the volume within the polymeric structure that is not occupied by molecules. It has a great influence on the physical properties and durability of polymers.[10-13] Consequently, since the characterization of the free volume is related to the mechanical and thermal history of the polymer, its investigation is of great interest.[14,15] The use of PALS in free volume characterization is unique. PALS is a non-destructive technique and is sensitive to a free volume on a molecular level.

PALS is based on measuring the lifetimes of positrons "injected" into a material.[16,17] Positrons emitted from a radioactive source enter the polymer matrix, thermalize, and may either annihilate with electrons or form positronium (Ps). The typical lifetime of the Ps depends on the spin state. The singlet state or para-positronium (p-Ps) annihilates in 0.1–0.2 ns. It is referred as τ_1. This value is lower than the typical lifetime of the positron itself, referred to as τ_2, which is in the range 0.3–0.5 ns. The triplet state or ortho-positronium (o-Ps) has a lifetime of 142 ns in vacuum; however, it decreases typically in a matter of a few nanoseconds: 1.5–4 ns. This is due to collisions of Ps with molecules (pick-off annihilation).[18,19]

In investigations of the free volume in polymer material, it is widely accepted that the longest lifetime component (τ_3 or τ_4) connected with the o-Ps is expected to give information on characteristics of the holes that appear due to the structural disorder in the amorphous regions in the polymer.[20,21] It has been found in amorphous polymers that τ_3 increases with an increase in the holes volume,[22] i.e. the o-Ps lifetime increases with the free volume. An increase of the free volume in the system means less overlap of the wave functions of the positron (that forms the o-Ps) and of the media electrons. Further, it is assumed that in glassy polymers the fraction of the positron forming o-Ps (I_3) is correlated to the density of holes in the material, but the exact nature of this correlation is not known.[23]

In semicrystalline polymers the picture is even more clouded, since one has to account for the many possible types of holes arising from the complex morphology that is commonly present in this class of materials, i.e. disordered regions between lamellae in the spherulites structure as well as the amorphous regions between the spherulites. In addition, the crystalline regions

are not clearly defined with sharp and clear boundaries or crystalline faces separating them from the surrounding amorphous regions. The crystallites themselves also contain many defects and dislocations arising from the extensive chain entanglements of molecules in the bulk state. The noncrystalline phase must be subdivided into the noncrystalline-amorphous and the crystalline-amorphous interfacial portions. The interfacial region is amorphous but has a constrained molecular mobility, due to the presence of crystallinity, and is usually described as the rigid-amorphous fraction.[24,25]

The relationship between the positron lifetime annihilation and the molecular characteristics of semicrystalline polymers has been the subject of vast number of academic research studies.[21] The observations of different authors about the relationship between the o-Ps lifetime and molecular structure of semicrystalline polymers can be summarized as follows. For several semicrystalline polymers the changes in the crystalline regions do not show any effect on the lifetime of the o-Ps annihilation. The lifetime spectra of the polymers are found to be best resolved in three-components, similar to in the case of the amorphous polymers. This has led to the conclusion that there is only one long-lived component ($\tau_3 \cong 1.5$–4 ns), regardless of the presence or absence of the crystalline phase. Some examples of semicrystalline polymers in this group are polyetheretherketone,[26] polyethyleneterephthalate (PET)[23] and polypropylene.[14] On the other hand, four lifetime components have been found for polyethylene (PE),[6] polyamides,[7] polytetrafluoronethylene[14] and 1,4-polybutadiene.[27] In this group of semicrystalline polymers two long-lived o-Ps components were obtained, where the first ($\tau_3 \cong 1$ ns) is attributed to o-Ps annihilation in the chain folded regions, and the second ($\tau_4 \cong 2.4$–4 ns) is attributed to pick-off annihilation of o-Ps entrapped in the free volume in the pure amorphous phase of the polymer. In the case of polyurethane/urea membranes obtained through the introduction of two soft segments, polypropylene oxide and polydimethylsiloxane, two long components (lifetimes τ_3 and τ_4) were ascribed to two Ps states decaying in different regions. The detection of the two long lifetimes in these membranes indicated the coexistence of two phases corresponding to separate domains of the two soft segments of the polydimethylsiloxane and polypropylene oxide membranes. [28]

A decrease in I_3 (the longest-lived component intensity) with increasing crystallinity has been reported for semicrystalline PET polyester.[23] However, the extrapolation gave $I_3 \cong 6\%$ at 100% crystallinity. It was concluded that the semicrystalline phase in PET contributed to the o-Ps formation. According to the authors' hypothesis presented in the article, the

inhomogeneous electron distribution existing in the crystal structure of PET is the reason why even small lattice distortions, such as long range thermal vibrations, can provide trapping sites for o-Ps formation in the crystalline phase in the regions of reduced atomic/electron density. Thus, the respective I_3 dependence on the crystallinity should be linear. The similarity of the structures of the PBCH segments and the PET molecules lead the author of this thesis to presume that similar results might be obtained for the PBCH homopolymer. However, in other semicrystalline polymers, such as PE, there is also evidence to suggest that the annihilation characteristics may be related to the average distance between crystallites, thickness of the crystallites, and the concentration of chain defects.[29] Furthermore, the Ps that is formed in crystalline and amorphous phases has also been assumed to tunnel through the interface between both phases, which complicates the situation.[21]

In the light of this somewhat ambiguous situation (the reliable number of fit for LT spectra and how to relate the PALS results to the polymers structure) the aim of this investigation was to determine whether any correlation exists between the mechanism of positron annihilation and the microstructure of the PDMS-PBCH copolymers and the respective homopolymers. It was hoped that this would shed further light on the relationship between the free volume of the copolymers and the morphological parameters (microphase separation and crystallinity), and the T_g of both the PDMS segment and PBCH segment in the copolymers. Copolymers with well-known structural and morphological parameters were reported in previous chapters (Chapters 3-5). Three different series were chosen in order to investigate the effect of the chemical composition (series C), the molar mass of the PDMS segment (series D) and the branching degree (series F) on the free volume of the PDMS-PBCH copolymers.

6.2 Experimental

6.2.1 PDMS-PBCH samples

The specimens under investigation were synthesized and characterized as described in Chapter 3. The morphologies of these copolymers were also investigated, as described in Chapters 4 and 5. The chemical and morphological characteristics of the studied samples are summarized in Table 6.1.

Table 6.1: Characteristics of three series of PDMS-PBCH copolymers (C, D, and F) investigated

Sample	PDMS in feed (wt %)	PDMS M_n (g/mol)	PDMS in the copolymer[a] (wt %)	Crystallinity ω_m[b] (%)	Branching index g[c]	Morphology type[d]
PDMS	100	-	100	0	-	-
PBCH	0	-	0.00	31.40	-	Spherulitic crystal
C-1	5	2000	4.74	23.40	-	Spherulitic crystal and PDMS spherical domains
C-2	10	2000	9.20	16.40	-	PDMS spherical domains
C-3	25	2000	22.70	14.10	-	PDMS spherical domains and bicontinuous
C-4	40	2000	35.76	9.61	-	bicontinuous
C-5	60	2000	52.10	6.10	-	PBCH spherical domains
D-1	10	1000	9.35	28.40	-	PDMS spherical domains
D-2	10	2000	9.20	16.40	-	PDMS spherical domains
D-3	10	4000	8.90	16.10	-	PDMS spherical domains
D-4	10	7000	9.10	13.10	-	PDMS spherical domains
D-5	10	10000	8.60	12.40	-	PDMS spherical domains
F-1	10	1000	9.10	25.60	0.94	PDMS spherical domains
F-2	10	1000	9.51	23.50	0.75	PDMS spherical domains
F-3	10	1000	9.32	22.60	0.62	PDMS spherical domains
F-4	10	1000	8.90	21.30	0.52	PDMS spherical domains
F-5	10	1000	9.44	15.50	0.47	PDMS spherical domains and bicontinuous

[a] determined by ^{1}H-NMR
[b] determined by WAXD
[c] determined by SEC-MALLS
[d] determined by AFM

6.2.2 Sample preparation

Two identical samples, approximately $2.5 \times 10 \times 10$ mm^3, were sandwiched around a positron source, made by evaporating carrier-free $^{22}NaCl$ solution onto aluminium foil (Figure 6.1). Positron lifetime measurements were performed using a fast-fast coincidence system with a time resolution of 240.34 ps full width of half maximum (FWHM) and a total of 1024 channel. The radioactive source (^{22}Na) was placed between two pieces of sample, for each sample, and wrapped very carefully in aluminium foil to ensure that the positrons interacted effectively with the material. The duration of each measurement was 80 min maximum, during which time 1×10^6 counts were collected.

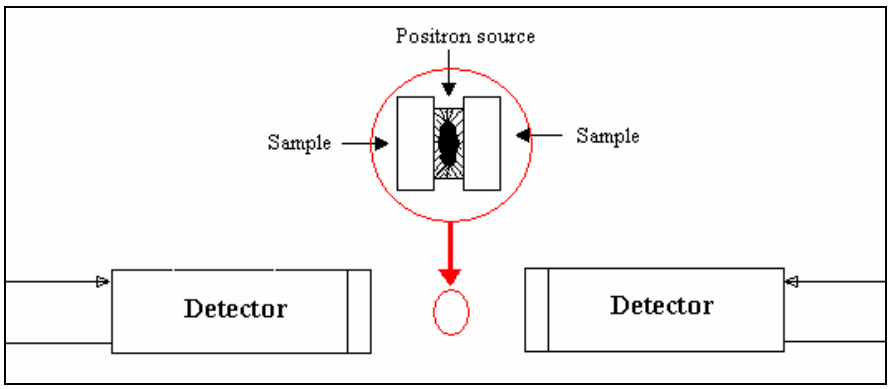

Figure 6.1: The radioactive source placed between the two copolymer samples.

6.2.3 Data analysis

Each positron annihilation spectrum, with a summit height of approximately 1×10^6 counts, was obtained at room temperature. Mathematically, using the PATFIT computer program, the spectra were analyzed as the sum of exponentials. The following procedure was used to analyze the LT spectra. The lifetime spectra for each sample were first analyzed in terms of three lifetime components, as illustrated in Figure 6.2.

Figure 6.2 shows the lifetime interval spectrum of PBCH homopolymer, representing the N coincidence time distribution that comes from the positron and the positronium annihilation processes. Mathematically, the spectra could be analyzed as the sum of exponentials. The applied equation for the fit is

$$N = D \exp(-\lambda_1 t) + C \exp(-\lambda_2 t) + B \exp(-\lambda_3 t) \qquad \text{[Eq 6.1]}$$

where *N* is the number of accumulated coincidences, the slopes λ are the rates of annihilation, *D*, *C* and *B* are the slope intercepts of each component at the zero time axis. The magnitudes of the three lifetimes τ_1, τ_2 and τ_3 suggest that they originate mainly from the annihilation of p-Ps, free positron and o-Ps, respectively.[16] The last parameter with the respective intensity (τ_3 and I_3) are the most important ones, because their analysis will determine the free volume and the physical–chemical characteristics of the media where the positron annihilation occurs.[21]

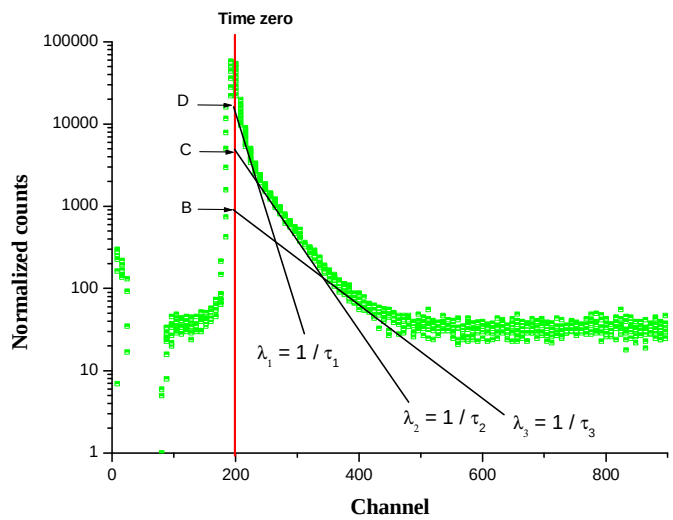

Figure 6.2: The three-components fit to the LT spectrum of PBCH.

Analysis of the measured spectra of PDMS-PBCH copolymers and only PBCH homopolymers by four lifetime components was also attempted, as shown in Figure 6.3. The applied equation in the fit in the Figure 6.3 is now:

$$N = D \exp(-\lambda_1 t) + C \exp(-\lambda_2 t) + B \exp(-\lambda_3 t) + A \exp(-\lambda_4 t) \qquad \text{[Eq 6.2]}$$

where *N* is the number of accumulated coincidences; and *D*, *C*, *B* and *A* are the slope intercepts of each component at the zero time axis.

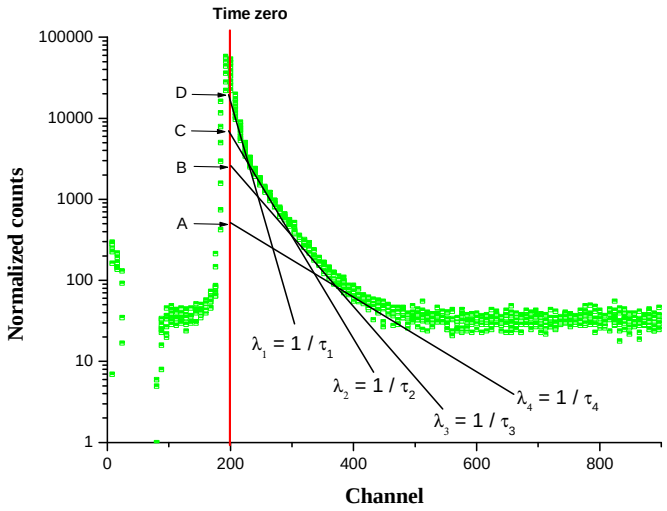

Figure 6.3: The four-components fit to the LT spectrum of PBCH.

The analysis was first applied without any constraints where the shortest of the four lifetimes was scattered in the range 0.1 and 0.3 ns, with very large variances fit. This lifetime is consistent with that of the p-Ps lifetime. In order to reduce the scatter of the points the final four lifetime analyses were carried out by fixing the intrinsic p-Ps lifetime at 0.125 ns. Further, the four-components fit was also applied by fixing τ_2 at 0.5 ns and τ_1 at 0.125 ns. However, negative values were obtained for several samples, with no significant improvement in the fit (high variances fit). Therefore the results of the four-components fit reported in this chapter were obtained when only τ_1 was fixed at 0.125 ns.

6.3 Results and discussion

6.3.1 PDMS and PBCH homopolymers

In the case of the PDMS homopolymer the LT spectrum was analyzed using the three-components unconstrained fit. As a result of the homogonous PDMS amorphous pure phase the three-components fit was suitable and applicable. The variance of the fits was also small, it is 1.1. However, in the case of the semicrystalline PBCH homopolymer the LT spectrum was analyzed using both the three-components unconstrained fit and the four-components constrained fit (using 0.125 ns for p-Ps annihilation lifetime (τ_1)). The variances of the fits were 1.13 and 1.6 for the three- and four-component fits, respectively. Table 6.2 shows the annihilation lifetime of the o-Ps (τ_3) and the corresponding intensity (I_3), which is indicative of the relative number of o-Ps annihilations. The radius and the volume of the holes, as well

as the free volume fraction, obtained using Eq 2.3, Eq 2.4 and Eq 2.5 are also listed in Table 6.2.

Table 6.2: The o-Ps characteristics of PDMS and PBCH homopolymers determined using the three-components fit

Sample	τ_3[a] (ns)	$\Delta\tau_3$[a] (ns)	I_3[b] (%)	ΔI_3[b] (%)	R[c](Å)	ΔR[c](Å)	fv[d] (Å^3)	Δfv[d] (Å^3)	ffv[e] (%)	Δffv[e] (%)
PBCH	2.06	0.012	19.42	0.098	2.10	0.007	110.00	0.97	3.21	0.06
PDMS	4.14	0.009	37.48	0.156	4.32	0.003	338.50	8.73	22.9	0.14

[a] the average lifetimes of the o-Ps
[b] the average intensities of the free volume holes
[c] the average radii of the free volume holes
[d] the average of the free volume holes
[e] the average of the free volume fractions

Regardless of constraints used in the four-components fit there was no significant improvement in the variance of the fit. The errors (standard deviations) in the lifetime and intensity of the o-Ps annihilation were higher than the respective values when the LT spectra were fitted with three exponential components. Thus, in PBCH homopolymers there was only one o-Ps component. If however, there were two components (one for the amorphous region and another for the crystallinity region), then they are very close to each other (at about 2.06 ns) and cannot be resolved mathematically. The suitability of the three-components fit for the PBCH polyester is consistent with that reported in literature for other polyesters, such as PET.[23]

Table 6.2 shows that about a quarter (22.9±0.12%) of the PDMS volume is free volume, which explains the very low T_g of this polymer (–123 °C). This value of the free volume fraction is larger than the value reported in literature for the PDMS pure homopolymer.[30] This variation might be a result of the difference in the degree of the crosslinking in the PDMS molecules. On the other hand, the free volume in the PBCH homopolymer, which has not been measured by PALS before, represents only 3.21±0.06% of the total volume of the polymers, even though the T_g of this polymer is lower than room temperature. The relatively low free volume fraction in the PBCH homopolymer can be attributed to the crystallinity degree in this polymer, determined using WAXD to be about 31.4% (see Section 4.3.1), resulting in a lower o-Ps yield. Therefore, the o-P lifetime and its intensity, as extracted from

the lifetime spectra, can provide an indication of the polymer's structure, and eventually provide more information on the region where the o-Ps could be annihilating.

6.3.2 PDMS-PBCH copolymers

Figures 6.4, 6.6 and 6.9 show the longest o-Ps lifetimes (τ_3 and τ_4) and intensities of the corresponding o-Ps (I_3 and I_4), as obtained after using the three- and four-components fits. In contrast to the homopolymers, the four-components fit in the copolymer series is necessary in order to understand the complex structure and morphology of such phase separated copolymer series and to have physical meaning of the lifetimes obtained. The three-components fits has the advantage that the fitting procedure is easer to apply than the four-components fits and gives a fitting usually very stable with small statistical scatter parameters (τ_i and I_i) in most of the cases compared with unconstrained four-components fits. However, constrained four-components fits in several samples of the PDMS-PBCH copolymers (namely C-1, C-2, D-1, D-2 and D-4) did show lower variance fit and less statistical scatter parameters than the three-components fits. In the complex semicrystalline copolymers with microphase separated morphology the three-components fits has no relevant physical meaning and gives only a more or less sufficient fit to the experimental data. Because of the structures of these semicrystalline PDMS-PBCH copolymers, positronium can form in both the crystalline (PBCH region) and amorphous (PBCH and PDMS regions) phases. The possible regions with free volume holes probed by o-Ps in these copolymers are in: (1) open amorphous texture and interfaces in spherulites, (2) interlamellar phase and lamellar defects, (3) interstitial cavity in the crystalline unit cell,[25] and the intermediate phase that forms between the PDMS domains and (4) the PBCH dominant phase.

Figure 6.4 shows the effect of the PDMS content on the lifetime (Figure 6.4(a)) and intensity (Figure 6.4(b)) of the o-Ps annihilation in series C, when both three- and four-components fits were used to analyses the LT spectra. The values of the lifetime and the intensity depend largely on the PDMS content in the copolymers. In the case of the PDMS-PBCH copolymers, when using a four-components fit there is an increase in long-lived component τ_4 and its intensity (I_4) as the PDMS content increases. This can be considered to be an indication of an increase in the free volume in the PDMS region. The increase in the τ_4 represents an increase in the size of the free volume holes in the PDMS phase. The increase in the intensity in the PDMS phase represents an increase in the number of the free volume holes and indicates the higher fraction of o-Ps annihilating in the PDMS phase as the PDMS content increases. The

free volume increases as the PDMS phase becomes the dominant phase and the morphology changes from small spherical domains of PDMS to larger domains, to bicontinuous phase, and then to small spherical domains of PBCH in a matrix of PDMS (see Table 6.1).

The shortest long-lived component τ_3 and its intensity (I_3) show an unstable increasing trend. This long-lived component (τ_3) can be attributed to the change in the free volume in PBCH phase. Here an interesting question arises: are the o-P characteristics in the PALS influenced by the presence of crystalline regions in the PBCH phase of the samples or not. The answer is clearly yes, since dislocation can form very easily in the crystalline region of the PDMS-PBCH copolymers and it is now particularly easier in PDMS-PBCH copolymers than in PBCH homopolymer.

It is also worthwhile considering the possibility that Ps trapping in dislocations or in vacancies that are associated with dislocations in the crystalline region of the PBCH segment could also affect the o-P characteristics in the PALS. Therefore, in order to understand the PBCH phase in more detail consideration of a five-components fit of the LT spectra is recommended. Such fits have been used for hypercrosslinked polystyrene, using both the PATFIT and MELT system.[3] The process of resolving five exponential components is extremely difficult and leads to large variances and was not done on the current data. Nevertheless, by using four-components fit the PDMS phase can be identified and understood clearly and this study is limited to four-component fit (using five-component fit might be object of another future study).

Therefore, in addition to, the microphase separation, the change in the crystallinity in PDMS-PBCH copolymers can have influence on the positron annihilation mechanism and increasing in the free volume in the PBCH region (τ_3) can be an evidence of looser packing of the PBCH macromolecular chains and of the formation of additional free volume at the phase boundaries. This might offer additional evidence of the formation of o-Ps in both the crystalline and amorphous phases, depending on the material under investigation, as was reported in several articles in the literature.[23] In this case the increasing I_3 as well as I_4 with PDMS content is most probably a result of the decreasing crystallinity in the PBCH phase. The increases in the τ_3, τ_4, I_3 and I_4 with an increase in the PDMS content shows a nonlinear relationship.

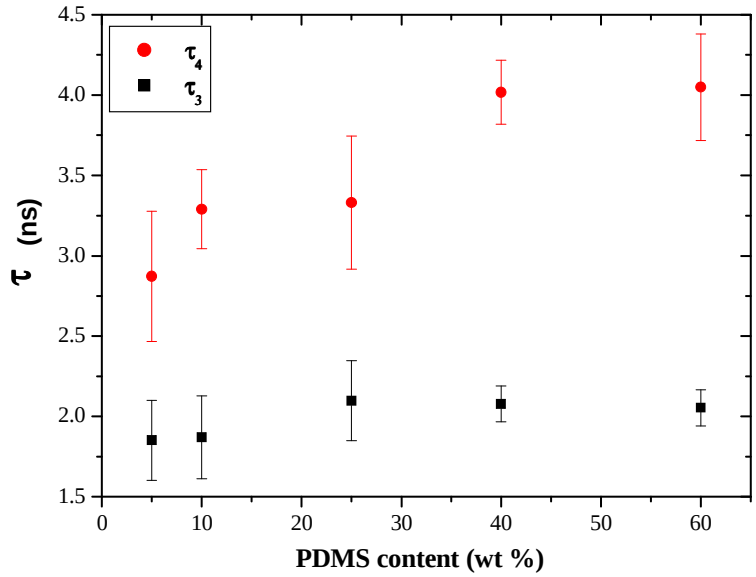

a)

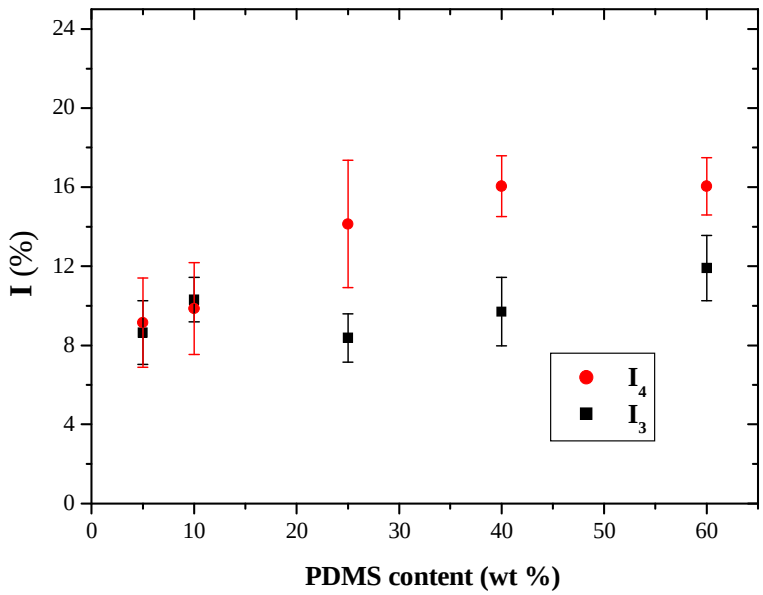

b)

Figure 6.4: Dependence of (a) o-Ps lifetime (τ) and (b) intensity (I) on the PDMS content in PDMS-PBCH copolymers (series C).

In copolymers with a high PDMS content (C-5) (60 wt %) the longest lifetime (τ_4) and intensity (I_4) were observed, meaning that these copolymers have a higher free volume of holes and a high density of such holes. This can be clearly seen from the radius of the free volume hole in Figure 6.5 and from the free volume values in Table 6.3.

Figure 6.5 shows the effect of the PDMS content on the radii of the free volume holes. Although in reality the free volume holes may not be completely spherical, the two free

volume radii R_3 and R_4 may be used as a rough estimate of the actual hole size. The smaller value (R_3) corresponds to the free volume holes in the PBCH phase and the larger one (R_4) to the free volume holes in the PDMS phase. Both radii of the free volume holes in Figure 6.5 increase as the PDMS content increases, which explains the decrease in the T_g values of the PDMS and the PBCH segments, as shown by the DMA results reported in Section 4.3.1.

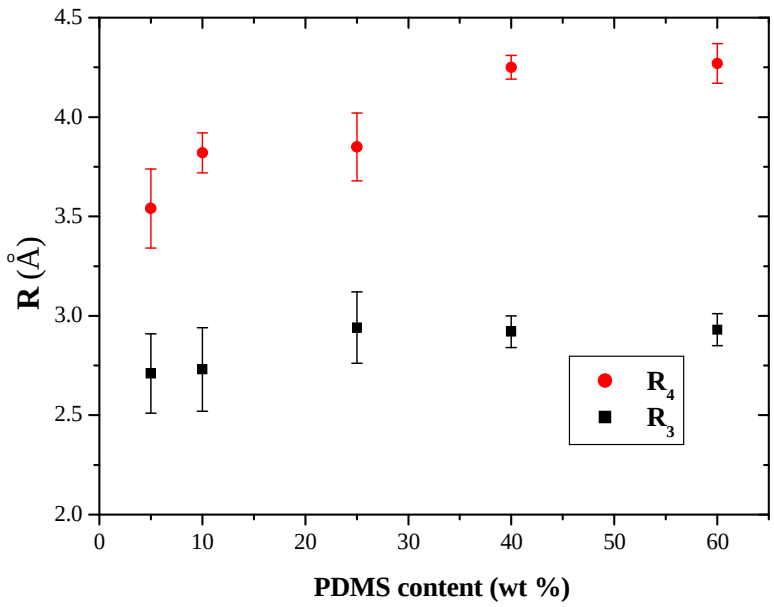

Figure 6.5: Effect of the PDMS content on the radius (R) of the free volume holes in series C.

The increase in the radius obtained for the PBCH phase in the copolymer when compared with the radius of the free volume holes in the PBCH homopolymer could be a result of the increase in the dislocations and imperfections in the PBCH phase in the copolymers due to the PDMS segment disruption of the lamella structure, as seen from the AFM images in Section 4.3.2. The change in the degree of crystallinity can lead to a change in the amorphous regions, and subsequently to a change in the lifetime and intensity of the o-Ps annihilations. No clear relationship can be drawn, however, between the degree of crystallinity and the o-Ps characteristics, because in all the PDMS-PBCH copolymer series the degree of crystallinity decreases as the PDMS content, the PDMS M_n and branching agent content increase, all of which can affect the o-Ps characteristics.

One can expect a higher free volume to occur due to both the microphase separation and the change in the degree of the crystallinity in the PDMS-PBCH copolymer. In other words, a high free volume and density is the result of the influence of the PDMS regions on the PBCH amorphous regions, and the PBCH amorphous regions in turn affect the neighbouring

crystalline structure of the PBCH region. Changing the crystalline regions as the PDMS content changes could result in broadening the amorphous regions as the PDMS content increases in between the crystalline regions of the PBCH folding chains in the lamella structure, as illustrated in the AFM images of copolymer C-1 (Figure 4.2). Obviously broadening the amorphous regions will lead to an increase in the size of the free volume holes in the intermediate region between the crystalline region and the amorphous region, and also in the crystalline region. In addition to the volume of the holes, Table 6.3 also shows the free volume fraction for the three PDMS-PBCH copolymer series (C, D and F).

Table 6.3: Free volume holes and free volume factions of the holes in three different PDMS-PBCH copolymer series based on the four-components fit

Sample	fv_3(Å^3)	Δfv_3(Å^3)	ffv_3(%)	Δ ffv_3(%)	fv_4(Å^3)	Δfv_4(Å^3)	ffv_4(%)	Δ ffv_4(%)	Total ffv (%)
C-1	102.5	8.70	0.72	0.18	187.3	31.6	3.08	1.41	3.80
C-2	103.8	8.70	0.69	0.19	234.7	18.9	4.16	1.52	4.85
C-3	104.7	11.60	0.84	0.38	239.5	31.7	6.09	2.19	6.93
C-4	103.4	12.00	1.58	0.54	322.5	14.7	9.31	1.31	10.89
C-5	105.7	11.30	1.30	0.60	326.5	24.4	9.43	1.55	10.73
D-1	79.6	8.70	2.43	0.84	198.5	21.1	2.68	1.39	5.11
D-2	85.4	12.20	1.58	0.40	234.7	11.2	4.16	1.39	5.74
D-3	111.8	11.30	2.22	0.65	313.1	26.1	6.62	1.31	8.84
D-4	111.3	14.80	1.97	0.55	319.7	30.3	5.86	1.48	7.83
D-5	112.5	11.10	1.95	0.46	326.5	31.1	7.58	1.57	9.43
F-1	84.9	21.81	1.01	0.66	195.0	23.89	5.30	1.93	6.31
F-2	96.2	20.22	0.69	0.48	205.7	22.87	5.23	1.77	5.92
F-3	106.7	19.64	0.84	0.62	239.5	20.25	6.43	1.68	7.27
F-4	115.8	17.80	0.63	0.47	280.1	24.53	5.93	2.21	6.56
F-5	126.2	27.19	0.78	0.65	293.8	31.64	4.31	1.69	5.09

Figure 6.6 shows the effect of the PDMS M_n on the lifetime (Figure 6.6(a)) and intensity (Figure 6.6(b)) of the o-Ps in series D. The o-Ps results detected in series D were similar to those for series C. The two long-lived components (lifetimes τ_3 and τ_4) of the o-Ps were generally smaller in the case of the copolymers with the shorter PDMS segment length. The two long-lived components increase as the PDMS molar mass increases in the copolymers. Once again the two long-lived components were ascribed to two o-Ps states decaying in different regions, indicating the coexistence of two phases corresponding to separate domains

of the two segments in the copolymers (PDMS phase and PBCH phase). This is confirmed by the TEM and the AFM results that described the presence of two phase morphology in this copolymer series (Section 5.3.2).

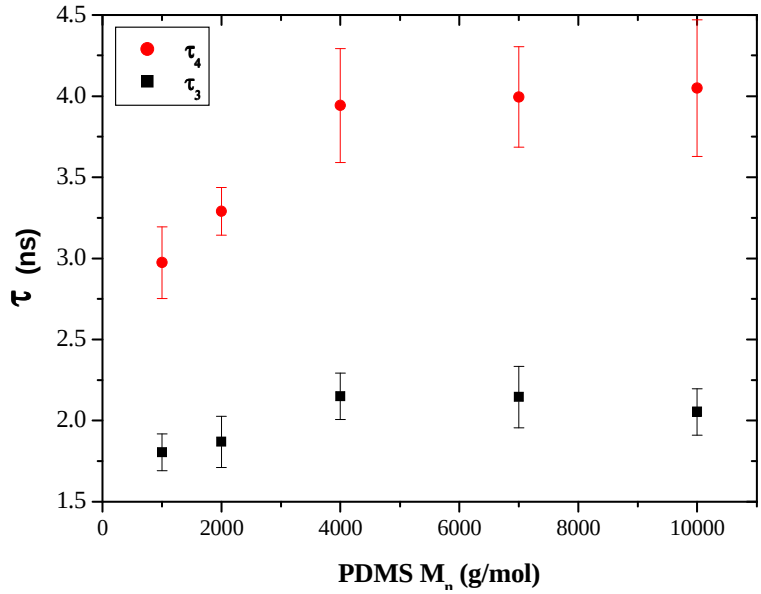

a)

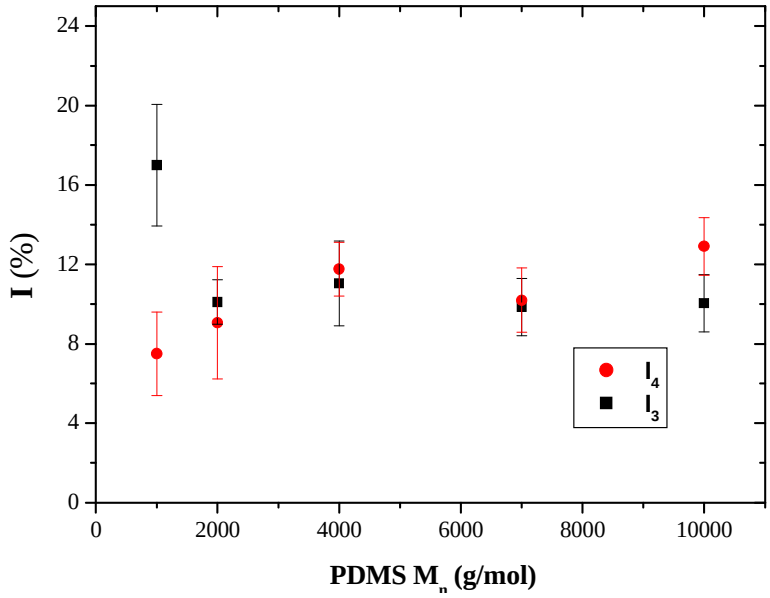

b)

Figure 6.6: Dependence of (a) o-Ps lifetime (τ) and (b) intensity (I) on the PDMS segment length in PDMS-PBCH copolymers (series D).

In Figure 6.6(b) the intensities (I_3 and I_4) showed opposite trends: I_3 decreases as the PDMS segment length increases, while I_4 increases. The D-2 copolymer showed the smallest intensity (specifically in the PBCH phase (I_3)). This can be attributed to the effect of the

intermediate phase. The size of the PDMS domains in this copolymer (see Section 5.3.2) is smaller than that in the other copolymers, which increases the surface contact between the PDMS and the PBCH, and thus a larger intermediate phase in this copolymer will be formed. The large scattering (the standard deviation or error) in both the o-Ps lifetimes and the intensities can be attributed to the various free volume holes sizes and to the uneven distribution of the holes in both copolymer phases.

Figure 6.7 shows the effect of the PDMS segment on the radii of the free volume holes in the PDMS and PBCH phases. The radii of the free volume holes, in both copolymer phases, increases as the PDMS segment length increases, which explains the decrease in the T_g values of the PDMS and the PBCH segments in this series (series D) of the copolymers, as described in Section 5.3.1.

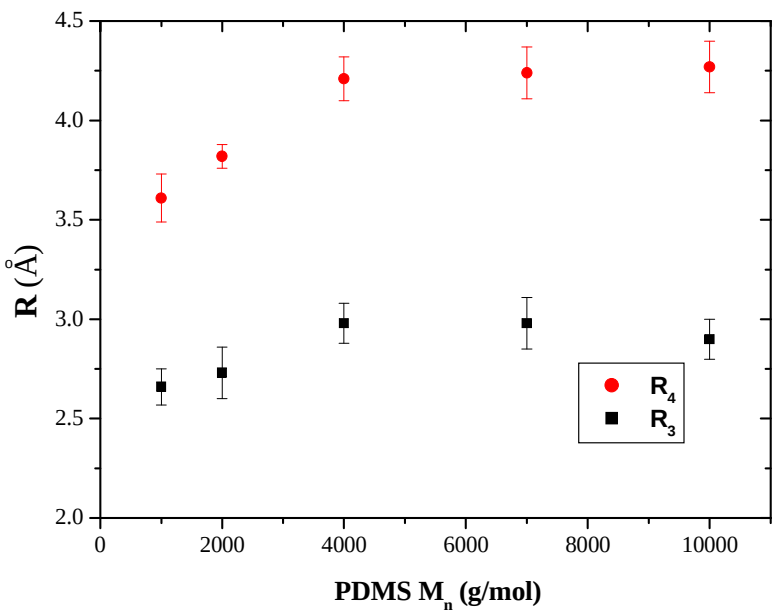

Figure 6.7: Effect of the PDMS segment length on the radius of the free volume holes in series D.

The free volume fraction was determined in both the PDMS and PBCH phases, based on the four-components fit parameters (τ_3, τ_4, I_3, and I_4) using Eq 2.5. The total fraction of the free volume in each copolymer was calculated as the sum of the free volume fractions in both phases. The results of the total fraction of the free volume are visually illustrated in Figure 6.8. The free volume fraction is directly related to the mechanical properties of the polymers. This parameter can be thought of as the product of the average hole size and the hole concentration.[21] Figure 6.8 illustrates the difference in the free volume fractions of the

copolymers series C, D and F, as well as the free volume fractions of homopolymers PBCH and PDMS. There is a significant change in the free volume fractions in all the copolymers series. Copolymers C-5 has the largest free volume fraction and C-1 has the smallest.

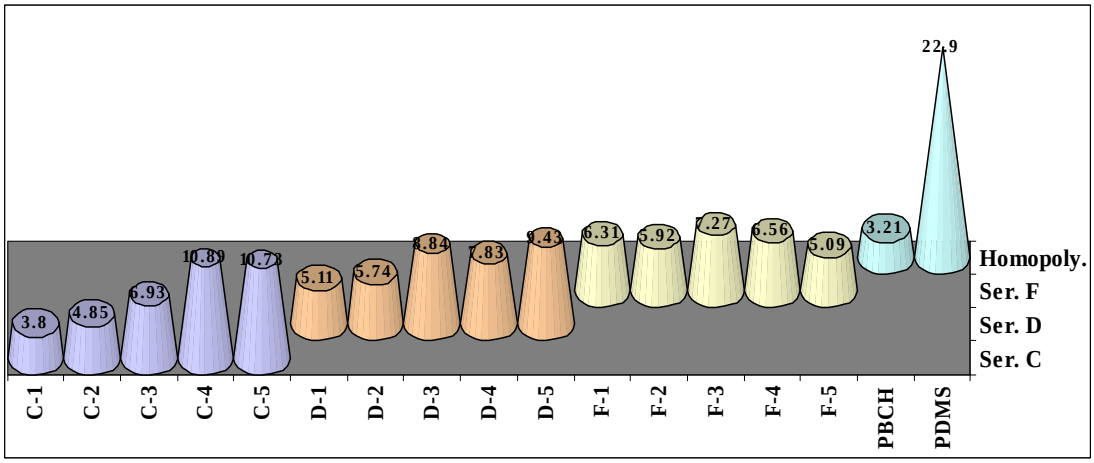

Figure 6.8: Visual representation of the total fraction of the free volume in the copolymer series C, D and F, and PBCH and PDMS homopolymers, calculated as a sum of fraction of the free volumes obtained from the two long-lived components.

Figure 6.9 shows the effect of the branching agent on the o-Ps characteristics: changes take place in the o-Ps lifetime (Figure 6.9(a)) and intensity (Figure 6.9(b)) with a change in the branching agent content. In this case no matter which number of components fit was used there was an increasing trend in the o-Ps lifetimes as the branching agent content increases. This was in contrast to the intensities, which showed a decreasing trend. The morphology investigation of this series described in the previous chapters (see also Table 6.1) showed that all the samples have spheres of PDMS domains in a matrix of PBCH, although the F-5 copolymer showed small regions of bicontinuous phase on the surface of the sample. This similarity in the morphology, as well as the chemical compositions (10 wt % PDMS), might be the reason why all the copolymers in this series (series F) showed a similar trend when three- and four-components fit were used. Once again, the large scattering in both the o-Ps lifetimes and the intensities can be attributed to the variation in the free volume hole sizes and uneven distribution in both copolymer phases. The increase in the τ_3 and τ_4 reflects an increase in the mean size of the free volume holes in the PBCH and PDMS phases, respectively. However, the decreasing trend of the I_3 and I_4 indicates a smaller amount of o-Ps annihilated in both phases.

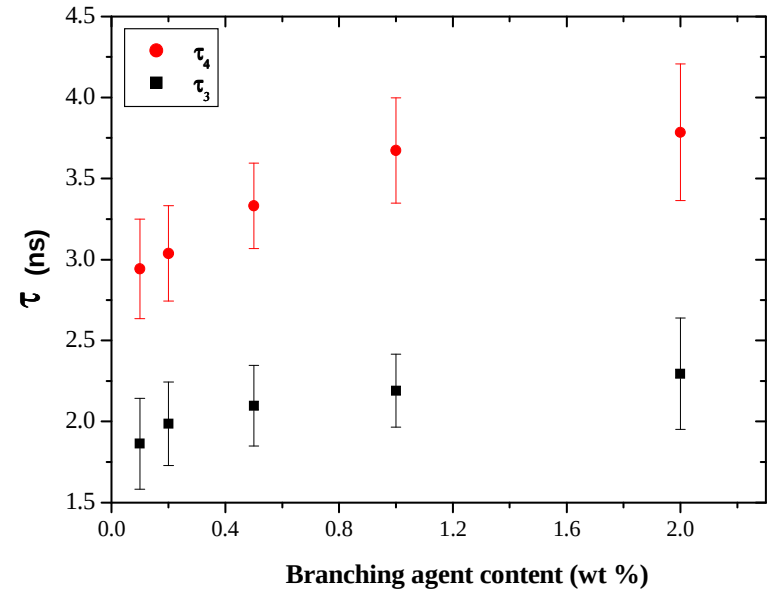

a)

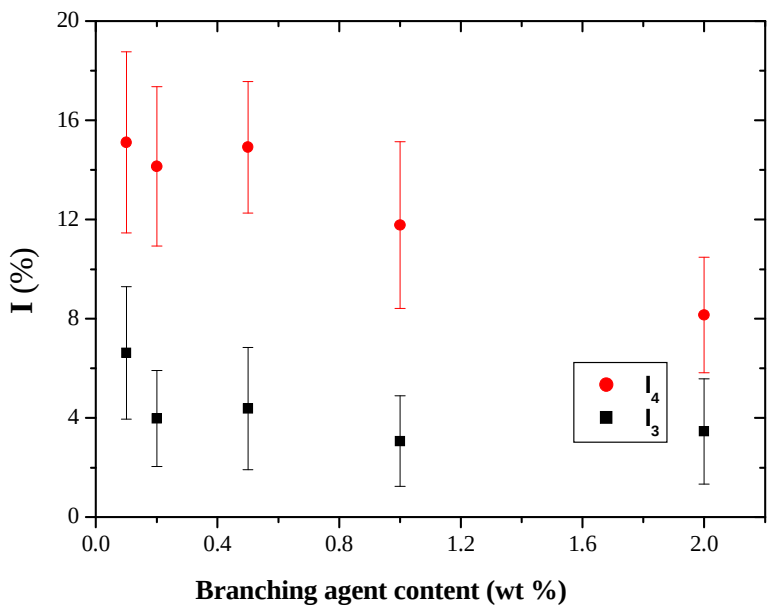

b)

Figure 6.9: Dependence of (a) o-Ps lifetime and (b) intensity on the branching agent content in PDMS-PBCH copolymers (series F).

Furthermore, in series F there is a significant increase in the both the τ_3 and τ_4 (Figure 6.9(a)) when the branching agent content increases from 0.1% to 1%, and both remain almost constant when the branching agent content increases from 1% to 2%. This can also be seen in the radius of the free volumes holes (both R_3 and R_4), as shown in Figure 6.10. Figure 6.10 shows the effect of the branching agent content on the radius of the free volume holes. The trend of the change in radius appears similar to the o-Ps lifetime trend. Although there is no

change in the radius of the free volume holes between F-4 and F-5 the fraction of the free volume (ffv) (Figure 6.8) does not show steady change, as in the actual free volume (fv) and the lifetime of the o-Ps. This indicates the effect of the intensity of the free volume on the free volume fractions and thus effect of the intensity on the glass transition and the mechanical properties of the copolymer.

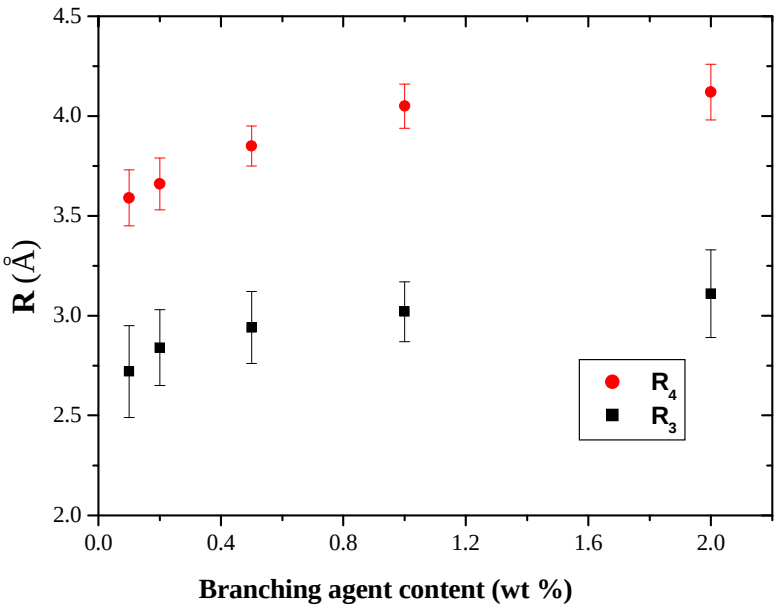

Figure 6.10: Effect of the branching agent content on the radius (R) of the free volume holes in series F.

6.3.3 Glass transition temperature and free volume

Figure 6.11 shows a comparison between the effect of the PDMS content, PDMS segment length and the branching agent content on the free volumes (both fv_3 and fv_4) and the T_g values of the PBCH segment and the PDMS segment in the PDMS-PBCH copolymers. The large scattering in the free volumes in the copolymer segments compared with that in the homopolymers could be due to uneven sizes and density of the free volume holes in the copolymer.

The agreement between the trends in the T_g values and the free volumes as a function of PDMS content can be seen in Figures 6.11(a) and 6.11(b). It is obvious that as the PDMS content increases the free volume increases, and thus the T_g values of the PDMS and PBCH segments in the PDMS-PBCH copolymers decrease. The increase in the free volume of the PDMS phase is clearer than that in the PBCH phase.

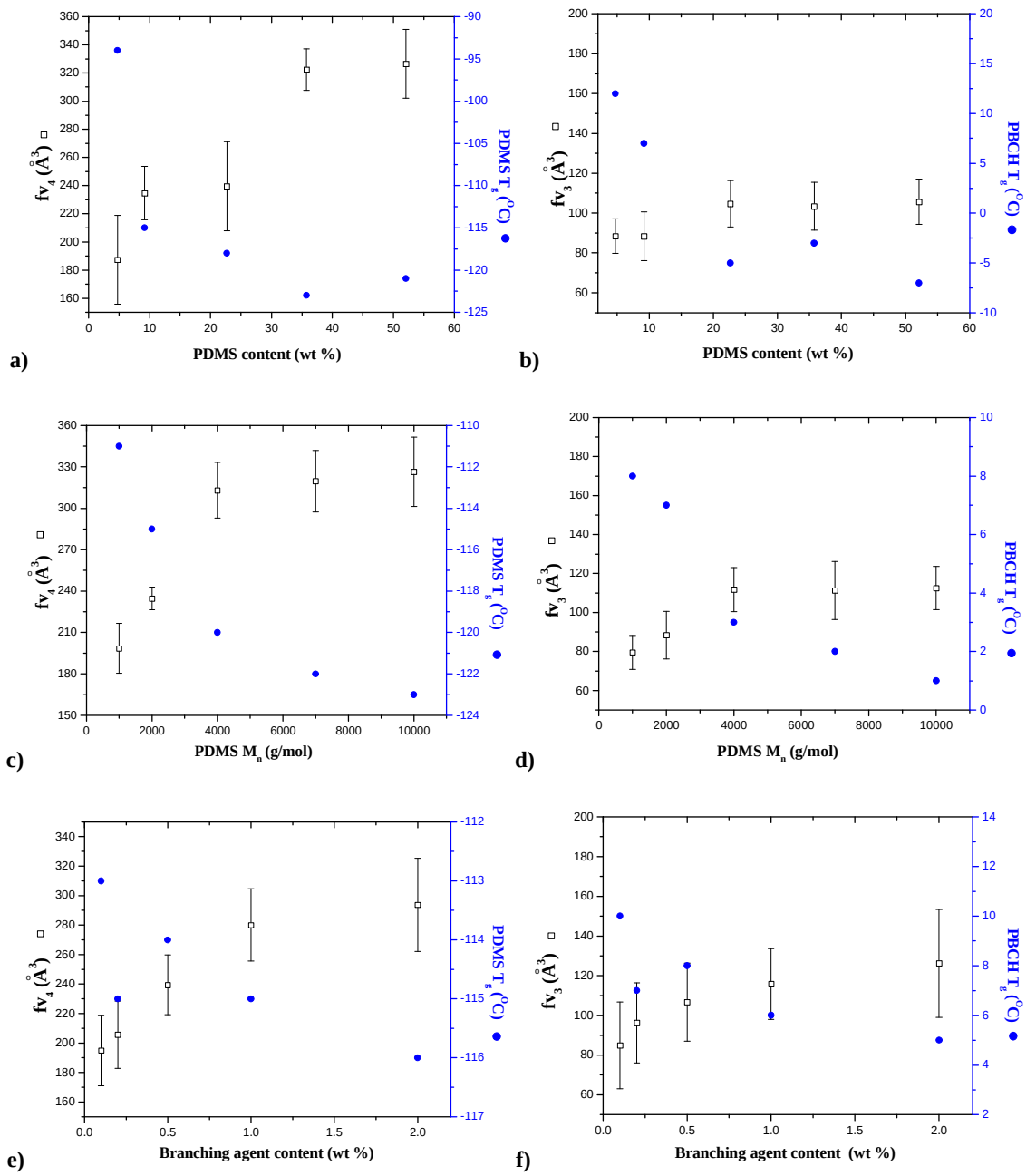

Figure 6.11: The effects of the PDMS content, PDMS M_n and the branching agent content on the o-Ps lifetime and the T_g values of the PDMS and PBCH segments in the PDMS-PBCH copolymers.

An increase in free volume holes of the PDMS and PBCH segments in the copolymers is also observed when the PDMS M_n increases in series D (Figures 6.11(c) and 6.11(d)). This increase in the free volume lead to decreases in T_g values of both PDMS and PBCH segments. The free volume increases as the PDMS M_n increases first (PDMS M_n increase from 1000 to 2000 g/mol) and then remains almost constant, while the T_g of the PDMS segment and the PBCH segment decrease as the PDMS segment length increases. However,

overall, the change in the free volume holes in both phases as a function of PDMS segment length was very clear. In the case of the branched PDMS-PBCH copolymers a good agreement is also obtained between the changes in the T_g values of both the PDMS and PBCH segments and the change in the free volume holes as a function of branching agent content (see Figures 6.11(e) and 6.11(f)). From the above results one can see clearly the agreement between the PALS (fv) results and the DMA results (T_g).

6.4 Conclusions

The ability to determine the free volume in PDMS-PBCH semicrystalline copolymers using the PALS technique was investigated. The free volumes of the PDMS and PBCH homopolymers were determined using PALS. The LT spectra were analyzed using the three-components fit. In the case of the PDMS-PBCH copolymer series, where the three-components fit becomes meaningless, the LT spectra of the PDMS-PBCH copolymer series were analyzed using the four-component fit. The results showed that the mean lifetime of o-Ps reflects the size of the free volume holes, and the lifetime of o-Ps found to be very sensitive to changes in the free volume caused by changes in the molecular structure of the copolymers. It also appeared that the crystal structure and the phase separation morphology could affect the free volume of the PDMS-PBCH copolymers.

The free volume in three different series of PDMS-PBCH semicrystalline copolymers was determined using the PALS technique. In the first series the PDMS content was varied, in the second series the PDMS M_n was varied, and in the third series the branching degree was varied. In the first series, it was found that increasing the PDMS content leads to an increase in the intensity of Ps and the lifetime of the o-Ps. The results obtained for the second series also showed an increasing trend in the intensity and the lifetime of the o-Ps as the PDMS M_n increases. In the third series, however, variation in the branching degree, showed a very clear increasing trend in the o-Ps lifetime and decreasing trend in the intensity as the branching degree increases.

The free volume values and the glass transition temperatures of the PDMS and PBCH segments in the PDMS-PBCH copolymers showed that the results obtained by using the PALS technique are in good agreement with the results obtained by using the DMA technique.

6.5 References

1. He, C.; Suzuki, T.; Shantarovich, V. P.; Ma, L.; Matsuo, M.; Kondo, K.; Ito, Y. *Physics Letters A* 2003, 313(3), 223-230.
2. He, C.; Suzuki, T.; Ma, L.; Matsuo, M.; Shantarovich, V. P.; Kondo, K.; Ito, Y. *Physics Letters A* 2002, 304(1-2), 49-53.
3. He, C.; Suzuki, T.; Shantarovich, V. P.; Kondo, K.; Ito, Y. *Chemical Physics* 2003, 286(2-3), 249-256.
4. Dlubek, G.; Bondarenko, V.; Pionteck, J.; Supej, M.; Wutzler, A.; Krause-Rehberg, R. *Polymer* 2003, 44(6), 1921-1926.
5. Al-Qaradawi, I. Y. *Radiation Physics and Chemistry* 2003, 68(3-4), 467-470.
6. Danch, A.; Osoba, W.; Stelzer, F. *European Polymer Journal* 2003, 39(10), 2051-2058.
7. Dutta, D.; Bhattacharyya, A.; Ganguly, B. N. *Journal of Membrane Science* 2003, 224(1-2), 127-135.
8. Winberg, P.; Eldrup, M.; Maurer, F. H. J. *Polymer* 2004, 45(24), 8253-8264.
9. Wang, Z. F.; Wang, B.; Qi, N.; Ding, X. M.; Hu, J. L. *Materials Chemistry and Physics* 2004, 88(1), 212-216.
10. Pethrick, R. A. *Current Opinion in Solid State and Materials Science* 2002, 6(3), 221-225.
11. Sathyanarayana, P. M.; Shariff, G.; Thimmegowda, M. C.; Ashalatha, M. B.; Ramani, R.; Ranganathaiah, C. *Polymer Degradation and Stability* 2002, 78(3), 449-458.
12. Huang, Y.; Paul, D. R. *Polymer* 2004, 45(25), 8377-8393.
13. Kilburn, D.; Bamford, D.; Lüpke, T.; Dlubek, G.; Menke, T. J.; Alam, M. A. *Polymer* 2002, 43(25), 6973-6983.
14. Sánchez, V.; López, R.; Fucugauchi, L. A.; Ito, Y. *Journal of Applied Polymer Science* 1995, 56(7), 779-791.
15. Ito, Y. *Radiation Physics and Chemistry* 2000, 58(5-6), 551-554.
16. Procházka, I. *Materials Structure* 2001, 8(2), 55-60
17. DeMaggio, G. Positron annihilation as a probe of polymer thin films, surfaces, and interfaces. PhD, University of Michigan, United States, 1997.

18. Kansy, J.; Consolati, G.; Dauwe, C. *Radiation Physics and Chemistry* 2000, 58(5-6), 427-431.

19. Uedono, A.; Ito, K.; Nakamori, H.; Ata, S.; Ougizawa, T.; Ito, K.; Kobayashi, Y.; Cao, X.; Kurihara, T.; Oshima, N.; Ohdaira, T.; Suzuki, R.; Akahane, T.; Doyama, M.; Matsuya, K.; Jinno, S.; Fujinami, M. *Nuclear Instruments and Methods in Physics Research, Section B: Beam Interactions with Materials and Atoms* 2008, 266(5), 750-754.

20. Pethrick, R. A. *Progress in Polymer Science* 1997, 22(1), 1-47.

21. Jean, Y. C.; Mallon, P. E.; Schrader, D. M., *Principles and Applications of Positron and Positronium Chemistry*. First ed.; World Scientific Publishing, Singapore, 2003; pp 253-280.

22. López-castañares, R.; Olea-cardoso, O.; Vázquez-moreno, F.; Lizama-soberanis, B.; Camps-carvajal, E.; Angeles-anguiano, E.; Castaño, V. *Bulgarian Journal of Physics* 2002, 29(3-4), 155-178.

23. Li, X.; Gidley, D. W.; Hristov, H. A.; Yee, A. F. *Polymer* 1994, 35(1), 14-17.

24. Androsch, R.; Wunderlich, B. *Polymer* 2005, 46(26), 12556-12566.

25. Cheng, M.-L.; Sun, Y.-M.; Chen, H.; Jean, Y. C. *Polymer* 2009, 50(8), 1957-1964.

26. Kobayashi, Y.; Haraya, K.; Hattori, S.; Sasuga, T. *Polymer* 1994, 35(5), 925-928.

27. Bartos, J.; Sausa, O.; Bandzuch, P.; Zrubcová, J.; Kristiak, J. *Journal of Non-crystalline Solids* 2002, 307-310, 417-425.

28. Ferreira Marques, M. F.; Gordo, P. M.; Kajcsos, Zs.; Lopes Gil, C.; de Lima, A. P.; Queiroz, D. P.; de Pinho, M. N. *Radiation Physics and Chemistry* 2007, 76 (2), 129–133.

29. Balta Calleja, F. J.; Serna, J.; Vicente, J.; Segovia, M. A. *Journal of Applied Physics* 1985, 58(1), 253.

30. Li, B.; Xu, D.; Jiang, Z.; Zhang, X.; Liu, W.; Dong, X. *Journal of Membrane Science* 2008, 322(2), 293-301.

Chapter Seven

Surface Morphology of PDMS-s-PBCH Copolymers and HPLC-LC-transform Microscopic Hyphenated Techniques

Abstract

The surface morphology of the alternating polydimethylsiloxane-polybutylenecyclohexanedicarboxylate segmented (PDMS-s-PBCH) multiblock copolymer (series E) was investigated and compared to their analogies of PDMS-PBCH random multiblock copolymer in series C and D. The complex morphology of both copolymers (random and alternating) was further investigated using a novel high performance liquid chromatography-atomic force microscopy (HPLC-AFM) offline coupling hyphenated techniques. The hyphenated coupling techniques were developed to provide information on the morphology as a function of the PDMS content and distribution and the copolymer molar mass. In these techniques the copolymers were first fractionated, based on their molar mass, using size exclusion chromatography (SEC), and based on their chemical composition, using gradient elution chromatography (GEC). First hyphenated technique was carried out using SEC and AFM, which provides information on the copolymer morphology of each similar molar mass fraction (narrow molar mass distribution). The average chemical composition of the copolymer was obtained using Fourier-transform infrared spectroscopy (FTIR). Although the PDMS segment content along the copolymers molar mass distribution was investigated by SEC-LC-transform-FTIR the effect of the PDMS content on the copolymer fractions morphology was investigated using AFM. The second hyphenated technique was carried out using GEC and AFM, which provides information on the copolymer morphology of each similar chemical compositions fraction and narrow PDMS distributions. The spherical domains of the PDMS are the dominant type of morphology in all the fractions of the copolymers as in the bulk copolymer. In several copolymer fractions, however, the morphology showed three phases simultaneously. Other hyphenated techniques of high performance liquid chromatography-digital pulsed force mode of AFM (HPLC-DPFM-AFM) were proposed. Here the collected fractions from both SEC and GEC were subjected to adhesive force mapping using the pulsed-force mode of the AFM. This provides a new type of two-dimension separation of the copolymers: in the first dimension the copolymers separated using HPLC (either SEC or GEC) and in the second dimension the adhesive force of each copolymer fraction was mapped to obtain distribution based on the adhesive force of that fraction.

Keywords: PDMS copolymers, SEC-LC-transform-AFM, GEC-LC-transform-AFM.

7.1 Introduction

The complexity of block copolymers (particularly multiblock copolymers) has forced polymer science researchers to seek new analytical techniques that are capable of giving a more detailed picture of the copolymer characteristics, such as microstructure, composition, properties and morphology. Fractionation of a copolymer gives fractions with defined distributions (mainly molar mass or chemical compositions) and allows for subsequent physical or chemical testing of the respective fractions. It is a valuable and widely used technique.[1] One of the most useful and effective ways of performing fractionations on copolymer systems is by using chromatographic systems. This is due to its speed and high resolving power.[2,3] The chromatography process may be defined as those in which the solute is transferred between two phases, one of which is stationary and the other moving, often traversing a long tube called a column.[4] Three main forms of liquid chromatography (LC) have been used in the past to fractionate polymers: SEC, LC-CC and GEC.[5,6] Both the chromatography systems that were used in this study (SEC and GEC) were discussed in detail in Section 2.5.

In order to characterize heterogeneous copolymers it is necessary to separate not into unique molecules into a series of narrower molar mass distribution fractions. This is required in order to obtain a more detailed picture of the copolymer structure. These separated fractions may be required for further analysis such as the chemical composition or the microstructure investigate by a wide range of techniques such as Fourier-transform infrared spectroscopy (FTIR).[7-9]

Incorporation of PDMS into polyesters has been shown to yield several attractive properties while retaining many of the excellent properties of the corresponding homopolymers.[10] Two different experimental procedures were used in this work to synthesize multiblock segmented polydimethylsiloxane-polybutylenecyclohexanedicarboxylate (PDMS-s-PBCH) copolymers: a one-prepolymer method, based on a method developed by Kiefer et al.,[11] and a two-prepolymer method, based on a method developed by O'Malley et al.[12] for PDMS-aliphatic polyester copolymer. Depending on the copolymerization procedure a random or perfectly alternating multiblock copolymer was obtained. Because the focus of this study is aimed to investigate the morphology of the random copolymers only limited study on the surface morphology of alternating PDMS-s-PBCH multiblock copolymers was preformed in this chapter using AFM. This is done in an attempt to compare their morphology with the

complex morphology of the random PDMS-s-PBCH copolymers. However this chapter mainly devoted to describe the fractionation of selected samples of both type of the PDMS-PBCH copolymers, using chromatography techniques and to observe the surface morphology of the collected fractions.

SEC allowed fractionations based on the hydrodynamic volume (molar mass) of the copolymers and was coupled to FTIR using a LC-transform device. Using FTIR-LC-transform technique provides a clear chemical composition characterization of the PDMS-PBCH copolymers at specific molar mass distributions. GEC profile of THF and hexane solvents was also developed to be suitable for the PDMS-s-PBCH copolymer systems. GEC technique was used to fractionate based on the chemical compositions of the copolymers and also used to confirm the copolymer formation and purity as was discussed in Chapter 3.

Moreover, the fractionated copolymers, which were deposited directly on the germanium disc were redissolved and divided either into three fractions based on the molar mass or into two fractions based on the chemical composition. The redissolved polymers were used to make new thin films. Morphological characterization of the thin films of the copolymer fractions was carried out using the AFM technique in tapping mode. These offline coupling hyphenated techniques between the HPLC and the AFM were developed to provide morphology information as a function of the PDMS distribution or the copolymer molar mass and PDMS content, and they can be extended to be used for other copolymer systems. They also allow for morphology comparison between the bulk morphology of the copolymer and the fractions morphologies.

One selected sample of the PDMS-s-PBCH copolymer was fractionated and its collected fractions were subjected to adhesive force mapping (without redissolving the fractions) using the pulsed-force mode of AFM. This offered a new type of hyphenated techniques that can give two-dimensional distribution of the copolymers. The first distribution was created by the physically fractionate the copolymers using HPLC (either SEC or GEC) and from which, six and nine fractions were collected from SEC and GEC, respectively. The second distribution was created for each copolymer fraction obtained from the HPLC by mapping and distributing the adhesive force to from adhesive force distribution of that fraction. The adhesive force distribution is closely related to the chemical composition distribution of the copolymer surface.

7.2 Experimental

7.2.1 PDMS-s-PBCH samples

The alternating PDMS-s-PBCH copolymers (series E) were characterized in Chapter 3. Although the term alternating is used to describe series E copolymers, the copolymers chains of this series might content part with various PBCH segment lengths as discussed in Section 3.3.2.2. The relevant characteristics for this chapter of the selected copolymers for chromatography fractionations are summarized in Table 7.1.

Table 7.1: The characteristics of the PDMS-s-PBCH copolymers with 2000 g/mol PDMS M_n

Sample	PDMS in feed (wt %)	PDMS[a] (wt %)	PDMS-PBCH M_n[b] (g/mol)	Crystallinity ω_m[c] (%)	Crystallinity ω_{mPES} (%)
C-2	10	9.2	17171	16.4	18.0
C-3	25	22.7	20239	14.1	18.2
E-2	10	13.1	18235	17.8	20.5
E-3	25	27.2	17420	15.2	20.8

[a] PDMS content in the copolymer determined using ^{1}H-NMR

[b] Copolymers molar mass determined using SEC

[c] Degree of crystallinity determined using WAXD

Samples C-2 and C-3 are random PDMS-s-PBCH copolymers with PDMS segment length of 2000 g/mol. On the other hand samples E-2 and E-3 are alternating PDMS-s-PBCH copolymers with PDMS and PBCH segment lengths of 2000 and 940 g/mol, respectively. The degree of crystallinity of both E-2 and E-3 was determined using WAXD in the same manners as the random PDMS-s-PBCH copolymers described in Section 4.3.1.

7.2.2 Characterization techniques

7.2.2.1 Fractionation by size exclusion chromatography

SEC analyses were carried out using a dual pump HPLC system comprising of the following units: Waters 2690 separation module (Alliance) and Agilent 1100 series variable wavelength detector. THF was used as solvent with the flow rate set at 1 mL/min. A Mixed-E column packed with Pl gel silica particles (3 μm diameter) was used. The column temperature was set at 30 °C. Samples (5 mg/mL) were prepared in THF.

7.2.2.2 Fractionations by gradient elution chromatography

GEC was used to monitor the chemical composition of PDMS-PBCH copolymers by fractionation using a mixture of THF and hexane as eluant with a flow rate of 1 mL/min. The solvent gradient profile used for all GEC analyses was illustrated in Section 3.2.5.5. The separation was performed on the same a dual pump HPLC used for fractionation by SEC (Section 7.2.2.1).

7.2.2.3 SEC-LC-FTIR analysis

SEC-LC-transform-FTIR analysis was performed to determine the PDMS content throughout the copolymer samples. Separation according to molar mass by SEC was the first step of SEC-LC-transform-FTIR. In the second step of SEC-LC-transform-FTIR fractions are automatically deposited on a germanium disc. The germanium disc was then inserted into a FTIR spectrometer for chemical composition analysis. From the obtained FTIR spectra a profile of the PDMS content as a function in the molar mass distribution of the copolymer is created. The infrared spectra were obtained with a Perkin Elmer 1650 FTIR.

7.2.2.4 Surface morphology investigation of the PDMS-s-PBCH copolymers

All AFM images were obtained on a multimode AFM that described in Section 4.2.2.4 using a low resonance frequency silicon cantilever with a resonance frequency of about 60 kHz and a spring constant of k = 50 N/m. All experiments were carried out under ambient conditions. The scan rate was set in the range of 0.5 to 0.7 Hz. All AFM images were enhanced in the Veeco imaging software program and subjected to a plane fitting and flattening procedure, which eliminates the image bow resulting from non-linear scanner movement. Additionally, digital filtering was carried out to remove noise and clarify the structures present in the image. Only noise and image artefacts were eliminated using lowpass filtering. The typical sequence of the applied image treatment was: auto-flattening, planefit, and lowpass filtering.

In order to collect fractions for AFM analysis, from both the chromatography fractionation techniques (SEC and GEC), an LC-transform supported with a germanium disk was used. Small pieces of mica approximately 5 x 5 mm^2 were attached to the germanium disk and the eluted samples were collected on the mica pieces. Each eluted copolymer sample from the SEC system and GEC system was collected on two or three mica pieces, according to the broadness of the distribution. When the copolymer was fractionated based on the molar mass three fractions were collected whereas only two fractions were collected when the copolymer

was fractionated based on the chemical composition. Due to the rough surface of the directly deposited films (which prevented direct morphology imaging) all the fractions were redissolved and smooth thin films were made from samples of 0.5% in THF. These smooth thin films were placed in a vacuum oven at 25 °C for 24 h before the surface morphology investigation was carried out using AFM. One of the selected copolymers was fractionated and its collected fractions were subjected (without redissolving) to adhesive force mapping using pulsed-force mode of the AFM in order to relate the results of more than three adhesive force fraction measurements to the elution time. Thus the adhesive forces on nine different areas on the eluted copolymers surface were carefully measured. A typical example of the AFM adhesive force image of a PDMS-PBCH copolymer and the corresponding distribution histogram is shown in Figure 7.1.

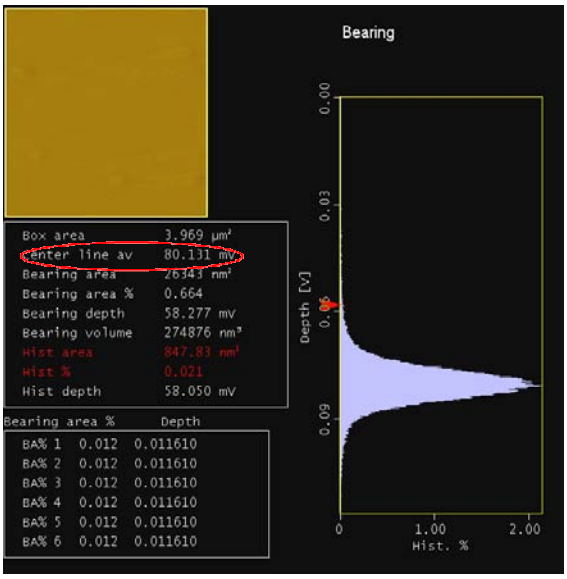

Figure 7.1: Typical example of the AFM adhesive force image of a PDMS-PBCH copolymer and the corresponding voltage distribution histogram.

The distribution histograms are calculated automatically during sample scanning. The adhesive force (F) is calculated using the following equation:

$$F = V \times k \times S \qquad \text{[Eq 7.1]}$$

where V is the average voltage value from the adhesion images, *k* is the spring constant of the AFM cantilever (2.8 N/m) and S is the sensitivity of the photodiode (500 nm/V). The V value is obtained for each AFM image by using bearing analysis (it is a method of plotting and analyzing the distribution of surface height over a sample). The average of the adhesive

force was determined as an average of five adhesion images: each image of these images consists of 256 x 256 single measurements in the observed areas of approximately 2 x 2 μm^2. All measurements were carried out under the same conditions. The distribution histograms of the adhesive force images were calculated using Eq 7.1 and the voltage distribution histograms.

7.3 Results and discussion

Before commencing with this section, it is considered necessary to mention three important points. First, the initial PDMS content in the copolymerization feed are used in the discussion for the sake of simplicity. Second the discussion of the surface morphology of the obtained fractions is limited to only the phase images of the AFM, due to the limited information that can be obtained from the height images of the AFM (as was elaborated in Section 4.3.2). Third, the GEC results were discussed in details in Chapter 3.

7.3.1 Surface morphology of alternating PDMS-s-PBCH copolymers

Figure 7.2 shows the AFM phase images obtained for the alternating PDMS-s-PBCH multiblock copolymers. In the case of 5 wt % PDMS content copolymer (E-1) (Figure 7.2(a)) small spherical domains were observed. The average diameter of these domains is approximately 25 ± 5 nm. In contrast to the random PDMS-s-PBCH copolymers with 5 wt % PDMS content (PDMS M_n 2000 g/mol) (Section 4.3.2) no a spherulitic crystal structure was observed for the alternating PDMS-s-PBCH multiblock copolymers. This is attributed to either the slightly high PDMS content in the alternating copolymers or the fact that the one-prepolymer method may allow the PBCH segment in the copolymer chain to grow with randomly and short and very long chains can be formed, with no interruption by PDMS segments. The very long PBCH segment length can be sufficient to allow the PBCH segment to fold in a lamella crystal order and then to form a spherulitic structure. This is not likely to occur for the alternating copolymers with a relatively short PBCH segment length in the two-prepolymer method.

Figure 7.2(b) shows AFM phase images of the 10 wt % PDMS content PDMS-PBCH alternating multiblock copolymer. A slightly different morphology to the 5 wt % PDMS content copolymer morphology was observed for this higher PDMS content copolymer (E-2). Once again, spherical of PDMS domains appear in the phase images with average diameter of approximately 40 ± 10 nm. The bright areas that appear in Figure 7.2(b) for the alternating

PDMS-s-PBCH multiblock copolymers with 10 wt % PDMS (PDMS M_n 2000 g/mol) could be either remains of PBCH homopolymer or crystalline PBCH segments in the copolymer that are confined in the matrix of the amorphous phase of the copolymer in the form of crystalline domains (a height variation effect is also possibility). A similar type of bright areas was attributed to crystalline domains of polybutyleneterephthalate when polybutyleneterephthalate polyethylene oxide PDMS multiblock copolymers were investigated using AFM tapping mode by Dahrouch and coworkers.[13]

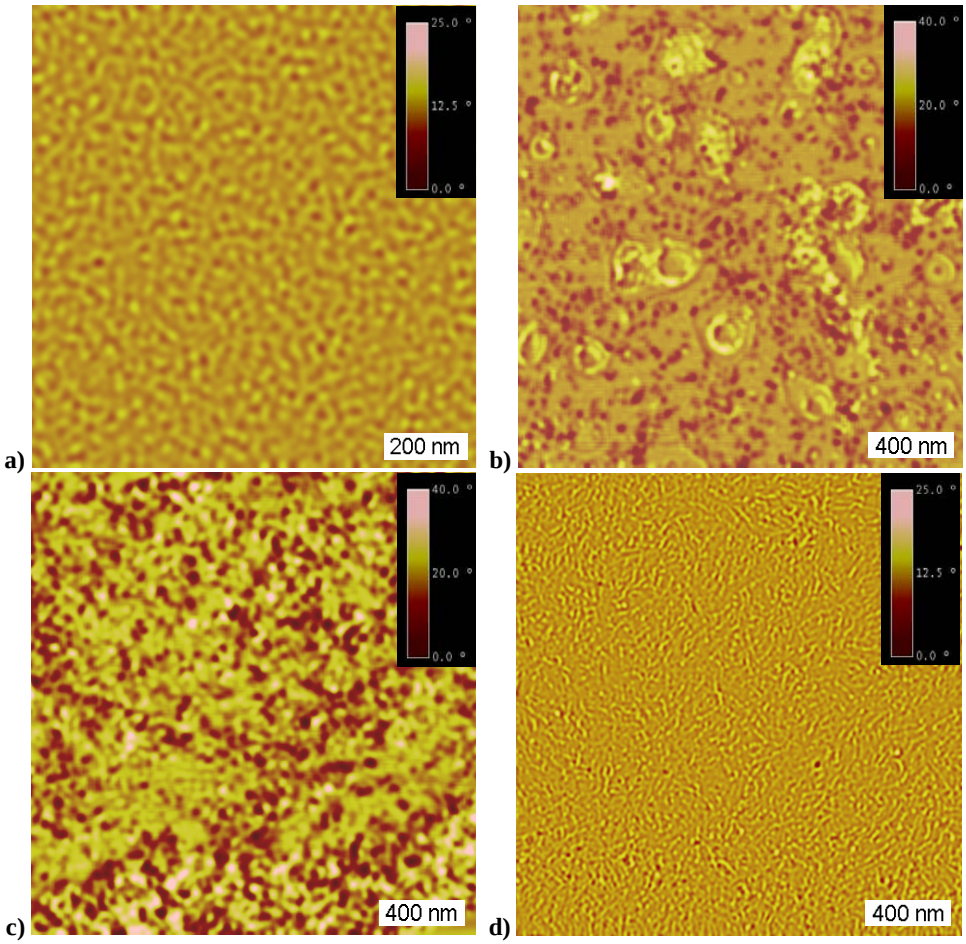

Figure 7.2: AFM phase images of thin films of PDMS-PBCH alternating multiblock copolymers: (a) 5 wt % PDMS (PDMS M_n 2000 g/mol) (b) 10 wt % PDMS (PDMS M_n 2000 g/mol) (c) 25 wt % PDMS (PDMS M_n 2000 g/mol) (d) 10 wt % PDMS (PDMS M_n 1000 g/mol).

The spherical PDMS domains were also observed for the other alternating PDMS-PBCH multiblock copolymers E-3 and E-4 as shown in Figure 7.2(c) and Figure 7.2(d) respectively. The average diameter of the PDMS domains was increased to 60 ± 10 nm as the PDMS content increased to 25 wt % (PDMS M_n 2000 g/mol) in the E-3. The only possible explanation for the increase in the PDMS domain size is the possibility of PBCH segment is

trapped inside. Although the length of the PBCH segment in this copolymer can not be shorter than 940 g/mol but because of the large length of the PDMS segment (2000 g/mol) the PBCH link between two PDMS molecules can easily trapped in between and thus inside the PDMS domains, which increase the PDMS segment length drastically to 7000 g/mol. When the PDMS segment length decreased to 1000 g/mol (10 wt % PDMS) in the E-4 the average diameter of these domains became approximately 20 ± 5 nm. All the alternating PDMS-s-PBCH copolymers showed PDMS spherical domains with average diameters smaller than that observed for their analogies of random PDMS-s-PBCH copolymers (Sections 4.3.2 and 5.3.2). This can be attributed to the restriction of the PDMS segment movement in the alternating PDMS-s-PBCH copolymer chains created as a result of the relatively constant length of the PBCH segment with minimum length (M_n) of 940 g/mol. Obviously this restriction of the PDMS segment movement becomes less in the random PDMS-s-PBCH copolymers, in which the length of the PBCH segment may go down to only one repeating unit of ester.

The variation in the synthesis method leads to different surface morphologies for several random and alternating PDMS-s-PBCH copolymers, while the same type of morphologies was obtained for others. In order to fully understand the complex morphology of the PDMS-s-PBCH copolymers four copolymers were selected for investigations (see Table 7.1): two samples with different surface morphologies (C-2 and E-2) and two samples with similar surface morphologies (C-3 and E-3).

7.3.2 HLPC-LC-transform-AFM investigation of PDMS-PBCH copolymers

Figure 7.3 illustrates the SEC-LC-transform-FTIR results for a random PDMS-PBCH copolymer with 10% PDMS content (sample C-2). The Gram-Schmidt plot that obtained after SEC fractionation is overlaid with the Si-O/C=O ratio. The Si-O band is at 1051 cm^{-1} and C=O band is at 1730 cm^{-1} wavelengths. The result shows that in this sample the low copolymer molar mass fraction contains more PDMS (Si-O/C=O) than that the higher molar mass fraction. Figure 7.3 also shows the surface morphology of the fractions collected from SEC for this PDMS-PBCH copolymer. The fractions surfaces were imaged via tapping mode AFM at ambient temperature. Only the resulting phase images are shown here. The thermodynamic incompatibility of the PDMS soft segment and the PBCH hard segment results in a two-phase microstructure as discussed previously in Chapter 4 and 5. Spherical domains of PDMS are observed in the surface morphology of all the fractions. It is interesting

to note the pattern or the order that can be seen in the first fraction, which has a high molar mass, and a low PDMS content determined from the FTIR results. A similar pattern of order has been reported for the bulk morphology of other di-block and tri-block copolymers.[14-16] Thus this order or pattern here indicates that the main bulk of this fraction most likely consists of PDMS-PBCH di-block or tri-block copolymers. Although similar spherical PDMS domains were observed for the unfractionated copolymer (see Section 4.3.2), this type of order has not been seen for C-2 copolymer without using sample fractionations techniques.

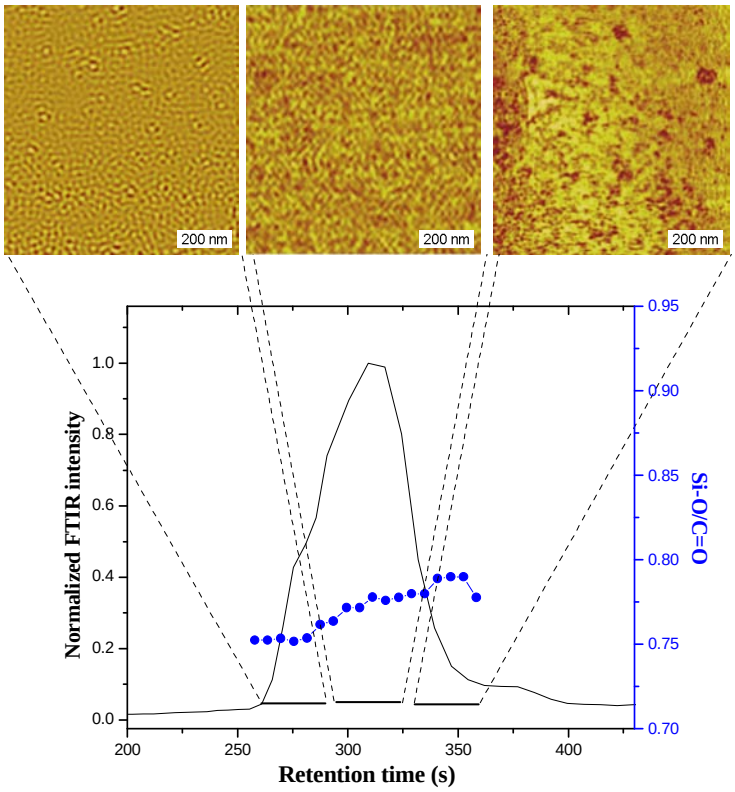

Figure 7.3: A Gram-Schmidt plot overlaid with the ratio of Si–O/C=O FTIR bands and AFM images for each assigned fraction of a random PDMS-PBCH multiblock copolymer with 10 wt % PDMS content.

Figure 7.4 shows the results obtained when the copolymer was fractionated by GEC, based on the chemical composition. The obtained surface morphology shows large PDMS domains in a rich PDMS fraction (first fraction in Figure 7.4). The sizes of these domains appear larger than that of the PDMS domains in the fractions obtained from SEC fractionation of this copolymer. In this image some of the domains begin to connect with each other, which was not observed in the bulk morphology of this copolymer in Section 4.3.2. This eventually will lead to a change in the type of morphology from spheres to a bicontinuous phase, as will be discussed later in this section for the 25 wt % PDMS content copolymer.

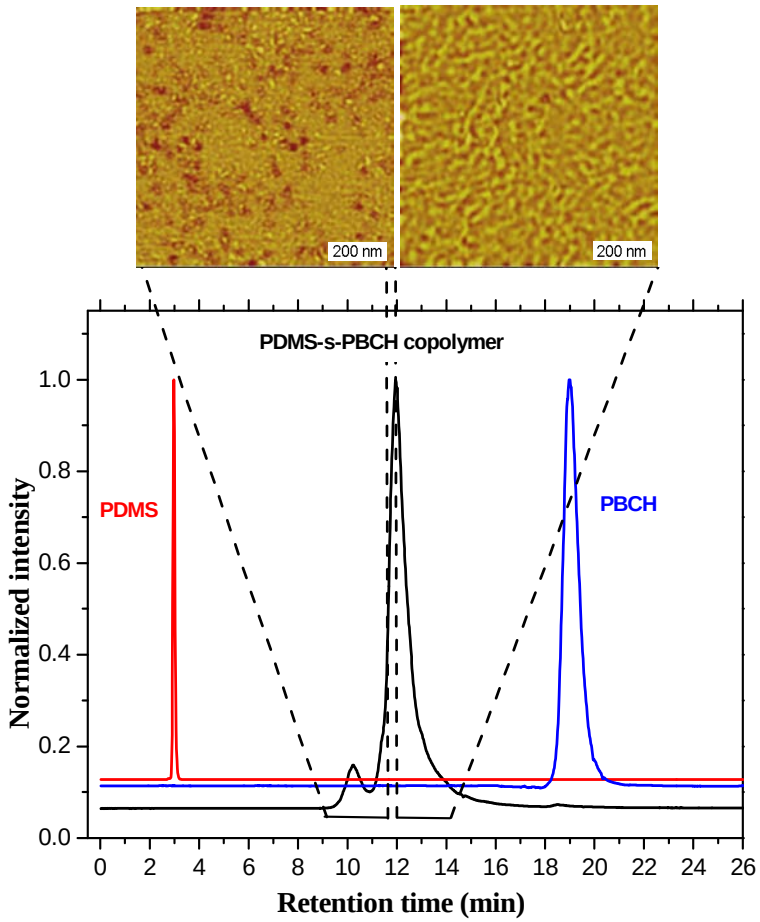

Figure 7.4: GEC result for PDMS, PBCH homopolymers and a random PDMS-PBCH multiblock copolymer with 10 wt % PDMS content and AFM images for each assigned fraction of the copolymer (Chapter 3).

Figure 7.5 shows the SEC-LC-transform-FTIR results (plotted as Gram-Schmidt plot) and the surface morphology of the collected fractions for alternating PDMS-s-PBCH copolymers (sample E-2) with 10 wt % PDMS content. In this copolymer the ratio of Si-O/C=O, which illustrates the PDMS content across the copolymer molar mass distribution, shows no significant change in the PDMS content as the M_n of the copolymer changes. This indicates that all the copolymer chains have relatively the same PDMS content, as is expected for alternating copolymers. The two phase structures of the PDMS domains dispersed in a continuous PBCH hard phase were evidenced by AFM observation. Figure 7.5 shows the PDMS domains on the surface in the AFM phase images that correspond to both high and medium molar mass fractions (first fraction and second fraction in Figure 7.5 respectively). These fractions were obtained when the 10 wt % PDMS content alternating PDMS-s-PBCH copolymers were fractionated, based on the molar mass.

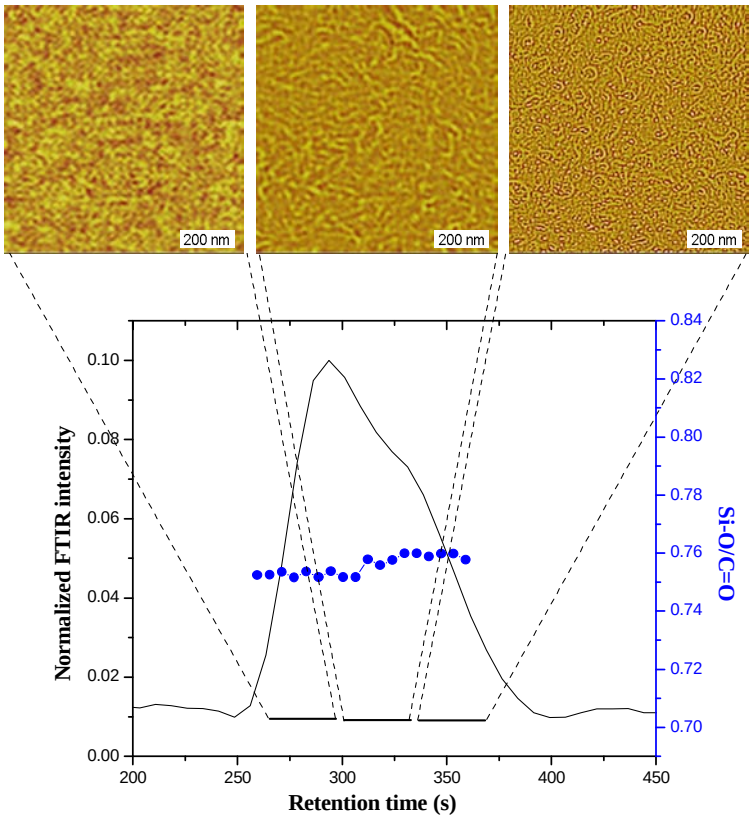

Figure 7.5: A Gram-Schmidt plot overlaid with the ratio of C=O/Si–O FTIR bands and AFM images for each assigned fraction of alternating PDMS-PBCH multiblock copolymer with 10 wt % PDMS content.

In the low molar mass fraction (third fraction), however, in addition to the PDMS domains, very bright domains are also observed. These bright domains have relatively irregular sizes and are not uniformly distributed in the PDMS-s-PBCH copolymer amorphous matrix. These domains could be either due to the height variation effect or due to the presence of crystalline phase. The crystalline phase in this case might be from remains of PES homopolymer or PES segment in the copolymers. A similar type of morphology for the unfractionated copolymers was observed (Figure 7.2). However, here the bright domains seem to be much smaller and can be seen much clearer. The PDMS-PBCH copolymer matrix in several areas in the low molar mass fraction image also shows a secondary morphology looks like worm morphology or lamella-like morphology. This type of morphology seems to be similar to the type of morphology that usually obtained from di and triblock copolymers. In fact the low molecular mass alternating PDMS-PBCH copolymer fraction can be made of a di or triblock copolymer molecules.

Figure 7.6 shows GEC analysis of the sample E-2. The small peak at a retention time of about 18 min corresponds to a small amount of PBCH homopolymer still present in the copolymer. In the AFM image of the rich PBCH fraction the matrix of the PDMS-PBCH copolymers also shows some lamella morphology, which was described in low molecular mass fraction in Figure 7.5 as an attempt of forming lamella morphology, which interrupted with the bright domains. Although the PBCH has been removed from the fractionated copolymers, the bright domains still appear in the phase image of the second fraction in Figure 7.6. This proves that these bright domains are in fact not crystalline domains of PBCH homopolymers. This leaves only two possibilities can be used to explain the nature of the bright domains. These are: amorphous copolymer with various height or crystalline domains of PBCH segment in the copolymer chains. In the case of the latter possible explanation this type of morphology can be modelled by the fringed-micelle model very easily as shown in Figure 7.7.

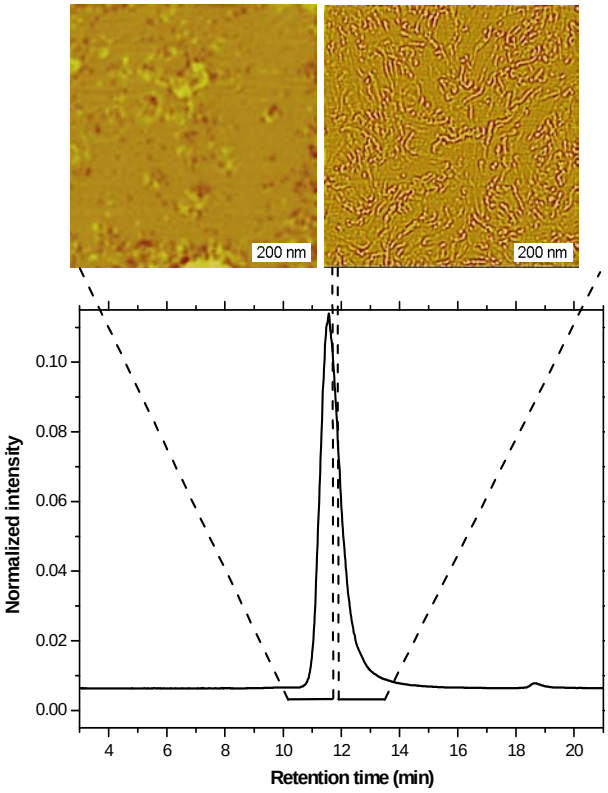

Figure 7.6: GEC results and AFM images for each assigned fraction of alternating PDMS-PBCH multiblock copolymer with 10 wt % PDMS content (Chapter 3).

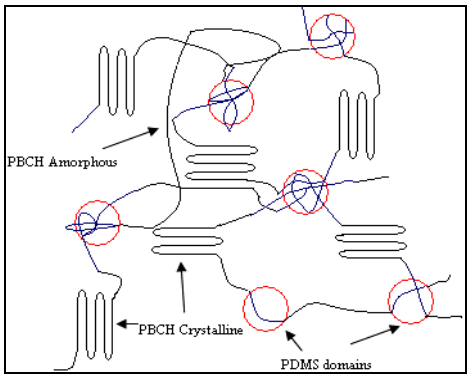

Figure 7.7: Schematic representation of the fringed-micelle model, showing the crystallinity of PBCH segments in the PDMS-PBCH copolymers.

Figure 7.7 shows clearly that the PDMS segment in the copolymer chains are disrupting the large crystal order of the PBCH segment in this copolymer and the small length of the PBCH segment also leads to the creation of small domains of PBCH crystals in the matrix of the PDMS-s-PBCH amorphous phase.

Figure 7.8 shows the Gram-Schmidt plot overlaid with the ratio of Si–O/C=O FTIR bands of the random PDMS-PBCH when the PDMS content was increased to 25 wt % in the copolymer (sample C-3). The PDMS content along the molar mass distribution of the copolymer seems to be relatively constant, but they do not necessarily have a similar distribution along the copolymer chains. Figure 7.8 also shows the surface morphology of the PDMS-PBCH fractions obtained from AFM. In this copolymer (C-3) all the collected fractions from the SEC-LC-transform show morphology similar to the morphology of the bulk copolymer (Section 4.3.2). The PDMS domains can be seen for the fractions as for the bulk in the polyester matrixes. On the other hand when the copolymer is fractionated based on the chemical composition (Figure 7.9); bright domains were observed as well in the low PDMS content fraction. Once again these bright domains might be either due to the height variation effect or due to PBCH crystalline segments in the copolymers. Furthermore the DSC and WAXD results discussed earlier in Section 4.3.1 and Section 5.3.1 provides conformation of the presence of such crystalline phase in the unfractionated copolymers and the observation of the PBCH crystalline phase in several fractions of fractionated copolymers implies the existence of this PBCH crystalline phase in the unfractionated copolymer as well.

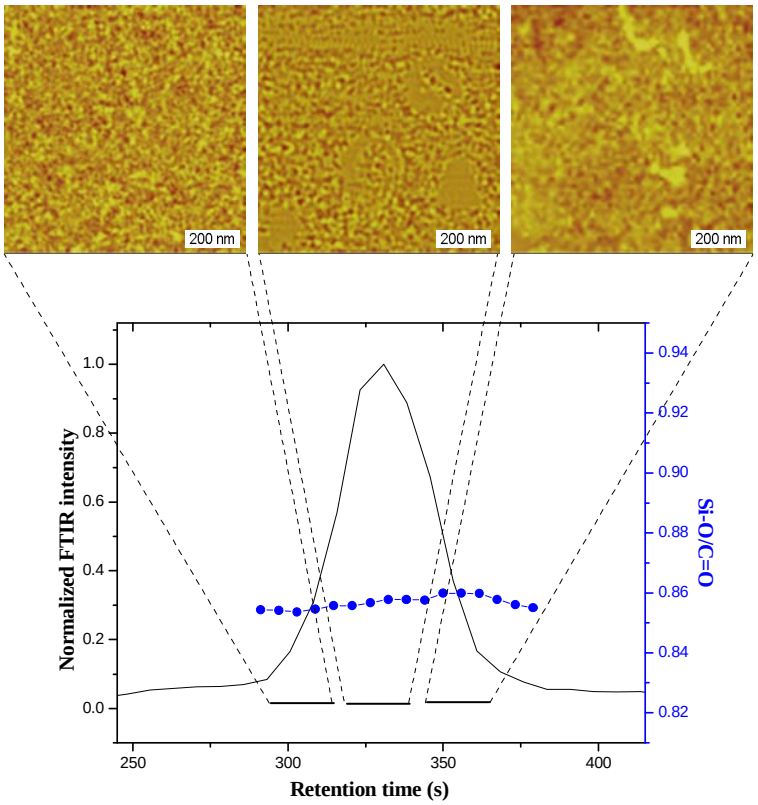

Figure 7.8: A Gram-Schmidt plot overlaid with the ratio of Si–O/C=O FTIR bands and AFM images each assigned fraction of a random PDMS-PBCH multiblock copolymer with 25 wt % PDMS content.

Once again this type of morphology can be modelled by the fringed-micelle model (shown in Figure 7.7). However, close look in the rich PBCH copolymer fraction (Figure 7.9) also revealed the lamella morphology interrupted with the segregation of the PDMS in to spherical domains and also with the bright domains, which are more likely related to the PBCH crystalline regions. The rich PBCH copolymer image shows a poorly ordered microphase-separated structure resembling more ordered type of structure that can be typically obtained from diblock copolymers. Although it is well known that the most important driving factor for the phase separated morphologies in the PDMS-organic copolymers is the low solubility parameter of the PDMS compared with that of the organic segment (δ = 7.3–7.5 $Cal^{½}cm^{-3/2}$),[17] the crystallization of the PBCH segment in the microdomain can also be considered to be another driving force for the phase separation in the PDMS-PBCH semicrystalline system. In this case, due to the low glass transition temperature of the PDMS segment, the crystallization of the PBCH segments will be confined within nanoscale domains. The crystallization in nanoscale domains has been reported in literature for diblock copolymers with strongly segregated systems with rubbery

blocks.[18-20] Although the fascinating morphology of the three phases has been observed in several of the unfractionated copolymers, none is as clear as shown in the fractionated copolymers. This is a clear indication of the advantages of using the newly proposed HPLC-LC-transform-AFM offline hyphenated techniques for investigating the complex morphology of multiblock PDMS copolymers.

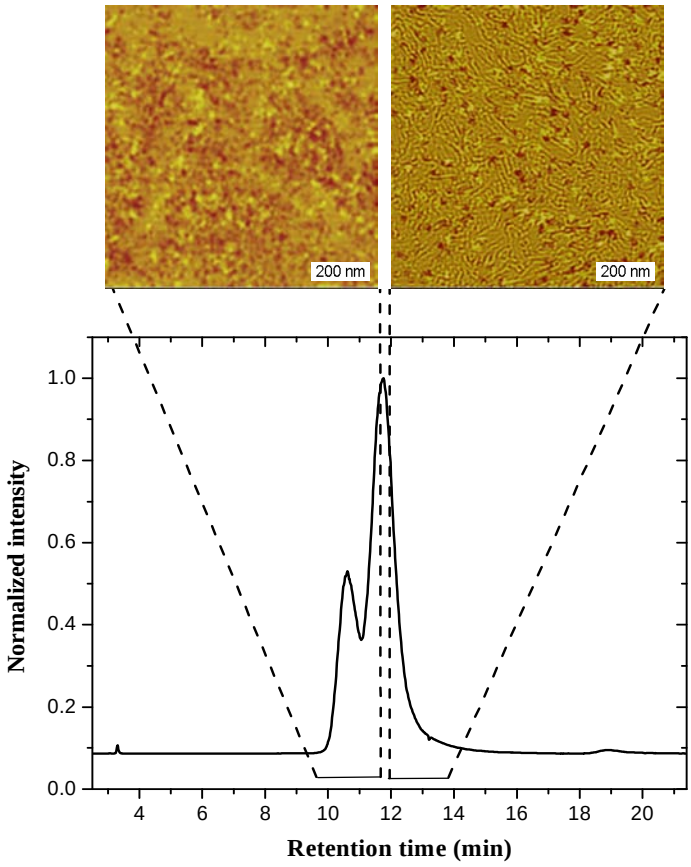

Figure 7.9: GEC results and AFM images for each assigned fraction of a random PDMS-PBCH multiblock copolymer with 25 wt % PDMS content (Chapter 3).

Figure 7.10 shows SEC-LC-transform-FTIR results for the alternating multiblock copolymer with 25 wt % PDMS content (sample E-3). There is a slight increase in the average PDMS content in the low molar mass fractions of the copolymer. Consistently, the AFM phase images show spherical domains of PDMS in the amorphous lamella morphology of PDMS-s-PBCH copolymer matrix. Although the PDMS content is high in this fraction the bright domains are still seen. This illustrated the fact that in the copolymer chains themselves there is a phase separations as can be detected from the presence of three type of morphology in the same image.

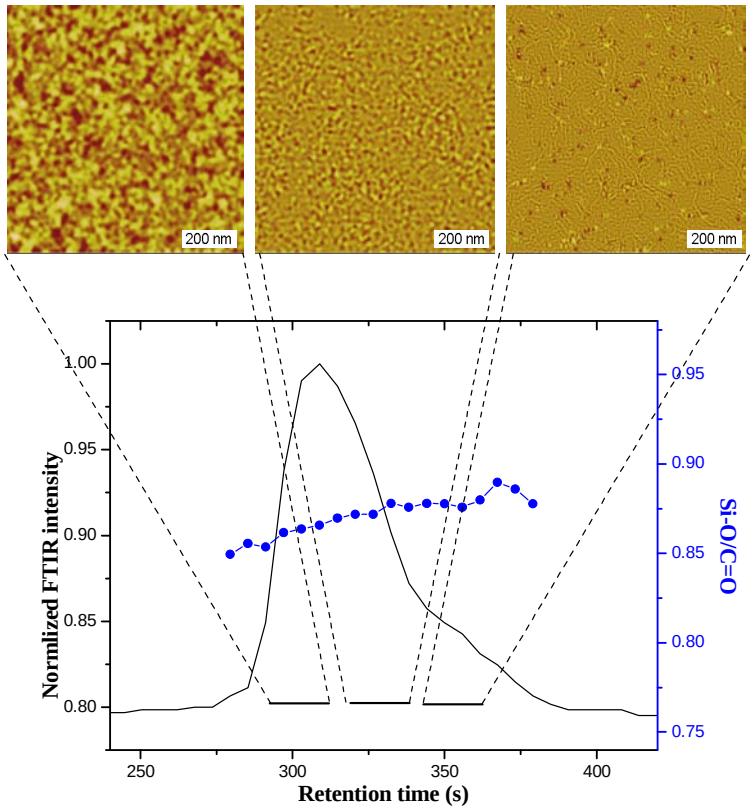

Figure 7.10: A Gram-Schmidt plot overlaid with the ratio of Si–O/C=O FTIR bands and AFM images for each assigned fraction of an alternating PDMS-PBCH multiblock copolymer with 25 wt % PDMS content.

Figure 7.11 shows the GEC results and the surface morphology of the collected fractions for alternating PDMS-PBCH copolymers (sample E-3) with 25 wt % PDMS content. Two types of morphology are obtained: PDMS domains in a matrix of PBCH for the low PDMS content fraction, and the rich PDMS content fraction shows bicontinuous phase type morphology with a few PDMS domains scatter in the images as well. Comparison of the fractions morphologies in Figures 7.10 and 7.11 with the bulk copolymer morphology in Figure 7.2(c) of E-3 copolymer showed largely changes in the morphology as the heterogeneity of the copolymer changes.

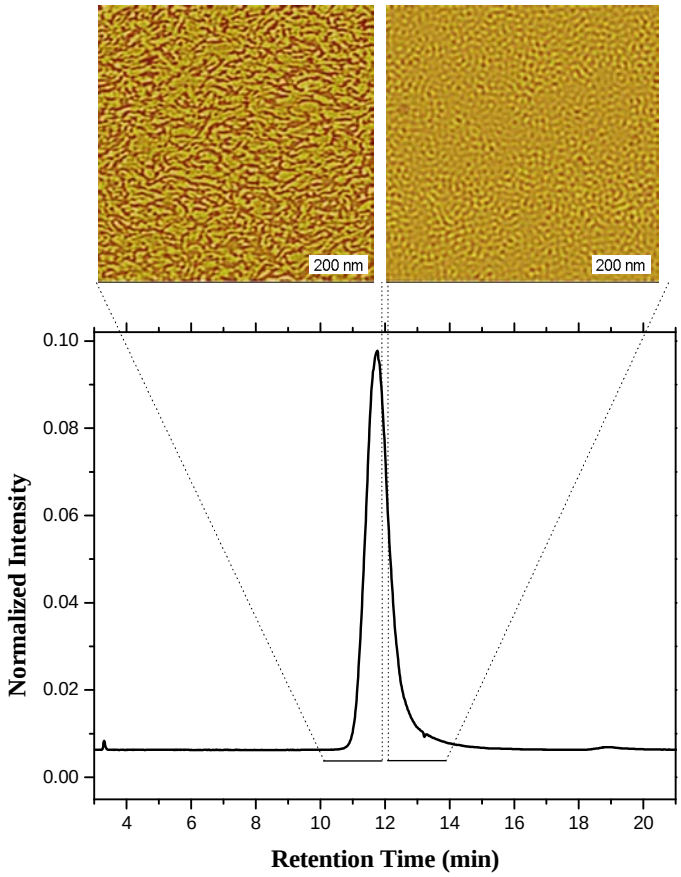

Figure 7.11: GEC results and AFM images taken for each assigned fraction of an alternating PDMS-PBCH multiblock copolymer with 25 wt % PDMS content (Chapter 3).

7.3.3 Adhesive force investigation of PDMS-PBCH copolymer fractions

Another new hyphenation technique is proposed, namely the HPLC-DPFM-AFM technique. In this technique the collected fractions from the HPLC system (using either GEC or SEC) are subjected to adhesive force mapping using the pulsed-force mode of the AFM. The results obtained from the GEC-DPFM-AFM technique are presented in Figures 7.12–7.14 for a selected random PDMS-PBCH multiblock copolymer with 10 wt % PDMS content. This sample was chosen to be presented as a typical example of the adhesive force investigation of PDMS-PBCH copolymer fractions for three reasons. First, the most obvious reason is due to the representative results that were obtained for this sample using this technique. Second, a variety of morphologies were recorded for this copolymer from the previously mentioned hyphenated technique. Third, it is necessary to have a relatively large variation in the PDMS content along the molar mass distribution in order to illustrate the validly of using the adhesive force measurement to indicate the chemical composition change on the copolymer surface.

Figure 7.12 shows the average adhesive forces for each copolymer fraction, and the PBCH and PDMS homopolymers, calculated using Eq 7.1. Although the average value of the adhesive force is easily measured for each fraction, a more refined statistical approach can be used. This uses the displayed histogram with bearing analysis, and is calculated using Eq 7.1 and the voltage distribution histograms.

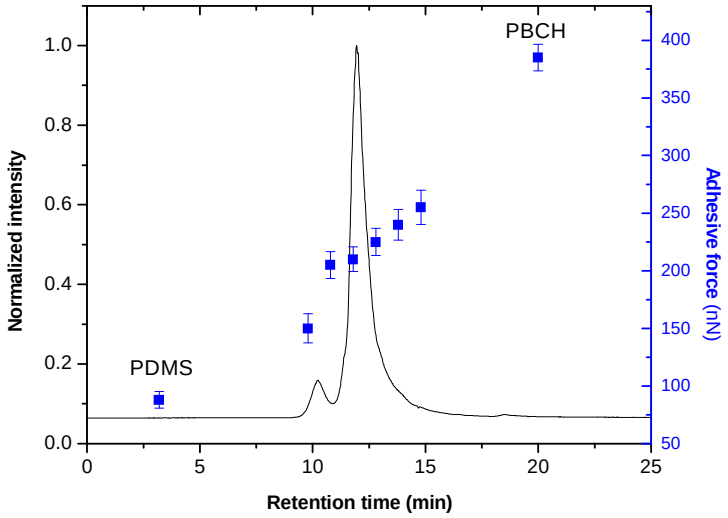

Figure 7.12: GEC-DPFM-AFM results for a PDMS-PBCH random multiblock copolymer with 10 wt % PDMS content.

The histogram of the adhesive force shown in Figure 7.13 reveals the adhesive force distribution on the surface of each fraction of the copolymers from 256 x 256 single measurements. The adhesive force of each copolymer fraction was mapped and distributed automatically based on the adhesive force to produce the histogram of the adhesive force distribution. The histogram in fact shows the chemical distribution on the surface of each fraction. It is clear that some fractions have broader distribution than others, which indicates that the broader the distribution is the greater is the variation in chemical composition and functional groups in the sample.

Using a Gaussian fit the broadness of the adhesive force distribution peaks was quantified using the full width at half maximum (FWHM) values. The obtained results are presented in Table 7.2. The broadest fraction is fraction-6 and the narrowest fraction is fraction-2. The PDMS homopolymer shows the smallest FWHM value, indicting that it has the narrowest broadness as would be expected.

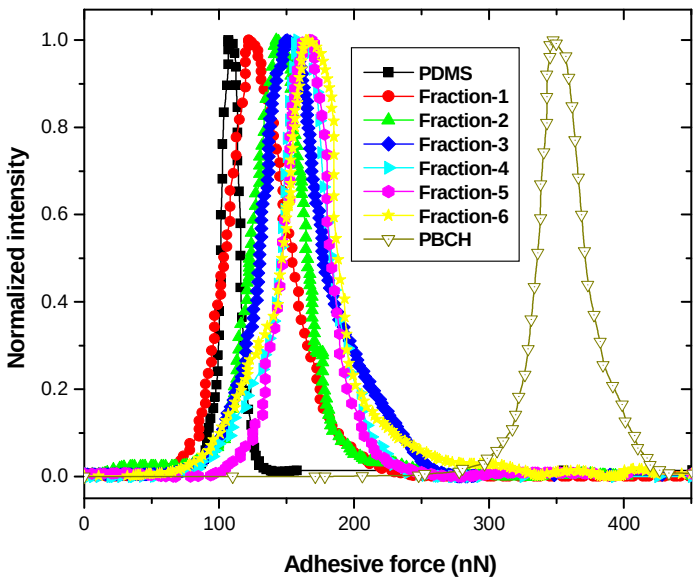

Figure 7.13: Adhesive force distribution of the PDMS and PBCH homopolymers and six fractions of PDMS-PBCH random multiblock copolymer with 10 wt % PDMS content obtained from the SEC-DPFM-AFM.

Figure 7.13 also shows the adhesive force distribution of both PDMS and PBCH homopolymers. All the adhesive force distributions of the fractions are situated between the maximum (PBCH) and the minimum (PDMS) distributions of the homopolymers and are shifted towards the PBCH as the PBCH content increases in the copolymers. Significantly, however, all the copolymer fractions distributions show some overlapping with the PDMS distribution. The overlapping can be clearly seen in the 2D plot (Figure 7.14).

Table 7.2: FWHM of the PDMS the PBCH homopolymers and the C-2 copolymer as well as the HPLC-DPFM-AFM fractions adhesive force distribution peaks

GEC-DPFM-AFM		SEC-DPFM-AFM	
Fraction no.	FWHM	Fraction no.	FWHM
PDMS	15	Fraction-1	43
Fraction-1	40	Fraction-2	52
Fraction-2	37	Fraction-3	45
Fraction-3	39	Fraction-4	61
Fraction-4	47	Fraction-5	42
Fraction-5	42	Fraction-6	34
Fraction-6	50	Fraction-7	31
PBCH	37	Fraction-8	28
-	-	Fraction-9	38

Figure 7.14 shows the contour plots of the adhesive force and the retention time of each fraction obtained from GEC. PDMS and PBCH homopolymers are also included in the 2D plot. The fact that three complete separated distributions were observed confirms the PDMS-PBCH copolymers formation. The increase in the adhesive force as the retention time increases (indicated by the white line in the 2D plot) shows that the copolymer has been fractionated based on the chemical compositions.

Fraction-6 obtained from GEC-DPFM-AFM shows the largest FWHM, which illustrates the variety of the chemical composition of this fraction. The largest FWHM can also be seen from the broadness of the PDMS-s-PBCH distribution in the right side when it is compared with the left side of the PDMS-s-PBCH distribution. The high PDMS content copolymer at lower retention time has an average adhesive force and distribution relatively similar to that of the PDMS homopolymer. This indicates that in this fraction PDMS is dominant on the copolymer surface. With decreasing the PDMS content (large retention time) the broadening of the adhesive force distribution shifted toward that of the PBCH homopolymer indicating a less dominants PDMS on the copolymer surface.

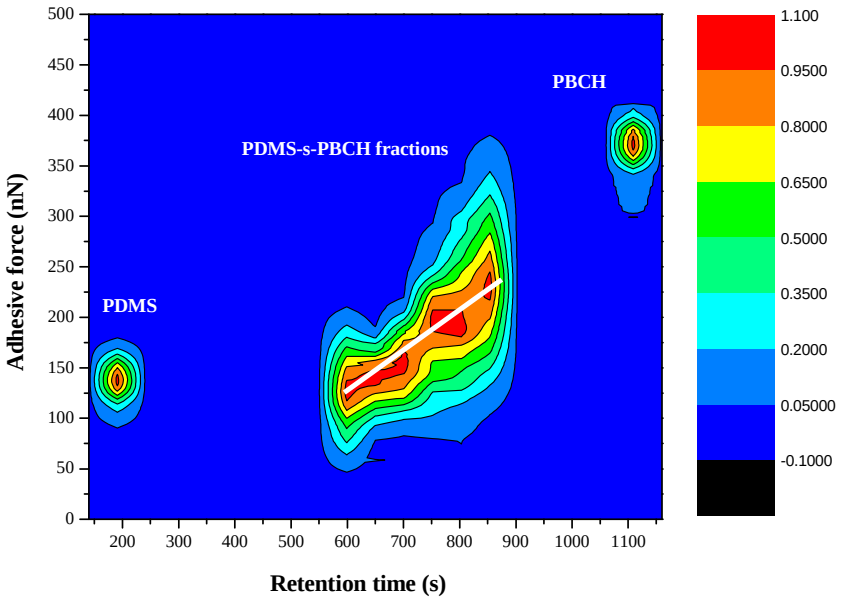

Figure 7.14: 2D plot of the GEC-DPFM-AFM results of sample C-2 associated with both homopolymers.

Figure 7.15 shows a typical example of SEC-DPFM-AFM results for a PDMS-PBCH random multiblock copolymer with 10 wt % PDMS content. The results of the average adhesive force values of the fractions are compared with the ratio of the Si-O/C=O obtained from the FTIR analysis that were previously presented in Figure 7.3. The comparison shows that the PDMS

content along the copolymer molar mass distribution is in relatively good agreement with the obtained average adhesive force values.

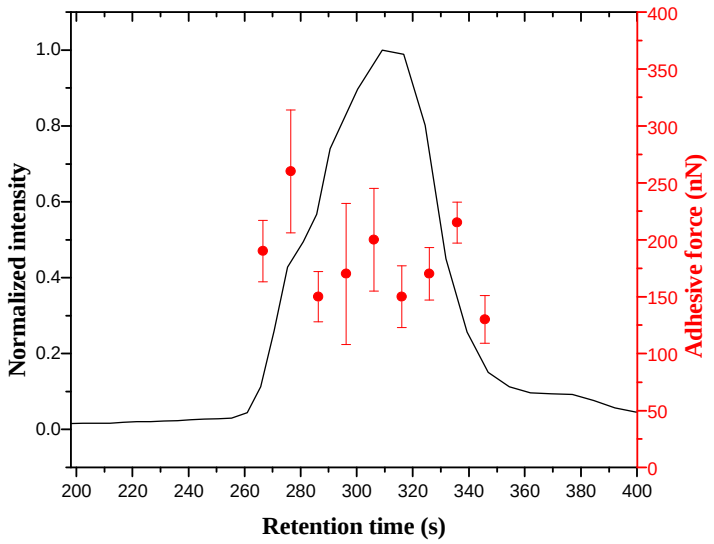

Figure 7.15: SEC-DPFM-AFM results for a PDMS-PBCH random multiblock copolymer with 10 wt % PDMS content.

Using the SEC-DPFM-AFM hyphenated technique, the C-2 copolymers were investigated. First the copolymer was fractionated in the HPLC system based on the molar mass (hydrodynamic volume). Then the adhesive force on the surface of the HPLC collected fractions were mapped and distributed as is illustrated in Figure 7.16, to create adhesive force for each fraction.

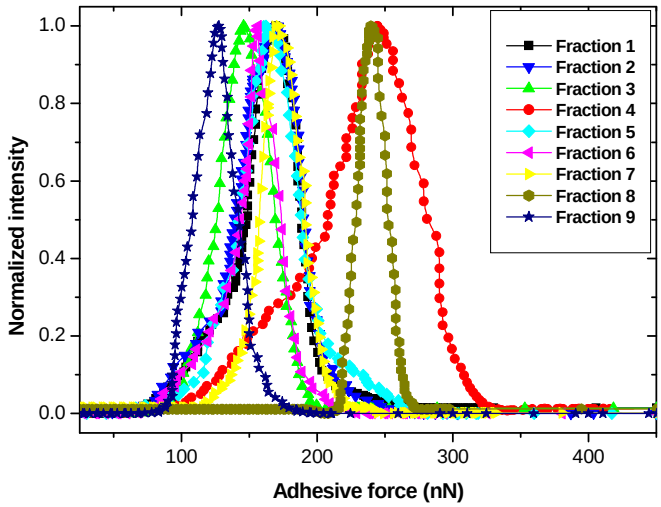

Figure 7.16: Adhesive force distribution of nine fractions of PDMS-PBCH random multiblock copolymer with 10 wt % PDMS content obtained from the SEC-DPFM-AFM.

The broadness of the adhesive force fractions that collected from SEC are also tabulated in Table 7.2. It is clear that the FWHM for fraction-4 is the largest of all the SEC fractions, which illustrates the variation of the chemical composition of the surface of the copolymer fractions. This also indicates that all the fractions consist of copolymer chains with varying PDMS content, which is a clear indication of the heterogeneity of this copolymer across the molar mass distribution. Therefore in the proposed (HPLC-DPFM-AFM) system, the data is collected and distributed to create new distribution of the fraction based on the adhesive force or the chemical composition, without the need for fractionation the copolymer on a preparative scale.

7.4 Conclusions

The surface morphology of the alternating PDMS-s-PBCH multiblock copolymer (series E) was investigated and compared to their analogies of random PDMS-s-PBCH multiblock copolymer in series C and D using AFM techniques. Similarly to the case of the PDMS-PBCH random multiblock copolymer, the AFM findings showed that the microphase separation occurred on the surface morphology of alternating PDMS-s-PBCH multiblock copolymers. The microphase separation here manifested in spherical micro-domains of PDMS types of morphology. The size of the PDMS domains increased as the PDMS content and molar mass increased, similar to the case in the random PDMS-PBCH copolymers.

In this chapter the complex morphology of both type of the PDMS-PBCH copolymer was further investigated using a new analytical technique. The PDMS-PBCH copolymers were fractionated using two different developed chromatography techniques: size exclusion chromatography and gradient elution chromatography. The PDMS content along the molar mass distribution was investigated using SEC-FTIR by off-line coupling techniques. Moreover, in this chapter a better understanding for the complexity of the morphology of the PDMS-PBCH multiblock copolymers was obtained using two new HPLC-AFM offline coupling techniques hyphenation. The two novel hyphenated offline coupling techniques were developed to provide morphology information as a function of PDMS distribution or copolymer molar mass and the PDMS content, namely SEC-AFM and GEC-AFM. These novel techniques provide a new way to study the morphology as a function of the copolymer molar mass (SEC-AFM) and as a function of the chemical composition (GEC-AFM). Although the fractions morphology of the investigated copolymers using, SEC-AFM did not show a very big or a significant change in the morphology, all the fractions morphology using

GEC-AFM did indeed show distinct differences in morphology. The morphology that observed in this chapter using the HPLC-AFM hyphenated techniques was much clearer than in the unfractionated copolymers using traditional techniques. However, the distinctive morphologies of lamellae order and the coexisting of more than of the bright domains in addition to the PDMS domains in a matrix with lamellae order were not observed in the previous chapters.

Furthermore, a new hyphenated technique of HPLC-DPFM-AFM was also proposed here. In the HPLC-DPFM-AFM hyphenated technique the collected fractions from the HPLC (either SEC or GEC) were subjected to adhesive force mapping using the digital pulsed-force mode of the AFM. This technique propose a two dimensions distribution of the copolymers in the first dimension the copolymers fractionated in HPLC column and the variation in the adhesive force of each collected fraction was measured and distributed based on the adhesive force to produce the adhesive force distribution for each fraction.

7.5 References

1. Julian, F. J.; Roger, S. P.; Manfred, J. R. C. *Reviews in Macromolecular Chemistry* 1966, 1(2), 393-434.
2. Striegel, A. M. *Analytical and Bioanalytical Chemistry* 2008, 390(1), 303-305.
3. Nikos, H.; Stergios, P.; George, F., *Block Copolymers: Synthetic, Strategies, Physical, Properties and Application*. First ed.; John Wiley and Sons, United States, 2003; pp 175-179.
4. Collins, E. A.; Bares, J.; Billmeyer Jr., F. W., *Experiments in Polymer Science*. First ed.; John Wiley and Sons, United States, 1973; pp 154-167.
5. Pasch, H., Analysis of complex polymers by interaction chromatography. In *Polymer Analysis Polymer Physics*, Springer, Berlin / Heidelberg, 1997; Vol. 128, pp 1-45.
6. Crompton, T. R., *Practical Polymer Analysis*. First ed.; Plenum Press, New York, 1993; pp 256-321.
7. Pasch, H., Hyphenated techniques in liquid chromatography of polymers. In *New Developments in Polymer Analytics I*, Springer, Berlin / Heidelberg, 2000; Vol. 157, pp 1-66.
8. Somsen, G. W.; Gooijer, C.; Brinkman, U. A. T. *Journal of Chromatography A* 1999, 856(1-2), 213-242.

9. Kok, S. J.; Arentsen, N. C.; Cools, P. J. C. H.; Hankemeier, T.; Schoenmakers, P. J. *Journal of Chromatography A* 2002, 948(1-2), 257-265.

10. Vuckovic, M. V.; Antic, V. V.; Dojcinovic, B. P.; Govedarica, M. N.; Djonlagic, J. *Polymer International* 2006, 55(11), 1304-1314.

11. Kiefer, L. A.; Yoon, T. H.; Glass T.E.; Jayaraman S.K.; McGrath J.E. *Journal of Polymer Science, Part A: Polymer Chemistry* 1997, 35(16), 3495-3506.

12. O'Malley, J.; Pacansky, T. J.; Stauffer, W. *Macromolecules* 1977, 10(6), 1197-1199.

13. Dahrouch, M.; Schmidt, A.; Leemans, L.; Linssen, H.; Götz, H. *Macromolecular Symposia* 2003, 199(1), 147-162.

14. Hamley, I. W., *Developments in Block Copolymer Science and Technology, Introduction to Block Copolymers.* University of Leeds, UK, 2004; pp 1-29.

15. Ruokolainen, J.; Tanner, J.; Ikkala, O.; ten Brinke, G.; Thomas, E. L. *Macromolecules* 1998, 31(11), 3532-3536.

16. Garstecki, P.; Holyst, R. *Macromolecules* 2003, 36(24), 9181-9190.

17. Yilgör, I.; McGrath, J., Polysiloxane containing copolymers: A survey of recent developments. In *Polysiloxane Copolymers/Anionic Polymerization*, Springer, Berlin / Heidelberg, 1988; Vol. 86, pp 1-86.

18. Zhang, F.; Chen, Y.; Huang, H.; Hu, Z.; He, T. *Langmuir* 2003, 19(14), 5563-5566.

19. Douzinas, K. C.; Cohen, R. E.; Halasa, A. F. *Macromolecules* 1991, 24(15), 4457-4459.

20. Hamley, I. W.; Fairclough, J. P. A.; Terrill, N. J.; Ryan, A. J.; Lipic, P. M.; Bates, F. S.; Towns-Andrews, E. *Macromolecules* 1996, 29(27), 8835-8843.

Chapter Eight

Conclusions and Recommendations

This chapter includes two main sections: conclusions that were drawn from this investigation and recommendations for future work. The conclusions are divided into two main parts: first the synthesis, characterization and properties of the copolymer, and second, the morphology investigation using traditional techniques and the new novel hyphenated techniques.

8.1 Conclusions

8.1.1 Synthesis, characterization and properties of the PDMS-PES copolymers

In this study five different molar masses of PDMS oligomer were successfully synthesized via equilibrium ring-opening polymerization. The PDMS oligomers were used to synthesize six series of semicrystalline multiblock PDMS-PES copolymers via a melt transesterification process under vacuum conditions. All the polymers obtained were characterized using various analytical techniques. The copolymers formation and homopolymer extraction were confirmed by developing a gradient solvent profile for GEC analysis.

Two of the six synthesized PDMS-PES copolymers were of the PDMS-s-PBA copolymer series and four series were of the PDMS-s-PBCH copolymers. The two PDMS-s-PBA copolymer series were synthesized using a one-prepolymer reaction method, in which the PDMS oligomers with constant chain length, and in varying PDMS concentrations, were reacted with BD and AA. In the first series the first stage of the polycondensation reactions was carried out in bulk, and in the second series in toluene. The results showed that the second synthesis method is a much more efficient method, in which higher molar mass copolymers and better PDMS incorporations are obtained.

Two series of PDMS-s-PBCH copolymers were also successfully synthesized via a one-prepolymer reaction method, by reacting the BD and DMCH in bulk either with constant PDMS chain length and varying PDMS concentrations or with different PDMS chain length and constant PDMS concentrations. The one-prepolymer method was also efficiently used to prepare the PDMS-br-PBCH copolymer series, using various quantities of branching agent and constant PDMS concentration and PDMS molar mass. One series of PDMS-s-PBCH copolymers was also synthesized using the two-prepolymer method. The reaction was carried out between PDMS with ester end groups and PBCH with hydroxyl end group. The segment length of PDMS and PBCH were kept constant and the relative composition was varied.

The results showed that the percentages of unreacted PDMS increased with an increase in the PDMS feed content and the PDMS molar mass in all the copolymers series. The PDMS-s-

PBA series had a higher quantity of unreacted PDMS than the PDMS-s-PBCH series; however all the copolymers showed good PDMS incorporation when a higher PDMS feed ratio was used. The increase in the quantity of unreacted PDMS with an increase the PDMS segment length is attributed to there being fewer functional groups available on the PDMS chain to react, as the molar mass of the PDMS increases for a constant weight present. On the other hand, the content of the branching agent in the branched copolymers has no clear effect on the unreacted PDMS percentages. The increase in the degree of branching as the branching agent content increases in the feed was confirmed by SEC-MALLS. The latter was used to determine the branching index. The chromatography techniques also showed a relatively random distribution of the PDMS segment over the entire molar mass distribution of the copolymers in most of the copolymers. DSC and WAXD results showed a significant reduction in crystallinity of the copolymers in all the copolymer series as the PDMS content, PDMS chain length and branching agent content increased. Due to the higher chain mobility of the PBA segment compared with the PBCH segment, the effect of the changes in the PDMS content on the crystallinity degree was greater in the PDMS-s-PBCH copolymers series than in the PDMS-s-PBA copolymers series. This was also attributed to the large difference in the polarity between the PDMS segment and the PBA segment, when compared with the PBCH segment, which may lead to a degree of mixing in the PDMS-s-PBCH copolymers series.

Variations in polyester type, PDMS content, segment length and degree of branching resulted in marked changes in the surface and bulk morphology, as well as the relative compositions of each component at the surface, as revealed from adhesive force measurements. The adhesive force results were correlated to the PDMS content in the bulk as well as to the PDMS segment length and branching degree. The surface of the PDMS-s-PES copolymers showed a very low surface energy compared to the PES homopolymers. The relationship between the segmented copolymers, composition and surface roughness generally increases with an increase in the PDMS content and the PDMS segment length, as well as the branching degree. In all cases a non-linear relationships were obtained.

8.1.2 Morphology of PDMS-PES copolymers

Microscopic, spectroscopic and thermal analytical techniques (AFM, TEM, DMA, DSC, WAXD and PALS) were used to investigate and identify the morphology of the PDMS-PES copolymers. The remarkable changes observed in the properties of PDMS-PES copolymers

such as T_g, T_m, surface energy, surface roughness and free volume were attributed to the variations in the copolymer morphology in terms of both microphase separation and crystallization. Changes in the copolymer morphology were investigated in terms of four factors: (1) the PES type (copolymer components), (2) the copolymer composition, (3) the length of one segment of the copolymers (PDMS segment length) and (4) the architecture of the copolymers (branching agent). The effect of the synthesis method of the copolymers on the morphology of selected samples was also investigated. The following conclusions can be made:

1) All the copolymers showed microphase separation as a result of the incompatibility between the PDMS segment and the polyester segment. Three types of surfaces and bulk morphologies were observed: spherical micro-domains of PDMS in a matrix of polyester, bicontinuous double diamond type morphology, and spherical micro-domains of polyester in a matrix of PDMS as the PDMS content increases. The findings showed that the diameters of the PDMS domains increased in proportion to the PDMS segment content and length in the segmented copolymers and to the degree of branching in the branched copolymers.

2) Spherulite crystal morphology was observed on the surface for both PBA and PBCH homopolymers and for PDMS-s-PBA and PDMS-s-PBCH copolymers with a 5 wt % PDMS content and 2000 g/mol PDMS segment length. It was also observed for a 10 wt % PDMS content and 2000 g/mol PDMS segment length for PDMS-s-PBA copolymers. PDMS-s-PBCH copolymers with 10 wt % PDMS did show spherulite crystal morphology but only when the PDMS segment length becomes 1000 g/mol.

3) PDMS domains were observed around the boundaries of the spherulites and between the lamellae crystal structures on the surface of the copolymers that showed spherulite crystal morphology. A heterogeneous distribution of the PDMS domains was also observed for these copolymers in the bulk morphology as a result of this segregation between the polyester lamellae. However, for several other copolymers with high PDMS content or PDMS segment length, the PDMS domains can be seen between the lamellae order of the polyester segments, in spite the fact that no spherulite was observed on the surface in these PDMS-PES copolymers.

4) The PDMS segment length and the branching degree had an unfavourable effect on the crystallization of the PBCH segment. Thus in the high PDMS content or long PDMS segment

length segmented copolymers and branched copolymers, the crystalline spherulites disappeared, and the morphology became more homogeneous. However, WAXD and DSC results showed relatively low degrees of crystallinity for all the segmented and branched copolymers series. This indicated that the crystallinity might be confined only in small regions. Results obtained when using the new hyphenated techniques for selected samples of PDMS-PBCH copolymers indicated small domains of crystalline regions. The crystalline domains of PBCH were detected in several fractions of the PDMS-s-PBCH copolymers.

5) Investigation of the free volume in PDMS-PBCH copolymers, using the PALS technique, showed that the mean lifetime of o-Ps reflected the size of the free volume hole. The LT spectra of the PDMS-PBCH copolymer series were analyzed using the four-component fit. It was proved that the mean lifetime of o-Ps very sensitive to the changes of the free volume caused by changes in the molecular structure of the PDMS-PBCH copolymers. The PALS results showed that the crystal structure and the phase separation morphology could affect the free volume of the PDMS-PBCH copolymers. From the PDMS content dependent measurements it was found that increasing the PDMS content leads to an increase in both the intensity of Ps and the lifetime of the o-Ps. The findings also showed an increasing trend in the intensity and the lifetime of the o-Ps as the PDMS segment length changed. The branching degree, however, showed an increase in the o-Ps lifetime and decrease in the intensity as the branching degree increases, which is in a very good agreement with the DMA results.

6) A better understanding of the complexity of the morphology of the PDMS-PBCH multiblock copolymers was achieved when hyphenation of two new HPLC-AFM offline coupling techniques was applied. These novel techniques provide a new way to study the morphology as a function of the copolymer molar mass (SEC-AFM) and as a function of the chemical composition (GEC-AFM). The distinctive morphology observed only by using this technique is the three phase morphology. The three phases were attributed to the PDMS and the PBCH amorphous phases and PBCH crystalline phase, which confirmed the DSC and WAXD results.

7) Lastly a two dimensional distribution of the copolymers was created by using another new type of hyphenated technique (HPLC-DPFM-AFM). In this hyphenated technique the collected fractions from the HPLC (either SEC or GEC) were subjected to adhesive force mapping using DPFM-AFM, and distributed based on the adhesive force, to produce the

adhesive force distribution for each fraction. Use of these hyphenated techniques can be extended to other copolymers, particularly copolymers with segments that have quite large differences in the adhesive force values.

8.2 Recommendations for future work

Incorporation of functionalized non-polar PDMS into polyesters (and copolyesters) may make it possible to upgrade all polyester matrices, particularly in terms of hydrolysis, impact, heat, and weather resistance. This can be extended to include relatively polar polyester monomers such as polybutyleneterephthalate (PBT). The PBCH-PDMS-PBCH, in this case, can be used to improve the compatibility between the polar monomers, of the PBT and the non-polar PDMS segments.

The synthesis of random polydimethylsiloxane-co-polyester of PBCH and PBT copolymers (PDMS-PBCH-PBT copolymers) with different PBCH and PBT content and constant PDMS content (10 wt %), via condensation polymerization under vacuum, is presented in Appendix C. The PBCH led to relative miscibility of the PDMS with the aromatic polyester and, due to the hydroxyl termination, covalent incorporation into the polyester backbone was also possible. This area needs further investigation, in terms of the copolymers characterization and the morphology investigation. The novel morphological investigation techniques that were introduced and used in this study could be applied to the PDMS-PBCH-PBT copolymers. Demonstration of the use of the GEC analysis for this copolymer is illustrated in Appendix C.

The use of any polymer in applications depends on the polymer properties, which is obviously controlled by the polymer morphology. The micro-heterogeneous morphological structures of PDMS-copolymers with domain dimensions of several hundred angstroms generate many of the novel and useful mechanical and surface properties. Thus the improvement of the properties for new applications needs to be investigated. One example is included in Appendix D, in which the electrospinning process was applied under different conditions for the PDMS-PBCH and PDMS-PBCH-PBT copolymers. As a result of the low T_g of the PDMS-PBCH copolymers no stable nanofibres was obtained. However, incorporating a PBT segment in the copolymer resulted in significant improvement in the nanofiber formation due to an increase in the T_g because of the high T_g of the PBT segment. This area of research needs to be further investigated in order to obtained good and applicable

nanofibers from these copolymers. These investigations should include consideration of copolymers with different PDMS content and PBT content. A morphology investigation of the output of the electrospinning should also be carried out, using observation techniques other than SEM technique, to investigate the effect of the electrospinning on the copolymer morphology. Preliminary studies of the electrospinning of the PDMS-PES copolymer from solutions have already shown promising results for the production of nanofibers (see Appendix D).

8.3 Posters and publications

- Part of this thesis was presented as a poster at the SACI National Convention, which took place in Stellenbosch, on 30 November – 5 December, 2008. The poster presented under the title of: Synthesis characterization and morphology investigation of PDMS-PBCH copolymer.

- Chapter 4 and small part of Chapter 3 were accepted for a publication and published online on 7 October 2009, as an article in the Journal of Applied Polymer Science, under the title of: Microscopic surface and bulk morphology of semi-crystalline polydimethylsiloxane–polyester copolymers, by ABE Abduallah and PE Mallon, {Journal of Applied Polymer Science, 155(3), 1518-1533 (2010)}.

Appendixes

Appendix A: PDMS oligomer

A-1 Example of a calculation of the target molar mass (M_m) of PDMS oligomers[1]

In order to prepare a 10 g sample of difunctional PDMS oligomer of 1000 g/mol molar mass the following calculation were made:

1. Quantity of the PDMS oligomer (in mole) is 10/1000 = 0.01 mol

2. Quantity of end-capping reagent (in mole) required equals to quantity of the PDMS oligomer = 0.01 mol

3. Quantity of end-capping reagent (in grams): 0.01 x 248.3 = 2.5 g

4. Therefore the quantity of D_4 = quantity of PDMS oligomer – quantity of end capping reagent: D_4 = 10 – 2.5 = 7.5 g

It is well known from the literature[2,3] that the product of the equilibrium ring opening polymerization of D_4 in bulk is a mixture of linear PDMS with, maximum, 15 wt % cyclic molecules. This means the small quantity of D_4 that will be used in the formation of the cyclic molecules will be: 7.5 x 15/100 = 1.125 g.

Therefore, the quantity of D_4 required yielding approximately 10 g of PDMS oligomer of 1000 g/mol molar mass is 7.5 + 1.125 = 8.625 g. Using similar calculations the quantity of the D_4 and the end-capping agent were determined for PDMS oligomers of other molar masses.

A-2 Calculation of PDMS molar mass for ^{1}H-NMR data[1]

The molar masses of the resultant amine-terminated polydimethylsiloxane oligomers were determined for ^{1}H-NMR data after thermal decomposition of the siloxanolate catalyst and removal of the cyclics by distillation. The chemical structure of the PDMS oligomer is shown in Figure A.1, as well as typical ^{1}H-NMR spectra of the five synthesized PDMS oligomers. The molar mass values were calculated using ^{1}H-NMR spectral data as follows:

1. Let the sum of the integration of the chemical shifts due to the four $–CH_2$ protons (δ 2.6 ppm) attached to the chain end = V. Thus integration of the chemical shift for one proton in the chain end X = V / 4

2. The molar mass of the end group is M_m (EG) = 116 g/mol

3. Let the integration of the chemical shifts due to the six $-CH_3$ protons (δ 0.07 ppm) attached to the backbone = W. Thus the area for one proton in each single repeating unit in the backbone is Y = W / 6

4. The molar mass of the repeat unit SiO $(CH_3)_2$ is M_m (RU) = 74.16 g/mol

5. Immediately at the chain end group one atom of oxygen is missing, as is shown in the left side of the PDMS chain in the Figure A.1.

Therefore the molar mass of one oxygen (O) atom must be subtract from the total molar mass M_m (O) =16 g/mol

6. The M_m was determined by substituting the above values in the following equation, [Eq A.1]:

$$M_m = [(Y/X)\, M_m(RU)] + M_m(EG) - M_m(O) \qquad \text{[Eq A.1]}$$

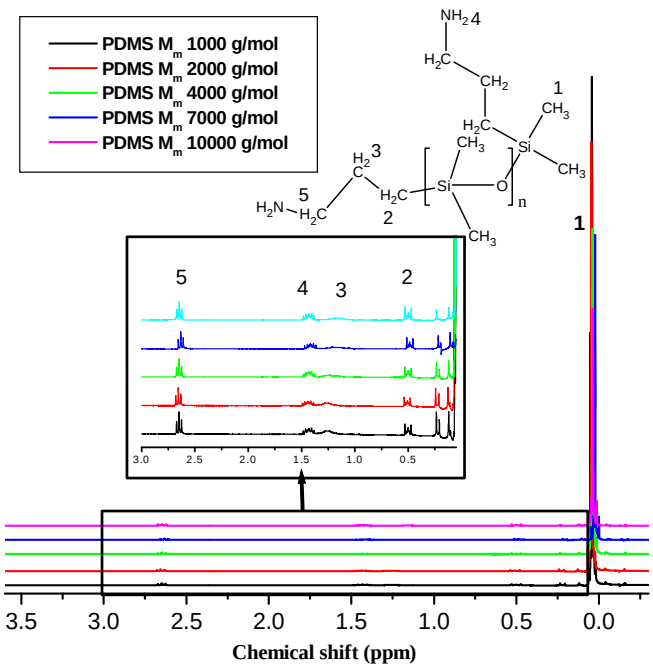

Figure A.1: ^{1}H-NMR spectra of PDMS oligomers of various molar masses.

A.3 PDMS amino end group deactivation reaction[4]

In order to deactivate the NH_2 end group of the PDMS oligomer benzophenone was reacted with the amine group. This reaction was carried out to avoid possible interference of this group with the silica gel that was used as a packing material in the SEC columns, during SEC.

Approximately 5 x 10^{-4} mol (1.00 g) of the PDMS oligomer was placed in a test tube with an excess of benzophenone (1.2 x 10^{-3} mol, 0.22 g). Activated molecular sieve were added to absorb the water evolved from the reaction, which aided in driving the reaction to completion. The test tube was capped with a rubber septum with a needle outlet. The test tube was placed in oil bath at 125 °C, and the reaction continued for 12 h. The crude reactor product was dissolved in hexane and the excess benzophenone was recrystallized, and filtered. ^{1}H-NMR was performed to make sure that the entire NH_2 end group was deactivated. The products were run through a small laboratory chromatography column and the outcome of the column was used in SEC analysis. The size of samples introduced onto the column, and the output and the absorbed PDMS, are illustrated in Table A.1.

Table A.1: The size of samples introduced onto the laboratory chromatography column, and the output and the absorbed PDMS

Sample	PDMS input (mg)	PDMS output (mg)	Absorbed PDMS (mg)
1000	90	81	9
2000	90	83	7
4000	90	80	10
7000	90	82	8
10000	90	81	9

Figure A.2 shows typical examples of ^{1}H-NMR spectra for deactivated end group of the PDMS, (2000 g/mol M_m PDMS oligomer). Spectrum (a) shows the chemical shifts at δ 7.1 – 7.6 ppm, due to the aromatic group in the oligomer chain end. The decrease in the intensity of the chemical shift at δ 2.6 ppm can be used as an indication of the occurrence of the deactivation reaction. However, as indicated by the chemical shift at δ 2.6 ppm, some of the NH_2 end groups were not deactivated. Hence the deactivate reaction was repeated at a higher temperature of 140 °C. This lead to a shift the equilibrium of in the reaction towards the reaction output (product), and seen clear in spectrum (b). In the spectrum (b) the dramatic decrease in the intensity of the chemical shift at δ 2.6 ppm indicates that the reaction has been relatively completed successfully.

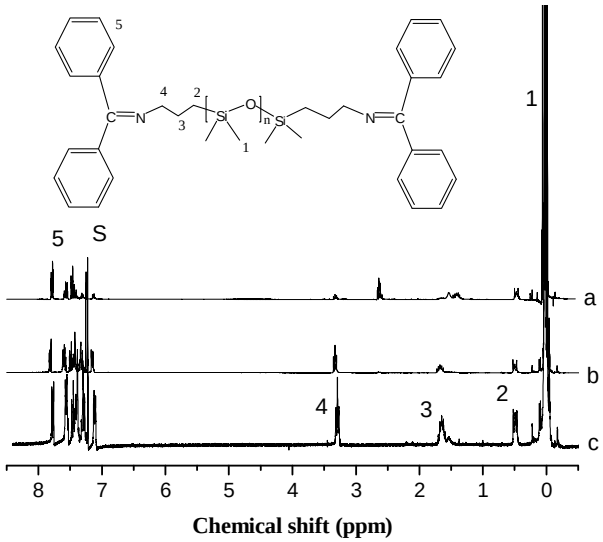

Figure A.2: ^{1}H-NMR spectra of PDMS oligomer (a) after blocking the NH_2 end group (at 125 °C), (b) after repeating the blocking of the NH_2 end group (at 140 °C), and (c) after running the polymer through a chromatography column packed with silica gel.

To ensure that no PDMS with amino end groups was present in the polymer, and avoid the possibility of blocking the SEC column, the polymer was run through a chromatography column to catch any trace of PDMS with amine end group as it shown in the spectrum (c) in Figure A.2. The collected polymer was isolated, and its molar mass determined safely by SEC.

A.4 References

1. David, P. W. Polydimethylsiloxane containing block copolymers: synthesis and characterization of alternating poly(arylene ether phosphine oxide)-b-siloxane and segmented nylon 6,6-b-siloxane copolymers. PhD in Chemistry, State University Virginia, United States, 2001, pp 129-133.
2. Kendrik, T. C.; Parbhoo, B. M.; White, J. W., *Chain Polymerization Part II: Polymerization of Cyclosiloxanes*. First ed.; Pergamon Press, Oxford, 1989; Vol. 4, pp 459-492.
3. Brook, M. A., *Silicon in Organic, Organometallic, and Polymer Chemistry*. First ed.; John Wiley and Sons, United States, 2000; pp 256-274.
4. Bowens, A. D. Synthesis and characterization of poly(siloxane imide) block copolymers and end-functional polyimides for interphase applications. PhD in Chemistry, State University Virginia, United States, 1999, p 97.

Appendix B: PDMS-PBCH copolymers

B.1 Determination of the composition of the copolymer

It was necessary to determine whether if all the PDMS charged to the reactor was actually incorporated into the copolymer or not. Thus both PDMS-PBA and PDMS-PBCH copolymers were purified using a solvent / non solvent method. This was performed in two steps. In the first step chloroform solvent and a mixture of methanol and isopropanol non solvent was used. In the second step THF solvent and hexane non solvent was used. The pure copolymers were then dried under vacuum at 40 °C for at least 20 hours. Samples of dry copolymers were then dissolved in d-chloroform and analysis by ^{1}H-NMR. The copolymers were and Compositions were determined by using the integration of the chemical shifts at δ 0.07 ppm ($I(CH_3)_{PDMS}$) and the integration of the chemical shifts at δ 4.1 ppm ($I(OCH_2)_{HS}$), using equations Eq. B.1 and Eq. B.2.

$$X_{HS} = \{ I(OCH_2)_{HS} /4\} / \{ I(OCH_2)_{HS} /4 + [I(CH_3)_{PDMS} /(6*DP_{PDMS})]\} \qquad \text{[Eq. B.1]}$$

where X_{HS} is the molar fraction of the polyester hard segment. The molar fraction of the PDMS segment is $X_{PDMS} = 1 - X_{HS}$. In Eq. B.1 the molar fraction was obtained based on one mole of PDMS oligomer, with varying degrees of polymerization (DP_{PDMS}): from low M_m to high M_m, as follows 13, 26, 46, 82, and 123 unites. The corresponding mass fractions are given by

$$HS\% = [X_{HS} M_{HS} / (X_{HS} M_{HS} + X_{PDMS} M_{PDMS})] * 100 \qquad \text{[Eq. B.2]}$$

where HS% is the weight percent of the hard (PBA or PBCH) segments, M_{HS} the molar mass of the base unit of the hard segment and M_{SS} the molar mass of the soft PDMS segment.[1] The M_{HS} PBA or PBCH base units are 190 and 212 g/mol, respectively. The M_{PDMS} ranges from 1000 to 10000 g/mol depending on the molar mass of the PDMS in the copolymerization feed. The weight percent of the soft (PDMS) segments (SS%) = 100 – HS%.

B.2 Pilot study of the morphology of the PDMS-PES copolymer

The PDMS-s-PBCH copolymer with 5 wt % PDMS content (unless otherwise stated) was selected to be investigated to determine the best conditions of sample preparation for morphology investigations. Three methods of film preparation were considered, namely casting method, spin coating method and spreading at the air water interface method. Etching

treatment for the surface samples also considered. The morphology was investigated using AFM and also scanning electron microscope (SEM) for only treated samples.

B.2.1 Film preparation using the casting method

Solutions of four different copolymers concentrations were used, 6%, 3%, 0.5% and 0.2%. The topography and phase AFM images of the films of the copolymers 6%, 3% and 0.2% are shown in Figure B.1. Results obtained for the 0.5% copolymers solutions, which showed spherulite crystal structure, were reported and discussed in Section 4.3.2. When more concentrated solutions of 6% and 3% copolymers were used, fibrillar morphology or a nano-ribbon-like structure was formed, as shown in Figure B.1 (a and b) and Figure B.1 (c and d), respectively. The type of morphology of the 3% concentration sample can be distinguished also as lamella morphology, which seems to be similar to the type of morphology that was obtained by Ibarboure et al.[2] for pol-γ-benzyl-$_L$-glutamamte-PDMS-pol-γ-benzyl-$_L$-glutamamte copolymer. In the corresponding height images, in Figure B.1, the individual threads or nano-ribbons are not as easily visible as in the phase images. It is important to notice that the appearance of the semicrystalline spherulite morphology for PDMS-s-PBCH copolymers is critically dependent on the film thickness.

On the other hand, when a dilute solution was used (0.2%), discontinuous deposits were formed, as shown in Figure B.1 (e and f). In order to obtained reliable information about the bulk morphology of the sample using AFM surface analyses it was necessarily to obtained thin copolymer film as much as possible. By trial and error of different concentrations between 3% and 0.2% copolymers, the best thin continues film was obtained from 0.5% copolymer concentration. Therefore 0.5% copolymer concentration was used in the morphology investigations and films as showed in Chapters 4, 5 and 7.

Higher magnification of the copolymer films prepared from the 3% solution shows soft amorphous spots, as seen in Figure B.2. This is most likely related to PDMS segregation. The fact that spherulites and ribbon-like structures as well as small amounts of spherical segregations were observed in these copolymers suggests that liquid-liquid demixing had occurred, where the major part of the phase-separated PDMS segments seems to be present as spheres in-between the crystalline phase of PBCH.

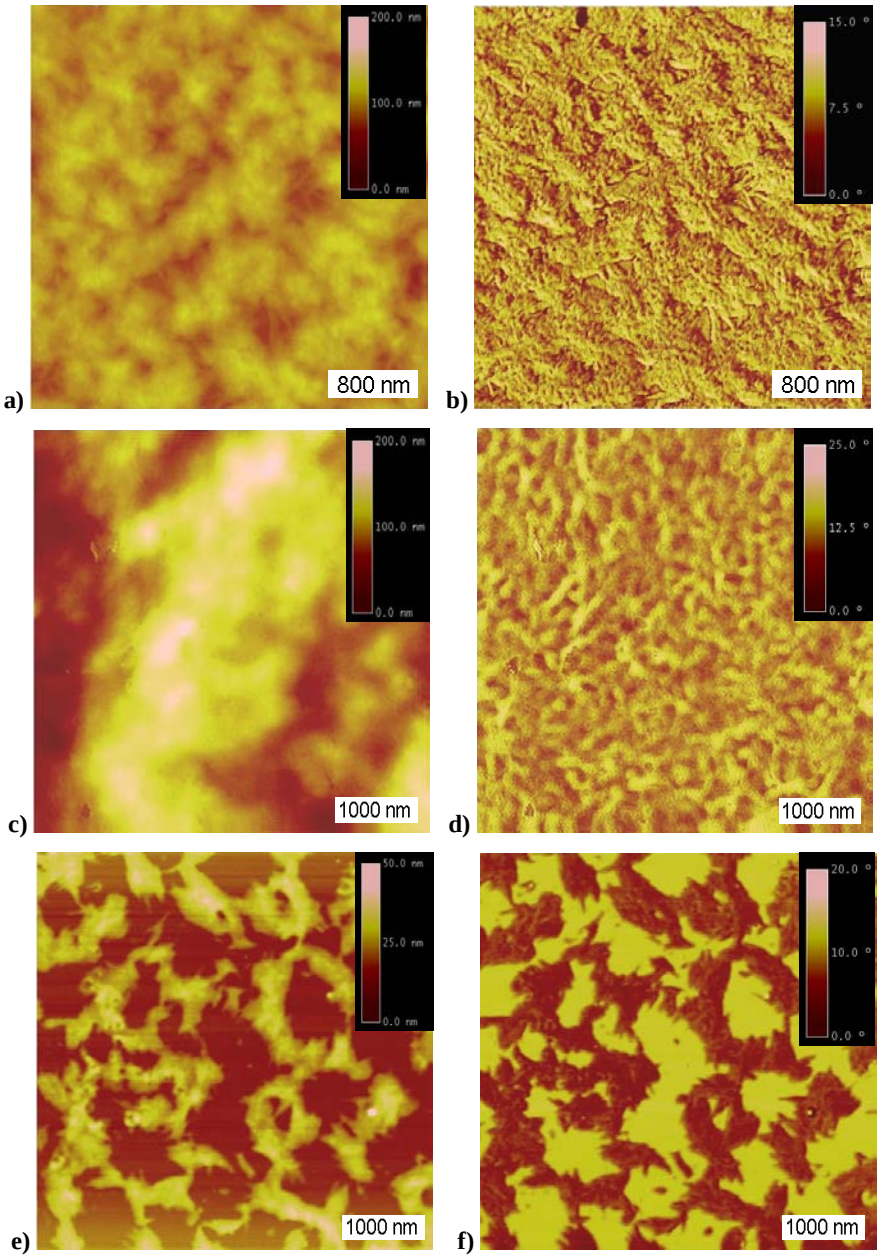

Figure B.1: Topography and phase AFM images of thin films of PDMS-s-PBCH copolymers with 5 wt % PDMS (Mn PDMS 2000 g/mol): copolymer concentrations (a and b) 6%, (c and d) 3% and (e and f) 0.2%.

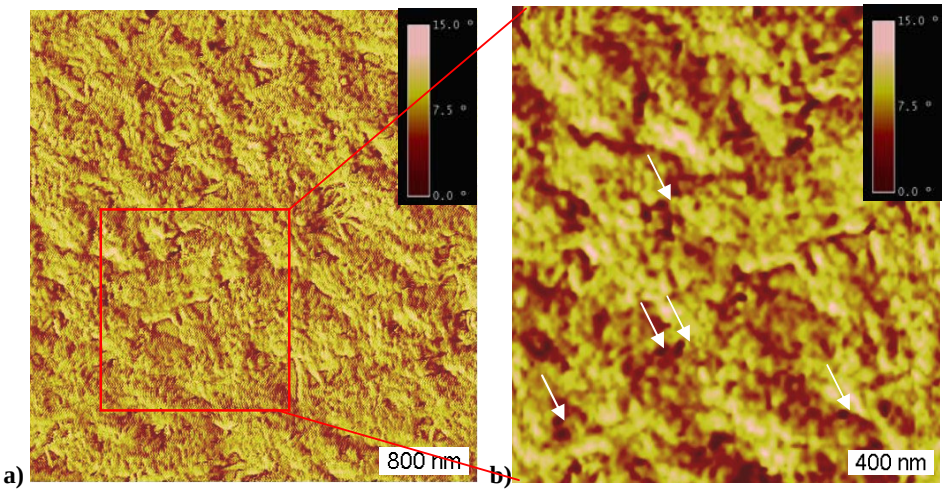

Figure B.2: AFM phase images of thin films of PDMS-s-PBCH copolymers with 5 wt % PDMS content and a copolymer concentration 3%, showing PDMS segregation between the nano-ribbon structures.

B.2.2 Film preparation using the spin coating method

The spin coating method was also applied to form films from a 0.5% solution PDMS-s-PBCH copolymer (5 wt % PDMS content). The surface morphology observed in this case is illustrated in Figure B.3. This copolymer film exhibited a slightly different surface morphology from the films prepared by the casting method. The presence of spherulites was detected, as in the case of the casting method (Chapter 4) but here their size is smaller than in the case of the cast films.

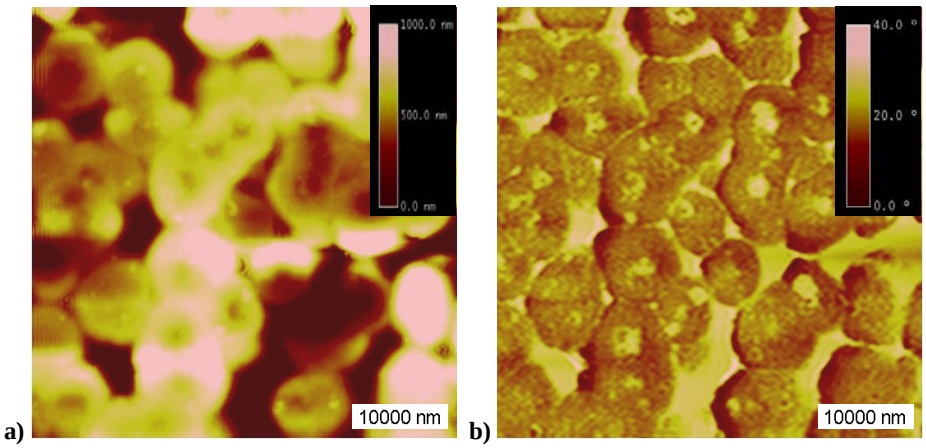

Figure B.3: Topography (a) and phase (b) AFM images of thin films of a PDMS-s-PBCH copolymer with 5 wt % PDMS obtained from spin coating method .

The diameters of the spherulites shown in Figure B.3 are 7–10 μm. This morphology most probably arises from the spin coating method that brings the system into non-equilibrium

conditions, which can significantly slow down the spherulites growth rate, in comparison to the casting method, due to rapid solvent evaporation.

B.2.3 Film preparation using spreading at the air-water interface method

Using this method a sample of 0.5% PDMS-s-PBCH copolymer (5 wt % PDMS) in THF solvent was spread at the air-water interface to form a thin film. Due to the relatively high density of the PBCH segment, two layers formed. The first, which is expected to be very rich in the PDMS segment, was formed on the top of the water at the air-water interface, and the second, which is expected to be rich in polyester segment chains of the copolymers formed at the bottom of the beaker. Both layers were collected on freshly cut mica pieces and their surfaces imaged using AFM. The results of the morphology of both layers are shown in Figure B.4.

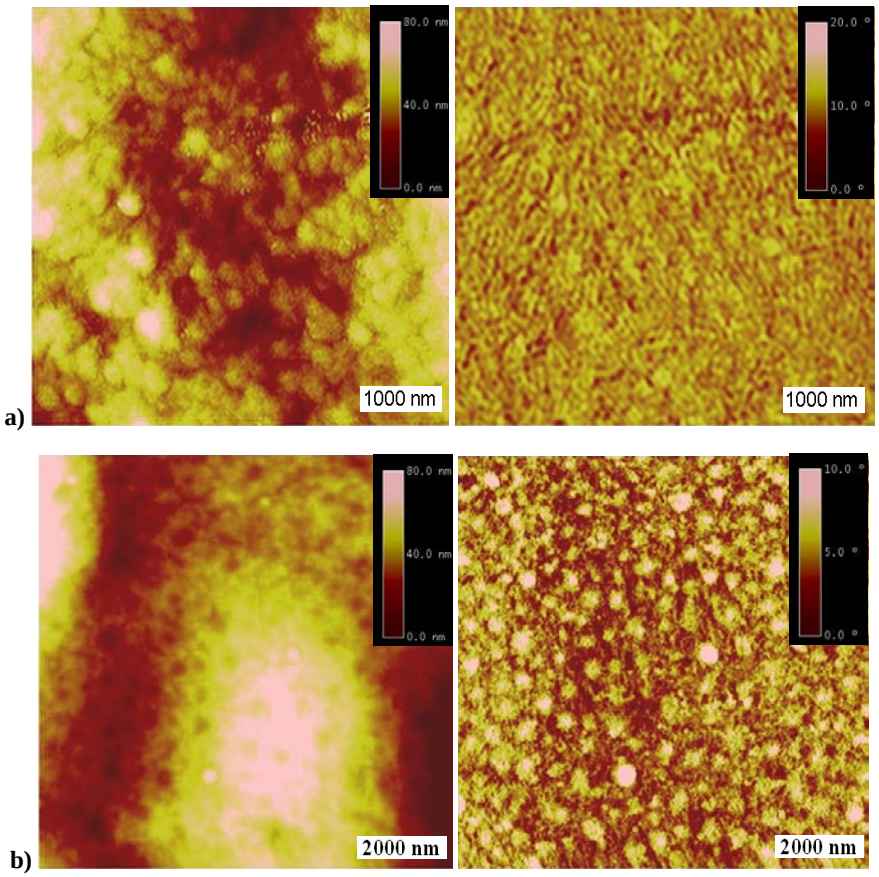

Figure B.4: Typical examples of AFM height and phase images for (a) the top layer and (b) the bottom layer of PDMS-s-PBCH copolymers with 5% PDMS, obtained for films prepared by spreading at the air-water interface method.

The spherical domains of the PDMS are clearly observed in the top layer in the AFM phase images in Figure B.4(a). The bottom layer, which is rich with the PBCH segment, shows bright regions. These regions are attributed to the crystalline domains of the PBCH segments.

B.2.4 Morphology of treated samples

In the case of PDMS-s-PBCH copolymers (at 5 wt % PDMS content) spherulites and PDMS domains between the lamella structures were observed by AFM, without any sample treatment. Although DSC results for higher PDMS content copolymers (C-2 sample, 10 wt % PDMS) showed a quite high crystallinity degree, the AFM results showed neither spherulites nor PDMS domains between the lamellae. Therefore, in order to observe the spherulites and the PDMS domains between the lamellae structure HCl vapour was used to etch away the amorphous regions on the surface of a thin film that was made using 10 wt % PDMS content copolymers. After the etching process the copolymer samples were washed with distilled water and then the surfaces of the copolymers were imaged using AFM. The obtained results for the 10 wt % PDMS content copolymers are shown in Figure B.5 and Figure B.6 after etching for 10 and 24 h, respectively.

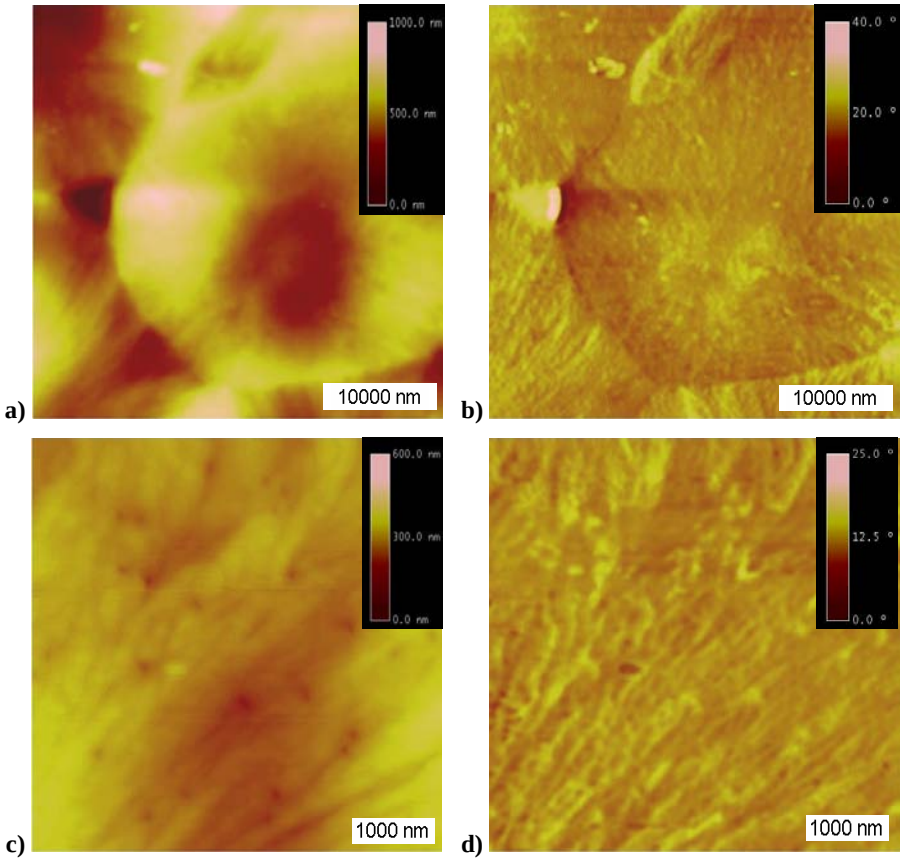

Figure B.5: AFM height (a, c) and phase (b, d) images for etched PDMS-PBCH copolymers with 10% PDMS content, after 10 h etching.

In both cases the height images (Figure B.5 (c) Figure B.6 (a and c)) show the effect of the etching as holes, which can be seen as dark spots in the AFM height images. The lamellae are clearly shown in Figure B.6 in the phase images b and d. As a result of the high surface roughness of the etched copolymer it was very difficult to investigate the rest of the copolymers series using the AFM technique.

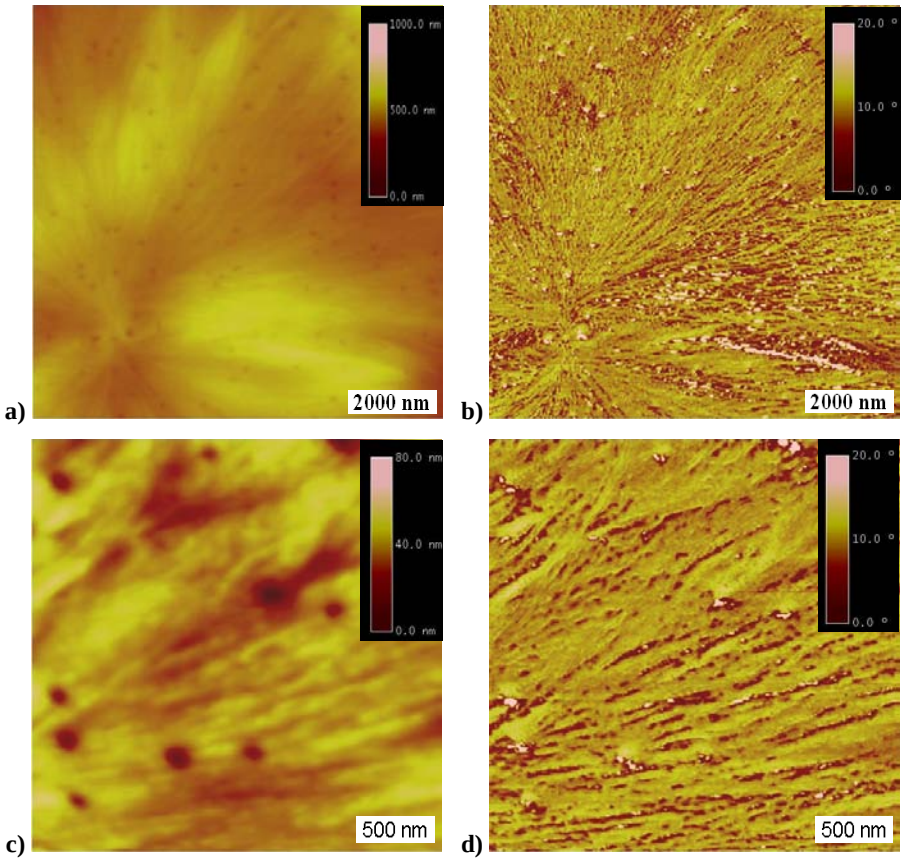

Figure B.6: AFM height (a, c) and phase (b, d) images of etched PDMS-PBCH copolymers with 10% PDMS content, after 24 h etching.

Thus the surface morphology of ten thin etched films of the PDMS-PBA and PDMS-PBCH copolymers were also examined by scanning electron microscopy (SEM), using a Leo® 1430VP Scanning Electron Microscope (Stellenbosch University). Prior to imaging, the samples were sputter-coated with a thin gold layer. The thin films were prepared by casting a 1 wt % solution of PDMS-s-PES in chloroform, using freshly prepared mica plates as substrate. The deposited films were dried under ambient conditions for 24 h before exposing the films to HCl vapour for 24 h to etch the amorphous region away.

Figure B.7 shows SEM images of (a) PDMS-s-PBA and (b) PDMS-s-PBCH copolymers (at 5 wt % PDMS content). The same type of morphology observed for these copolymers in

Section 4.3.2 without surface treatment was observed here after the HCl treatment. However, there were two disadvantages in the SEM images. The internal structure of the spherulites was clearer in the AFM images than in SEM images, and the effect of the etching on degradation of the sample can be also seen (Figure B.7 (b)).

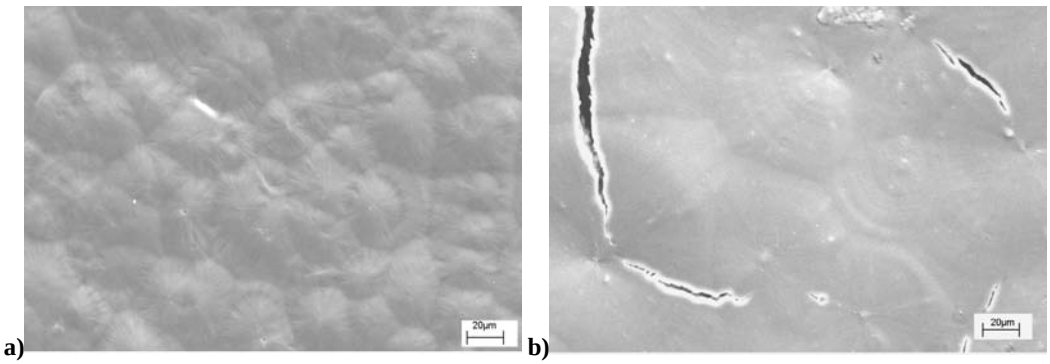

Figure B.7: SEM images of thin films of (a) PDMS-s-PBA and (b) PDMS-s-PBCH copolymers with 5% PDMS (Mn PDMS segment 2000 g/mol).

In the case of 10% PDMS-s-PBCH copolymers, after etching the amorphous region away and then using SEM analysis, the spherulitic crystal structure was observed for both B-2 and C-2, as shown in Figure B.8.

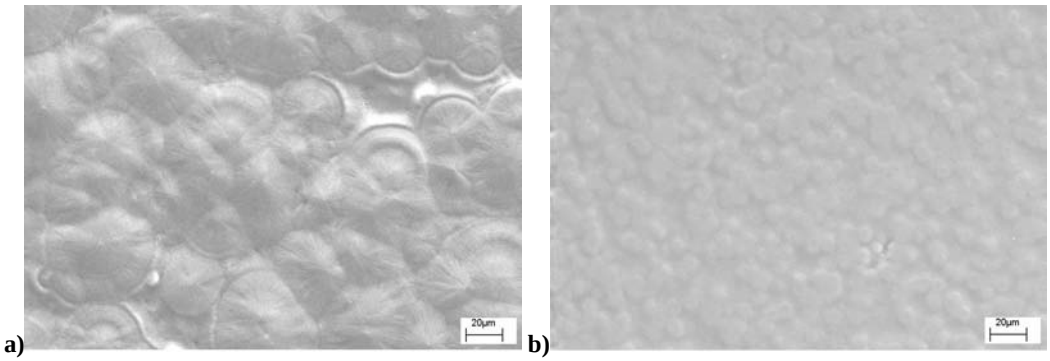

Figure B.8: SEM images of thin films of (a) PDMS-s-PBA and (b) PDMS-s-PBCH copolymers with 10% PDMS (Mn PDMS segment 2000 g/mol).

Figure B.9 shows SEM images of etched samples of the PDMS-s-PBA and PDMS-s-PBCH copolymers with various PDMS content. Samples B-3 and C-3 (25% PDMS) shows small spherulites, as can be seen in Figures B.9 (a) and B.9 (b), respectively.

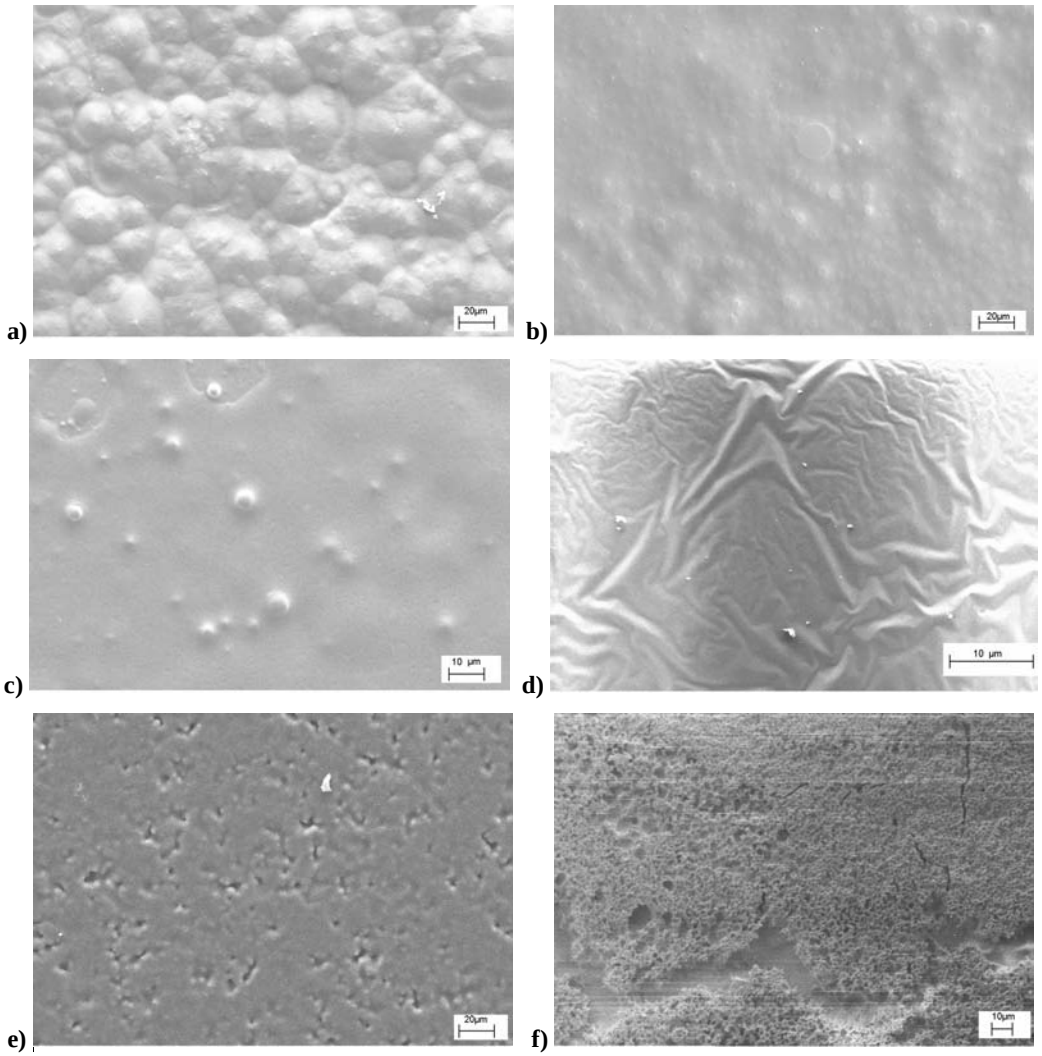

Figure B.9: SEM images of thin films of PDMS-s-PBA and PDMS-s-PBCH copolymers with 25% (a and b), 40% (c and d) and 60% (e and f) PDMS, respectively.

However, the spherulites for sample B-3 copolymers are more clearly seen than for sample C-3. After comparing the size of the spherulites in the SEM images one can conclude that as the PDMS content increase so the size of the spherulites become smaller, which obviously leads to a decrease in the T_m of the copolymers (as was discussed in Section 4.3.1). In the case of higher PDMS content copolymers (Figure B.9 (c, d, e and f)), no spherulites can be seen, even after HCl sample treatment.

B.3 References

1. Vuckovic, M. V.; Antic V. V.; Dojcinovic B. P.; Govedarica M. N.; Djonlagic J. *Polymer International* 2006, 55(11), 1304-1314.

2. Ibarboure, E.; Papon, E.; Rodríguez-Hernández J. *Polymer*, 2007, 48(13), 3717-3725.

Appendix C: PDMS-polybutylene 1,4-cyclohexane dicarboxylate-co-terephthalate (PDMS-PBCH-PBT) copolymers

C.1 Synthesis of PDMS-PBCH-PBT copolymers

A series of segmented PDMS-PBCH-PBT copolymers (series G) was prepared using a polyesterification method, in a three-step polymerization reaction. In the first step the amino end groups were converted to ester groups by reacting PDMS oligomers with excess DMCH. In the second step BD and DMCH were added in a similar way and ratio to those used in the PDMS-PBCH synthesis described previously in Section 3.2.3.2. The reaction was carried out in a similar manner to the synthesis of the PDMS-PBCH copolymers (Section 3.2.3.2). The reaction was allowed to proceed with slow nitrogen flow at 160 °C for three hours. The third step commenced when the DMT was added in the required percentage, based on the amount of the DMCH. The reaction was allowed to proceed further with a slow nitrogen flow at 180 °C for another two to three hours. At the end of the copolymerization an aliquot of titanium catalyst was added before taking the reaction to a reduced pressure in order to reach high conversions. The final temperature reached was 240 °C under high vacuum. The copolymerization reaction is illustrated in Scheme C.1.

In order to investigate the effect of the PBT content on the copolymer's properties, four segmented copolymers of polydimethylsiloxane-copolyester were synthesized utilizing PDMS oligomers with similar molar masses (1000 g/mol). The PDMS content in the polymerization feed was kept constant at 10 wt %.

The reaction was carried out in a reactor to which a distillation arm was connected. Methanol that evolved during the reaction and the excess butanediol at the end of the reaction were removed via the distillation arm.

Although it is reported in literature that PDMS-PBT multiblock copolymers with up to 60 wt % of PBT content are completely soluble in chloroform,[1] when polycaprolactone was used as a linkage between the PDMS and PBT segments similar to the PBCH in our copolymer systems, the entire series of our PDMS-PBCH-PBT copolymers was only partially soluble in chloroform. Due to the fact that PBT is not soluble in chloroform, Soxhlet extraction of the soluble copolymer was carried out. The yield of the copolymerization was determined gravimetrically and then by adding 80 wt % of chloroform solvent a white mixture was obtained.

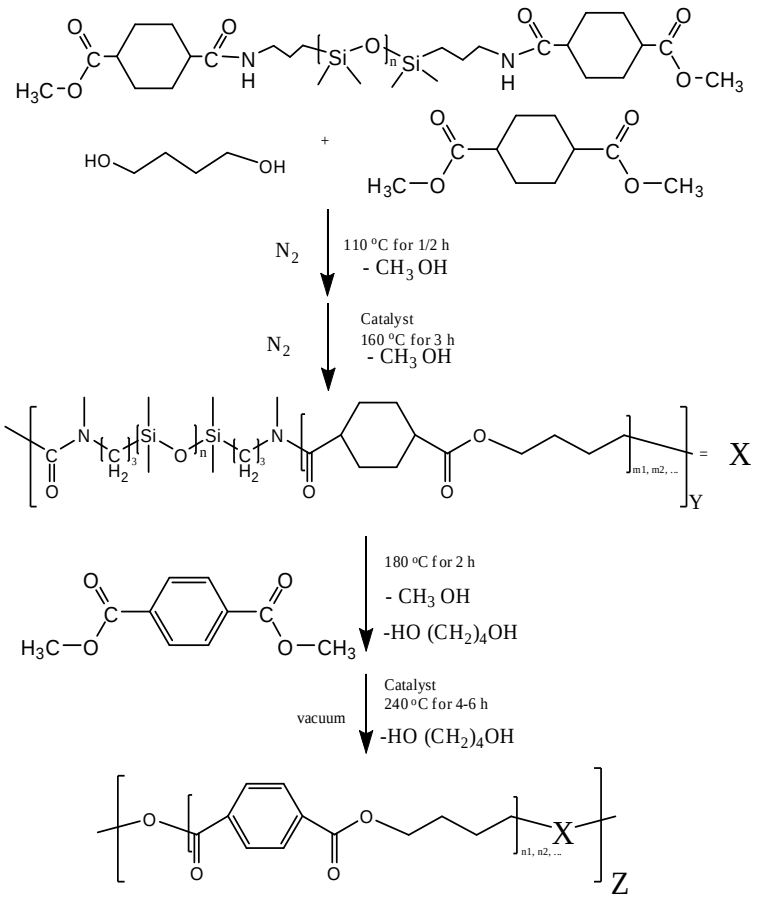

Scheme C.1: Synthesis of segmented PDMS-PBCH-PBT copolymers

The extraction was continued for 24 h. The insoluble fractions were dried under vacuum for 24 h at 40 °C and then the masses of the fractions determined. The soluble fractions were further extracted in order to remove the PDMS and the PBCH homopolymers, as illustrated in Figure C.1.

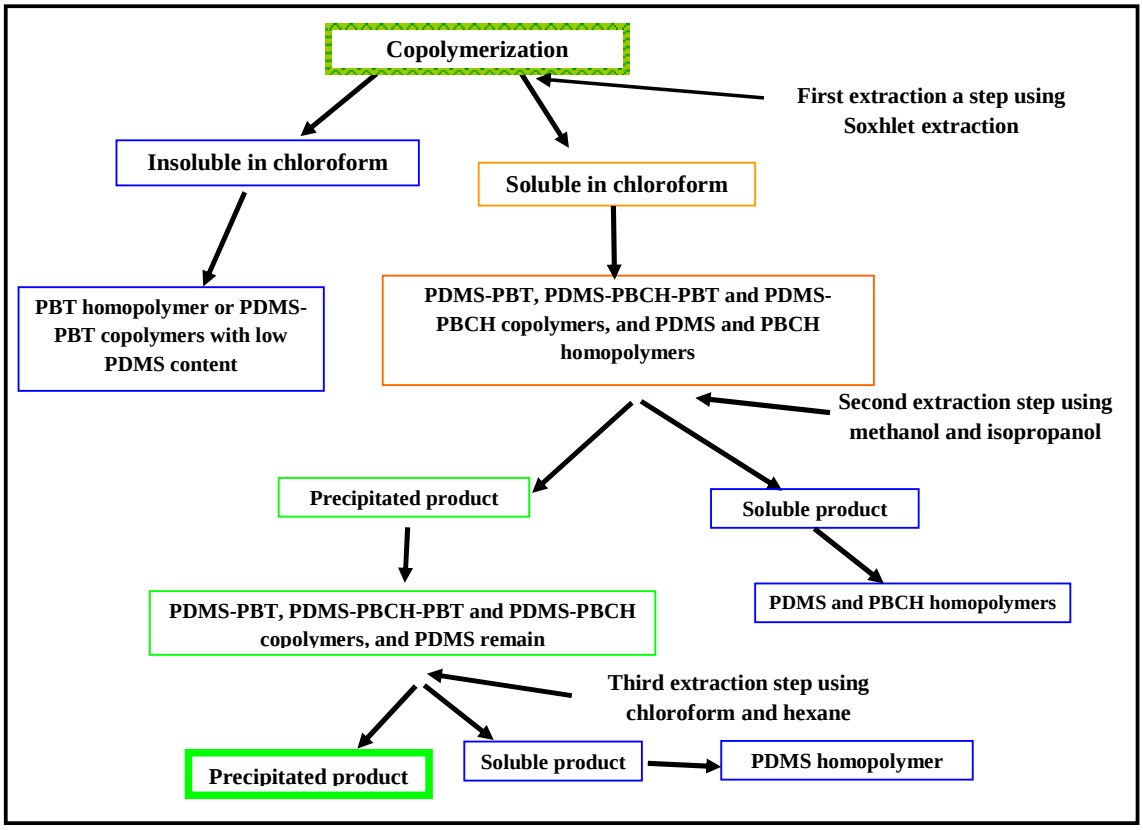

Figure C.1: Schematic illustration of the extraction steps for purification of the PDMS-PBCH-PBT copolymers.

The soluble fractions were investigated by GEC after each extraction step. Figure C.2 shows the gradient profile that was used in the GEC analyses using hexane and chloroform as solvents.

Figure C.3 shows a typical example of the results obtained from GEC for the soluble fraction of the G-4 sample. The PDMS-PBCH-PBT fraction is at about 13.5 min retention time. The other side products (such as PDMS, PBCH homopolymers, PDMS-PBCH and PDMS-PBT and PBCH-PBT) can also be seen at different retention time as shown in the Figure C.3. Even after three extraction steps, the PDMS homopolymer and PDMS-PBT copolymer remained in the PDMS-PBCH-PBT copolymers.

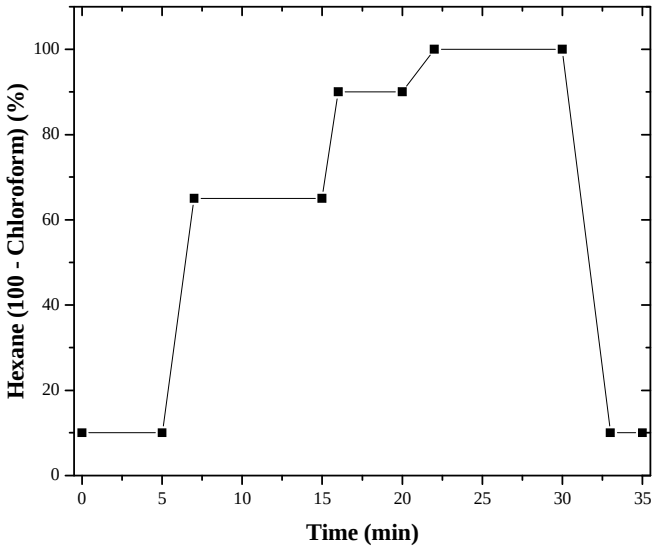

Figure C.2: Gradient elution profile used in HPLC to fractionate PDMS-PBCH-PBT copolymers (stationary phase: Nucleosil C18 5 µm, mobile phase: chloroform/hexane; ELSD detector, flow rate 1 mL/min). ***The gradient was started at 10:90 of (chloroform/hexane, (v/v)), held constant for 5 min, then changed linearly within 2 min to 65:35 (chloroform/hexane, (v/v)), and held constant for 8 min and then changed linearly within 1 min to 90:10(chloroform/hexane, (v/v)), and held constant for 4 min and then changed linearly within 2 min to 100:0 (chloroform /hexane, (v/v)) and held constant for 8 min and then changed linearly within 3 min to 10:90 (chloroform /hexane, (v/v)) and held constant for 3 min.***

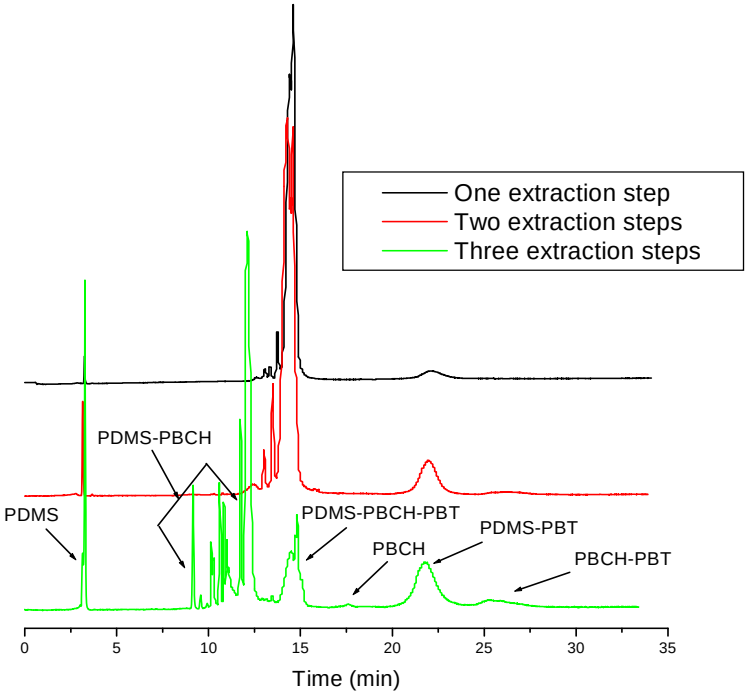

Figure C.3: Typical example of GEC results of the soluble fraction of PDMS-PBCH-PBT copolymers (G-4).

C.2 Structure and composition of the PDMS-PBCH-PBT copolymers

The structure and composition of the PDMS-PBCH-PBT copolymers were determined by ^{1}H-NMR spectroscopy. A typical ^{1}H-NMR spectrum of a PDMS-PBCH-PBT copolymer (sample G-4) is shown in Figure C.4. All the chemical shifts in the spectrum were assigned to the chemical structure of the copolymer according to the Cambridge Soft Chem. Office 2006 using the NMR-prediction software program.

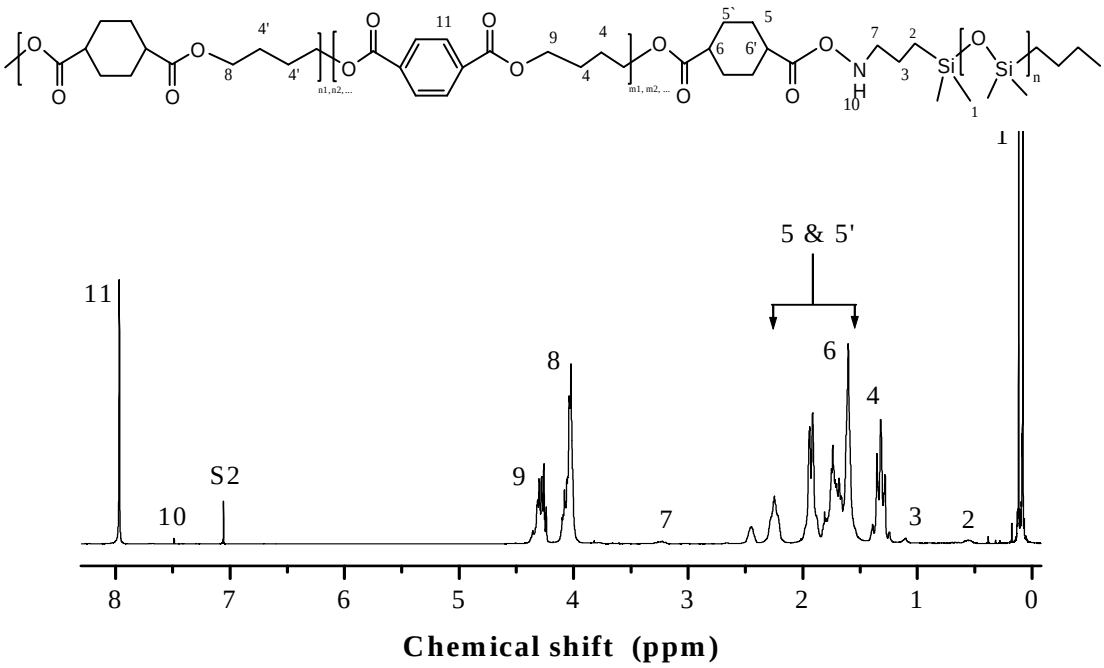

Figure C.4: Typical ^{1}H-NMR spectrum of PDMS-PBCH-PBT copolymers (sample G-2).

The PBCH and PBT molar fractions, with respect to 1 mol of PDMS segment, which has a degree of polymerization of 13 units, were calculated from ^{1}H-NMR spectra using the integration of the chemical shifts at δ = 4.3 ppm ($I(OCH_2)_{PBT}$), δ = 4.1 ppm ($I(OCH_2)_{PBCH}$) and δ = 0.07 ppm ($I(CH_3)$PDMS), and then applying the following equations:

$$X_{PBCH} = \{I(OCH_2)_{PBCH}/4\}/\{[I(OCH_2)_{PBCH} + I(OCH_2)_{PBT}]/4 + I(CH_3)_{PDMS}/(6*13)\} \quad \text{[Eq C.1]}$$

$$X_{PBT} = \{I(OCH_2)_{PBT}/4\}/\{[I(OCH_2)_{PBCH} + I(OCH_2)_{PBT}]/4 + I(CH_3)_{PDMS}/(6*13)\} \quad \text{[Eq C.2]}$$

$$X_{PDMS} = 1 - X_{PBT} - X_{PBCH} \quad \text{[Eq C.3]}$$

where X_{PBCH} is the molar fraction of the PBCH segment, X_{PBT} is the molar fraction of the PBT segment and X_{PDMS} is the molar fraction of the PDMS segment. The molar fractions

here were obtained based on one mole of PDMS oligomer with a molar mass of 1000 g/mol. The corresponding mass percentages are given by

$$\text{PBCH wt \%} = [X_{PBCH} M_{rPBCH} / (X_{PBCH} M_{rPBCH} + X_{PBT} M_{rPBT} + X_{PDMS} M_{PDMS})] * 100 \quad \text{[Eq C.4]}$$

$$\text{PBT wt \%} = [X_{PBT} M_{rPBT} / (X_{PBCH} M_{rPBCH} + X_{PBT} M_{rPBT} + X_{PDMS} M_{PDMS})] * 100 \quad \text{[Eq C.5]}$$

$$\text{PDMS wt \%} = 100 - \text{PBT\%} - \text{PBCH\%} \quad \text{[Eq C.6]}$$

where PBCH wt % is the mass percent of the PBCH segments and M_{rPBCH} is the molar mass of the base unit of the PBCH segment (212 g/mol). The PBT wt % is the mass percent of the PBT and M_{rPBT} is the molar mass of the base unit of the PBCH segment (206 g/mol). The PDMS wt % is the mass percent of the soft PDMS segment and the M_{PDMS} is the molar mass of the PDMS segment (1000 g/mol). Table C.1 shows a summary of the results obtained.

Table C.1: Chemical compositions of PDMS-PBCH-PBT copolymer series

Sample	Polymerization feed			Actual copolymers composition determined from ^{1}H-NMR spectra		
	PDMS wt %	PBT wt %	PBCH wt %	PDMS wt %	PBCH wt %	PBT wt %
G-1	10	10	80	8.9	78.8	12.3
G-2	10	20	70	9.2	68.6	22.2
G-3	10	30	60	9.1	56.4	34.5
G-4	10	40	50	9.3	48.4	42.3

The values of the mass ratios of the PBCH, PBT and PDMS segments determined from the ^{1}H-NMR spectra agree with the values of feed compositions of the reaction mixture in the copolymerization reactions.

The incorporation of the PBT segment into the copolymer chains was proven by Soxhlet extraction using chloroform. It is well known that the PBT homopolymer is insoluble, while the PDMS-PBCH copolymers are soluble in chloroform. The results obtained after the Soxhlet extraction showed that all the samples comprised both a soluble and an insoluble fraction. The chemical compositions of the soluble and insoluble fractions were investigated by ^{1}H-NMR spectroscopy. The spectra of both fractions contained signals of Si–CH_3 protons from the PDMS segments and signals of aromatic rings from the PBT segments, in addition to the PBCH signal at δ 4.1 ppm. The chemical compositions of all fractions were determined

using the equations Eq C.1 – Eq C.6. The results are tabulated in Table C.2. The extracted and insoluble fractions differ in their compositions and contain considerably different amounts of PDMS, PBCH and PBT segments. However, it can be concluded that both the extracted and insoluble fractions have a segmented (multiblock) structure.

Table C.2: ^{1}H-NMR analysis of chloroform soluble and insoluble fractions of the PDMS-PBCH-PBT copolymer series

Sample	Soluble fraction in chloroform			Insoluble fraction in chloroform		
	PDMS wt %	PBCH wt %	PBT wt %	PDMS wt %	PBCH wt %	PBT wt %
G-1	12.3	84.3	3.4	7.2	41.2	51.6
G-2	12.5	74.5	13.0	5.8	32.2	52.2
G-3	13.6	74.0	12.4	4.5	34.1	61.4
G-4	14.3	70.3	15.4	3.4	24.4	72.2

The insoluble fractions of the copolymer contained 51.6 – 72.2 wt % PBT segments while the soluble fractions contained only 3.0 – 15.4 wt %. The soluble fractions of the PDMS-PBCH-PBT copolymer with 15.4 wt % content PBT were used in a preliminary electrospinning investigation, as described in Appendix D.

C.3 Intrinsic viscosity measurements

The intrinsic viscosities of the products of the copolymerization, as well as the soluble (chloroform) and insoluble fractions were determined using Ubbelohde viscometer in solvents ratio of 70 to 30 of trichloroethylene and phenol mixture. The measurement of efflux times is carried out at 25 °C, by visual observation of the passage of the liquid meniscus past two lines marked on the viscometer, at which times a stopwatch is started and stopped. An Ubbelohde viscometer, with a regular size of 10 ml, was calibrated at 25 °C according to the general procedure given in ISO3104, ISO3105, BS188, IP Method 71 and ASTM Method D445. The kinematic viscosity η (mm^2/s) of a liquid may be calculated from a mean measured flow time t (s) using the formula:

$$\eta = Ct \qquad \text{[Eq C.7]}$$

where C is a constant = 0.004855 (mm^2/s)/s. The Ubbelohde viscometer was used for measurement of dilute solution viscosity of PDMS in order to determine the intrinsic viscosity [η] of the PDMS-PBCH-PBT copolymers. The results tabulated in Table C.3.

The Mark and Houwink constants of the PDMS-copolyester copolymers are not reported in literature and thus the molar masses for these new copolymers were not obtained. However, from the viscosity values one can predict which copolymer might have the higher molar mass (G-4), and which the lowest one (G-2).

Table C.3: The intrinsic viscosity [η] of PDMS-PBCH-PBT copolymers (series G)

Sample	Copolymerization product [η]	Soluble fraction [η]	Insoluble fraction [η]
G-1	0.27	0.26	0.29
G-2	0.22	0.22	0.24
G-3	0.25	0.23	0.28
G-4	0.28	0.27	0.32

C.4 References

1. Antic, V. V.; Vuckovic; M. V., Djonlagic; J. *Journal of the Serbian Chemical Society*, 2007, 72 (2), 139-150.

Appendix D: Preliminary study of electrospinning of segmented and branched polydimethylsiloxane-polyester copolymers

In this section the electrospinning of three types of PDMS-polyester copolymers is briefly discussed: PDMS-s-PBCH copolymers, PDMS-br-PBCH copolymers and PDMS-PBCH-PBT copolymers.

D.1 Introduction

Nanofibers can be produced by a number of techniques such as drawing, template synthesis, phase separation, self-assembly and electrospinning.[1] Electrospinning is a rapid, simple, and relatively inexpensive method to fabricate high aspect ratio, submicron diameter size fibres with high surface area. Figure D.1 illustrates the electrospinning apparatus, in its simplest form. The apparatus comprises of a syringe to hold the polymer solution, a syringe pump, two electrodes, a DC voltage supply in the kV range, and a ground collector.

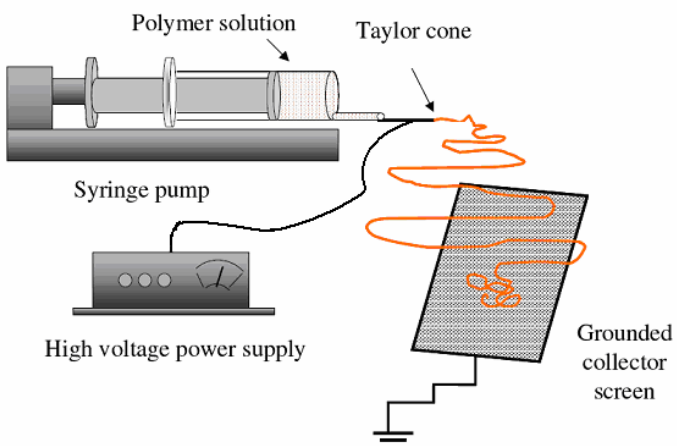

Figure D.1 Schematic representation of the electrospinning process and apparatus used in our laboratory for electrospinning of polydimethylsiloxane-polyester copolymers.

Typically, during electrospinning, the polymer solution is connected to a large electric potential and the polymer solution is delivered to the tip of a small capillary, and an external electric field is applied. The electrical charge that develops at the surface of the polymer solution interacts with the external electric field, resulting in the emission of a steady fluid jet that thins as it accelerates towards the collector. A so-called Taylor cone forms due to the competing forces of the static electric field and the liquid's surface tension. The jet can experience a whipping instability, leading to bending and stretching of the jet, observed as loops of increasing size. The whipping jet then thins substantially, while travelling the short

distance between the electrodes. The presence of polymer in solution leads to the formation of fine solid fibres as the solvent evaporates. The charge on the fibres eventually dissipates into the surrounding environment.[2]

The resulting product is a non-woven fibre mat that is composed of tiny fibres with diameters between 50 nanometres and 10 microns.[3] Potential applications of such nanofibres include filtration and composite materials, catalyst supports, optical and chemical sensors, drug delivery, and electrospun non-woven biodegradable fabrics that can be used as adhesion barriers, for wound dressing and tissue engineering. Several recent reviews have comprehensively summarized significant advances in the electrospinning area.[1, 4]

Forming sub-micron sized fibres from segmented or branched PDMS copolymers with functional groups is imperative for tailoring the functionality and utility of non-woven fibre membranes. Not much research has focused on the influence of copolymer composition and molecular architecture on the electrospinning performance. In this section, attempts at the electrospinning of selected segmented and branched PDMS-PES copolymers with different PDMS content and segment length is discussed. Due to the low surface energy of the PDMS segments the nanofibers obtained are expected to have super-hydrophobic surfaces, which could increase the possible applications of the PDMS-PES copolymers.

D.2 Experimental

Table D.1 shows a summary of the molecular masses and the chemical compositions of the copolymers. The detailed characteristics of the C-2 and F-2 copolymers were discussed in the main part of the thesis, while G-4 was described in Appendix C.

Table D.1: Summary of the characteristics of the PDMS-polyester copolymers investigated

Sample	PDMS M_n (g/mol)	PDM[a] (wt %)	PBCH[a] (wt %)	PBT[a] (wt %)	M_w [b] (g/mol)	g[c]
C-2 (D-2)	2000	9.20	90.8	0.00	27719	-
F-2	1000	9.51	9.51	0.00	33950	0.75
G-4	1000	14.30	70.30	15.40	-	-

[a] Measured by ^{1}H-NMR
[b] Measured by SEC
[c] Measured by SEC-MALLS

These PDMS-polyester copolymer samples were used in a pilot study in order to identify the optimum electrospinning conditions. To the best of my knowledge none of these copolymers have been spun before using electrospinning or any other techniques. The electrospinning of these copolymers samples was carried out using various experimental conditions. Small changes in the electrospun fibres (determined using SEM) were obtained by varying the solution concentration (viscosity), and the voltage or the electric filed. In all cases chloroform was used as a solvent. Tables D.2, D.3 and D.4 tabulate the electrospinning conditions used and discussed, and the respective results obtained.

D.3 Exploring the nano-fibre formations from the PDMS-s-PBCH copolymers

The PDMS-s-PBCH copolymer properties that might affect the fibre formation are the M_n (27,000 g/mol) and the T_g values (10 and 123 °C, for the PBCH and PDMS segments, respectively), as well as the low rate of the crystallization of the PBCH segment. These factors can affect the entanglement as well as the solidification of the polymer when the solvent evaporates, and thus affect the formation and the stability of the nanofibers.

As is illustrated in Table D.2, experiments were carried out in which both the concentration of the copolymer solution and the voltage were changed in nine experiments. The most important fixed electrospinning condition here, in addition to the polymer characteristics, is the distance between the needle and the ground collector (20 cm) and the flow rate (0.08 ml/min) in the chloroform solvent.

Electrospun fibres of the PDMS-s-PBCH copolymer were collected at two different ground collector temperatures: using water as the grounded collector at room temperature (25 °C), and using water and ice as the grounded collector (at 0 °C).

Table D.2: Electrospinning parameters used in a pilot study of PDMS-s-PBCH copolymers and a summary of the results according to SEM

Experiment no.	Electric field (kV)	Copolymer concentration (wt %)	Results obtained when using water at 25 °C	Results obtained when using ice/water at 0 °C
1	15	10	Film with some droplet spread	Film with some droplets spread on the film and evidence of collapsed fibres
2	15	20	Film with some droplets spread on the film	Many droplets or beads, with no clear evidence of fibre formation
3	15	30	Many droplets, with no fibre formation	Many droplets, with evidence of collapsed fibres
4	20	10	Rough film with a spread of small and big droplets or beads	Film with small spread of droplets, with evidence of collapsed fibres
5	20	20	Film with many of beads and droplets	Film with many of beads and droplets
6	20	30	Clear evidence of nanofiber formation	Clear evidence of nanofiber formation
7	25	10	A few droplets, with evidence of collapsed fibres	A few droplets, with evidence of collapsed fibres
8	25	20	A few droplets, with evidence of collapsed fibres	A few droplets, with evidence of collapsed fibres
9	25	30	Clear evidence of nanofiber formation	Clear evidence of nanofiber formation with small diameter of nanofiber

Figure D.2 shows the SEM images of the fibres obtained when using the first grounded collector. The effect of changing the voltage from 15 to 20 to 25 kV, for the three different copolymer concentrations of 10, 20 and 30 wt %, can be seen very clearly.

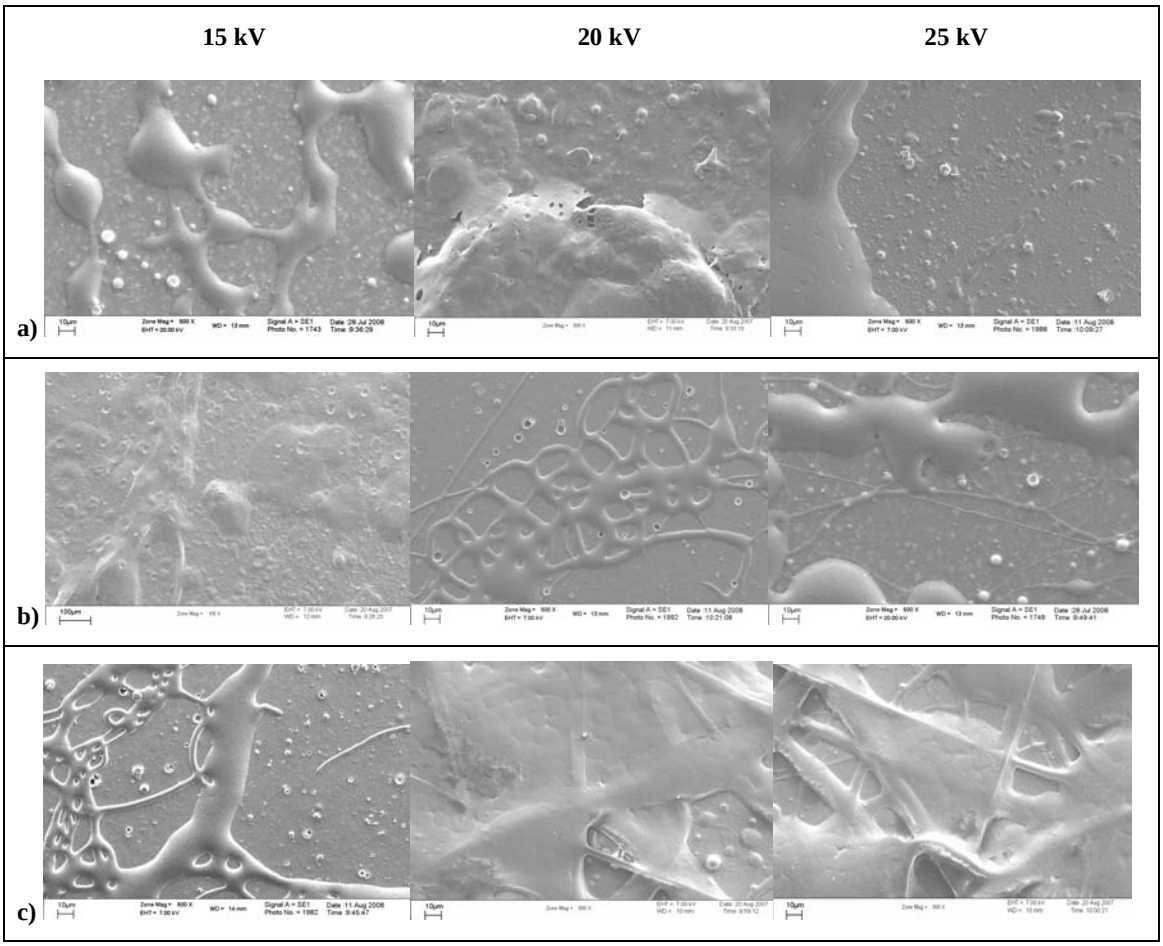

Figure D.2: SEM images of electrospun fibres of PDMS-PBCH copolymers, at a concentration of (a) 10 wt %, (b) 20 wt % and (c) 30 wt %, at various voltages, and using water as a ground collector.

For all the voltages used, and a copolymer concentration if 10 wt %, no clear evidence of fibre formation can be seen. However, when the copolymer concentration was increased to 30 wt % and 20 and 25 kV were used, clear evidence of fibre formation can be seen in Figure D.2. The chloroform was expected to diffuse too rapidly into the water (if any still remains when fibres hit the surface of ground collectors. The stability of these fibres is not good, and they collapse at room temperature. This can also be seen for a 20 wt % concentration at 20 and 25 kV. Thus collapse is most probably due the T_g values of the copolymers being below room temperature. The slow crystallization rate of the PBCH segment in these copolymers can also cause difficulties in obtaining stable nanofibers. The nanofibers formed, therefore, collapse as soon as they hit the grounded collector, and formed smooth or rough films, depending on the solution concentration and the voltage.

The second attempt to obtained nanofibers was carried out by decreasing the temperature of the ground collector. This was done by using water and ice as ground collector at –5 to 5 °C. Figure D.3 shows the SEM images of nanofibers obtained when the copolymers were spun and by using water and ice as ground collector.

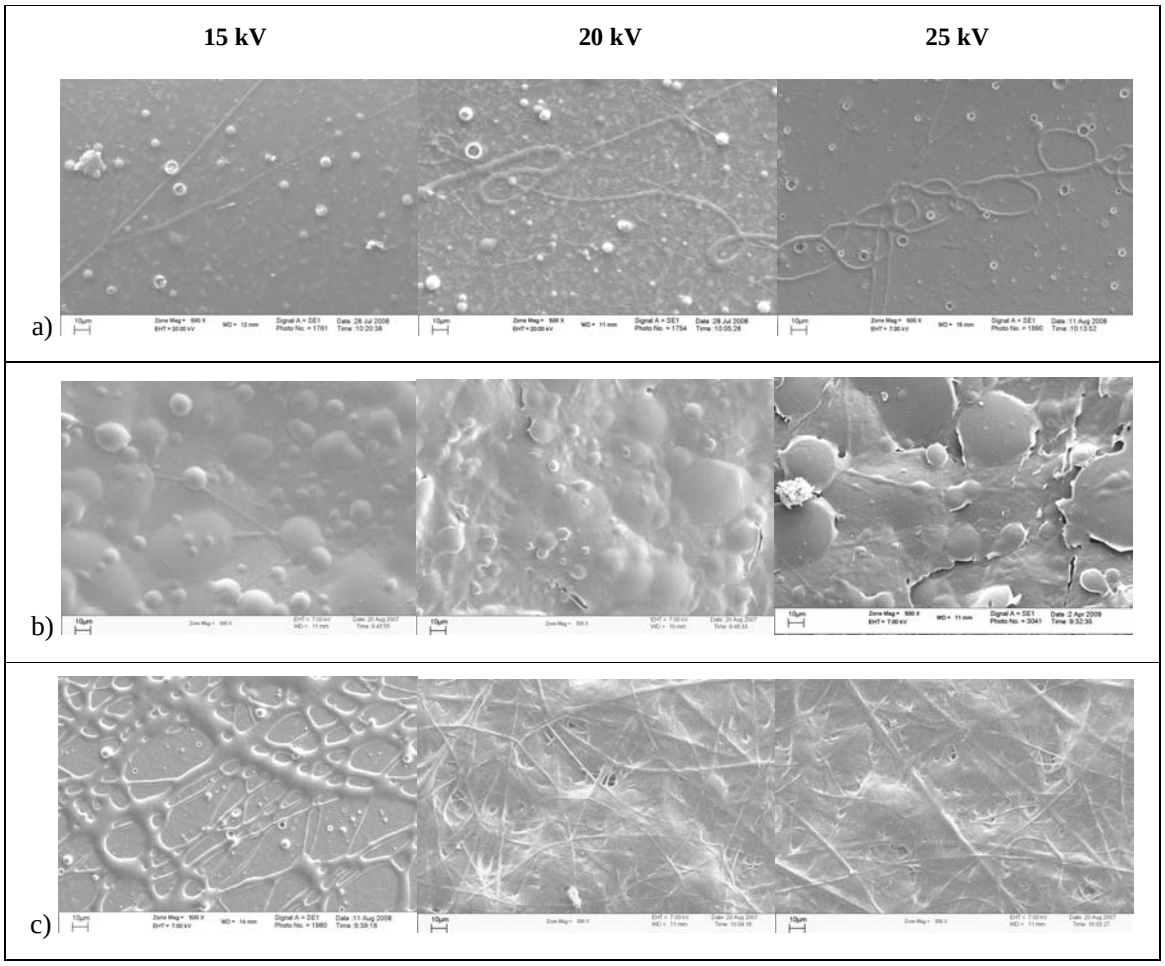

Figure D.3: SEM images of electrospun fibres of PDMS-PBCH copolymers, at a concentration of (a) 10 wt %, (b) 20 wt % and (c) 30 wt %, at various voltages, and using water/ice as a ground collector.

Although there were not great improvements using water and ice as the ground collector, it is clear that the size of the unstable nanofibers obtained at 30 wt % concentration and at 20 kV and 25 kV from the ice and water ground collector was smaller than that obtained when only water is used as the ground collector.

The third attempt carried out to obtain nanofibers involved increasing the number of entanglements in the copolymer by introducing branches in the copolymer structures. These results are discussed in the following section.

D.3 Exploring the nano-fibre formations from the PDMS-br-PBCH copolymers

The branching effect in the PDMS-br-PBCH is another factor that can affect nanofiber formation from the electrospinning process. The branches can, in fact, affect both the T_g of the copolymer and the entanglement of the copolymer chains. Table D.3 shows the electrospinning conditions used to spin the PDMS-br-PBCH samples and a summary of the results obtained for this copolymer.

Table D.3: Electrospinning parameters used in a pilot study of PDMS-br-PBCH copolymers and a summary of the results according to SEM

Experiment no.	Electric field (kV)	Copolymer concentration (wt %)	Results obtained (according to SEM images, see Figure D.4)
1	15	10	Clear film with some droplets and no nanofiber formation
2	15	20	Film with some droplets spread on the film
3	15	30	Many droplets or beads with no real fibre formation
4	20	10	As for experiment no. 1
5	20	20	Film with many beads or droplets
6	20	30	Some nanofibers can be seen in between the beads
7	25	10	Film with many small droplets spread on the film
8	25	20	Many beads with a few nanofibers
9	25	30	As for experiment no. 6

Although in several SEM images in Figure D.4 there is evidence of fibre formation, it is clear that no significant improvement was obtained in the stability of the formed fibres. Further, it can be seen that for the 30 wt % concentration at 20 and 25 kV, fewer nanofibers were formed than formed under similar conditions in the PDMS-PBCH segmented copolymers. This might be due to the decrease in the crystallinity degree as well as the ability of the copolymer to stretch, due to the relatively high concentration of such branches in the copolymer chains. This is in addition to the low T_g, which allow the formed nanofibers to collapses. Therefore, the ability of the PDMS-PBCH segmented copolymer to crystallize from solution can, in fact, lead to better fibre formation. Furthermore, the ability to crystallize cannot lead to stable nanofibers unless the crystallize rate is relatively fast, but not too fast. A

too rapid crystallization may cause the polymer to solidify before stretching, and forming fibres.

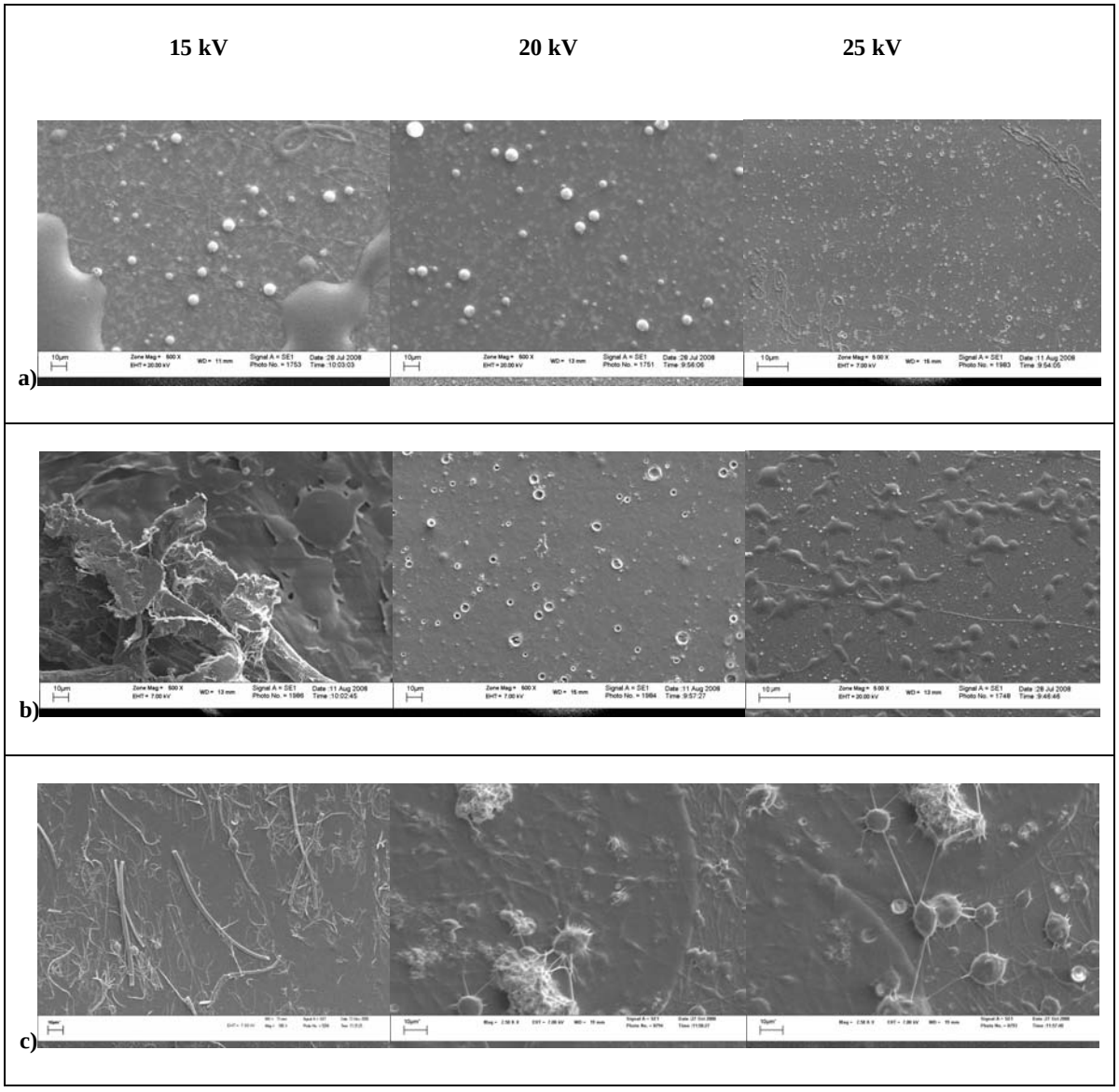

Figure D.4: SEM images of electrospun fibres of PDMS-br-PBCH copolymers, at a concentration of (a) 10 wt %, (b) 20 wt % and (c) 30 wt %, at various voltages and by using water as a ground collector.

The main reason why nanofibers of these copolymers collapse after formation is the low T_g. In order to overcome the above mentioned obstacles, another attempt was made by changing the copolymer structure. In order to increase both the T_g of the copolymer and the rate of the crystallization, PBT segments were incorporated into the copolymers chains. The synthesis method of PDMS-PBCH-PBT copolymer was described in Appendix C.

D.4 Exploring the nano-fibre formations from the PDMS-PBT-PBCH copolymers

One sample of the PDMS-PBCH-PBT copolymer (the fraction of sample G-4 soluble in chloroform) was used in this pilot study in order to investigate the possibility of obtaining nanofibers. The electrospinning process used here was similar to that used for PDMS-PBCH copolymers in order to determine the effects of solution concentration (viscosity) and voltage or electric field on nanofiber formation as well as on the morphological features. Many experiments were carried out but no noticeable improvement was really achieved. Table D.4 shows selected electrospinning conditions that were used to spin the samples and a summary of the obtained results.

Table D.4: Electrospinning parameters used in a pilot study of PDMS-PBCH-PBT copolymers and a summary of the results according to SEM

Experiment no.	Electric field	Copolymer concentration	Results obtained (according to SEM images, see Figure D.5)
1	15	10	Clear film and no sign of nanofiber formation
2	15	20	Film with some droplets spread on the film
3	15	30	Many droplets or beads, with no real fibre formation
4	20	10	Film with some droplets spread on the film
5	20	20	Film with many beads or droplets
6	20	30	Some nanofibers can be seen in between the beads
7	25	10	Film with many droplets spread on the film
8	25	20	Many beads with a few nanofibers
9	25	30	As for experiment no. 8

In Figure D.5 all the SEM images show clear evidence of nanofiber formation with many beads. The size of these beads seems to be unaffected by using various experimental conditions. The copolymer droplets and beads that are observed to form from the electrospinning of solutions of dilute concentration (10 wt %) is due to insufficient chain entanglement. As the concentration increases to (20 or 30 wt %), droplets and beaded fibres are observed, as well as uniform fibres between the beads at 20 kV. Use of the low electric field strength (voltage) (15 kV) for the highly concentrated solution (30 wt %) does however,

results in droplets and beaded fibres of PDMS-PBCH-PBT copolymers; the nanofibers are hardly evident. The GEC result showed in Figure C.3 also indicate the possibility of the remains of some PBCH homopolymer and PDMS-PBT copolymers. This indicates that the beads might be a mixture of these polymers and the PDMS-PBCH-PBT copolymers.

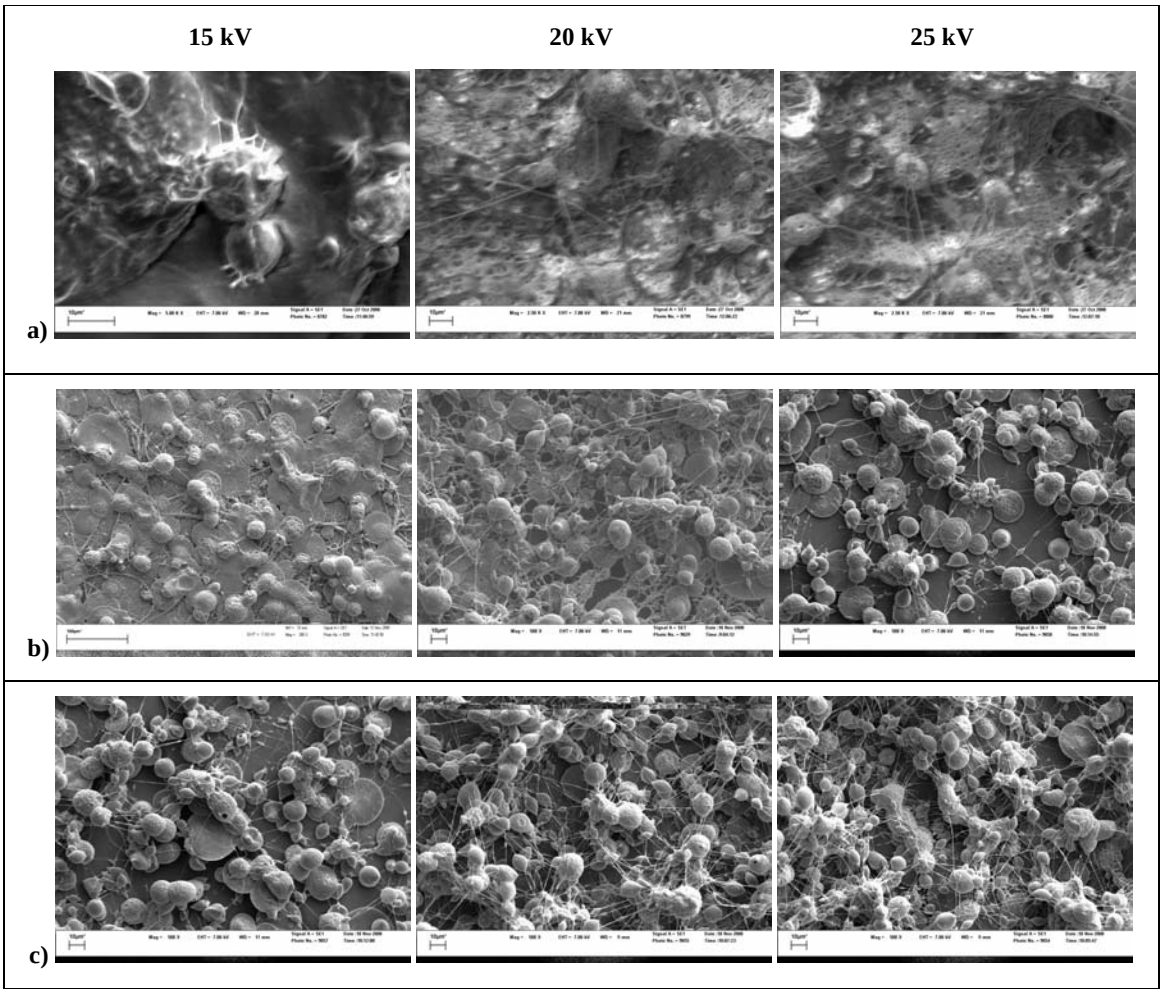

Figure D.5: SEM images of electrospun fibres of PDMS-PBCH-PBT copolymers, at a concentration of (a) 10 wt %, (b) 20 wt % and (c) 30 wt %, at various voltages, and using water as a ground collector.

D.5 Conclusion

Although no completely uniform fibres have yet been observed for any of the investigated PDMS-polyester copolymers, the results of this study are promising in terms of producing nanofibers using electrospinning PDMS-polyester copolymers from solutions. These copolymers are expected to form nanofibers with a super-hydrophobic surface as a result of the PDMS segment and the high surface areas of such fibres. This could open the door for further applications for these materials. Obviously much work is still needed to be done in

this area of PDMS-polyester copolymers. This can take two or three routes: improve the electrospinning conditions, and increase the PBT content in the copolymer while still maintaining the solubility of the obtained copolymer. Electrospinning from the melt is another possibility.

D.6 References

1. Ramakrishna, S.; Fujihara, K.; Teo, W.-E.; Lim, T.-C.; Ma, Z., *An Introduction to Electrospinning and Nanofibers.* First ed.; World Scientific Publishing Company, Singapore, 2005.
2. Patanaik, A.; Anandjiwala, R. D.; Rengasamy, R. S.; Ghosh, A.; Pal, H. *Textile Progress* 2007, 39(2), 67-120.
3. Koski, A.; Yim, K.; Shivkumar, S. *Materials Letters* 2004, 58(3-4), 493-497.
4. Thandavamoorthy, S.; Bhat, G. S.; Tock, R. W.; Parameswaran, S.; Ramkumar, S. S. *Journal of Applied Polymer Science* 2005, 96(2), 557-569.